Computational Intelligence and Neuroscience

# Recent Advances in Brain Signal Analysis: Methods and Applications

Guest Editors: Victor Hugo C. de Albuquerque, Plácido Rogerio Pinheiro, João Paulo Papa, João Manuel R. S. Tavares, Ronaldo Parente de Menezes, and Carlos A. S. Oliveira

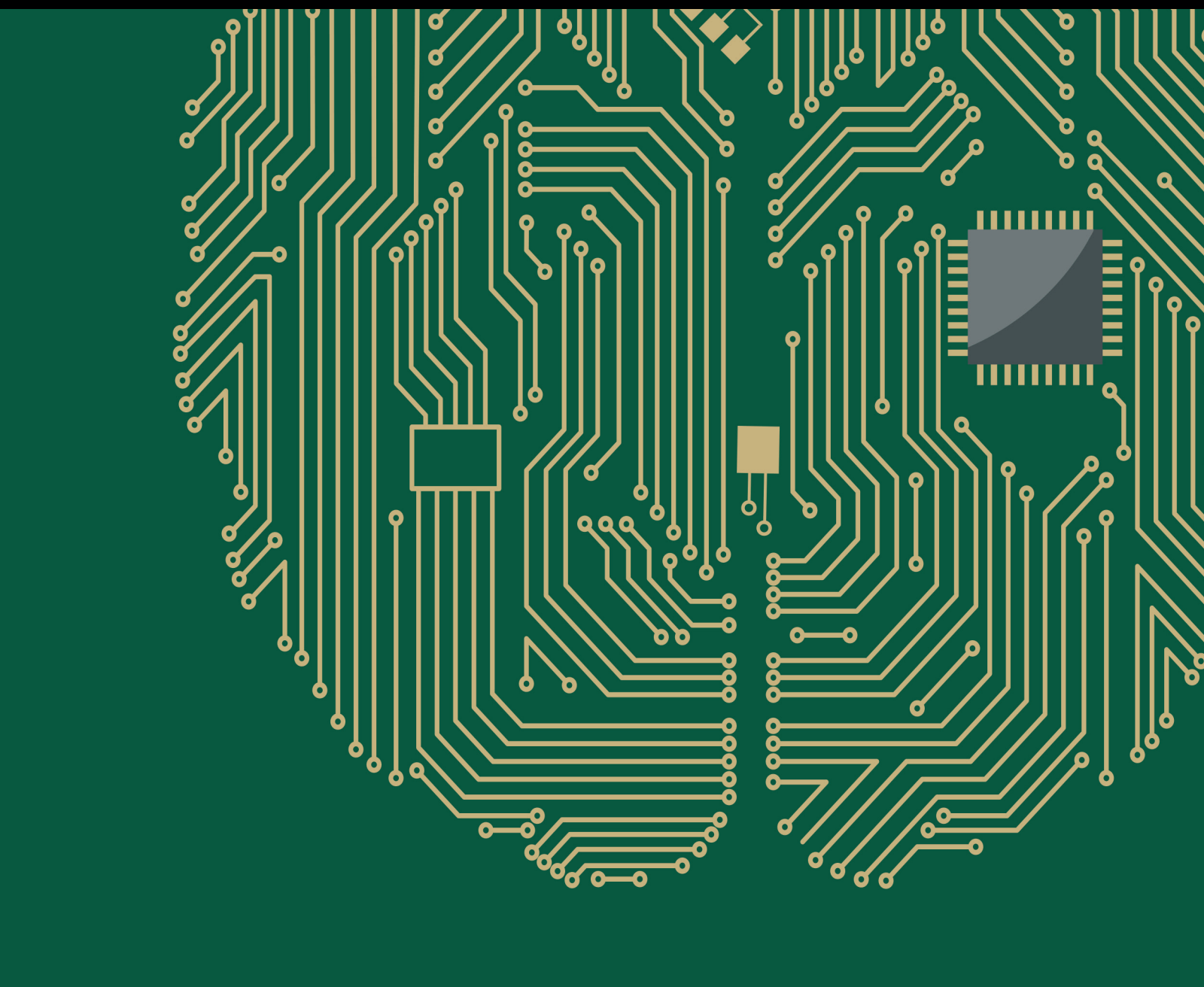

# Recent Advances in Brain Signal Analysis: Methods and Applications

# Recent Advances in Brain Signal Analysis: Methods and Applications

Guest Editors: Victor Hugo C. de Albuquerque, Plácido Rogerio Pinheiro, João Paulo Papa, João Manuel R. S. Tavares, Ronaldo Parente de Menezes, and Carlos A. S. Oliveira

# Editorial Board

# Contents

Hindawi Publishing Corporation
Computational Intelligence and Neuroscience
Volume 2016, Article ID 2742943, 2 pages
http://dx.doi.org/10.1155/2016/2742943

*Editorial*

# Recent Advances in Brain Signal Analysis: Methods and Applications

**Victor Hugo C. de Albuquerque,[1] Plácido Rogerio Pinheiro,[1] João Paulo Papa,[2] João Manuel R. S. Tavares,[3] Ronaldo Parente de Menezes,[4] and Carlos A. S. Oliveira[5]**

[1] *Programa de Pós-Graduação em Informática Aplicada, Universidade de Fortaleza, Fortaleza, CE, Brazil*
[2] *Universidade Estadual Paulista Júlio de Mesquita Filho, Bauru, SP, Brazil*
[3] *Instituto de Ciência e Inovação em Engenharia Mecânica e Engenharia Industrial, Departamento de Engenharia Mecânica, Faculdade de Engenharia, Universidade do Porto, Porto, Portugal*
[4] *Florida Institute of Technology, Melbourne, FL, USA*
[5] *University of Florida, Gainesville, FL, USA*

Correspondence should be addressed to Victor Hugo C. de Albuquerque; victor.albuquerque@unifor.br

Received 22 August 2016; Accepted 22 August 2016



## 1. Introduction

Signal processing and analyses have been extensively used in the field of Neuroscience. For example, (semi)automatic brain-based systems have been increasingly used in various medical applications such as disease prevention, detection and diagnosis of diseases, rehabilitation, smart environments education, serious games and entertainment, security and authentication, biometry, and mobile, as well as new equipment for signal acquisition. These systems are introduced in the literature as accurate, fast, complementary, and alternative devices to aid specialists in their decision making, to facilitate the analysis and interpretation of brain signals, and to reduce and/or eliminate errors [1, 2]. The main objective of this special issue is to promote a discussion on the recent advances related to Brain Signal Analysis from novel methods or applications in order to identify innovative, current, and important contributions to the field of Neuroscience. This special issue of this journal contains 9 original works selected from the 23 submitted. These studies address new trends in novel methods and techniques applied to different applications.

## 2. Computational Intelligence

First of all, I. Martišius and R. Damaševičius developed a prototype of a three-class brain-computer interface system, based on the Steady State Visually Evoked Potentials (SSVEP) paradigm and the Emotiv EPOC headset, to control an online target shooting game implemented in the OpenViBE software. Moreover, S.-K. Kim et al. explored the effects of smartphone push notification delivery during a task according to the level of smartphone overuse, using the event related potential (ERP). The authors concluded that the smartphone presented sensitive reactions associated with notifications during tasks. In addition, J. M. de Oliveira et al. described a virtual environment for patients to engage in a therapeutic game for neuropsychomotor rehabilitation that integrates patient and the proposed virtual environment. In this work, the system recognizes and tracks hands and fingers (Leap Motion sensor) as well as the electroencephalographic sensor (MindWave) responsible for measuring attention levels during task execution. Furthermore, H. G. Yeom et al. examined whether similar rhythmic oscillations with time delays exhibited in macroscopic neural activity at a low frequency during reaching movements from magnetoencephalography (MEG) signals using jPCA showed that the neural mechanism of skilled movements was similar to that of rhythmic movements. Also, K. Yano and T. Suyama presented a novel fixed low-rank spatial filter estimation for brain-computer interface systems applied to recognizing emotions elicited through movies. On the other hand, N. T. Haumann

et al. compared results achieved by applying popular methods for reducing artifacts in MEG and EEG signals of the auditory evoked Mismatch Negativity responses in healthy adult subjects. Jointly, R. Grandchamp and A. Delorme proposed the Brainarium, a novel pedagogical and artistic approach based on brain-computer interface technologies, which can deliver and illustrate scientific knowledge, as well as a new framework for scientific exploration. Besides, J. Hori and S. Takasawa proposed an inverse filter that optimizes filtering properties using a sigmoid function applied to human experimental data of visually evoked potentials. These authors concluded that the estimation accuracy is improved and the localized dipole distribution is obtained with less noise. Finally, N. S. Bastos et al. evaluated the use of a data mining technique combined with brain-computer interface systems to assess the behavior of the brain of blind and sighted people in a spatial activity.

## Acknowledgments

The guest editors wish to thank all the authors and reviewers for helping to improve the works published here.

*Victor Hugo C. de Albuquerque*
*Plácido Rogerio Pinheiro*
*João Paulo Papa*
*João Manuel R. S. Tavares*
*Ronaldo Parente de Menezes*
*Carlos A. S. Oliveira*

## References

[1] T. C. Handy, *Brain Signal Analysis: Advances in Neuroelectric and Neuromagnetic Methods*, The MIT Press, London, UK, 2009.

[2] M. A. Arbib, *The Handbook of Brain Theory and Neural Networks*, MIT Press, London, UK, 2nd edition, 2003.

Hindawi Publishing Corporation
Computational Intelligence and Neuroscience
Volume 2016, Article ID 4204385, 12 pages
http://dx.doi.org/10.1155/2016/4204385

*Research Article*

# The Brainarium: An Interactive Immersive Tool for Brain Education, Art, and Neurotherapy

**Romain Grandchamp[1,2] and Arnaud Delorme[3,4,5]**

[1] *Laboratoire de Psychologie et NeuroCognition, Université de Grenoble, Grenoble, BSHM, 1251 av Centrale CS40700, 38058 Grenoble Cedex 9, France*
[2] *CNRS, UMR 5105, Grenoble, France*
[3] *Centre de Recherche Cerveau et Cognition (CerCo), Université Paul Sabatier, Pavillon Baudot, Hopital Purpan, BP 25202, 31052 Toulouse Cedex 3, France*
[4] *CNRS, UMR 5549, Toulouse, France*
[5] *Swartz Center for Computational Neuroscience, Institute of Neural Computation (INC), University of San Diego California, La Jolla, CA 92093-0559, USA*

Correspondence should be addressed to Romain Grandchamp; romain.grandchamp@gmail.com

Received 13 April 2016; Accepted 30 June 2016

Academic Editor: Victor H. C. de Albuquerque



Recent theoretical and technological advances in neuroimaging techniques now allow brain electrical activity to be recorded using affordable and user-friendly equipment for nonscientist end-users. An increasing number of educators and artists have begun using electroencephalogram (EEG) to control multimedia and live artistic contents. In this paper, we introduce a new concept based on brain computer interface (BCI) technologies: the Brainarium. The Brainarium is a new pedagogical and artistic tool, which can deliver and illustrate scientific knowledge, as well as a new framework for scientific exploration. The Brainarium consists of a portable planetarium device that is being used as brain metaphor. This is done by projecting multimedia content on the planetarium dome and displaying EEG data recorded from a subject in real time using Brain Machine Interface (BMI) technologies. The system has been demonstrated through several performances involving an interaction between the subject controlling the BMI, a musician, and the audience during series of exhibitions and workshops in schools. We report here feedback from 134 participants who filled questionnaires to rate their experiences. Our results show improved subjective learning compared to conventional methods, improved entertainment value, improved absorption into the material being presented, and little discomfort.

## 1. Introduction

This century has been marked by the development of new brain imaging techniques, which have allowed us to better understand how our brain functions when we experience different mental states. The brain appears as a key integrative organ where a variety of inputs are simultaneously processed and combined: exteroceptive stimuli, that is, stimulations coming from the external world, proprioceptive inputs that provide body state information, or interoceptive inputs such as thoughts, emotions, and other inner experiences [1]. This processing is the result of lifelong learning, shaping, and adaptation of our neural system through our interaction with the world [2].

With the discovery of some of the core processes underlying brain electrical activity, we have found a new way of looking at the brain of living beings, obtaining insights on the functioning of their perceptual and inner spaces. When groups of several thousand neurons in the brain, sitting at close distances from each other and oriented in the same direction, are firing synchronously, their joint electrical activity adds up and generates an electrical field that is strong enough to be captured on the scalp. As a result of technological developments in electronics, signal processing, and

computer science, we are now able to record different electrical brain rhythms with millisecond precision and process this activity in real time by placing electrodes on subjects' head. The technique of electroencephalography (EEG) is now widely used both in fundamental and in clinical research, as well as a diagnostic tool in clinical environment. In addition to basic research and clinical applications, EEG rhythms have been recently used to control computers in real time. In Brain Machine Interface (BMI) or Brain Computer Interface (BCI) [3–5] characteristic patterns of EEG activity during specific mental activity are mapped to a given computer command. Some BCI systems allow controlling a mechanical device, a graphical interface, or a video game using thoughts only. Subjects may voluntarily learn to retrain specific brain EEG patterns in order to correct pathological activity of the brain. This specific range of application is called neurofeedback or neurotherapy [6–8].

When EEG began to be recorded in the 1930s, researchers realized that several typical rhythms could be distinguished in the brain electrical activity recorded at the surface of the scalp. The first "brainwave" was identified by the father of electroencephalography, Berger [9]. It was denominated using the first Greek letter, alpha, and became the "alpha" rhythm, which is a brain rhythm that oscillates at about 10 cycles per second (10 Hertz). This rhythm is particularly active when a person is awake, resting with his/her eyes closed or while relaxing [10, 11]. Using alpha brainwaves to create or modulate sound and/or music has been pioneered by Lucier [12] as recently as 1965. Later in 1969, Kamiya showed that it was possible to voluntary control the alpha brain rhythm and modulate audio feedback in real time [13].

Following technical and theoretical progresses in neuroscience, computer science, and signal processing, EEG signals have recently been used in new ways [14, 15]. With the development of affordable and user-friendly EEG systems, the last few years have seen an increasing number of art projects using brain electrical activity as an input or way to produce or modulate artistic content such as computer graphics, animations, music, and choreography. Several performances have been created around the concept of music generation using brainwaves [16–19]. The Global Mind Project (http://www.globalmindproject.com/) is an example of such an artistic project. This system allowed for audio-video rendering of brain data, which, when combined with live interactive performance, has helped further develop new interactive artistic productions. According to Clarke, an Honorary Fellow in the Department of Culture and Communication at the University of Melbourne, "drawn together in a coalescence of self and technology, the artists connected to the EEG headsets are presented as both automata – self-operating machines – and intentional, self-activating beings, that have the ability to affect and be affected by the on-screen imagery generated" [20].

Another recent realization developed by a team of Rensselaer Polytechnic Institute students is Yehuda Duenyas' Infinity Simulator which involves control of a 3D automated rigging system using specific brainwave patterns [21]. This device led to the creation of the Ascent project (http://the-ascent.co/), a live-action, participatory theatrical experience that combines mind-control and levitation via an automated custom-built lifting platform system.

Our system uses similar ideas with the important addition of an immersive environment. This is the first time to our knowledge that *real time EEG* recordings are being displayed in a *full dome immersive environment* allowing *direct spatialization* (spatial transposition) of brainwave data. One of the main originality and strengths of our system is also the brain metaphor regarding the shape of the device. Among developed applications, it allows projecting EEG topographic activity directly on the dome surface of a planetarium as if viewers were standing at the centre of the brain, looking up at electrical brain activity projected on the scalp.

The "Brainarium" (originally "Cerveaurium" in French) was initially designed to present neuroscience concepts in a fun, attractive, and interactive way for educational and entertainment purposes, by mixing art and science. In the method section of this paper, we will first present the general concept and architecture of the system in order to outline and illustrate its general functioning, describe a first performance that was designed for the Brainarium, and detail the specific implementation of the performance using open source software platforms. In the Result and Critical Reception section, we then mention the context in which our device has been used during exhibitions at museums and during "The Brain's Awareness Week" and present data on audience's experience in the Brainarium. In Discussion, we finally introduce potential extension and further development of our system in the fields of education, entertainment, arts, and more specifically its possible benefits in clinical applications such as neurotherapy.

## 2. Methods

*2.1. Concept and General Design.* Figures 1 and 2 summarize the architecture of the system and the different hardware it is comprised of. EEG signal is acquired on a person present in the dome. As shown in these figures, we used the Emotiv Epoc headset (Emotiv, Inc.), which includes 14 metal electrodes recording electrical brainwaves on the surface of the scalp at a frequency of 240 Hz (240 samples per second), but any EEG system compatible with BCI software can potentially be used. The signal is then transmitted, using a wireless connection, to a computer. This processing unit handles the signal processing part and calculates the control signals, which will be used to drive multimedia contents. Visual representations are finally projected onto a planetarium dome via a video projector equipped with a hemispherical lens (the system can be adapted to project on a hemispheric mirror which will reflect the image on the dome surface rather than directly project on the dome using a hemispheric lens). The system can be upgraded to multiprojector full dome systems but the main advantage of using a transportable inflatable dome and monoprojector hemispheric projection system is that it decreases the overall cost and allows an itinerant use. The computer display adapter should have two video outputs in order to allow simultaneous control of the different software on one screen and output to the video projector for the dome. In addition, a video splitter was used to send the video signal

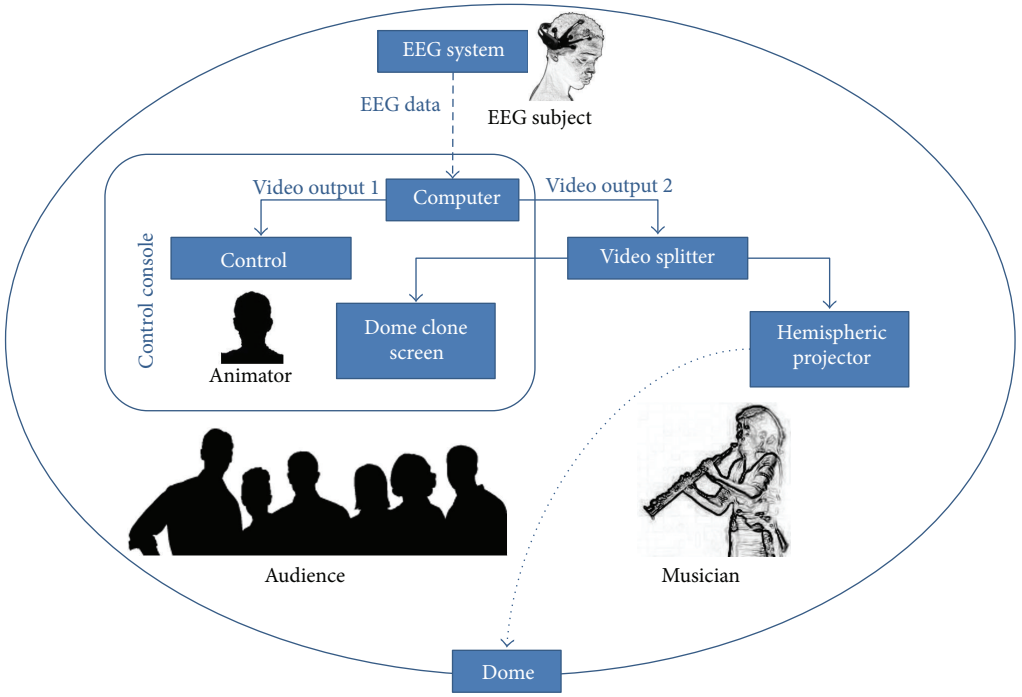


Figure 1: General principle of the Brainarium. EEG is recorded using the Emotiv headset and sent to a computer that computes brain rhythm activity in real time and projects it on the planetarium dome.

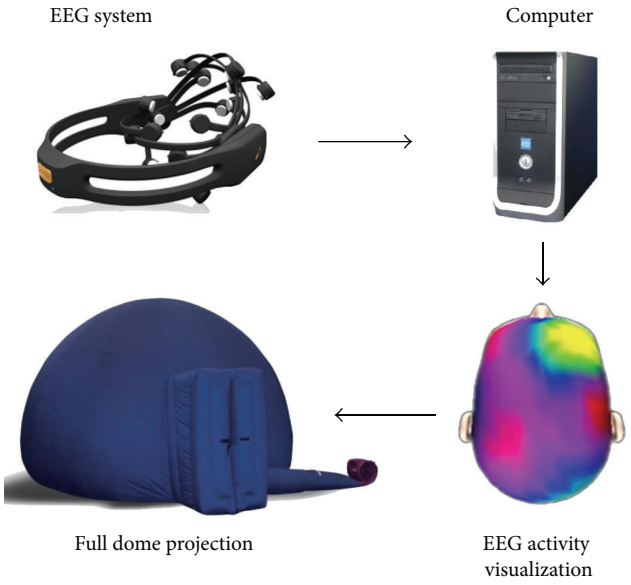


Figure 2: Flow chart of the different modules of the Brainarium.

to a second screen so that the person driving the performance could see what was being projected.

If the system is used in the context of an art and science performance, brain electrical activity may be recorded from a member of the audience, an organizer of the projection, or an artist who participates in the event. Our device opens a wide range of possibilities among which we have integrated and used the following for a first performance:

(i) Interaction with animation in computer graphics through electrical brain(s) activity(ies).

(ii) Visualization of a brain rhythm (Alpha rhythm) associated to the suppression of visual input when the subject closes his eyes or relaxes.

(iii) Real time presentation of topographies of brain electrical activity.

(iv) Interactive presentation of brain's structures on a 3D brain model.

After presenting the general implementation of the system, the next sections will be devoted to description of each one of these applications.

*2.2. General Implementation.* Our set-up is based on combining a hemispheric projection system such as the one used in a planetarium, a hemispheric projection surface, and a brain computer interface system. Since every functional block of the system is modular, various solutions may be developed depending on budgetary constraints and available material. As we are writing this paper, the cost of building such a system could range from about US$5,000 to about a hundred thousand dollars when using research grade apparatus; the intermediate set-up we present here costs about US$40,000 although we also provide suggestions on how to build a similar system for a lesser amount.

For projection, we used a transportable planetarium system, which comprised a Digitarium® Delta Portable Digital Planetarium System [22] and a Digitalis™ Portable Dome [23] which has a diameter of 7 meters. However, both

hemispheric projection systems and projection surfaces may be made at a lesser cost using custom made tools [24–26]. We implemented a low cost solution to replace the Digitarium Delta Portable Digital Planetarium System. This solution is composed of four parts: a full HD video projector (Acer H7531D), a condensator (Rodenstock TV Heligon 75 mm F/D = 1.1 can be replaced by a classical 50 mm with F/D = 1.4 combined with a +4 diopters lens as well), a 50 mm 45° mirror mount (Skywatcher), and a fisheye lens (Peleng 8 mm f3.5 fisheye lens). The dome we used was made of a thick fabric inflated by a powerful fan. This solution makes it more convenient to transport and set up the system compared to a rigid dome solution. However, this method has the drawback of having to leave the fan turned on in order to keep the dome inflated. Even if the sound of the fan is not covering the sounds played inside the dome, it still creates a distracting background noise.

The control console was composed of a classic personal computer equipped with a dual screen graphic card powerful enough to handle HD projection and two LCD monitors. One of the LCD monitors was used to control the demonstration. On the second graphical output, a video splitter was used to send the display signal to both a control LCD monitor and the video projector. For the EEG signal acquisition, the research edition package of Emotiv Epoc headset was used [27]. Emotiv Epoc is a wearable EEG "headset" composed of 14 gold-plated electrodes. In order to record electrical signals generated by the brain, each electrode is covered by a small felt-based pellet that acts as a bridge between the electrode and the scalp. These pellets have to be soaked in a saline solution, of water mixed with salt, which allows electrical conduction from the skin to the metal electrode through the pellet. The advantages of using this system are that it is relatively low in cost compared to clinical or research oriented devices. It is also wireless, fast, and easy to set up and provides some level of spatial resolution since it has 14 electrodes. However, clinical or research EEG systems with better signal quality can be used if available. Dry active electrodes would be the most adapted for such a system as they provide acceptable signal quality with a minimum preparation time but they are still expensive to date compared to the Emotiv Epoc solution.

The complete list of software used to run the system is depicted in Table 1. Except from the Emotiv software suite (the basic software package provided with the Epoc headset by Emotiv), the software used to do signal processing and visualization is all part of the open source community. For the fractal application, the software package "Mind Your OSC" was used to collect data from Emotiv Control Panel software and send it as an Open Sound Control (OSC) [28] stream to visualization software. The interactive fractal video was displayed using the vvvv software (https://vvvv.org/), a graphical programming environment for easy prototyping and development. The vvvv software application is designed to facilitate handling of large media environments with physical interfaces, real time motion graphics, audio, and video that can simultaneously interact with many users. The freely available OpenVibe software [29] was used for signal acquisition, signal processing, and visualization of the EEG

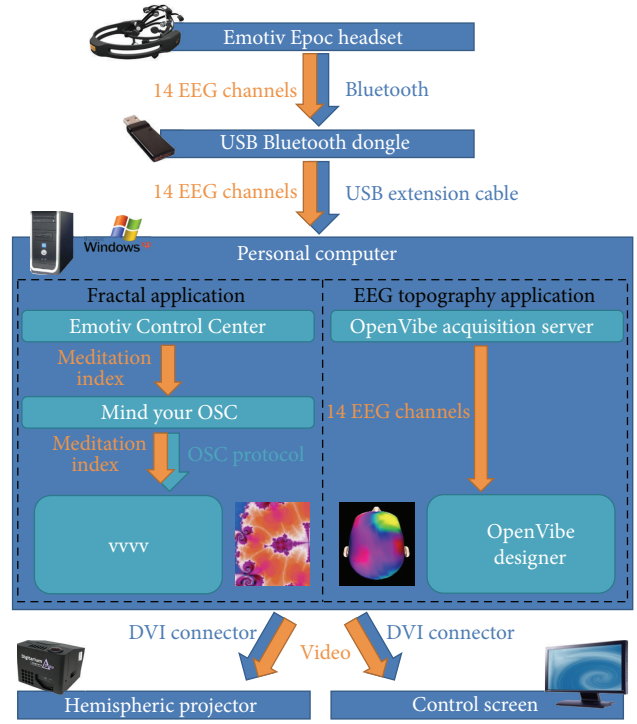


Figure 3: Set-up of the Brainarium for two different application examples: the fractal dynamical zoom application and the EEG topography application.

data in the context of the EEG topography application. Finally, the 3D brain model application has been developed using Blender (https://www.blender.org/), a free open source 3D content creation suite, and rendered by its embedded real time full dome plugin [30]. We are making available all additional plugin and software developed for our application under an open source license [31].

*2.3. Performance Design and Implementation.* In this section we detail technical implementation of each application used for the different phases of the original performance designed for the Brainarium.

*2.3.1. Brain-Controlled Animation of Fractals.* This application is an example of live interaction. Figure 3 depicts the general architecture of the hardware and software for this application.

We first placed the EEG cap on the subject's head. Ideally, the subject's alpha brainwaves should be large compared to the overall electromagnetic noise. Since individual brains show different electrical rhythmic activities, some subjects can exhibit low amplitude alpha oscillations and this might make it more difficult to process the signal without the use of advanced artifact rejection techniques. Due to time limitation between sessions, we often asked a preselected person with known high amplitude alpha rhythm (i.e., easily observable on the signal trace) to be the subject.

After checking electrodes contact quality and signal quality, a calibration step lasting approximately two minutes

Table 1: List of hardware and software applications required for setting up the Brainarium.

| Software | Operating system | Function |
|---|---|---|
| Emotiv Control Center | MS Windows | Acquire EEG data and transmit it to the software "Mind Your OSC" |
| Mind Your OSC | MS Windows | Receive data from Emotiv Control Center and transmit them to vvvv using OSC protocol |
| vvvv | MS Windows | (i) Receive OSC data packets from "Mind Your OSC"<br>(ii) Calibrate the system<br>(iii) Compute the video speed<br>(iv) Display hemispheric video |
| OpenVibe Acquisition Server | MS Windows or Linux | Acquire EEG data and transmit it to OpenVibe Designer |
| OpenVibe Designer | MS Windows or Linux | (i) Collect data from OpenVibe Acquisition Server<br>(ii) Process EEG signal (extract alpha frequency band)<br>(iii) Compute and display real time EEG topography |
| Blender | MS Windows or Linux | Display a 3D brain model in the Game Engine with a full dome display mode |

is performed in order to evaluate some statistical features of the signal of interest's amplitude for the selected subject such as its mean and standard deviation. We used the index "Meditation" provided by the Emotiv Control Panel as the control signal. Since it has not been made public by Emotiv, we do not have the exact formula used to compute this index out of the raw EEG signal. However, it is known to be positively correlated with the alpha rhythm and relaxation. Emotiv indexes result from a statistical analysis based on a large normative database collected of many subjects and are therefore already normalized. However, a calibration procedure is still used in order to adapt the system to subject's specific statistics. In our case, we used the standard deviation and the mean value of the "Meditation" index over the calibration period as a reference value to tune the feedback set-up.

During the first minute of calibration we asked the subject to keep his eyes open and during the second minute we ask him to keep his eyes closed. Even if the subject has already performed the experiment, it is important to repeat the calibration step since EEG features widely vary throughout the day and from one day to another. "Meditation" values are calculated for both the eyes-closed and the eyes-open period and are used to calibrate the system to allow balanced behaviour of the visual feedback animation. Once calibration is performed, the session starts with the video feedback being projected on the dome and the audience enters the dome. In the meantime, a professional musician is improvising based on the visual display. This allows creating a complete interactive feedback loop between the subject wearing the EEG device and the musician (Figure 4(a)). The musician uses inspiration of what he sees on the dome to play music and adapt it. Furthermore, he can engage in an interplay with the wearer of the EEG and can try to induce changes in what is displayed.

The "Meditation" measure controls the display projected on the dome. We used a zoom into Mandelbrot's ensemble fractal as visual feedback. More details about the video used are given in following paragraphs; we focus here on the interaction configuration. The speed and direction (forward or backward) of the zoom depends on the brainwaves of the subject wearing the EEG cap. The system was set up so that the animation was played forward, as if diving or moving forward into the fractal, when the current alpha wave amplitude generated by the subject was over its mean level. By contrast, when the current alpha wave amplitude was lower than its mean level, the animation was played

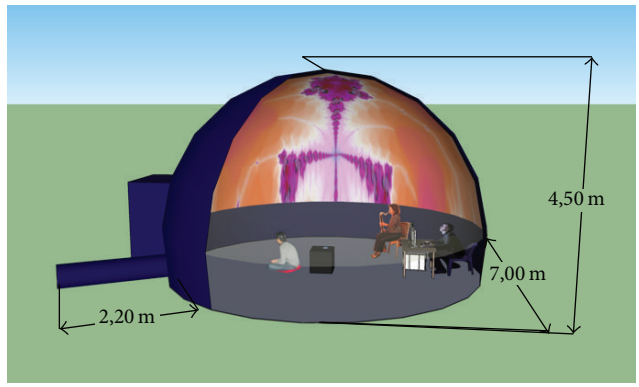


(a)

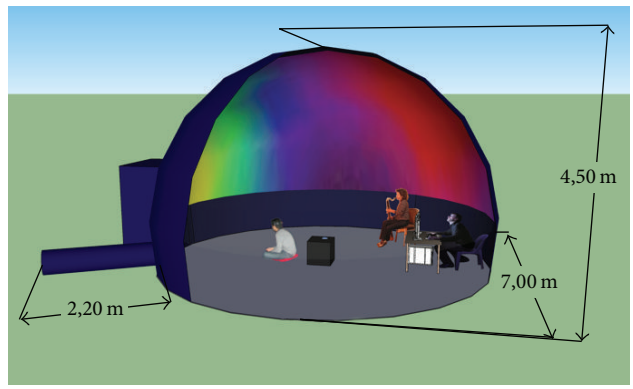


(b)

Figure 4: Brainarium represented as a 3D model with exact dimensions (the public is not shown on the rendering). (a) shows the projection of fractals and (b) shows the projection of subject's scalp topographies.

backward, as if travelling away from the fractal. The speed of the animation was modulated by the difference between the current value of the alpha "Meditation" wave amplitude and its mean amplitude; that is, zooming becomes faster as the current value is further away from the mean. As a result, a "Meditation" value equal to the mean value would result in a static image.

The shapes projected on the dome are fractals. A 2D fractal is a mathematical expression, which may be represented as a 2D image. We choose to use fractals because, in addition to their aesthetic dimension, more and more research is showing that certain aspects of brain activity or even its own structure share some features with fractals [32–35]. Because fractals are based on mathematical expressions, there is no theoretical limit to the resolution of fractal images making it possible to zoom in on a small portion of the image and expanding it indefinitely. Another feature of fractal images is that their structure is preserved regardless of the "zoom." Finally, fractal images are self-similar representations. If the appropriate "zoom" is applied to a fractal image, the same image may be found again. An interesting feature resulting from the use of a fractal animation is that it produces an immersive tunnelling effect.

Fractal images presented in the Brainarium were made dynamic by zooming in or out in the fractal image. The animation used in the Brainarium was "a precalculated journey into the heart of the Mandelbrot fractal set" (http://www.hd-fractals.com/), which is named after Benoit Mandelbrot, the mathematician who studied and popularized it [36]. The video used in our demonstration features a 2^760 zoom in the Mandelbrot fractal set and it was produced by Teamfresh (http://www.hd-fractals.com/), an independent production company which specialized itself in rendering fractal animations. We used a commercially available High Definition version of the animation. The fractal video control application has been specifically implemented for this project using vvvv, a graphical programming environment for easy prototyping and development (https://vvvv.org/). We have made the vvvv patches developed for this application freely available [31].

*2.3.2. EEG Real Time Topography Application.* Specific software for this application can be seen in Figure 3. During the second part of the performance, participants observe EEG raw brainwaves, followed by their representation as topography or how EEG brainwaves are distributed on the surfaces of the scalp. These EEG topographies may be likened to topographies used in elevation maps for hiking. Instead of representing the terrain elevation on the Earth surface, colors represent the strength of a specific brainwave at different locations on the head surface. In our case, we focused on brainwaves in a frequency band ranging from 8 to 12 Hz called the alpha band. Alpha brainwave amplitudes vary quickly in time and space and this dynamic may be rendered as animated colored maps on the dome. The topography is represented using either classic 2D spherical projection or an interactive 3D head model from OpenVibe software [29]. Using this set-up, participants may observe that when the subject closes his eyes, alpha wave amplitudes increase on the part of the dome that represents the back of the head. The part of the brain that is activated is called the occipital region, which is a brain area largely devoted to visual processing. When this region does not process visual information, that is, when the subject closes his eyes, alpha waves tend to increase in this brain area. Another way to increase alpha wave amplitude over the entire brain is to ask the subject to enter a deep relaxation state but this requires more training from the subject and this is more difficult to achieve in a single session: we have succeeded to perform the second part of this demonstration with only a few subjects. While the brain dynamic is shown on the dome, a musician is simultaneously playing his instrument, trying to help the subject to go into deeper relaxation states and simultaneously giving him auditory feedback about his relaxation state using his own interpretation of ongoing EEG patterns (Figure 4(b)). We have made available under an open source license the OpenVibe software scenario we developed to display alpha wave topography [31].

*2.3.3. Neuroanatomy Using a 3D Interactive Brain Model.* After the two interactive real time EEG sessions, the last part of our demonstration interactively showed different parts of the cortex in human brain volume. Despite the BCI being not involved in this part, we still want to describe it briefly to keep the description of the system's features complete. On the basis of gross topographical conventions, the cortex can be classified into four lobes: the temporal lobe, occipital lobe, parietal lobe, and frontal lobe. The system developed using Blender Game Engine (https://www.blender.org/) allows manipulating the 3D model in order to show the different lobes and introduce some of basic neuroanatomy concepts. We implemented rotation around different axis, zooming in and out for projection of these 3D models on the dome. The 3D models are rendered using the "Blender embedded full dome plugin" to compensate deformation due to the dome-specific projection lens and surface. We are making publicly available the Blender file we developed [31].

## 3. Results and Critical Reception

The innovative aspect of our project was to combine real time brain electrical activity visualization tools with an immersive full dome environment. Participants were seated inside the space enclosed by the projection dome, which induces a special atmosphere and feeling. In addition, scientific and artistic content interactive display exploited the analogy between the shape of the projection space and the near spherical shape of the brain (see Methods). What participants heard was not necessarily limited to what was being played inside the dome, as the material used for the projection surface was not soundproof. Nevertheless, acoustic properties of the dome were specific to its hemispheric shape, and this tended to enhance participants' experiences.

The Brainarium was inaugurated during "The Brain's Awareness Week," an event organized every year in all large European cities. For a week, series of exhibits are set up to present to the general public the latest advances in brain

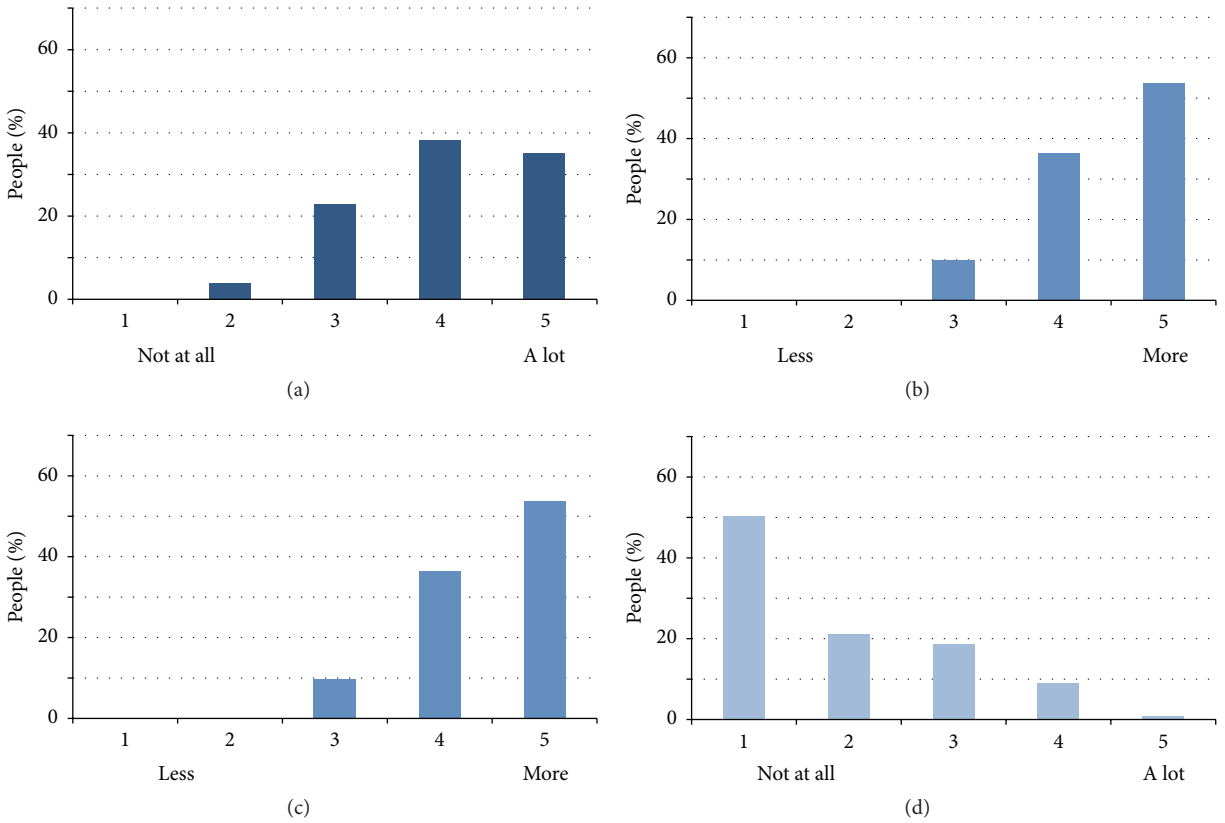


Figure 5: (a) Improved learning. (b) Entertainment. (c) Absorption. (d) Discomfort.

research. During "The Brain's Awareness Week" 2013, we performed more than 17 sessions demonstrating the Brainarium to more than 200 visitors. Following this encouraging start, our demo was also presented in Paris during the Cognitive Sciences Forum in the "Couvent des Cordeliers," at the Medical School of Paris, where it proved to be a very popular animation with more than 180 visitors in one day. Our project was also featured on the most popular newspaper of South-West France (6 million readers), "La Depeche," and also mentioned on local radio stations. It is now regularly requested for performances in more and more cities across France and Belgium, for workshops in primary and secondary schools, and for various national events such as the French National Science Week.

A questionnaire was filled in by participants after the performance to collect their feelings and how their experience in the Brainarium compares to traditional conferences and lectures they attended.

This questionnaire allowed us to collect demographic data about participants, on four closed questions with Likert scales, and an open text field where subject could give us their feedback freely. The first question asked the participant if he or she feels this type of demonstration promotes learning and memory compared to a conventional conference. Answer was given on a 5-point Likert scale ranging from 1 ("not at all") to 5 ("a lot"). The second question asked the participant whether it was more entertaining than a traditional conference or course. Answer was given on a 5-point Likert scale ranging from 1 ("less entertaining") to 5 ("more entertaining"). Question three addressed whether participant was more or less absorbed by the presentation on the 3D dome compared to a presentation on a conventional rectangular screen. Answer was given on a 5-point Likert scale ranging from 1 ("less absorbed") to 5 ("more absorbed"). Finally, the fourth question asked if the participant felt discomfort (i.e., if he felt dizzy) due to the presentation on the 3D dome. Answer was given on a 5-point Likert scale ranging from 1 ("not at all") to 5 ("a lot"). We collected data on a total of 134 participants in two distinct performance places, during four different days. 52 participants were men and 82 were woman with an average age of $30.4 \pm 17.3$ years old across all participants (minimum age was 7; maximum age was 80).

Results from the questionnaire are shown in Figure 5. Our results show improved subjective learning compared to conventional methods, improved entertainment value, improved absorption into the material being presented, and little discomfort with no participant experiencing strong discomfort.

## 4. Discussion

Planetarium domes have previously been used to display various contents. However, to our knowledge, this is the first time that real time EEG data is being shown in such an environment. Our demonstration appeared to arouse some

level of popular success and seemed to provide participant with a new type of interactive experience. Thus, we have made all the tools we developed available in the public domain for anyone interested in reproducing our demonstration.

In the following sections, we will focus on four domains of application in which the Brainarium may potentially be used and further developed: education applications, entertainment applications, art applications, and immersive neurofeedback applications.

*4.1. Education and Training Applications.* The current Brainarium set-up already provides educational material to explain some basic concepts in Cognitive Sciences. We are currently exploring the possibility of showing content using stereoscopic projection methods, with the goal of providing an even more intense immersive experience to the public.

We currently focus on porting two classical BCI applications to the dome environment and developing pedagogical materials. The first application involves visualizing brain electrical activity related to emotion. Recent studies have reported that it is possible to differentiate emotional reactions and states using EEG in real time [14, 37]. When the participant wearing the EEG headset is experiencing a given emotion, an appropriate dynamical pattern reflecting the subject's emotion would be shown on the dome. The second application involves visualizing brain electrical activity associated with real and imagined body movements. Execution or mental visualization of body movement gives rise to typical brain rhythms [38]. These rhythms are recorded at the scalp surface and may be used to control visual display or even robotic devices. Moreover, results brought by fMRI studies on these domains can be shown to complement the explanations, showing brain areas and brain processes involved. The ultimate goal is to use the interactive and immersive dimensions to create and stimulate curiosity, attention, and interest in order to serve pedagogical purposes.

*4.2. Entertainment Applications.* The Brainarium could potentially be used as an immersive environment for BCI based games. BCI appear as a potential new way to gain control over a video game or a virtual world [39, 40]. Several EEG products specifically developed for BCI games have recently been made available to the general public in the form of commercial games (Star Wars Force Trainer and Mindflex by Matel, Inc.) and video games (Mindout: http://www.mindoutgame.com/, Free [41]). Several game studios have even specialized to solely design BCI games (MindGames: http://mindgames.is/, Dreams of Danu: http://www.dreamsofdanu.com/).

Immersive environments such as hemispheric projection surfaces have been already used for video games (e.g., with Blender full dome compatible Game Engine) [30], but never in conjunction with BCI systems. Moreover, it has been pointed out in a previous study by Lalor et al. [42] that subjects report that the multimodal feedback, such as the visuoauditive feedback delivered by the Brainarium, is useful in learning to control the game by suggesting that immersion increases sensation and therefore provides a more enjoyable game experience.

However, the engagement in the task of controlling the game using brainwaves might be too demanding and might degrade game experience. Nelson et al. [43] showed that concentration on the BCI task interacted with the feelings of presence in a virtual reality environment. However, they report as well that over time BCI control became more automatic for subjects as their brain adapts to the device, which allowed them to be gradually more absorbed by the virtual reality environment and feel more present. This description varies from what most subjects who experience the same virtual environment without BCI report: initially participants feel a high sense of presence which gradually drops as they realize the limitations of the virtual environment [44].

But what does the dome bring compared to a classic head mounted virtual reality device such as 3D goggles? An experiment studied the experience of users in an immersive device called the Cave [45], a room in which the user is presented with high-resolution stereo-pair images projected in real time on 3 walls and the floor, which provides an experience similar to a dome environment. They compared the experience of users in several environments: no immersion, head mounted 3D goggles, and the Cave. Subjects rated the Cave as providing a more immersive experience than all other conditions. Subjects also reported that the Cave was more comfortable than the head mounted goggles. There are numerous potential causes of visual discomfort when viewing stereo displays [46]. One of them is the vergence-accommodation conflict, that is, small amounts of left/right asymmetries, which is potentially present in all conventional stereo [47]. These results argue in favour of dome or room based systems for producing highly immersive environments.

*4.3. Art Applications.* More and more exploratory work using digital media and interactive devices are emerging on the art scene, leading to the relatively new field of interactive art. This developing genre of art usually has the public providing input in order to determine some parts or characteristics of the created content. Interactive art provides a ground for dialogue between the artist and the public through the potential of actions or reactions, introducing either intentional or passive ways to act upon the artwork.

The Brainarium is specific in the sense that the participant brainwaves are the source of interactivity. The artist may modulate multimedia artwork projected on the dome based on participant brainwaves. As mentioned for the education application parts, the artist may be able to extract subject's emotion and adapt the art forms being shown on the dome. Our system finally opens up the possibility to live coparticipation involving one or several participants wearing EEG headsets.

*4.4. Medical Applications Using Immersive Neurofeedback.* Neurofeedback is a type of brain computer interface application used in clinical environments to help to treat pathological traits [48–51]. Neurofeedback is being used to treat neuropsychological pathologies, epilepsy, ADHD, addiction, and depression [6, 52, 53], and to improve performance (stress management, creativity, attention and focus, and control of impulsivity [7, 8, 54–57]). The idea behind neurofeedback

is that pathological mental states generate abnormal brain rhythms. By training patients to control their brain rhythms and suppress the pathological ones, it might be possible to treat specific mental pathologies. Note that neurofeedback is not yet widely accepted in the scientific and medical communities although recent neuroscientific works indicate some level of clinical efficacy and a bright future for this discipline [58–62].

Recent research results brought evidence that, in the context of neurofeedback training, immersion tends to improve training efficiency compared to classic feedback on a 2D screen [63]. As stated by Lécuyer et al. [64], virtual reality (VR) technologies provide motivating, safe, and controlled conditions that enable improvement of BCI learning. As reported in a recent review by Pfurtsheller et al. [65], a realistic virtual and immersive environment enhances the feeling of presence, task performance, and also cortical activation [66–68]. Studies indicate that the more game-like and engaging neurofeedback applications often resulted in a better performance [69, 70]. Subjects report the games are more stimulating and that multimodal immersive feedback is useful [42].

Previous studies have used virtual reality goggles with neurofeedback [63] but neurofeedback has never been performed in immersive environments like the one we are presenting here. Immersive environments could potentially offer numerous other benefits to patients, such as reduced training time, improved classification accuracy, increased sense of immersion and presence in an artificial setting, and reduced boredom or fatigue [71]. Finally, in the context of a therapeutic neurofeedback session, the dome environment provides a unique environment for enhanced intimacy between the patient and the therapist.

In the specific field of emotion regulation, fMRI neurofeedback recently brought very promising results [72–76]. However and despite the difficulty of recording subcortical regions of the brain involved in emotion generation, result obtained with EEG recordings [14, 15, 37] could be extended and refined in order to benefit from the high temporal resolution of the EEG and target in particular cortical areas involved in emotion monitoring and regulation [77]. Independent component analysis and source reconstruction methods could potentially be used to improve EEG spatial resolution and signal to noise ratio. Cannon et al. [78] showed that limbic lobe and hippocampal activity can be recorded and visualized using LORETA during affective memory recall. In another study, Cannon et al. [79] showed that it was possible to learn to self-regulate activity in anterior cingulated gyrus, an area of the brain known to be involved in both cognitive and affective processes. ICA neurofeedback and LORETA neurofeedback are indeed possible in an immersive set-up such as the Brainarium. Following recent developments in the field of virtual reality technology, several studies argued in favour of several benefits from using virtual reality in treatment of various pathologies or disorders related to emotions such as anxiety disorders (for a review see [80]). Bringing together BCI and VR could potentially help to not only better monitor and therefore optimize the therapy, but also give birth to new therapeutic techniques.

## 5. Conclusion

We described the first interactive system allowing real time spatialized visualization of electrical brain activity in a brain-like shaped immersive environment. This device was initially intended to deliver scientific knowledge using a pedagogical medium at the crossing between art, science, and technology. Its modular architecture allows extending and adapting it to various implementation solutions leveraging the costs to different contexts of deployment. This innovative concept can be further developed into a rich variety of applications in educational, entertainment, art, and medical domains.

## Competing Interests

The authors declare that they have no competing interests.

## Acknowledgments

The authors wish to thank the Art and Science Association "Les Chemins Buissonniers" that collaborated on this project, the association "La Ligue de l'Enseignement" that lent the dome for the demos, the association "InCOGnu" who provided the Emotiv Epoc headset, and Isabelle Cirla, the professional musician who played during the live exhibits. This project was supported by a grant in neuroinformatics from the FRM Foundation and a grant from the French Ministry of Research on brain computer interfaces.

## References

[1] C. S. Sherrington, *The Integrative Action of the Nervous System*, Yale University Press, New Haven, Conn, USA, 1906.

[2] H. R. Maturana and F. J. Varela, *The Tree of Knowledge: The Biological Roots of Human Understanding*, New Science Library/Shambhala Publications, 1987.

[3] J. R. Wolpaw, N. Birbaumer, D. J. McFarland, G. Pfurtscheller, and T. M. Vaughan, "Brain-computer interfaces for communication and control," *Clinical Neurophysiology*, vol. 113, no. 6, pp. 767–791, 2002.

[4] B. Z. Allison, E. W. Wolpaw, and J. R. Wolpaw, "Brain-computer interface systems: progress and prospects," *Expert Review of Medical Devices*, vol. 4, no. 4, pp. 463–474, 2007.

[5] C. S. Nam, G. Schalk, and M. M. Jackson, "Current trends in Brain-Computer Interface (BCI) research and development," *Journal of Human-Computer Interaction*, vol. 27, no. 1, pp. 1–4, 2010.

[6] J. Gruzelier and T. Egner, "Critical validation studies of neurofeedback," *Child and Adolescent Psychiatric Clinics of North America*, vol. 14, no. 1, pp. 83–104, 2005.

[7] J. Gruzelier, T. Egner, and D. Vernon, "Validating the efficacy of neurofeedback for optimising performance," *Progress in Brain Research*, vol. 159, pp. 421–431, 2006.

[8] T. Thompson, T. Steffert, T. Ros, J. Leach, and J. Gruzelier, "EEG applications for sport and performance," *Methods*, vol. 45, no. 4, pp. 279–288, 2008.

[9] H. Berger, "Über das Elektrenkephalogramm des Menschen," *Archiv für Psychiatrie und Nervenkrankheiten*, vol. 87, no. 1, pp. 527–570, 1929.

[10] E. D. Adrian and B. H. C. Matthews, "The berger rhythm: potential changes from the occipital lobes in man," *Brain*, vol. 57, no. 4, pp. 355–385, 1934.

[11] G. Pfurtscheller, C. Neuper, and W. Mohl, "Event-related desynchronization (ERD) during visual processing," *International Journal of Psychophysiology*, vol. 16, no. 2-3, pp. 147–153, 1994.

[12] A. Lucier, "Statement on: music for solo performer," in *Biofeedback and the Arts, Results of Early Experiments*, D. Rosenboom, Ed., pp. 60–61, Aesthetic Research Center of Canada Publications, Vancouver, Canada, 1976.

[13] J. Kamiya, "Operant control of the EEG alpha rhythm and some of its reported effects on consciousness," in *Altered States of Consciousness*, pp. 519–529, John Wiley & Sons, New York, NY, USA, 1969.

[14] Y.-P. Lin, J.-R. Duann, J.-H. Chen, and T.-P. Jung, "Electroencephalographic dynamics of musical emotion perception revealed by independent spectral components," *NeuroReport*, vol. 21, no. 6, pp. 410–415, 2010.

[15] G. Leslie, A. Ojeda, and S. Makeig, "Towards an affective brain-computer interface monitoring musical engagement," in *Proceedings of the 5th Humaine Association Conference on Affective Computing and Intelligent Interaction (ACII '13)*, pp. 871–875, Geneva, Switzerland, September 2013.

[16] S. Mann, J. Fung, and A. Garten, "DECONcert: bathing in the light, sound, and waters of the musical brainbaths," 2007.

[17] G. Leslie and T. Mullen, "MoodMixer: EEG-based Collaborative Sonification," in *Proceedings of the International Conference on New Interfaces for Musical Expression*, Oslo, Norway, June 2011.

[18] T. Mullen, R. Warp, and A. Jansch, "Minding the (transatlantic) gap: an internet-enabled acoustic brain-computer music interface," in *Proceedings of the International Conference on New Interfaces for Musical Expression*, Oslo, Norway, May-June 2011.

[19] E. R. Miranda and A. Brouse, "Interfacing the brain directly with musical systems: on developing systems for making music with brain signals," *Leonardo*, vol. 38, no. 4, pp. 331–336, 2005.

[20] J. Clarke, *Spectacle of the Mind*, Global Mind Project, 2009, http://www.academia.edu/199451/Spectacle_of_the_Mind.

[21] Tkoranyi, *Xxxy's Infinity Simulator Connects Emotiv Headset to Theatrical Flying Rig*, Neurogadget, 2011.

[22] Digitalis Education Solutions, "Digitarium Delta Digital Planetarium System," In: Digitalis Education Solutions, 2011, http://www.digitaliseducation.com/products-digitarium_delta.html.

[23] Digitalis Education Solutions, *Digitalis Portable Planetarium Domes*, 2011, http://www.digitaliseducation.com/domes.html.

[24] Y. Lhoumeau and L. Ruiz, "Lhoumeau Sky-System (Numeric Planetarium with Fisheye)," 2010, http://www.lss-planetariums.info/index.php.

[25] P. Bourke, "Digital fulldome, techniques and technologies," in *Proceedings of the Graphite Conference*, ACM SIGGRAPH, Perth, Australia, December 2007.

[26] P. Bourke, "Using a spherical mirror for projection into immersive environments," in *Proceedings of the 3rd International Conference on Computer Graphics and Interactive Techniques in Australasia and South East Asia*, pp. 281–284, Dunedin, New Zealand, 2005.

[27] Emotiv Inc, "Emotiv EPOC Software Development Kit," Emotiv—Brain Computer Interface Technology, 2010, https://github.com/Emotiv.

[28] M. Wright, "OpenSoundControl," in *OpenSound Control*, 2011, http://archive.cnmat.berkeley.edu/OpenSoundControl/.

[29] Y. Renard, F. Lotte, G. Gibert et al., "OpenViBE: an open-source software platform to design, test, and use brain-computer interfaces in real and virtual environments," *Presence: Teleoperators and Virtual Environments*, vol. 19, no. 1, pp. 35–53, 2010.

[30] P. Bourke and D. Felinto, "Blender and immersive gaming in a hemispherical dome," *GSTF International Journal on Computing*, vol. 1, no. 1, 2010.

[31] R. Grandchamp, "Downloads," Romain Grandchamp's Homepage, 2011, https://sites.google.com/site/romaingrandchamp/cerveaurium/downloads.

[32] E. Pereda, A. Gamundi, R. Rial, and J. González, "Non-linear behaviour of human EEG: fractal exponent versus correlation dimension in awake and sleep stages," *Neuroscience Letters*, vol. 250, no. 2, pp. 91–94, 1998.

[33] R. Ferenets, T. Lipping, A. Anier, V. Jäntti, S. Melto, and S. Hovilehto, "Comparison of entropy and complexity measures for the assessment of depth of sedation," *IEEE Transactions on Biomedical Engineering*, vol. 53, no. 6, pp. 1067–1077, 2006.

[34] D. S. Bassett, A. Meyer-Lindenberg, S. Achard, T. Duke, and E. Bullmore, "Adaptive reconfiguration of fractal small-world human brain functional networks," *Proceedings of the National Academy of Sciences of the United States of America*, vol. 103, no. 51, pp. 19518–19523, 2006.

[35] P. A. Carpenter, C. J. Davia, and R. L. Vimal, "Catalysis, perception, and consciousness," *New Mathematics and Natural Computation*, vol. 5, no. 1, pp. 287–306, 2009.

[36] B. B. Mandelbrot, "Fractal aspects of the iteration of $z \to \lambda z$ (1–z) for complex $\lambda$ and z," *Annals of the New York Academy of Sciences*, vol. 357, no. 1, pp. 249–259, 1980.

[37] Y.-P. Lin, C.-H. Wang, T.-L. Wu, S.-K. Jeng, and J.-H. Chen, "EEG-based emotion recognition in music listening: a comparison of schemes for multiclass support vector machine," in *Proceedings of the 2009 IEEE International Conference on Acoustics, Speech, and Signal Processing (ICASSP '09)*, pp. 489–492, IEEE, Taipei, Taiwan, April 2009.

[38] G. Pfurtscheller and F. H. Lopes da Silva, *Event-Related Desynchronization*, Elsevier Health Sciences, Philadelphia, Pa, USA, 1999.

[39] B. Reuderink, "Games and brain-computer interfaces: the state of the art," WP2 BrainGain Deliverable, HMI, University of Twente, Enschede, The Netherlands, 2008.

[40] A. Nijholt, D. P.-O. Bos, and B. Reuderink, "Turning shortcomings into challenges: brain-computer interfaces for games," *Entertainment Computing*, vol. 1, no. 2, pp. 85–94, 2009.

[41] Emotiv, Emotiv Application Store. In: Emotiv—Brain Computer Interface Technology, 2010, http://emotiv.com/product-category/applications/.

[42] E. C. Lalor, S. P. Kelly, C. Finucane et al., "Steady-state VEP-based brain-computer interface control in an immersive 3D gaming environment," *EURASIP Journal on Applied Signal Processing*, vol. 2005, no. 19, pp. 3156–3164, 2005.

[43] W. T. Nelson, L. J. Hettinger, J. A. Cunningham, M. M. Roe, M. W. Haas, and L. B. Dennis, "Navigating through virtual flight environments using brain-body-actuated control," in *Proceedings of the IEEE Virtual Reality Annual International Symposium*, pp. 30–37, IEEE Computer Society, Albuquerque, NM, USA, March 1997.

[44] M. Garau, H. R. Widenfeld, A. Antley et al., "Temporal and spatial variations in presence: a qualitative analysis," in *Proceedings of the International Workshop on Presence*, pp. 232–239, Valencia, Spain, January 2004.

[45] C. Cruz-Neira, J. Leigh, M. Papka et al., "Scientists in wonderland: a report on visualization applications in the CAVE virtual reality environment," in *Proceedings of the IEEE Symposium on Research Frontiers in Virtual Reality*, pp. 59–66, San Jose, Calif, USA, October 1993.

[46] F. L. Kooi and A. Toet, "Visual comfort of binocular and 3D displays," *Displays*, vol. 25, no. 2-3, pp. 99–108, 2004.

[47] T. Shibata, J. Kim, D. M. Hoffman, and M. S. Banks, "The zone of comfort: predicting visual discomfort with stereo displays," *Journal of Vision*, vol. 11, no. 8, article 11, 2011.

[48] N. Birbaumer and L. G. Cohen, "Brain-computer interfaces: communication and restoration of movement in paralysis," *The Journal of Physiology*, vol. 579, no. 3, pp. 621–636, 2007.

[49] E. Buch, C. Weber, L. G. Cohen et al., "Think to move: a neuromagnetic brain-computer interface (BCI) system for chronic stroke," *Stroke*, vol. 39, no. 3, pp. 910–917, 2008.

[50] N. Birbaumer, A. Ramos Murguialday, C. Weber, and P. Montoya, "Chapter 8 Neurofeedback and Brain-Computer Interface. Clinical Applications," *International Review of Neurobiology*, vol. 86, pp. 107–117, 2009.

[51] W. Wang, J. L. Collinger, M. A. Perez et al., "Neural interface technology for rehabilitation: exploiting and promoting neuroplasticity," *Physical Medicine and Rehabilitation Clinics of North America*, vol. 21, no. 1, pp. 157–178, 2010.

[52] H. Heinrich, H. Gevensleben, and U. Strehl, "Annotation: neurofeedback—train your brain to train behaviour," *Journal of Child Psychology and Psychiatry and Allied Disciplines*, vol. 48, no. 1, pp. 3–16, 2007.

[53] M. B. Sterman, "Basic concepts and clinical findings in the treatment of seizure disorders with EEG operant conditioning," *Clinical EEG Electroencephalography*, vol. 31, no. 1, pp. 45–55, 2000.

[54] E. Angelakis, S. Stathopoulou, J. L. Frymiare, D. L. Green, J. F. Lubar, and J. Kounios, "EEG neurofeedback: a brief overview and an example of peak alpha frequency training for cognitive enhancement in the elderly," *The Clinical Neuropsychologist*, vol. 21, no. 1, pp. 110–129, 2007.

[55] T. Egner and J. H. Gruzelier, "Learned self-regulation of EEG frequency components affects attention and event-related brain potentials in humans," *NeuroReport*, vol. 12, no. 18, pp. 4155–4159, 2001.

[56] B. Zoefel, R. J. Huster, and C. S. Herrmann, "Neurofeedback training of the upper alpha frequency band in EEG improves cognitive performance," *NeuroImage*, vol. 54, no. 2, pp. 1427–1431, 2011.

[57] P. Wiener, "Neurotherapy in adult management of stress: developmental aspects of the adult immune system," *Journal of Adult Development*, vol. 18, no. 2, pp. 66–69, 2011.

[58] H. Gevensleben, B. Holl, B. Albrecht et al., "Distinct EEG effects related to neurofeedback training in children with ADHD: a randomized controlled trial," *International Journal of Psychophysiology*, vol. 74, no. 2, pp. 149–157, 2009.

[59] J. P. Hamilton, G. H. Glover, J.-J. Hsu, R. F. Johnson, and I. H. Gotlib, "Modulation of subgenual anterior cingulate cortex activity with real-time neurofeedback," *Human Brain Mapping*, vol. 32, no. 1, pp. 22–31, 2011.

[60] I. H. C. H. M. Philippens and R. A. P. Vanwersch, "Neurofeedback training on sensorimotor rhythmin marmoset monkeys," *NeuroReport*, vol. 21, no. 5, pp. 328–332, 2010.

[61] S. Wangler, H. Gevensleben, B. Albrecht et al., "Neurofeedback in children with ADHD: specific event-related potential findings of a randomized controlled trial," *Clinical Neurophysiology*, vol. 122, no. 5, pp. 942–950, 2011.

[62] R. J. Schafer and T. Moore, "Selective attention from voluntary control of neurons in prefrontal cortex," *Science*, vol. 332, no. 6037, pp. 1568–1571, 2011.

[63] J. Gruzelier, A. Inoue, R. Smart, A. Steed, and T. Steffert, "Acting performance and flow state enhanced with sensory-motor rhythm neurofeedback comparing ecologically valid immersive VR and training screen scenarios," *Neuroscience Letters*, vol. 480, no. 2, pp. 112–116, 2010.

[64] A. Lécuyer, F. Lotte, R. B. Reilly, R. Leeb, M. Hirose, and M. Slater, "Brain-computer interfaces, virtual reality, and videogames," *Computer*, vol. 41, no. 10, pp. 66–72, 2008.

[65] G. Pfurtscheller, R. Leeb, J. Faller, and C. Neuper, "Brain-computer interface systems used for virtual reality control," in *Virtual Reality*, J.-J. Kim, Ed., chapter 1, pp. 3–20, InTech, Rijeka, Croatia, 2011.

[66] L. Jäncke, M. Cheetham, and T. Baumgartner, "Virtual reality and the role of the prefrontal cortex in adults and children," *Frontiers in Neuroscience*, vol. 3, pp. 52–59, 2009.

[67] S. Lee and G. J. Kim, "Effects of visual cues and sustained attention on spatial presence in virtual environments based on spatial and object distinction," *Interacting with Computers*, vol. 20, no. 4-5, pp. 491–502, 2008.

[68] M. Slater, A. Steed, and Y. Chrysanthou, *Computer Graphics and Virtual Environments: From Realism to Real-Time*, Addison Wesley, 2002.

[69] J. D. Bayliss, S. A. Inverso, and A. Tentler, "Changing the P300 brain computer interface," *Cyberpsychology and Behavior*, vol. 7, no. 6, pp. 694–704, 2004.

[70] D. Oude Bos and B. Reuderink, "BrainBasher: a BCI game," in *Proceedings of the Extended Abstracts of the International Conference on Fun and Games*, vol. 4, pp. 36–39, Eindhoven, Netherlands, October 2008, http://doc.utwente.nl/65050/.

[71] R. Ron-Angevin, M. A. Lopez, and F. Pelayo, "The training issue in brain-computer interface: a multi-disciplinary field," in *Bio-Inspired Systems: Computational and Ambient Intelligence*, J. Cabestany, F. Sandoval, A. Prieto, and J. M. Corchado, Eds., vol. 5517 of *Lecture Notes in Computer Science*, pp. 666–673, Springer, Berlin, Germany, 2009.

[72] V. Zotev, R. Phillips, K. D. Young, W. C. Drevets, and J. Bodurka, "Prefrontal control of the amygdala during real-time fMRI neurofeedback training of emotion regulation," *PLoS ONE*, vol. 8, no. 11, Article ID e79184, 2013.

[73] D. E. J. Linden, I. Habes, S. J. Johnston et al., "Real-time self-regulation of emotion networks in patients with depression," *PLoS ONE*, vol. 7, no. 6, Article ID e38115, 2012.

[74] V. Zotev, F. Krueger, R. Phillips et al., "Self-regulation of amygdala activation using real-time fMRI neurofeedback," *PLoS ONE*, vol. 6, no. 9, Article ID e24522, 2011.

[75] A. Caria, R. Sitaram, R. Veit, C. Begliomini, and N. Birbaumer, "Volitional control of anterior insula activity modulates the response to aversive stimuli. A real-time functional magnetic resonance imaging study," *Biological Psychiatry*, vol. 68, no. 5, pp. 425–432, 2010.

[76] S. J. Johnston, S. G. Boehm, D. Healy, R. Goebel, and D. E. J. Linden, "Neurofeedback: a promising tool for the self-regulation of emotion networks," *NeuroImage*, vol. 49, no. 1, pp. 1066–1072, 2010.

[77] K. N. Ochsner and J. J. Gross, "The cognitive control of emotion," *Trends in Cognitive Sciences*, vol. 9, no. 5, pp. 242–249, 2005.

[78] R. Cannon, J. Lubar, K. Thornton, S. Wilson, and M. Congedo, "Limbic beta activation and LORETA: can hippocampal and related limbic activity be recorded and changes visualized using LORETA in an affective memory condition?" *Journal of Neurotherapy*, vol. 8, no. 4, pp. 5–24, 2004.

[79] R. Cannon, J. Lubar, A. Gerke, K. Thornton, T. A. Hutchens, and V. McCammon, "EEG spectral-power and coherence: LORETA neurofeedback training in the anterior cingulate gyrus," *Journal of Neurotherapy*, vol. 10, no. 1, pp. 5–31, 2006.

[80] A. Gorini and G. Riva, "Virtual reality in anxiety disorders: the past and the future," *Expert Review of Neurotherapeutics*, vol. 8, no. 2, pp. 215–233, 2008.

Hindawi Publishing Corporation
Computational Intelligence and Neuroscience
Volume 2016, Article ID 6391807, 10 pages
http://dx.doi.org/10.1155/2016/6391807

*Research Article*

# Discovering Patterns in Brain Signals Using Decision Trees

**Narusci S. Bastos, Diana F. Adamatti, and Cleo Z. Billa**

*Federal University of Rio Grande (FURG), Rio Grande, RS, Brazil*

Correspondence should be addressed to Narusci S. Bastos; naruscibastos@gmail.com

Received 29 April 2016; Revised 26 July 2016; Accepted 2 August 2016

Academic Editor: Placido Rogerio Pinheiro



Even with emerging technologies, such as Brain-Computer Interfaces (BCI) systems, understanding how our brains work is a very difficult challenge. So we propose to use a data mining technique to help us in this task. As a case of study, we analyzed the brain's behaviour of blind people and sighted people in a spatial activity. There is a common belief that blind people compensate their lack of vision using the other senses. If an object is given to sighted people and we asked them to identify this object, probably the sense of vision will be the most determinant one. If the same experiment was repeated with blind people, they will have to use other senses to identify the object. In this work, we propose a methodology that uses decision trees (DT) to investigate the difference of how the brains of blind people and people with vision react against a spatial problem. We choose the DT algorithm because it can discover patterns in the brain signal, and its presentation is human interpretable. Our results show that using DT to analyze brain signals can help us to understand the brain's behaviour.

## 1. Introduction

Neuroscience is the scientific study of the nervous system. And with new technologies emerging, such as Brain-Computer Interface (BCI) systems, new discoveries can be made in this area. But analyzing and interpreting data collected from these BCI systems is not an easy job, so software tools have been developed in order to aid scientists in this area.

This work proposes a methodology that uses a data mining technique, called decision tree (DT), to discover patterns in brain signals and presents a model (a decision tree) that is easily interpretable. To show how our methodology works, we use a case scenario where we examine the brain signals of blind people and sighted people in spatial activity.

Blindness is a severe or total change of one or more elementary functions of vision; it affects the ability to perceive color, size, distance, shape, position, or movement in a given space [1]. The expression "visual impairment" refers to the spectrum ranging from blindness to low vision. There are two types of blind people: congenitally blind and acquired blind. The congenitally blind people have the cognitive system based on only 4 senses since birth, without any reference to visual elements, unlike the acquired blind ones, who have to adapt their cognitive system to their new condition [2].

The nervous system is responsible for the reception, storage, and release of information. It is a complex system consisting of various structures and specialized organs with different functions [3]. It can be divided into sensory system, which is responsible for collecting information about the organism and the environment; motor system, which organizes and executes actions; and the associative system. In this work, we focus our study on the sensory system, since it is known that individuals with visual impairments have their orientation capacity compromised [4].

BCI systems are tools (hardware and software) that allow a way of communication between the brain and the computer. They usually capture and process neural activities of the brain, and they do not require other stimuli, such as muscle movements [5]. There are different kinds of BCI; in this work, we used an EEG- (electroencephalogram-) based BCI system to collect brain signals. The EEG records brain electrical activity measured on the surface of the scalp and it is capable of capturing brain activity every millisecond due to a high temporal resolution. Most BCI systems provide only brainwaves and graphics (such as brain maps) tools to analyze

the brain activity. In this work, we propose the use of data mining to analyze the brain's behaviour.

Data mining (DM) is the process of extracting or mining knowledge from a large volume of data and there are several algorithms that can be used to discover patterns in a dataset [6]. This work focuses on the use of decision trees for knowledge discovery in a dataset of brain signals of blind (visual impairment) and sighted people during an activity involving spatial abilities in order to discover whether there is a difference in their brain activity.

This work is divided into five sections. Section 2 presents a theoretical background, such as brain areas and their functions, visual impairment, BCI systems, and data mining. Section 3 provides the materials and methods we used. Section 4 presents the obtained results, and finally Section 5 presents conclusions and future works.

## 2. Theoretical Background

*2.1. Brain Areas and Their Functions.* The brain is the main component of the nervous system. It is responsible for all mental operations such as concentration, thinking, learning, and motor control. These capabilities are implemented through neurons, which can currently be explained by neuroscience.

Human brain is divided into two hemispheres, right and left. Initially, there was a belief that there was one dominant hemisphere and the other was dominated. However, this concept has become outdated, and now there is a belief that there are actually two specialized hemispheres. Thus, each hemisphere is responsible for a set of functions that end up working together.

Anatomists usually divide the brain into major regions, called lobes, whose boundaries are not always accurate but transmit an initial idea of regional location. There are five lobes: four external and one internal, located in the lateral sulcus [7]. The four external lobes are the following: frontal lobe, which is located in the forehead; parietal lobe, which is located under the cranial bone with the same name; temporal lobe, which is associated with the tempora; and occipital lobe, which is located in the occipital cranial bone. The fifth lobe, the insula lobe, can only be seen when the lateral sulcus is opened [7, 8]. There are many other structures situated in the central nervous system (CNS), but in this work we investigate only the four visible lobes because the BCI system that we used does not have access to the insula lobe.

Each lobe has specialized functions: the occipital lobe is primarily concerned with the sense of vision; it is divided into multiple distinct visual areas, in which the biggest one is the primary visual cortex. The parietal lobe is partially dedicated to the sense of touch; it is responsible for body sensitivity functions and spatial recognition. The temporal lobe contains the primary auditory cortex; it processes audio data, specific aspects of vision, language understanding, and some aspects of memory. Finally, the frontal lobe is responsible for cognitive actions, memory, and movement [8, 9].

*2.2. Visual Impairment.* The visual impairment, in any degree, compromises a person's ability to orient and move in space with security and independence [10]. So, people with visual impairment or blindness compensate this visions lack of information using other senses: hearing, smell, touch, and taste [11].

*2.3. Brain-Computer Interface Systems.* BCI systems are a set of tools that enable communication between a brain and a computer. The main objective of BCI systems is to provide interaction between a user and an external device, such as computers, switches, or prostheses, using only brain signals. There are different ways to collect brain signals; one of them is to use the electroencephalography (EEG). The EEG is based on detecting brain electrical activity through electrodes applied to the scalp [12].

The signals that are captured by an EEG equipment are the potential differences between regions of the cortex. These electrical signs are generated due to the flow of ions between the different neurons of the brain. When a neuron is activated, it is polarized, generating an action potential that can be propagated to other neurons, provoking a flow of information [13].

The records acquired through the electrodes represent the intensity of brainwaves. They can vary between 0 $\mu$V and 200 $\mu$V, and they have frequency ranging from 0.3 Hz to 100 Hz. The resulting signal of an EEG shows peaks related to existence of electric activity, indicating a general spatial location of brain activity, because this signal is the sum of the activity of a large number of neurons communicating with each other [14].

*2.3.1. Actichamp and Acticap.* The Actichamp tool is developed by Brain Vision LLC. It is a modular amplification system that incorporates large components for electrophysiological analysis as EEG, event-related brain potentials (ERP), and BCI. It was used in conjunction with Acticap, which is a cap with 32 electrodes, and it is inserted into the scalp of a person. It has the channels of the international standard "10–20." The Acticap is connected to the Actichamp amplifier, to transmit the signals captured by the electrodes. Figure 1 shows how the electrodes are distributed throughout the cap.

The locations for each electrode are calculated to be in the intersection of the lines between standard cranium landmarks (see Figure 1). The name of each electrode indicates the region of the brain: FP indicates the prefrontal lobe; F, frontal lobe; T, temporal lobe; C, the central groove; P, parietal lobe; and O, occipital lobe. The number or the second letter identifies the hemispheric location: Z is the zero line in the center of the head; even numbers represent the right hemisphere; odd numbers represent the left hemisphere. The numbers are displayed in ascending order with increasing distance from the center [15, 16].

Table 1 shows the brain areas, the channels that constitute each area, and the abilities of each region.

*2.3.2. OpenVibe Software.* OpenVibe is a software platform dedicated to designing, testing, and using Brain-Computer

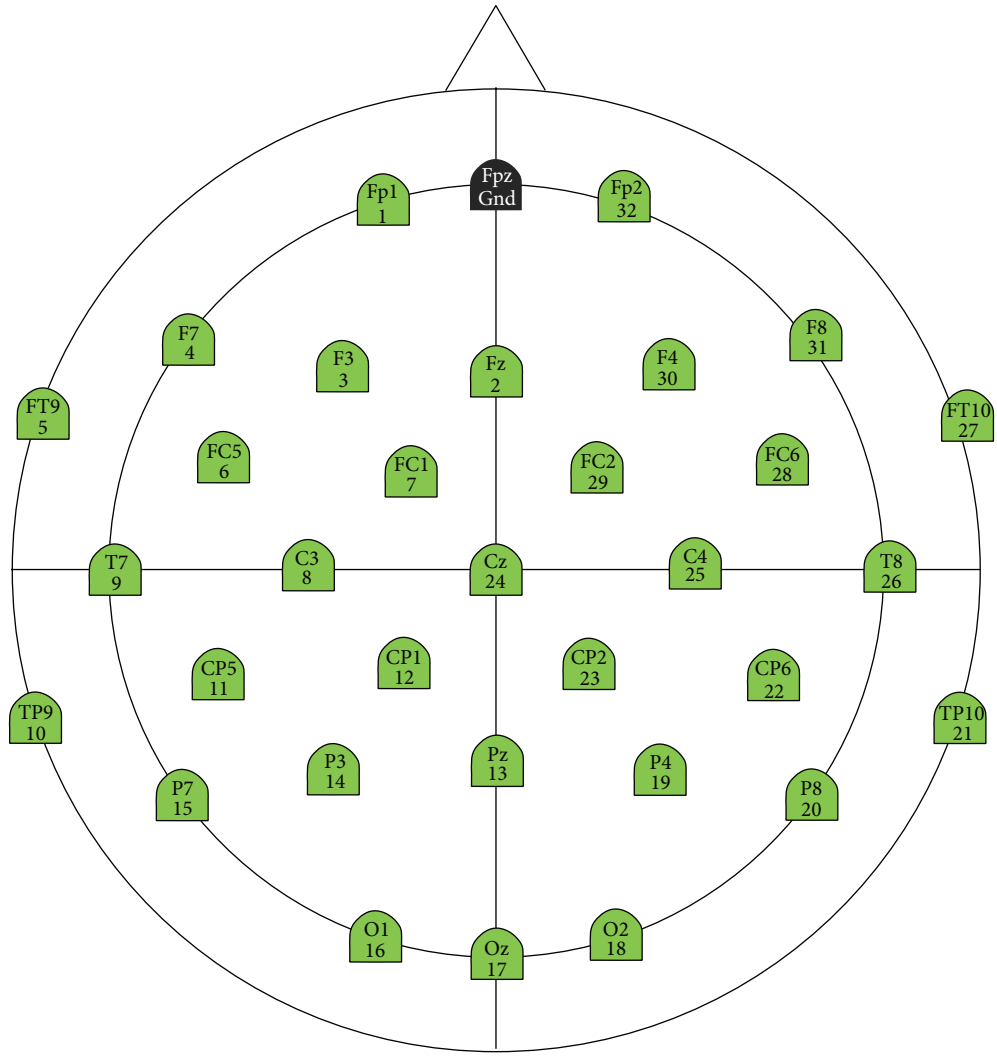


Figure 1: Location of the electrodes in Acticap.

Table 1: Brain region, electrodes, and proprietary functions.

| Brain region | Electrode | Proprietary functions |
|---|---|---|
| Frontal lobe | Fp1, Fp2, Fz, F7, F3, Fz, F4, F8, FC5, FC1, FC2, FC6, FT9, FT10. | Executive functions (management of cognitive/emotional resources on a given task) |
| Temporal lobe | T7, TP9, T8, TP10. | Perception of biological motion |
| Parietal lobe | P7, P3, Pz, P4, P8. | Somatosensory perception, spatial representations, and tactile perceptions |
| Occipital lobe | O1, Oz, O2. | View images (including during a dialogue) |

Interfaces. The configuration for use with Actichamp is predefined; the software communicates automatically with the signal capture tool. OpenVibe presents a very simple interface, where the user can set through an algorithm (automata) features that meet the needs of the task.

*2.4. Data Mining.* Data mining (DM) is the process of extracting or mining knowledge from a large volume of data. DM involves the study of tasks and techniques, where tasks are a specific class of problems and techniques are the groups of solutions to solve them [6].

Alencar et al. [17] point out that one of the most accepted definitions of data mining by researchers in the field is the one given by Fayyad et al. [18], which states the following: "database knowledge extraction is the process of identifying valid, new, potentially useful and understandable patterns embedded in the data."

Table 2: Classifiers accuracy percentage [20].

| Classifier | PA |
|---|---|
| ANN | 81.6% |
| LDA | 24.0% |
| DT | 75.6% |

Data mining is one step in a broad process known as Knowledge Discovery in Database (KDD). KDD is the process of finding knowledge in data. In this context, DM is the step of obtaining the information [6].

Descriptive tasks are focused on discovering patterns that describe data in a way that human being can understand. The main descriptive tasks are association rules and clustering. Predictive tasks search for patterns to infer new information about the existing data or to predict the behaviour of new data. The main predictive tasks are classification and regression [6, 19].

The difference between predictive and descriptive methods consists in the fact that descriptive methods do not require a precategorization of records; that is, it is not necessary target in an instance; in predictive methods, the dataset has a predefined target variable and records are categorized in relation to it.

## 3. Related Work

In the last years, a lot of work has been developed using data mining algorithms and, in some of them, these algorithms are used to perform classification tasks in brain signals.

Ishfaque et al. [20] report an experiment with several different classifiers in order to identify if a subject is moving his/her right hand forward or backward or his/her left hand forward or backward, thereby establishing a classification problem of 4 classes. In their experiment, they collect brain signals, using EEG-based BCI, of blindfolded subjects doing random movements of their right and left hands.

Ishfaque et al. [20] collected brain activities from 19 electrodes. The data was processed in the time domain, so their dimensionality was reduced from 19 columns to 5 columns using Principal Component Analysis (PCA). The amplitude of all four classes differentiated in time made the remaining data clearly separable.

After the data was collected, Ishfaque et al. [20] tested different types of classifiers in order to analyze the performance of each one. They use the following classifiers: Artificial Neural Networks (ANN), Linear Discriminant Analysis (LDA), and DT. To evaluate the results, they use a confusion matrix and accuracy percentage (AP). Both measures are used to check the accuracy of the classifiers.

According to the authors in [20], LDA, as expected, divided data linearly and because of that it did not present good classification ratings. On the other hand, ANN and DT reached good classification ratings, with ANN having better results. ANN accuracy percentage was 81.6%, DT accuracy percentage was 75.6%, and LDA accuracy percentage was 24.0%, as we can see in Table 2.

Table 3: Percentage of the accuracy of the classifiers in different datasets [21].

| Classifier | Dataset I PA | Dataset II PA |
|---|---|---|
| LDA | 82.86% | 84% |
| QDA | 78.57% | 79% |
| KFD | 80.71% | 81% |
| Linear SVM | 82.86% | 82% |
| Gaussian SVM | 84.29% | 84% |
| MLP | 80.71% | 81% |
| LVQ | 77.86% | 80% |
| $K$-NN | 84.29% | 83% |
| DT | 82.14% | 86% |

Another work that investigates machine learning algorithms in order to classify brain signals is the one of Wang et al. [21]. They made an experiment where subjects had identified left or right arrows and pressed the corresponding key on the keyboard. They collected two datasets using an EEG-based BCI system.

In the work of Wang et al. [21], they tested the following classification algorithms: LDA, Quadratic Discriminant Analysis (QDA), Kernel Fisher Discriminant (KFD) analysis, Support Vector Machines (SVM), Multilayer Perceptron (MLP), Learning Vector Quantization (LVQ), ANN, K-Nearest Neighbors (KNN), and DT. The unit of measurement for evaluation was the accuracy.

Wang et al. [21] conclude that Gaussian SVM and KNN reached good performance ratings in both datasets, while LVQ, QDA, KDF, and MLP reached the lowest ratings. Linear SVM and LDA presented similar performance. Wang et al. [21] point out that KNN is not commonly used to classify brain signals, but with the appropriate resources extraction and reducing the vector's dimension, KNN can reach good performance ratings. Table 3 shows the reached accuracy percentage of each classifier in the experiments of Wang et al. [21].

The works of Ishfaque et al. [20] and Wang et al. [21] compare classification algorithms to evaluate which one has better results to classify brain signals in a specific domain. They propose the use of different kinds of classifiers and measure their accuracy. In this work, we propose to use a classification algorithm, specifically DT, to discover patterns of reasoning in the brain. In other words, we do not propose to use DT to classify if the subject is performing a specific action; we are interested in discovering how the brain behaves when a specific task is proposed, and to investigate this brain's behaviour, we used a DT algorithm to discover patterns in the brain signals.

## 4. Methodology

Figure 2 is the flowchart of our methodology. Each box is described in detail in the following subsections.

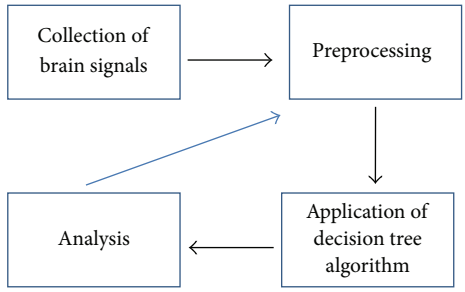


Figure 2: Methodology proposed in this work.

*4.1. Collection of Brain Signals.* We acquired the brain signals of 4 female individuals: 2 not blind and 2 blind people. The task we gave to them was to identify different 3D solid geometric shapes, in order to stimulate their spacial abilities. In our protocol, we used three objects: ball, cube, and parallelogram. All tests were performed with the approval of the Research Ethics Committee at the Health Area in Brazil, CCAAE: 344172114.3.0000.5324.

Detailed data collection is as follows:

(1) The data was collected in a private room, with only the subject and the researchers.

(2) The tools used to collect the brain signals were Actichamp and Acticap.

(3) Calibration of the equipment: the electrodes have to be stimulated until they showed enough impedance to make it possible to start the collection.

(4) The electrodes were connected to an audio recorder and the OpenVibe software was used for the acquisition and monitoring of brain signals.

(5) The eyes of the subject were blindfolded.

(6) Object one was given to the subject.

(7) The subject handled the object and verbalized the name of the object.

(8) Steps (6) and (7) were repeated with objects two and three.

Figure 3 shows the OpenVibe's automata used for brain signal acquisition and visual monitoring of them. The automata that follow the left side ending in "signal" display are performed, since the algorithms do not interfere with the signal acquisition. For signal acquisition, only the "acquisition client" and "GDF file writer" are used.

The "acquisition client" waits for data from the EEG and it distributes the signals to the scenario. The algorithm opens a socket to read the experiment information, sign, stimulus, and channels location data sent across the network.

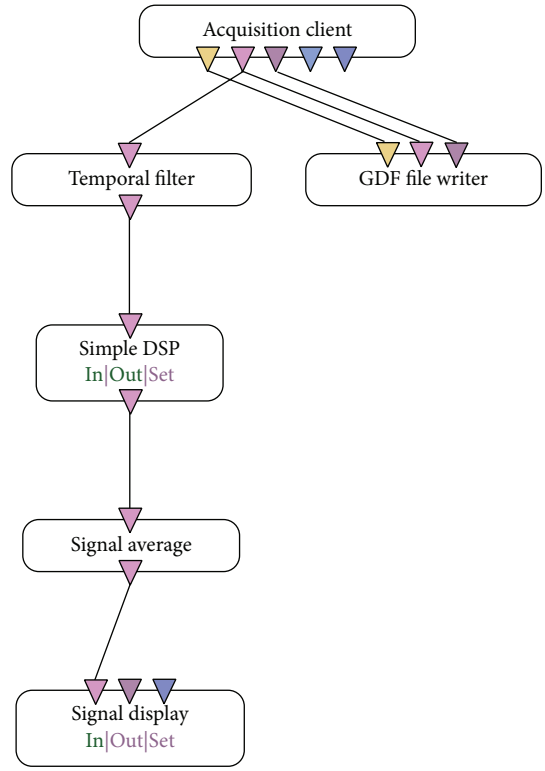


Figure 3: Automata used for the acquisition of brain signals.

The "GDF file writer" is a function that writes to disk a specific current output in standard file format GDF (Graph Exploration System). This "box" does not allow changes (the user can just inform the file name to be saved).

*4.2. Preprocessing.* The main steps of data preprocessing are

(1) conversion from GDF file to CSV file

(2) balancing data

(3) normalization

(4) grouping.

*4.2.1. Conversion from GDF File to CSV File.* For the conversion from GDF to CSV, it was necessary to create a scenario in OpenVibe software also containing the filters required for analysis of brain signals (Figure 4). This transformation was necessary because the CSV files can be read directly by the Weka data mining tool.

(1) "GDF file reader" has the following configuration:

(a) Samples per buffer: 32

(b) Subtracting physical minimum: false

(2) "Temporal filter" is used to filter the input signal (Figure 5).

The Butterworth filter is designed to introduce a flatter frequency response in the passband. The frequency ranges from 3.5 to 30 Hz, getting the theta, alpha, and beta waves.

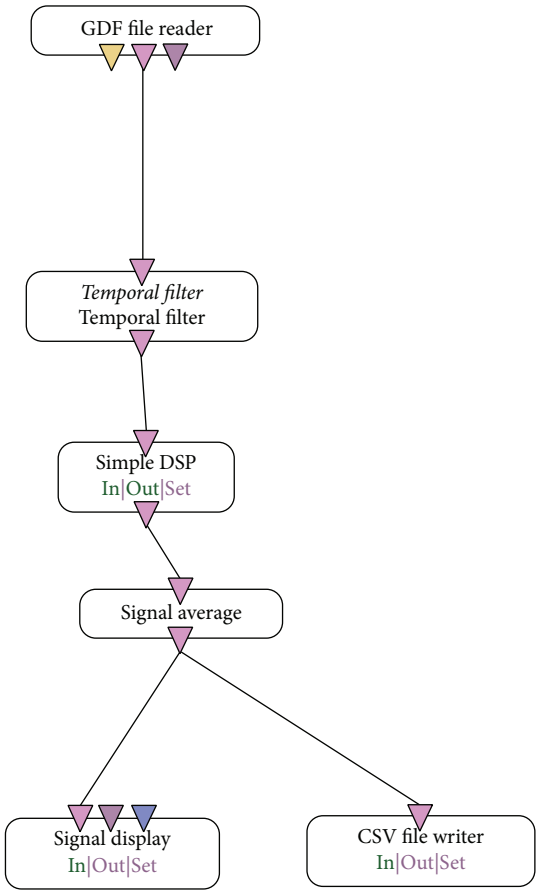


Figure 4: Automata to convert from GDF file to CSV file.

(3) "DSP filter" was set to $x * x$ to remove negative signs.

(4) "Signal average" was used to calculate the mean of each input sample and outputs a resulting signal.

(5) "CSV file writer" was used to record the filtered data in a CSV file.

(6) "Signal display" was used for monitoring the data during format conversion.

*4.2.2. Balance.* As a decision tree algorithm can be influenced by unbalanced data, we had to balance the data. Using the Weka software, we use a random filter to get 40 instances of each class. The number 40 was chosen because it was the number of instances of the class with less instances.

*4.2.3. Normalization.* The normalization step was done in Weka software, applying the filter "normalized," which transforms the values of the instances on a scale of 0 to 1.

*4.2.4. Grouping.* In order to identify temporal patterns, the data were grouped in a period of 1 second (10 instances). For each channel, the highest value was kept. So, at the end, each class had 4 instances, creating a new table with 16 instances.

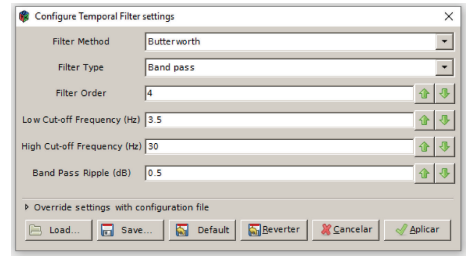


Figure 5: "Temporal filter" settings.

Time ≤ 14: cube (4.0)
Time > 14
| Time ≤ 30
| | Cp1 ≤ 0.072: interval (4.0)
| | Cp1 > 0.072: ball (4.0)
| Time > 30: parallelogram (4.0)
Number of leaves: 4
Size of the tree: 7

Figure 6: Algorithmic representation of the decision tree.

*4.3. Application of Decision Tree Algorithm.* In this study, we have used the J48 decision tree algorithm, which is a classification algorithm. The J48 tree decision (also called C4.5) is an algorithm that uses the method of divide and conquer to increase the predictive ability of decision trees. In this way, it always uses the best step assessed locally, without worrying if this step will produce the best solution, takes a problem, and divides it into several subproblems, creating subtrees between the root and the leaves. We used the Weka software to execute the J48 algorithm.

The Weka (Waikato Environment for Knowledge Analysis) is a collection of machine learning algorithms for data mining tasks. It was developed by the Department of Computer Science at the University of Waikato, New Zealand [22]. These algorithms can be applied directly or used by Java programs. Weka contains algorithms for preprocessing, classification, regression, clustering, and association rules [19].

*4.4. Analysis.* In a decision tree, each leaf node receives a class label. The nonterminal nodes, including the root node and other internal nodes, contain attributes test conditions to separate records that have different characteristics [23]. Figures 6 and 7 show an example of trees generated by the J48 algorithm. From the generated tree, we can extract some rules as follows:

(1) Time ≤ 14: cube.

(2) Time > 14, time ≤ 30, and CP1 ≤ 0.072: interval.

(3) Time > 14, time ≤ 30, and CP1 > 0.072: ball.

(4) Time > 14 and time > 30: parallelogram.

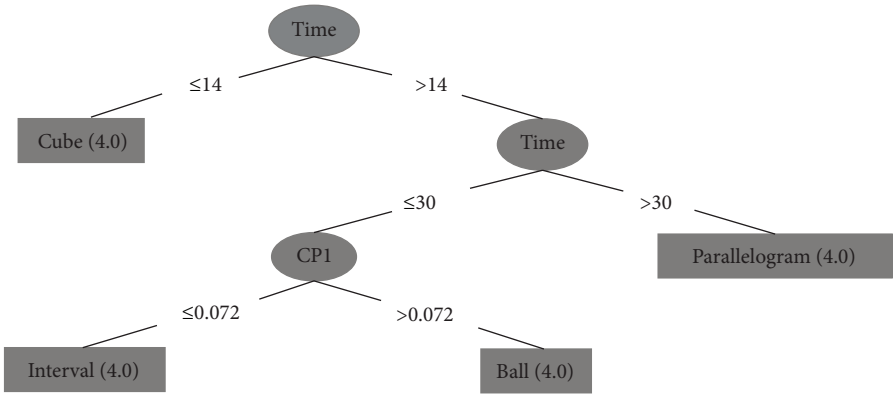


Figure 7: Graphical representation of the decision tree.

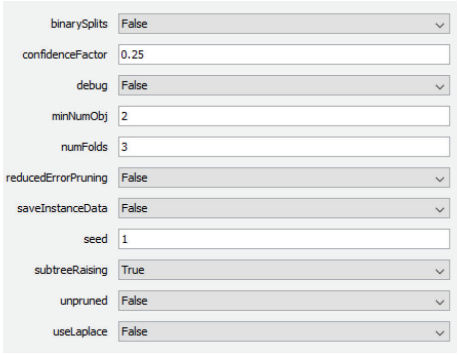


Figure 8: J48 parameters.

## 5. Results

During our research, we performed several experiments using the J48 algorithm with different settings. Firstly, the full set of examples was tested. In second place, some electrodes that we do not consider relevant were cut. Thus, instead of 32 channels (all), only 12 channels were used.

Beyond the above-mentioned settings, we also executed tests by varying the minimum number of instances per leaf (`minNumObj` in Weka), which is a parameter of the J48 algorithm. We tested the values 1%, 5%, and 10% of the total number of instances. The other parameters were set with the default values of Weka, as shown in Figure 8.

In most of these tests, we get good classification ratings, but the generated trees were very large and difficult to analyze. As our goal is not to classify new instances but to use decision trees to discover which areas of the brain had more significant activities, a tree with too many branches is not easy to analyze. We suppose that these trees were getting very large, probably, due to overfitting, since each tree leaf classified very few instances.

To avoid this overfitting, we grouped a subset of 10 consecutive instances. Each attribute received the highest value of its set (as mentioned in Section 4.2). So, in these tests, each instance contains the peak of each electrode in a larger period of time, representing in one instance a set with the highest values for each electrode during period of 1 second (approximately). With this configuration, we apply the DT algorithm to each subject's dataset. We executed them with the minimum number of objects set to 1%, because we had a small amount of instances of each class. The generated decision trees are shown in Figures 9, 10, 11, and 12 and they classify 100% correctly all the instances.

Figures 9, 10, 11, and 12 present the decision trees generated by the J48 algorithm, where (a) and (b) are two different ways to represent the same decision tree: (a) is a graphical representation of a tree and (b) is the algorithmic representation. Figures 9 and 10 represent the decision trees of two blind people. And Figures 11 and 12 represent the trees of sighted people.

In the trees of visual impairment individuals (congenital blindness) (Figures 9 and 10), the trees show that the channels presenting the most significant activities were at the parietal lobes (Figure 9: P4, P7; Figure 10: CP2) and at the front lobe (Figure 9: F7, Fp1; Figure 10: Fz, Fp1, FT9, and F7). As we mentioned before (Table 1), the parietal lobe is responsible for coordinating actions that are sensitive to skin, as the sense of touch. The frontal lobe coordinates motor activities, thinking, and speech.

In the trees of sighted individuals (blindfolded), according to Figures 11 and 12, the channels that presented significant activity correspond to the frontal lobe (Figure 11: FT10; Figure 12: F3, F7, and Fp1), parietal lobes (Figure 11: Pz), occipital lobes (Figure 11: Oz; Figure 12: O1), and central lobe (Figure 11: C4; Figure 12: C3). We can notice that, in all tests, blind and sighted individuals showed high activity in the frontal and parietal lobes, where the first is responsible for the organization of the thoughts and the second is responsible for the sense of touch. However, sighted people showed significant activity in the occipital lobe, which is responsible for the sense of vision. In blind people, this area was not activated, because the J48 algorithm considered the values of the occipital lobe's electrodes insignificant for the generated model.

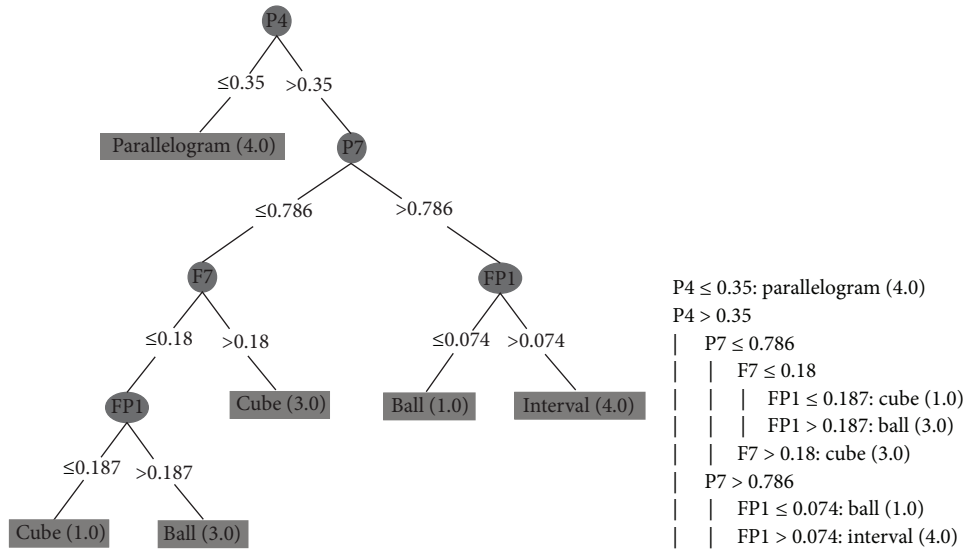


Figure 9: Blind person I: (a) DT's graphical representation and (b) DT's algorithmic representation.

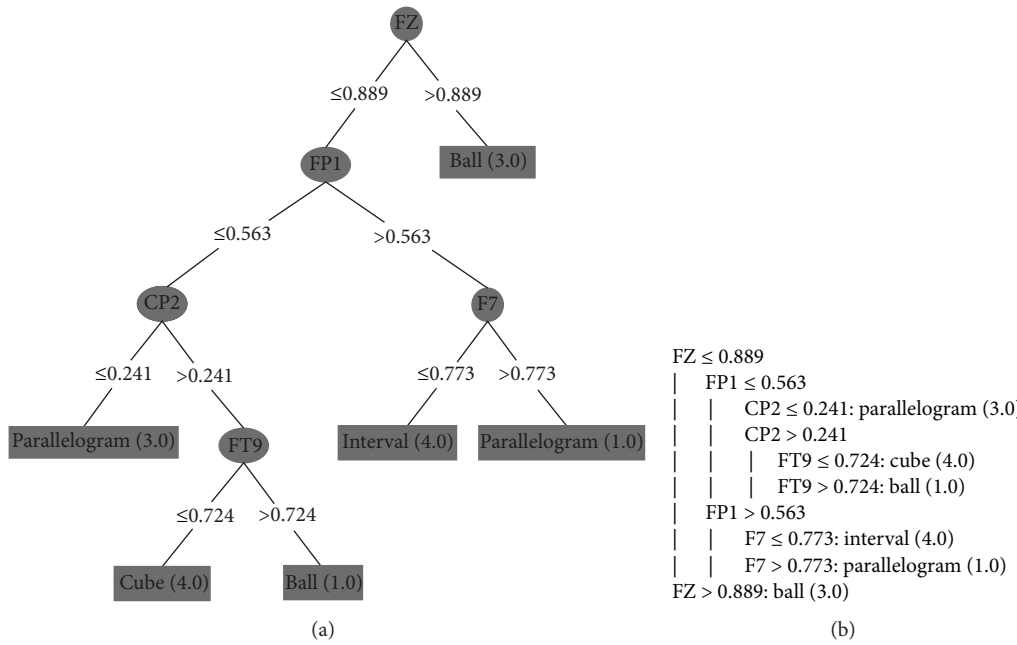


Figure 10: Blind person II: (a) DT's graphical representation and (b) DT's algorithmic representation.

## 6. Conclusion

This work analyzed four individuals, including two not blind people and two people with congenital visual impairment, in order to analyze brain activity during a spatial activity. For this analysis, we collect the brain signals with Actichamp tool and process these data with the Weka software to data mining. We choose the J48 data mining classification technique because it generates decision trees that are easy to analyze.

Based on the resulting decision trees, we can observe that sighted people had significant activity in the occipital lobe, which is responsible for the sense of vision, even when they are blindfolded. We suppose that this happened because they accessed the visual memory to aid them to identify the objects. However, blind people showed no significant activity in the occipital lobe in the model created by the J48 algorithm. Therefore, our experience suggests that the brains of blind people and people with normal vision have different ways of

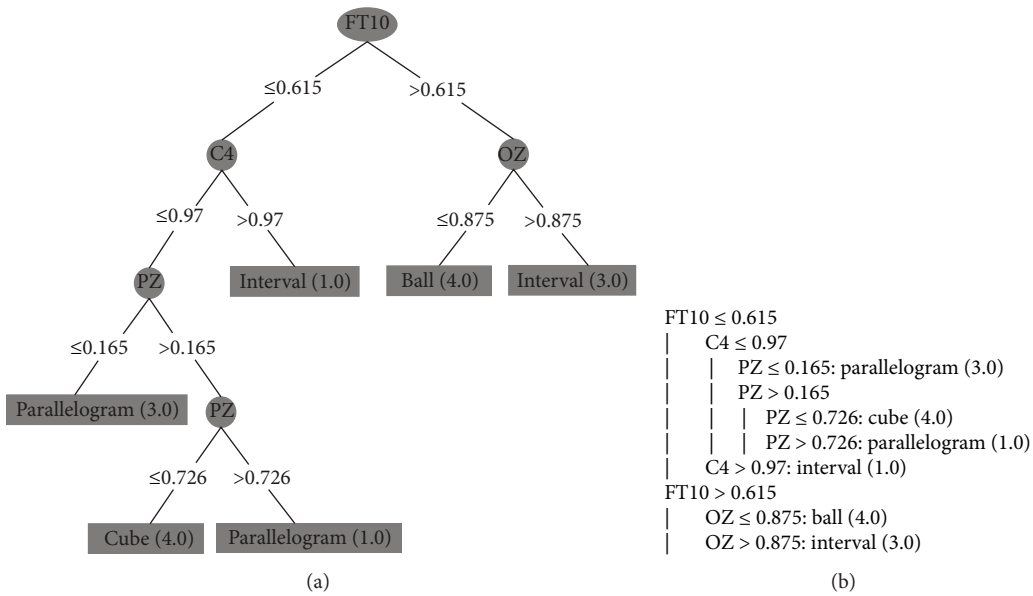


Figure 11: Sighted person I: (a) DT's graphical representation and (b) DT's algorithmic representation.

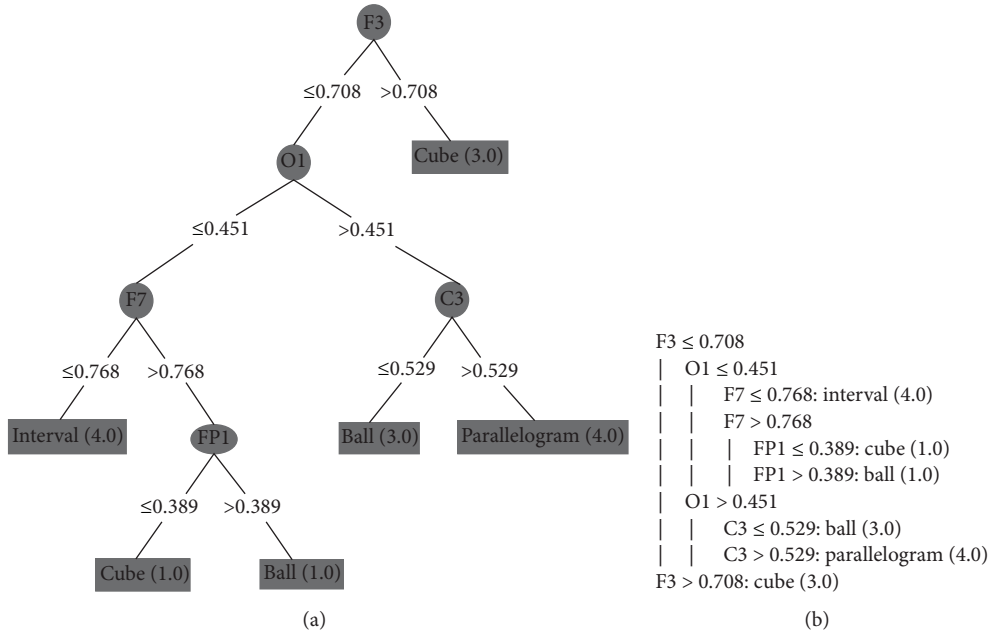


Figure 12: Sighted person II: (a) DT's graphical representation and (b) DT's algorithmic representation.

carrying out spatial activities, even if they are placed in the same situation (people with vision were blindfolded).

As future works, we intend to expand the study with a larger number of people. We also intend to apply the methodology in other neuroscience studies, since DT can be used to discover patterns and understand brain signals in many different kinds of problems.

## Competing Interests

The authors declare that they have no competing interests.

## References

[1] E. D. de Sá, I. M. de Campos, and M. B. C. Silva, *Atendimento Educacional Especializado: Deficiência Visual*, MEC, SEESP, 2007 (Portuguese).

[2] V. Kastrup, "A Invention on fingertips: attention reversion in visually impaired people," *Psicologia em Revista*, vol. 13, no. 1, pp. 69–90, 2007.

[3] C. Eyzaguirre, *Physiology of the Nervous System. Year Book Medical*, First Thus Edition, 1st edition, 1969.

[4] M. Gil, *Cadernos da TV Escola—Deficiência Visual*, MEC-Secretaria de Educação a Distância, Brasília, Brasil, 2000 (Portuguese).

[5] S. Machado, M. Cunha, B. Velasques et al., "Brain-computer interface: new prospects for rehabilitation," *Revista Neurociências*, vol. 17, no. 4, pp. 329–335, 2009 (Portuguese).

[6] R. B. Pereira, A. Plastino, B. Zadrony, L. H. C. Merschmann, and A. A. Freitas, "Lazy attribute selection: choosing attributes at classification time," *Intelligent Data Analysis*, vol. 15, no. 5, pp. 715–732, 2011.

[7] M. R. Lourenço, P. P. Garcez, R. Lent, and D. Uziel, "Temporal and spatial regulation of interneuron distribution in the developing cerebral cortex—an *in vitro* study," *Neuroscience*, vol. 201, pp. 357–365, 2012.

[8] M. S. Gazzaniga, T. F. Heatherton, and M. A. V. Veronese, *Psychological Science: Mind, Brain and Behavior*, edited by W. W. Norton, 2006.

[9] R. Lent and F. Tovar-Moll, "How can development and plasticity contribute to understanding evolution of the human brain?" *Frontiers in Human Neuroscience*, vol. 9, article 208, 2015.

[10] Secretária de Educação Especial, *Subsídios para a Organização e Funcionamento de serviços de educação especial*, Ministério da Educação e do Desporto, Secretária de Educação Especial, Brasília, Brazil, 1995 (Portugueses).

[11] S. D. Silveira Nunes and J. F. B. Lomonaco, "Desenvolvimento de conceitos em cegos congênitos: caminhos de aquisição do conhecimento," *Psicologia Escolar e Educacional*, vol. 12, no. 1, pp. 119–138, 2008 (Portuguese).

[12] D. J. McFarland and J. R. Wolpaw, "Brain-computer interfaces for communication and control," *Communications of the ACM*, vol. 54, no. 5, pp. 60–66, 2011.

[13] M. Kugler, I. N. Mukai, H. S. Lopes, and V. Pilla Junior, "Recognition of EEG patterns related to evoked potentials by intermittent photo-stimulation," in *Proceedings of the International Conference on Mathematics and Engineering Techniques in Medicine and Biological Sciences*, pp. 344–350, CSREA Press, Las Vegas, Nev, USA, 2001.

[14] I. Oliveira, L. Carrico, N. Guimaraes, T. Chambel, and C. Teixeira, *Interfaces Computador-Cérebro: Extracção e Processamento de Características de Electroencefalogramas*, Department of Informatics, University of Lisbon, 2008 (Portuguese).

[15] A. Vallabhaneni, T. Wang, and B. He, "Brain-computer interface," in *Neural Engineering*, B. He, Ed., pp. 85–121, Kluwer Academic Publishers, New York, NY, USA, 2005.

[16] American Clinical Neurophysiology Society, "Guideline 5: guidelines for standard electrode position nomenclature," *American Journal of Electroneurodiagnostic Technology*, vol. 46, no. 3, pp. 222–225, 2006.

[17] A. B. Alencar, K. Börner, F. V. Paulovich, and M. C. F. de Oliveira, "Time-aware visualization of document collections," in *Proceedings of the 27th Annual ACM Symposium on Applied Computing (SAC '12)*, pp. 997–1004, ACM, Trento, Italy, March 2012.

[18] U. Fayyad, G. Piatetsky-Shapiro, and P. Smyth, "From data mining to knowledge discovery in databases," *AI Magazine*, vol. 17, no. 3, pp. 37–53, 1996.

[19] U. Fayyad, *Advances in Knowledge Discovery and Data Mining*, AAAI Press, Menlo Park, Calif, USA, 1st edition, 1996.

[20] A. Ishfaque, A. J. Awan, N. Rashid, and J. Iqbal, "Evaluation of ANN, LDA and decision trees for EEG based brain computer interface," in *Proceedings of the IEEE 9th International Conference on Emerging Technologies (ICET '13)*, pp. 1–6, IEEE, Islamabad, Pakistan, December 2013.

[21] B. Wang, C. M. Wong, F. Wan, P. U. Mak, P. I. Mak, and M. I. Vai, "Comparison of different classification methods for EEG-based brain computer interfaces: a case study," in *Proceedings of the IEEE International Conference on Information and Automation (ICIA '09)*, pp. 1416–1421, Zhuhai, China, June 2009.

[22] J. Ferreira, *Data mining em banco de dados de eletrocardiograma [Tese de Douturado Instituto Dante Pazzanese de Cardiologia]*, Universidade de São Paulo, 2014 (Portuguese).

[23] P. N. Tan, M. Steinbach, and V. Kumar, *Introduction to Data Mining*, vol. 1, Pearson Addison Wesley, Boston, Mass, USA, 2006.

Hindawi Publishing Corporation
Computational Intelligence and Neuroscience
Volume 2016, Article ID 8404565, 10 pages
http://dx.doi.org/10.1155/2016/8404565

*Research Article*

# High-Resolution Cortical Dipole Imaging Using Spatial Inverse Filter Based on Filtering Property

**Junichi Hori[1] and Shintaro Takasawa[1,2]**

[1]*Graduate School of Science and Technology, Niigata University, Niigata 950-2181, Japan*
[2]*Terumo Corporation, Tokyo, Japan*

Correspondence should be addressed to Junichi Hori; hori@eng.niigata-u.ac.jp

Received 12 April 2016; Revised 15 July 2016; Accepted 7 August 2016

Academic Editor: Joao P. Papa



Cortical dipole imaging has been developed to visualize brain electrical activity in high spatial resolution. It is necessary to solve an inverse problem to estimate the cortical dipole distribution from the scalp potentials. In the present study, the accuracy of cortical dipole imaging was improved by focusing on filtering property of the spatial inverse filter. We proposed an inverse filter that optimizes filtering property using a sigmoid function. The ability of the proposed method was compared with the traditional inverse techniques, such as Tikhonov regularization, truncated singular value decomposition (TSVD), and truncated total least squares (TTLS), in a computer simulation. The proposed method was applied to human experimental data of visual evoked potentials. As a result, the estimation accuracy was improved and the localized dipole distribution was obtained with less noise.

## 1. Introduction

The spatial resolution of electroencephalogram (EEG) data is limited because of the small number of scalp surface electrodes used and the low conductivity of the skull. Therefore, it was difficult to specify brain electrical activity directly from the potential distribution measured on the scalp surface. Cortical dipole imaging that estimates the equivalent dipole source distribution on a virtual layer within a brain from the scalp potential has been proposed to solve this problem [1, 2]. According to cortical dipole imaging, brain electrical activity is represented by the equivalent dipole distribution without being restricted in the number and the direction of the signal sources.

The cortical dipole distribution is estimated from the scalp potentials by solving an inverse problem of the transfer matrix from the dipole layer to the scalp surface based on a head model. The solution of the inverse problem is influenced not only by the measurement noise but also by the error in the transfer matrix. The measurement noise originates in the measurement environment, caused by factors such as the variance of the electrode impedance, the environmental noise, and artifacts caused by eye blinks or body movements. On the other hand, the transfer matrix error originates in the distortion of the head model design such as errors of an electrode displacement, individual differences in head shape, and nonuniform electrical conductivity. Therefore, it is important to reduce the influence from both the measurement noise and the transfer matrix error for the EEG inverse solution of cortical dipole imaging.

Several spatial inverse filters have been proposed to reduce the influence of the measurement noise. Tikhonov regularization [3] and truncated singular value decomposition (TSVD) [4] were applied to truncate the noisy components. Use of a parametric projection filter incorporated with the statistical information on the noise has also been proposed [5, 6]. Moreover, the transfer matrix error was taken into consideration in the truncated total least squares (TTLS) method [7]. In this method, after scaling the covariance of the transfer matrix error to equal that of the measurement noise, the solution is estimated by minimizing the influence from both the measurement noise and the transfer matrix error. TTLS has been applied to a bioluminescence topography inverse problem [8] and an ECG inverse problem [9]. We applied TTLS to the inverse problem of cortical dipole imaging [10]. TTLS provided better results compared with

the traditional inverse methods when the transfer matrix was included in the forward problem.

In the present study, we paid attention to filtering property when solving the cortical inverse problem in order to improve the accuracy of cortical dipole imaging. Filtering property presents the amplitude characteristics by changing the singular value when singular value decomposition (SVD) is applied to the inverse solution. According to filtering property, the terms easily influenced by noise are reduced while the terms with less noise are passed. We estimated optimum filtering property using the least squares method (LS) in the simulation of several signal source configurations. An inverse filter model was constructed by approximating the filtering property with a sigmoid function. The proposed method was compared with traditional inverse techniques such as Tikhonov regularization, TSVD, and TTLS in computer simulation [11]. Based on the simulation results, our method was applied to human EEG data of visual evoked potential (VEP) [12]. The results indicated that the proposed method can provide better performance compared with traditional inverse techniques. In the present study, the restorative ability and applicability of the proposed method are defined by changing the signal and noise configurations and by applying these to several sets of experimental data. Concretely, the optimum parameter for the sigmoid function-based inverse filter is investigated by changing the depth of the signal source and the noise level.

## 2. Methods

*2.1. Cortical Dipole Imaging.* Cortical dipole imaging is one of the high-resolution EEG mapping techniques. A volume-conductor head model is used to estimate the cortical dipole distribution from measured scalp potentials. The head model is approximated by an inhomogeneous set of three concentric spheres that represent the scalp, the skull, and the brain, as shown in Figure 1 [2]. The radius of the scalp is set to 1 and the radii of the skull and the cortex are set to 94% and 87% of the scalp radius, respectively. The conductivity of the skull was set to $\sigma_1 = 0.0125$ and the conductivity of the cortex and the scalp was $\sigma_0 = 1.0$. A dipole layer was established inside of the cortex with arbitrary radius, $r_d$. A total of 1280 equivalent radial dipoles were uniformly arranged on the dipole layer to represent the dipole signal sources in a brain. Cortical dipole imaging has an advantage that there is no restriction on the number and direction of dipole sources.

The observation of the scalp potential $\mathbf{g}$ is modeled using the transfer matrix $\mathbf{A}$ from the dipole layer to the scalp surface as follows:

$$\mathbf{g} = (\mathbf{A} + \mathbf{E})\,\mathbf{f} + \mathbf{n}, \tag{1}$$

where $\mathbf{f}$ is the dipole distribution, $\mathbf{E}$ is the transfer matrix error, and $\mathbf{n}$ is the measurement noise. The transfer matrix $\mathbf{A}$ is determined from the geometry of the head model, the electrical conductivity involved, and the electrode and equivalent dipole source arrangements. The inverse problem

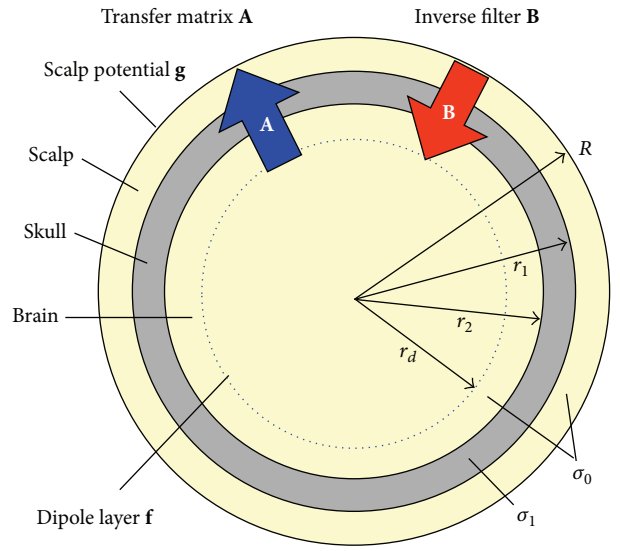


Figure 1: 3 sphere inhomogeneous volume-conductor head model.

should be solved to estimate the dipole distribution $\hat{\mathbf{f}}$ from the measured scalp potential $\mathbf{g}$:

$$\hat{\mathbf{f}} = \mathbf{B}\mathbf{g}, \tag{2}$$

where $\mathbf{B}$ is the inverse filter. As the method to construct the inverse filter, Tikhonov regularization [3] and TSVD [4] were proposed to reduce the influence of measurement noise. In addition, the TTLS method that reduces both the measurement noise and the transfer matrix error was investigated [7].

*2.2. Inverse Techniques.* The $m \times n$ transfer matrix is decomposed by

$$\mathbf{A} = \mathbf{U}\mathbf{\Sigma}\mathbf{V}^T, \tag{3}$$

where $\mathbf{U}$ and $\mathbf{V}$ are $m$th- and $n$th-orthogonal matrices and $\mathbf{\Sigma}$ is the singular value matrix:

$$\mathbf{\Sigma} = \left(z_{ij}\right) \in \mathbf{R}^{m\times n}, \quad z_{ij} = \begin{cases} \sigma_i, & \text{for } i = j, \\ 0, & \text{for } i \neq j, \end{cases} \tag{4}$$

$$\sigma_1 \geq \cdots \geq \sigma_r > 0,$$

$$\sigma_{r+1} = \cdots = \sigma_n = 0.$$

$\sigma_i$ $(i = 1, \ldots, n)$ represents singular values. $\mathbf{u}_i$ and $\mathbf{v}_i$ are left and right singular vectors, respectively. The parameter $r$ is the number of nonzero singular values.

In general, the inverse problem is solved by LS. The solution is described by

$$\hat{\mathbf{f}}_{\mathrm{LS}} = \sum_{i=1}^{r} \frac{\mathbf{u}_i^T \mathbf{g}}{\sigma_i} \mathbf{v}_i. \tag{5}$$

According to this method, the noise and error involved in the scalp potential $\mathbf{g}$ are enhanced by the terms of small

singular values. Tikhonov regularization and TSVD that estimate the solutions while suppressing the influence from the measurement noise overcome this problem. Tikhonov regularization is given by

$$\hat{\mathbf{f}}_{\mathrm{TIKH}} = \left(\mathbf{A}^T\mathbf{A} + \gamma\mathbf{I}\right)^{-1}\mathbf{A}^T\mathbf{g} = \sum_{i=1}^{r}\frac{\sigma_i^2}{\sigma_i^2+\gamma^2}\frac{\mathbf{u}_i^T\mathbf{g}}{\sigma_i}\mathbf{v}_i, \quad (6)$$

where $\gamma$ ($\gamma > 0$) is the regularization parameter [3]. TSVD is given by

$$\hat{\mathbf{f}}_{\mathrm{TSVD}} = \sum_{i=1}^{k}\frac{\mathbf{u}_i^T\mathbf{g}}{\sigma_i}\mathbf{v}_i, \quad (7)$$

where $k$ is the truncation parameter [4]. When the error is involved in the transfer function, the estimated solutions have bias in these methods. To reduce the influence of the transfer function error, TTLS was introduced [7]. The SVD for the augmented matrix $(\mathbf{A}, \mathbf{g})$ is given by

$$\begin{aligned}
&(\mathbf{A},\mathbf{g}) = \overline{\mathbf{U}}\,\overline{\mathbf{\Sigma}}\,\overline{\mathbf{V}}^T,\\
&\overline{\mathbf{U}} = \left(\overline{\mathbf{u}}_1,\ldots,\overline{\mathbf{u}}_m\right),\\
&\overline{\mathbf{V}} = \left(\overline{\mathbf{v}}_1,\ldots,\overline{\mathbf{v}}_{n+1}\right),\\
&\overline{\mathbf{U}}\,\overline{\mathbf{U}}^T = \mathbf{I}_m,\\
&\overline{\mathbf{V}}\,\overline{\mathbf{V}}^T = \mathbf{I}_{n+1},\\
&\overline{\mathbf{\Sigma}} = \left(\overline{z}_{ij}\right) \in \mathbf{R}^{m\times(n+1)}, \quad \overline{z}_{ij} = \begin{cases}\overline{\sigma}_i, & \text{for } i = j,\\ 0, & \text{for } i \neq j,\end{cases}\\
&\overline{\sigma}_1 \geq \cdots \geq \overline{\sigma}_r > 0,\\
&\overline{\sigma}_{r+1} = \cdots = \overline{\sigma}_n = 0.
\end{aligned} \quad (8)$$

When $k$ is a truncated parameter, the solution of TTLS is given by

$$\hat{\mathbf{f}}_{\mathrm{TTLS}} = -\overline{\mathbf{V}}_{12}\overline{\mathbf{V}}_{12}^{+} = -\frac{\overline{\mathbf{V}}_{12}\overline{\mathbf{V}}_{22}^T}{\left\|\overline{\mathbf{V}}_{22}\right\|_2^2}, \quad (9)$$

where

$$\overline{\mathbf{V}} = \begin{pmatrix}\overline{\mathbf{V}}_{11} & \overline{\mathbf{V}}_{12}\\ \overline{\mathbf{V}}_{21} & \overline{\mathbf{V}}_{22}\end{pmatrix}, \quad \overline{\mathbf{V}}_{11} \in \mathbf{R}^{n\times k}, \ \overline{\mathbf{V}}_{22} \in \mathbf{R}^{1\times(n+1-k)}. \quad (10)$$

$\mathbf{V}^+$ is the Moore-Penrose pseudoinverse of $\mathbf{V}$. The notation $\|\ \|_2$ denotes the Euclidian norm. In TTLS, the measurement noise and the transfer function error are combined by the augmented matrix. After decomposing the augmented matrix, the singular values that enhance the measurement noise and the transfer matrix error are truncated.

*2.3. Filtering Property.* These inverse solutions of Tikhonov regularization, TSVD, and TTLS are commonly expressed as

$$\hat{\mathbf{f}} = \sum_{i=1}^{r} p_i\frac{\mathbf{u}_i^T\mathbf{g}}{\sigma_i}\mathbf{v}_i, \quad (11)$$

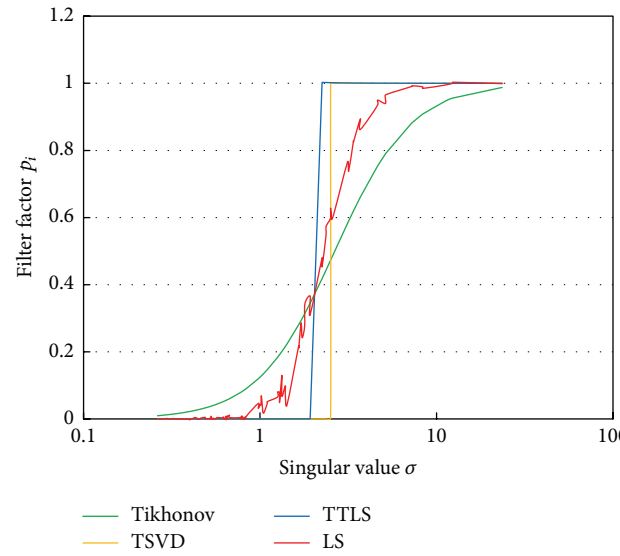


Figure 2: Filter factors of various inverse techniques against the singular value.

where $p_i$ is a filter factor. The filter factor $\{p_i\}$ $(i = 1,\ldots,r)$ is called a filter property [7, 11]. The filter factors $p_i$ of Tikhonov regularization, TSVD, and TTLS are derived by

$$\begin{aligned}
p_{i,\mathrm{TIKH}} &= \frac{\sigma_i^2}{\sigma_i^2+\gamma^2},\\
p_{i,\mathrm{TSVD}} &= \begin{cases}1, & \text{for } i = 1,\ldots,k,\\ 0, & \text{for } i = k+1,\ldots,r,\end{cases}\\
p_{i,\mathrm{TTLS}} &= \sum_{j=1}^{k}\frac{\overline{\mathbf{v}}_{n+1,j}^{\,2}}{\left\|\overline{\mathbf{V}}_{22}\right\|_2^2}\frac{\sigma_i^2}{\overline{\sigma}_j^2-\sigma_i^2}.
\end{aligned} \quad (12)$$

Figure 2 shows examples of the filter factors of Tikhonov regularization, TSVD, and TTLS against the singular values. The eccentricity of the signal sources was set to 0.6. Ten percent measurement noise and 10% transfer matrix error were added to the scalp potential and the transfer matrix, respectively. The radius of the dipole layer was set to 0.85. The singular value on the horizontal axis is displayed using a logarithmic scale. The terms for large singular values were passed while the terms for small singular values were attenuated in all filter factors. While the property of Tikhonov regularization was gradual, the properties of TSVD and TTLS were steep.

*2.4. Optimal Filtering Property Using Sigmoid Function.* When the actual dipole distribution is known, it is possible to find optimal filtering property by LS. The estimated optimal filtering property is shown in Figure 2. Filter factors were calculated using 100 kinds of signal source arrangement to adapt to various signal configurations. The estimated optimal filter property was intermediate between the property of Tikhonov regularization and the property of TSVD, as shown in Figure 2.

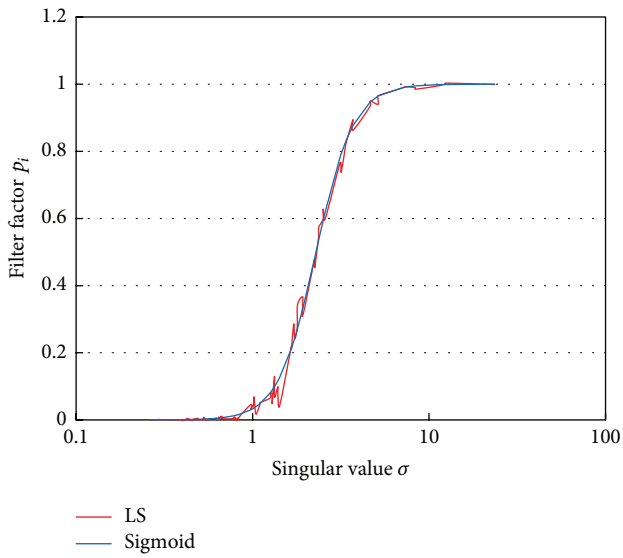


FIGURE 3: Optimal filter factors approximated by sigmoid function.

The filter factors have fluctuation because they were calculated using sampled signal sources. We approximated the filter property by a sigmoid function:

$$p_i = \frac{1}{1 + e^{-a(\log \sigma_i - \gamma)}} = \frac{1}{1 + \sigma_i^{-a} e^{a\gamma}}, \quad (13)$$

where $a$ is a gain parameter and $\gamma$ is a shift parameter. The approximated result of optimal filter factors by (13) is also shown in Figure 3. The optimal filtering property was changed according to the level of measurement noise, the transfer matrix error, and the depth of the signal sources. However, it is possible to approximate the filter factor by (13) with appropriate two parameters, $a$ and $\gamma$.

The aspect of the dipole distribution changes according to the depth of the signal source against the fixed dipole layer. The dipole distribution spreads so that the signal source is located in a deep position. The optimal filter when changing the depth of the signal source within the range 0.4–0.8 was estimated using the LS. The noise level was set to 0.1. The calculated optimal filter factors are plotted in Figure 4(a). The deeper the signal source was, the more singular values were suppressed by the filter property. It was confirmed that larger singular values were suppressed when the noise level was large. The sigmoid function in (13) was fitted to the obtained optimal filter factors as shown in Figure 4(b). The filter factors were well approximated with appropriate parameters.

In (13), it is necessary to estimate 2 parameters. There are calculation costs associated with this method, compared with traditional methods consisting of only 1 parameter. Thus, we investigated the relationship between 2 parameters. If one parameter is estimated, the other can be decided using the derived relationship equation. The relationship between 2 optimal parameters was repeatedly investigated by changing the depth of signal sources with a constant noise level. The relationship between the regularization parameter and the shift parameter in the sigmoid function is plotted in Figure 5. The relationships between 2 parameters for noise levels of 0.1 and 0.2 were approximated by linear equations. As a result, the filter factors can be estimated using only shift parameter $\gamma$.

This parameter relationship changed according to the noise level. In order to use the sigmoid function to determine the filter factors in actual EEG data, the parameter relationship should be decided using the information on noise level. However, the signal and noise components are intermingled in the observed EEG data. In such cases, independent component analysis (ICA) was applied to the EEG data to separate in the signal and noise components. ICA extracts independent sources from the observed signal based on statistical independence of the original signal. In a previous study, the noise component was precisely estimated from the subtraction of the separated signal component from the observed EEG data [13]. That is, the components without a signal component were assumed to be noise. The noise level was calculated by $\|\mathbf{n}\|_2/\|\mathbf{g}\|_2$.

*2.5. Parameter Estimation.* In actual application, the shift parameter $\gamma$ in the sigmoid function has to be determined as the same as the regularization parameter $\gamma$ in Tikhonov regularization and the truncated parameter $k$ in TSVD and TTLS [14–20]. If the actual dipole distribution is known, the parameter can be determined by minimizing the relative error between actual and estimated dipole distribution. However, the actual dipole distribution is unknown in practical situations. For such cases, the L-curve method was proposed to estimate the regularization parameter [14, 15]. In the L-curve method, the optimal regularization parameter is decided by minimizing both the estimated solution norm $\|\widehat{\mathbf{f}}\|_2$ and the residual norm $\|\mathbf{A}\widehat{\mathbf{f}} - \mathbf{g}\|_2$. The optimal parameter corresponds to the corner of the L-curve. As an estimation method for the corner of the L-curve, a curvature method that searches for the point of maximum curvature was proposed [16]. A minimal product method that estimates a minimum of the area $\|\mathbf{A}\widehat{\mathbf{f}} - \mathbf{g}\|_2 \cdot \|\widehat{\mathbf{f}}\|_2$ was also proposed [17].

## 3. Results

*3.1. Simulations.* Computer simulations were performed to evaluate the ability of the proposed inverse filter. A total of 128 electrodes were arranged uniformly on the scalp surface. The dipole layer with 1280 equivalent dipole sources was established with a depth of 0.85 inside of the brain. The numbers of electrodes and dipoles were set to be great enough to accomplish high spatial resolution, based on previous studies [2, 5]. Two radial signal sources with eccentricity of 0.6 were arranged with arbitrary position. Gaussian white noise was added as the measurement noise and the transfer matrix error.

First, we compared the inverse estimations of Tikhonov regularization, TSVD, TTLS, and the sigmoid function. Figure 6 shows the estimated results of dipole distributions for 2 radial signal sources with a depth of 0.6. The noise level and the error level were both set to 0.1. Figure 6 displays the top view of dipole distributions with normalized amplitude.

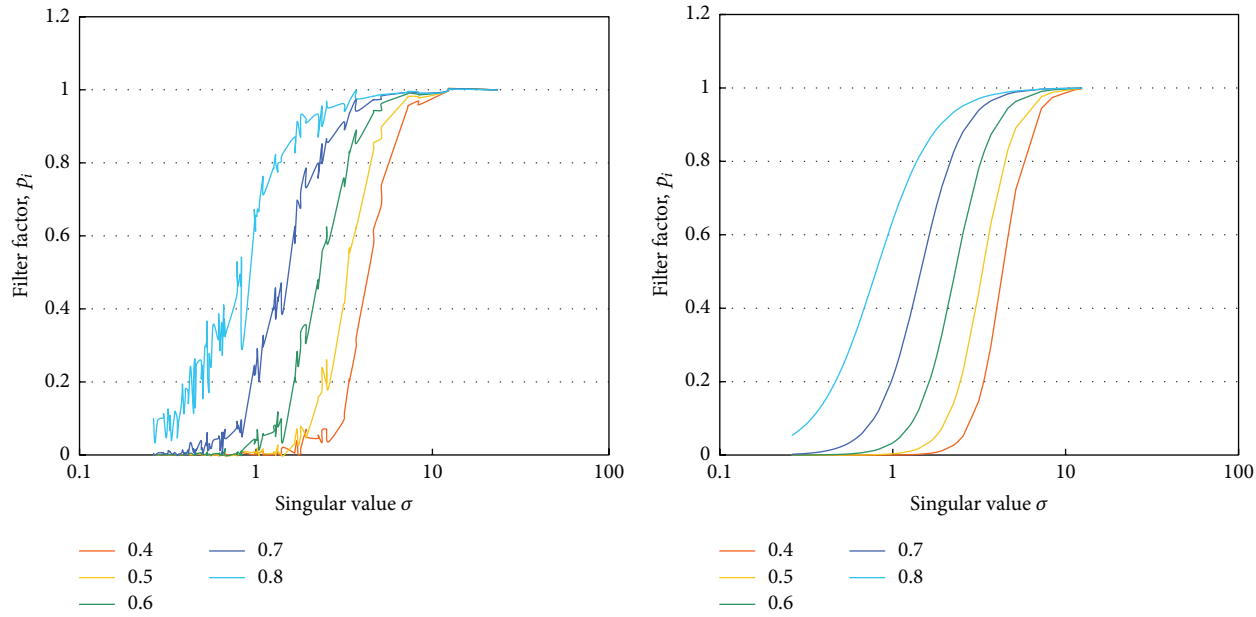


(a) Optimal filter factors calculated by least squares method

(b) Approximated filter factors by sigmoid function

FIGURE 4: Optimal filter factors by changing the depth of signal sources.

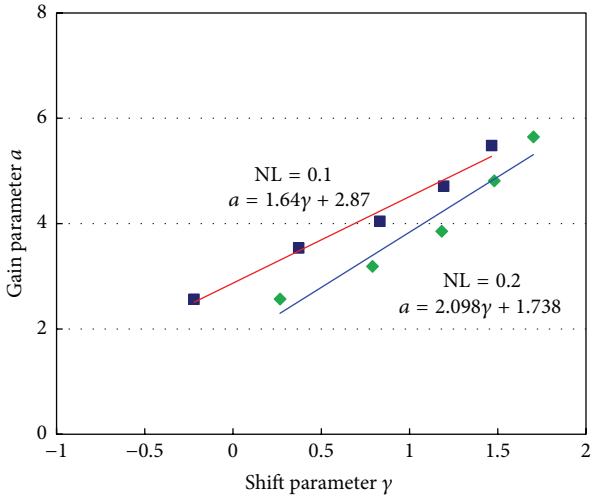


FIGURE 5: Relationship between shift parameter $\gamma$ and gain parameter $a$ in (9).

Two signal sources could be observed in the actual dipole distribution while the distribution of the scalp potential was spread over whole parietal region. The dipole distributions were estimated using Tikhonov regularization, TSVD, TTLS, and the sigmoid function. To avoid the influence of parameter estimation error, the regularization parameters were determined by minimizing the relative error when the actual dipole solution is supposed to be known. The result of Tikhonov regularization was influenced by noise. The localization was accomplished by the sigmoid function compared with TSVD and TTLS. The performance of TSVD was almost the same as that of TTLS.

Figure 7 shows the averaged relative error between actual and estimated dipole distributions with noise levels of 0.1 and 0.2. The error level was set to 0.1. The graphs show the average and standard deviation over 10 patterns of signal source arrangements. Dunnett's multiple comparison tests were applied to the data. The relative error of the sigmoid function is significantly smaller than that of the other methods. The performance of parameter estimation methods was examined in computer simulations. The curvature method and the minimal product method were compared by means of the relative error between actual and estimated dipole distributions. Figure 8 shows the relative errors with the noise levels of 0.1 and 0.2. The average and the standard deviation were obtained over 10 trials with various signal configurations. The relative error of the curvature method was significantly smaller than that of the minimal product method as a result of paired $t$-test. It was confirmed that the curvature method is more suitable for parameter estimation of sigmoid function than the minimal product method.

*3.2. Application to VEP.* Based on the simulation results, the proposed method was applied to human experimental data. The EEG data were measured from healthy subjects after obtaining informed consent according to the University of Illinois Ethical Review Board regulation. Ninety-four scalp electrodes arranged according to the expanded international 10-20 system were used for the EEG recording. The VEP to pattern reversal in the right half of the visual field was measured with intervals of 0.5 s. The VEP signals were averaged over 400 reversals. The sampling frequency was 1 kHz. The dipole layer was arranged with a radius of 0.85 to represent the visual-related signal sources. From the simulation result, the regularization parameter of the sigmoid

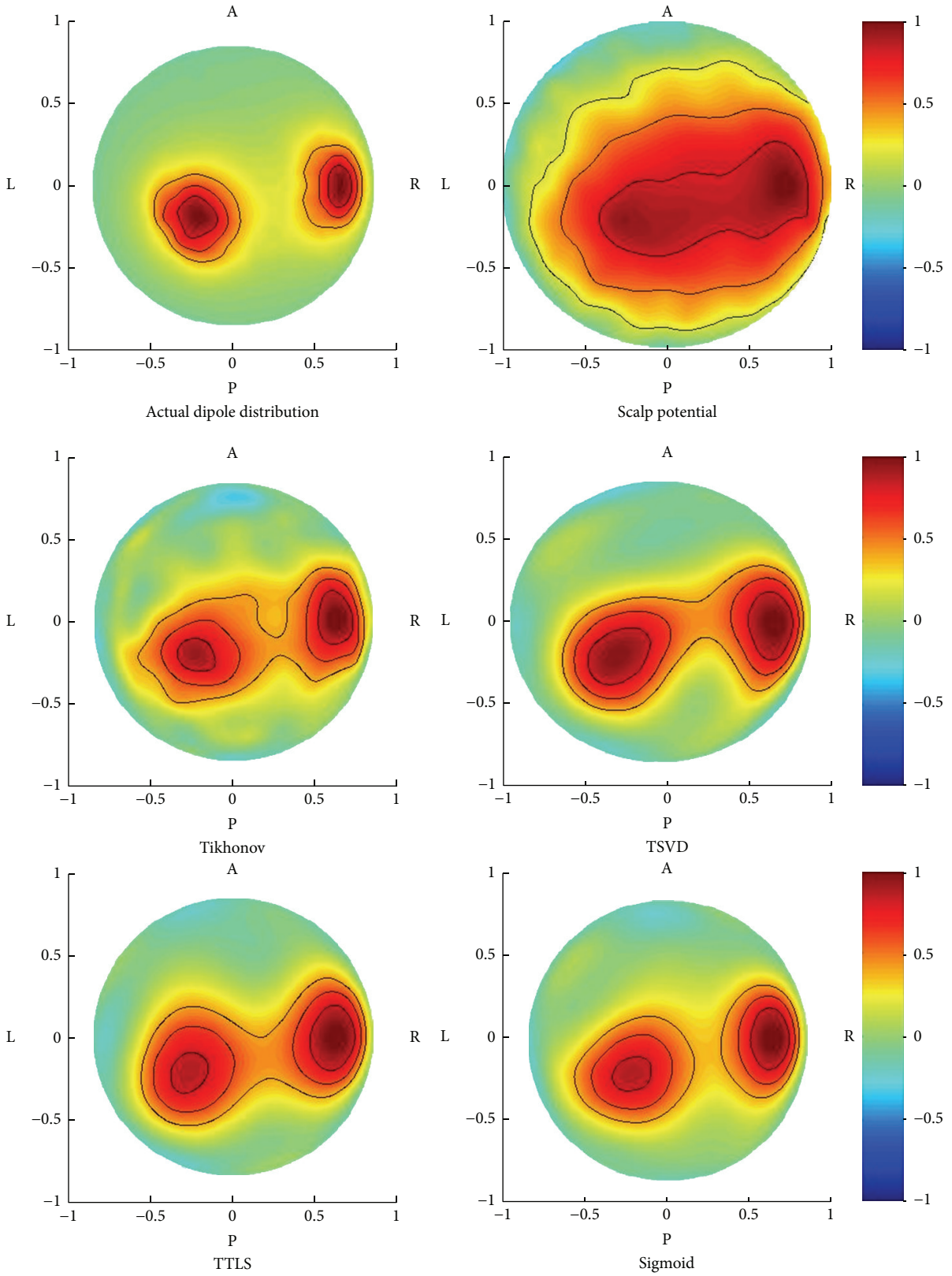


Figure 6: Simulation results of dipole distributions estimated by Tikhonov regularization, TSVD, TTLS, and sigmoid function. R: right; L: left; A: anterior; P: posterior.

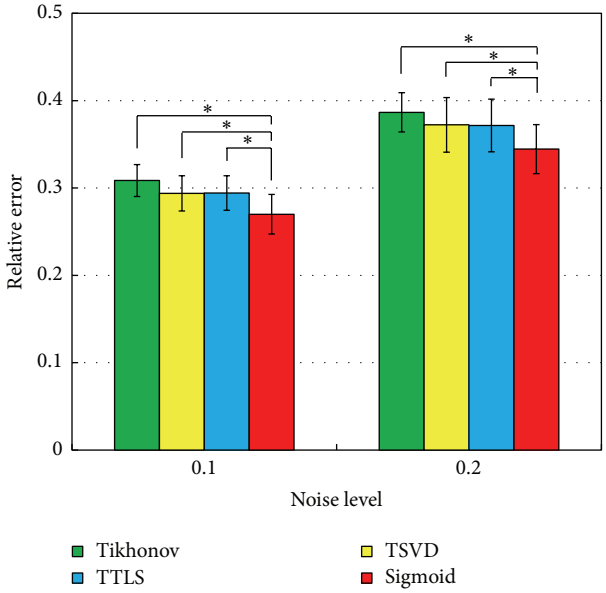


FIGURE 7: Relative errors of dipole distributions estimated by Tikhonov regularization, TSVD, TTLS, and sigmoid function ($N = 10$, $* < 0.05$).

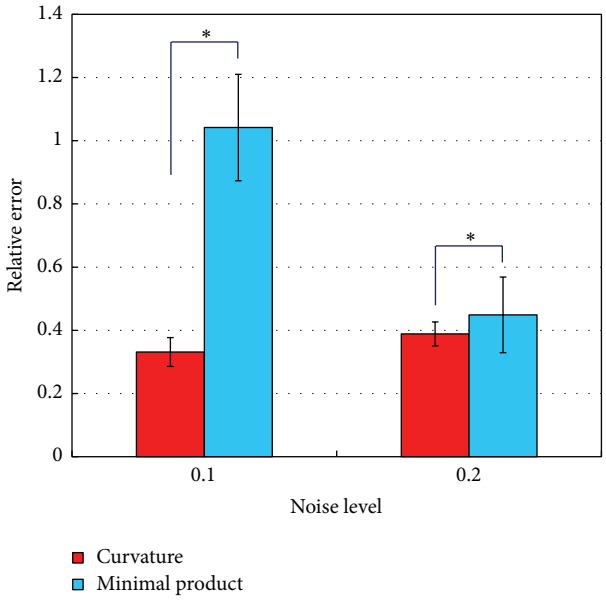


FIGURE 8: Comparison of parameter estimation methods ($N = 10$, $* < 0.05$).

function was estimated by means of the curvature method. Referring to a previous study, the curvature method was applied to Tikhonov regularization and the minimal product method was applied to TSVD and TTLS as the parameter estimation methods [10].

Positive potential was observed at about 100 ms after visual stimulus (P100). Cortical dipole imaging was applied at the positive peak (75 ms after the stimulus), followed by the propagation process (95 ms after the stimulus). Figure 9 shows the scalp potential and the dipole distributions estimated by Tikhonov regularization, TSVD, TTLS, and the proposed sigmoid function at 75 ms and 95 ms after stimulus (the results at other time intervals are omitted for want of space). The normalized maps were displayed when viewing from the posterior. The positive potential was distributed over the whole occipital region in the scalp potential map at 75 ms after stimulus. The signal was localized at the primary visual field in dipole distributions estimated by every method. The influence of noise was observed in the results of Tikhonov regularization and TSVD. The signal was more localized when TTLS and the sigmoid function were used. The positive potential was also distributed over the whole occipital region in the scalp potential map at 95 ms after stimulus. Two signal spots were visible in dipole distributions. From the viewpoint of signal separation, TSVD and the sigmoid function provided better results than Tikhonov regularization and TTLS.

## 4. Discussion

As shown in (13), the optimal filtering property was approximated using a sigmoid function with the singular value as a variable parameter. In the inverse problem of cortical dipole imaging, the number of singular values decayed exponentially as the singular values became large. Thus, the sigmoid function was fitted to the optimal filtering property based on the logarithm of a singular value.

The deeper the signal sources, the broader the dipole distribution. Broad mapping can be approximated with small number of singular values compared with sharp mapping. As a result, the larger singular values were depressed when the signal sources were located in deep positions. Moreover, when the noise level is large, the noise component must be suppressed in order to obtain high-fidelity dipole distribution. We confirmed that the larger singular values were depressed in noisy conditions.

Whenever the noise level and the depth of signal sources were changed, it was possible to fit the sigmoid function to the optimal filter factors estimated using LS. The cortical dipole distribution using the sigmoid function was more localized with less noise compared with the traditional methods. When the noise level increased, the relative error of every method increased. However, the relative error of the sigmoid function was smallest among the 4 inverse filters investigated. From these results, it was considered that highly precise estimation for cortical dipole imaging could be achieved by optimizing the filter factors.

In general, small singular values emphasize the noise included in the scalp potentials. The terms with small singular values were suppressed by filtering properties as shown in Figure 1. In addition, as explained in Section 2.4, the filtering property of the sigmoid function was intermediate between Tikhonov regularization and TSVD. This filter attenuates the terms with small singular values to reduce the noise while it passes the terms of large singular values to reconstruct the signal. The sigmoid function performs the signal reconstruction and noise reduction in a well-balanced manner.

The filter property based on the sigmoid function takes into consideration only measurement noise, while TTLS

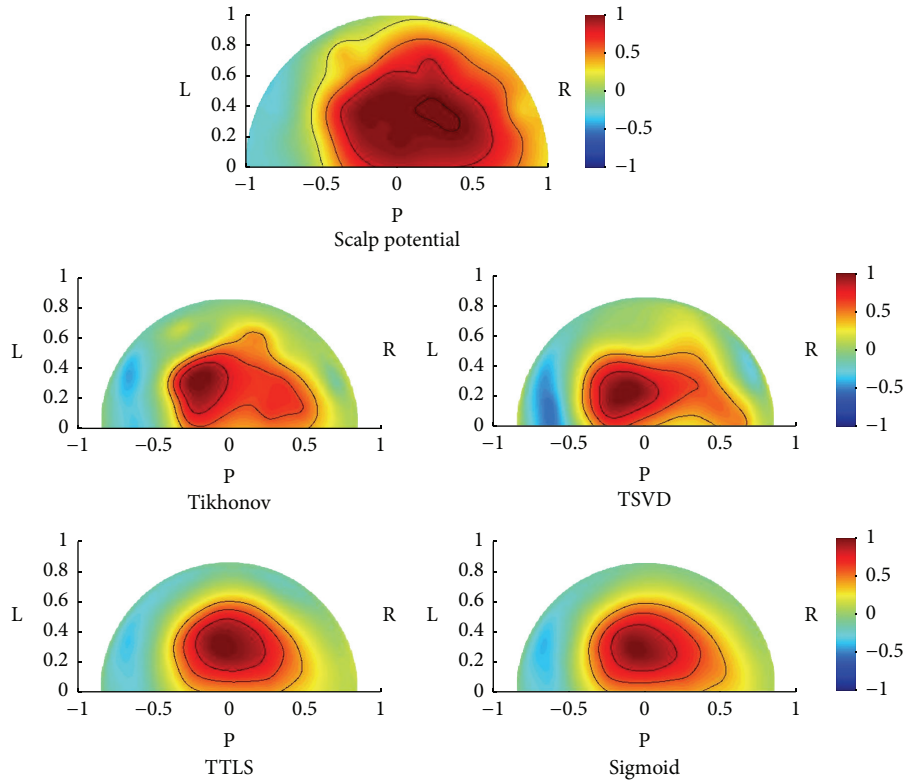


(a) 75 ms after visual stimulus

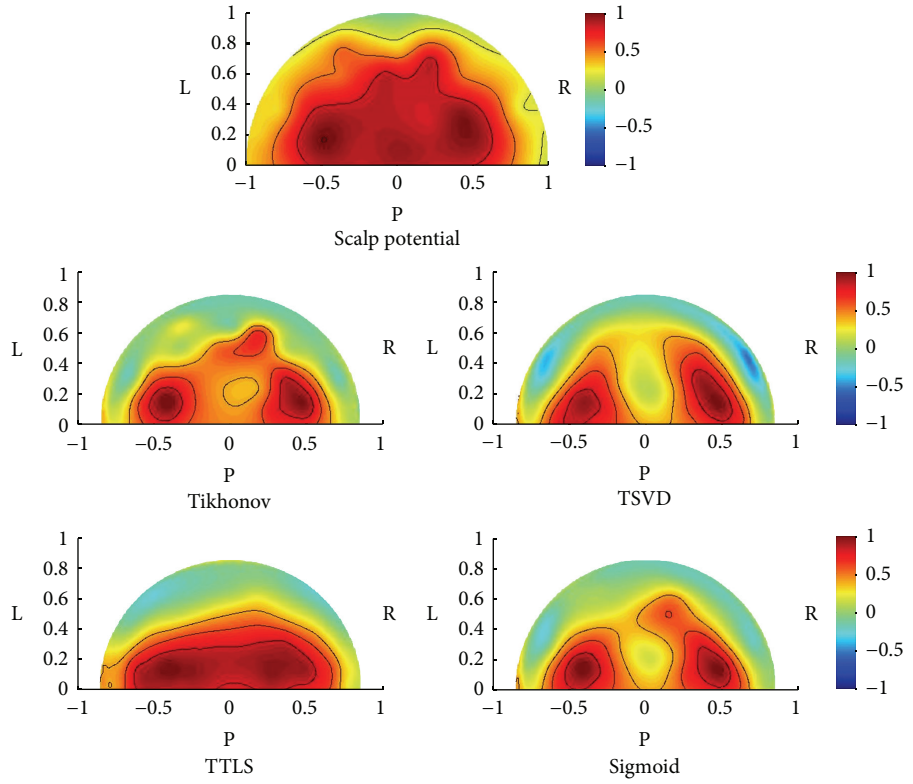


(b) 95 ms after visual stimulus

Figure 9: Estimated results of dipole distributions for VEP. R: right; L: left; P: posterior.

considers both the measurement noise and the transfer matrix error. The present simulation, considering the measurement noise and the transfer matrix error, suggested that the optimum filter property that considered the measurement noise properly was effective to obtain better inverse solutions. It is expected that the restorative ability would be improved by combining the sigmoid function-based inverse filter with TTLS.

As the method for estimating the regularization parameter of the sigmoid function, the curvature method was better than the minimal product method. In the previous study, it was reported that the curvature method was used for continuous values such as the regularization parameter of Tikhonov regularization while the minimal product was used for discrete values such as the truncated parameter of TSVD and TTLS [10]. The shift parameter $\gamma$ of the sigmoid function in (13) is a continuous value. Thus, the curvature method is suitable for the parameter estimation of the sigmoid function.

In the VEP experiment shown in Figure 9, the signal was localized at occipital region of cortical dipole distribution at 75 ms after visual stimulus. The activated area corresponds to the primary visual cortex and the results coincided with established physiological knowledge [21]. Both TTLS and the sigmoid function can localize the signal while suppressing the noise. The dipole distribution at 95 ms after visual stimulus showed two signals separated from one signal at 75 ms after visual stimulus. The visual signal caused at calcarine sulcus in the occipital region propagates through ventral and dorsal pathways [21]. It was possible to represent the process of signal propagation through ventral pathway using TSVD and the sigmoid function. In conclusion, regarding these two results, the sigmoid function was widely applicable in various situations and would be effective for human experimental data. It is difficult to evaluate the experimental performance quantitatively because the actual signal source is unknown. The experimental results of cortical dipole imaging have been evaluated visually in previous studies [10, 12, 13, 19]. The cortical imaging techniques may be evaluated by comparing with electrocorticogram invasively [22].

The proposed inverse filter supposed that the noise is uniformly distributed over the scalp surface. Actually, the noise is nonuniform because of the variation of the electrode impedance and physiological properties such as eye blink artifacts or body movements. In such cases, the parametric projection filter [5, 6] and parametric Wiener filter [23] can be effectively applied under nonuniform noise conditions. It is expected that cortical dipole imaging is improved by combining the sigmoid function-based filtering property and parametric projection or Wiener filter.

## 5. Conclusion

The spatial inverse filter was investigated based on filtering property aiming at high-resolution cortical dipole imaging. It was confirmed that the optimum filter factor depends on the noise level and the depth of signal sources. These results suggested that the filtering property can be designed by considering the signal and noise configuration. Moreover, the proposed method is of wide application for several types of experimental data. In computer simulations and human experiments using VEP, filtering property using the sigmoid function provided more localized dipole distribution with less noise compared with Tikhonov regularization, TSVD, and TTLS. For parameter estimation, the curvature method was suitable for the sigmoid function-based inverse technique. The proposed method will contribute to the visualization of cortical electrical activity in high resolution. We are planning to design filtering property using statistical information on noise distribution. Moreover, we would apply more realistic head models in the near future.

## Competing Interests

The authors declare that there is no conflict of interests regarding the publication of this paper.

## Acknowledgments

The authors would like to thank Professor B. He, University of Minnesota, who provided the experimental data. This research was supported in part by a Grant-In-Aid for Scientific Research (C) 26350496 from the Japanese Society for the Promotion of Science.

## References

[1] R. D. Sidman, M. R. Ford, G. Ramsey, and C. Schlichting, "Age-related features of the resting and P300 auditory evoked responses using the dipole localization method and cortical imaging technique," *Journal of Neuroscience Methods*, vol. 33, no. 1, pp. 23–32, 1990.

[2] Y. Wang and B. He, "A computer simulation study of cortical imaging from scalp potentials," *IEEE Transactions on Biomedical Engineering*, vol. 45, no. 6, pp. 724–735, 1998.

[3] A. N. Tikhonov and V. Y. Arsenin, *Solutions of Ill-Posed Problems*, Halsted Press, New York, NY, USA, 1977.

[4] P. C. Hansen, "The truncated SVD as a method for regularization," *BIT Numerical Mathematics*, vol. 27, no. 4, pp. 534–553, 1987.

[5] J. Hori and B. He, "Equivalent dipole source imaging of brain electric activity by means of parametric projection filter," *Annals of Biomedical Engineering*, vol. 29, no. 5, pp. 436–445, 2001.

[6] J. Hori, M. Aiba, and B. He, "Spatio-temporal cortical source imaging of brain electrical activity by means of time-varying parametric projection filter," *IEEE Transactions on Biomedical Engineering*, vol. 51, no. 5, pp. 768–777, 2004.

[7] R. D. Fierro, G. H. Golub, P. C. Hansen, and D. P. O'Leary, "Regularization by truncated total least squares," *SIAM Journal on Scientific Computing*, vol. 18, no. 4, pp. 1223–1241, 1997.

[8] X. He, J. Liang, X. Qu, H. Huang, Y. Hou, and J. Tian, "Truncated total least squares method with a practical truncation parameter choice scheme for bioluminescence tomography inverse problem," *International Journal of Biomedical Imaging*, vol. 2010, Article ID 291874, 11 pages, 2010.

[9] G. Shou, L. Xia, M. Jiang, Q. Wei, F. Liu, and S. Crozier, "Truncated total least squares: a new regularization method for the solution of ECG inverse problems," *IEEE Transactions on Biomedical Engineering*, vol. 55, no. 4, pp. 1327–1335, 2008.

[10] J. Hori and K. Takeuchi, "Cortical dipole imaging using truncated total least squares considering transfer matrix error," in *Proceedings of the 35th Annual International Conference of the IEEE Engineering in Medicine and Biology Society (EMBC '13)*, pp. 5410–5413, IEEE, Osaka, Japan, July 2013.

[11] S. Takasawa and J. Hori, "Improvement of cortical dipole imaging based on filtering property approximated by sigmoid function," *IEICE Technical Reports*, vol. 115, no. 229, pp. 1–6, 2015.

[12] S. Takasawa and J. Hori, "Improvement of cortical dipole imaging based on filtering property," *IEICE Technical Report*, vol. 114, no. 213, pp. 11–16, 2014.

[13] J. Hori and Y. Watanabe, "Cortical dipole imaging for multiple signal sources considering time-varying non-uniform noise," *IEEJ Transactions on Electronics, Information and Systems*, vol. 131, no. 11, pp. 1958–1965, 2011.

[14] N. P. Subramaniyam, O. R. M. Väisänen, K. E. Wendel, and J. A. V. Malmivuo, "Cortical potential imaging using L-curve and GCV method to choose the regularisation parameter," *Nonlinear Biomedical Physics*, vol. 4, no. 1, article 4, 2010.

[15] P. C. Hansen and D. P. O'Leary, "The use of the L-curve in the regularization of discrete ill-posed problems," *SIAM Journal on Scientific Computing*, vol. 14, no. 6, pp. 1487–1503, 1993.

[16] Y. Hosoda and T. Kitagawa, "Optimum regularization for ill-posed problems by means of L-curve," *The Japan Society for Industrial and Applied Mathematics*, vol. 2, no. 1, pp. 55–67, 1992.

[17] J. Lian and B. He, "A minimal product method and its application to cortical imaging," *Brain Topography*, vol. 13, no. 3, pp. 209–217, 2001.

[18] J. L. Castellanos, S. Gómez, and V. Guerra, "The triangle method for finding the corner of the L-curve," *Applied Numerical Mathematics*, vol. 43, no. 4, pp. 359–373, 2002.

[19] G. Rodriguez and D. Theis, "An algorithm for estimating the optimal regularization parameter by the *L*-curve," *Rendiconti di Matematica, Serie VII*, vol. 25, no. 1, pp. 69–84, 2005.

[20] P. C. Hansen, T. K. Jensen, and G. Rodriguez, "An adaptive pruning algorithm for the discrete L-curve criterion," *Journal of Computational and Applied Mathematics*, vol. 198, no. 2, pp. 483–492, 2007.

[21] M. W. Eyesenck and M. T. Keane, *Cognitive Psychology: A Student's Handbook*, Psychology Press, 2010.

[22] B. He, X. Zhang, J. Lian, H. Sasaki, D. Wu, and V. L. Towle, "Boundary element method-based cortical potential imaging of somatosensory evoked potentials using subjects' magnetic resonance images," *NeuroImage*, vol. 16, no. 3, pp. 564–576, 2002.

[23] J. Hori, T. Miwa, T. Ohshima, and B. He, "Cortical dipole imaging of movement-related potentials by means of parametric inverse filters incorporating with signal and noise covariance," *Methods of Information in Medicine*, vol. 46, no. 2, pp. 242–246, 2007.

Hindawi Publishing Corporation
Computational Intelligence and Neuroscience
Volume 2016, Article ID 6734720, 12 pages
http://dx.doi.org/10.1155/2016/6734720

*Research Article*

# A Novel Fixed Low-Rank Constrained EEG Spatial Filter Estimation with Application to Movie-Induced Emotion Recognition

**Ken Yano and Takayuki Suyama**

*Department of Dynamic Brain Imaging, Cognitive Mechanisms Laboratories, Advanced Telecommunications Research Institute International, 2-2-2 Hikaridai, Seika-cho, Soraku-gun, Kyoto 619-0288, Japan*

Correspondence should be addressed to Ken Yano; yanoken@atr.jp

Received 28 April 2016; Revised 15 June 2016; Accepted 19 June 2016

Academic Editor: Victor H. C. de Albuquerque



This paper proposes a novel fixed low-rank spatial filter estimation for brain computer interface (BCI) systems with an application that recognizes emotions elicited by movies. The proposed approach unifies such tasks as feature extraction, feature selection, and classification, which are often independently tackled in a "bottom-up" manner, under a regularized loss minimization problem. The loss function is explicitly derived from the conventional BCI approach and solves its minimization by optimization with a nonconvex fixed low-rank constraint. For evaluation, an experiment was conducted to induce emotions by movies for dozens of young adult subjects and estimated the emotional states using the proposed method. The advantage of the proposed method is that it combines feature selection, feature extraction, and classification into a monolithic optimization problem with a fixed low-rank regularization, which implicitly estimates optimal spatial filters. The proposed method shows competitive performance against the best CSP-based alternatives.

## 1. Introduction

Brain computer interfaces (BCIs) are a rapidly growing field of research that combines neurophysiological insights, statistical signal analysis, and machine learning. BCIs are generally designed based on a pattern recognition approach, that is, extracting features from EEG signals and using a classifier to identify the user's mental state from such features [1]. Those sequential approaches are called "bottom-up" schemes; given a large collection of single-trial EEG data, better representations of the data are extracted to finally obtain the classification output at the top. In contrast, discriminative or "top-down" approaches focus on predicting user intentions and are based on two criteria: the empirical prediction performance and the regularizer. Suitably chosen regularizers automatically induce sparse decomposition of the signal, which corresponds to conventional feature extraction [2].

This paper proposes a discriminative method using a low-rank regularizer to estimate spatial filters for extracting effective features under a study. The advantage of the proposed method is that it combines feature selection, feature extraction, and classification into a monolithic optimization problem with a low-rank regularization, because this approach includes spatial filter estimation in the optimization framework of statistical inference model. Under a suitable chosen regularizer, it induces the best inference model, which implicitly estimates optimal spatial filters under the regularization assumption.

Emotion classification from EEG data has attracted much attention recently [3, 4]. Emotion also plays an important role in human-human communication and interaction. The ability to recognize the emotional states of people is an important part of natural communication. This field of research is still relatively new, and there is still much to be

done to improve on existing elements in BCI but also to discover new possibilities.

For evaluation of the proposed methods, experiments were conducted to induce emotions by movies for dozens of young adult subjects and estimated the emotional states using the proposed method. The results were compared with conventional methods using a common spatial pattern (CSP).

This paper's contribution is the proposal and the explicit derivation of the fixed low-rank constrained discriminative approach and its application to emotion recognition with comparative analysis with conventional methods. This paper is organized as follows. Section 2 describes the background of emotion recognition from EEGs, and Section 3 describes the proposed method. Section 4 presents the data acquisition and experimental protocol. Section 5 describes the results and discussion. Section 6 concludes the paper.

## 2. Background

*2.1. Emotion in the Brain.* The limbic system which is like a cortical ring around the brain stem is responsible for initial emotional interpretation of the signals from the autonomic nervous system. The hypothalamus is responsible for processing the incoming signals and triggering the corresponding visceral physiological effects like a raised heart rate or galvanic skin response.

From the hypothalamus the stimuli information is passed on to the amygdala, which is important for learning to connect stimuli to emotional reactions (reward/fear) and for evaluating new stimuli by comparing them to past experience.

The amygdala is considered vital for emotion processing. However, since it is an underlying structure like the rest of the limbic system, it cannot be detected directly in recording from the scalp. The amygdala is connected to the temporal and prefrontal cortices, which is thought to be the way visceral sensations are interpreted cognitively, resulting in a consciously experienced feeling of an emotion [5].

The temporal lobe is essential for hearing, language, and emotion and also plays an important role in memory. The prefrontal lobe is involved in the so-called highest level of functioning. It is responsible for cognitive, emotional, and motivational processes. The prefrontal lobe is part of the frontal cortex, which is said to be the emotional control center and to even determine personality. It is involved in, among others, judgment and social behavior. These functions are very much based on the experience of emotions.

*2.2. Valence: Hemispherical Asymmetry.* Psychophysiological research has shown the importance of the difference in activation between the two cortical hemispheres in the reaction that subjects show toward stimuli. Left frontal inactivation is an indicator of a withdrawal response, which is often linked to a negative emotion. On the other hand, right frontal inactivation is a sign of an approach response, or positive emotion.

Harmon-Jones [6] suggests that the hemispherical differences are not an indication of affective valence, but of motivational direction (approach or withdrawal behavior to the stimulus). Affective valence does seem tightly linked to motivational direction. Therefore, the hemispherical asymmetry patterns do indicate the affective valence.

Davidson and Fox [7] found that 10-month-old infants exhibited increased left frontal activation in response to a film clip of an actress generating a happy facial expression as compared to a sad facial expression. Frontal cortical activity has been found to relate to facial expressions of positive and negative emotions as well.

## 3. Method

*3.1. General Framework.* Given a short high-pass filtered EEG segment, $X \in \mathscr{R}^{C\times T}$, where $C$ is the number of channels and $T$ is the number of time points, the data are first band-pass filtered at a band range being studied. A commonly used form of a second-order or power oscillation-based linear model can be written as follows:

$$f = b + \sum_{j=1}^{J} \theta_j \log\left(\mathrm{Var}\left(w_j^T X\right)\right). \tag{1}$$

Here, $\{w_j\}_{j=1}^{J} \in \mathscr{R}^{C\times J}$ is the spatial filters, $\{\theta_j\}_{j=1}^{J}$ are the weighting coefficients of the $J$ features, and $b$ is a bias term. The classifier first projects the signal by $J$ spatial filters. Next, it takes a logarithm of the power of the projected signal. Finally it linearly combines these $J$ dimensional features and adds bias.

To determine spatial filters $\{w_j\}_{j=1}^{J}$, CSP is often used [1]. Many variants of the original CSP have been proposed. [8]. Coefficients $\{\theta_j\}_{j=1}^{J}$ and $b$ are determined statistically from the training examples, that is, the pairs of trials and labels $\{X_i, y_i\}_{i=1}^{n}$ collected in the calibration phase. Label $y \in \{+1, -1\}$ corresponds to the binary classes being studied.

To briefly summarize CSP to compute spatial filter $w$, it is obtained by extremizing the following function:

$$J(w) = \frac{w^T \Sigma_{(+1)} w}{w^T \Sigma_{(-1)} w}, \tag{2}$$

where $\Sigma_{(c)}$ is the spatial covariance matrix of the EEG signals from class $c$ as follows:

$$\Sigma_{(c)} = \frac{1}{\left|\mathscr{I}_c\right|} \sum_{i\in\mathscr{I}_c} X_i X_i^T \quad (c \in +1, -1), \tag{3}$$

where we assume a zero mean for the EEG signal.

Since $J(w)$ remains unchanged if $w$ is rescaled, extremizing $J(w)$ is equivalent to extremizing $w^T\Sigma_{(+1)}w$ subject to the constraint $w^T\Sigma_{(-1)}w = 1$. Using the Lagrange multiplier method, this constrained optimization problem amounts to extremizing the following function:

$$L(\lambda, w) = w^T\Sigma_{(+1)}w - \lambda\left(w^T\Sigma_{(-1)}w - 1\right). \tag{4}$$

The spatial filter $w$ extremizing $L$ is such that the derivative of $L$ with respect to $w$ equals 0:

$$\begin{aligned}\frac{\partial L}{\partial w} &= 2w^T\Sigma_{(+1)} - 2\lambda w^T\Sigma_{(-1)} = 0 \Longleftrightarrow\\ \Sigma_{(+1)}w &= \lambda\Sigma_{(-1)}w \Longleftrightarrow\\ \Sigma_{(-1)}^{-1}\Sigma_{(+1)}w &= \lambda w.\end{aligned} \tag{5}$$

The spatial filters are the eigenvectors of $\Sigma_{(-1)}^{-1}\Sigma_{(+1)}$ which correspond to its largest and lowest eigenvalues.

*3.2. Proposed Model Calibration.* If we ignore the logarithm in (1), it can be reformulated as follows:

$$\sum_{j=1}^{J}\theta_j\left(w_j^T XX^T w_j\right) = \mathrm{Tr}\left(\Theta^T\Sigma\right), \tag{6}$$

where $\Theta = \sum_{j=1}^{J}\theta_j w_j w_j^T \in \mathscr{R}^{C\times C}$ and $\Sigma \in \mathscr{R}^{C\times C}$ is the covariance matrix of $X$. Finally we obtain

$$f = b + \langle\Theta, \Sigma\rangle. \tag{7}$$

Note that $\langle\Theta, \Sigma\rangle$ is the elementwise inner product of the two matrices. To determine parameters $(\Theta, b)$, logistic regression was employed with low-rank regularization of $\Theta$. This amounts to solving the following optimization problem with training examples:

$$\begin{aligned}\min_{\Theta,b}\quad & \sum_{i=1}^{n}\log\left(1 + e^{-y_i(b+\langle\Theta,\Sigma_i\rangle)}\right) + \sum_{i=1}^{c}\sigma_i\\ \text{s.t.}\quad & \mathrm{rank}(\Theta) = c,\end{aligned} \tag{8}$$

where $\sigma_i$ is the $i$th singular value of $\Theta$ and $c$ is the rank constraint of $\Theta$. The first term is convex. But since the low-rank constraint term is nonconvex, it is not guaranteed to find the optimal point. To solve this problem, the alternating direction method of multipliers (ADMM) [9] is employed with a hope that it has better convergence properties than other local optimization methods. For nonconvex problems, depending on the initial values, the solution can converge to different points.

The optimization problem is rephrased as follows:

$$\begin{aligned}\text{minimize}\quad & F(\Theta, b)\\ \text{subject to}\quad & \Theta \in C,\end{aligned} \tag{9}$$

where $C$ is the set of matrices with rank $c$. To solve it by ADMM, it can be rewritten as follows:

$$\begin{aligned}\text{minimize}\quad & F(\Theta, b) + G(\Xi)\\ \text{subject to}\quad & \Theta - \Xi = 0,\end{aligned} \tag{10}$$

where $G$ is the indicator function of $C$. The augmented Lagrangian (using the scaled dual variable) is

$$\begin{aligned}L_\rho(\Theta, b, \Xi, \Upsilon) = F(\Theta, b) + G(\Xi)\\ + \left(\frac{\rho}{2}\right)\|\Theta - \Xi + \Upsilon\|_2^2,\end{aligned} \tag{11}$$

where $\rho > 0$ is called the penalty parameter. So the iterative optimization of ADMM for this problem is

$$\begin{aligned}\Theta^{k+1} &= \arg\min_{\Theta,b}\left(F(\Theta, b) + \left(\frac{\rho}{2}\right)\left\|\Theta - \Xi^k + \Upsilon^k\right\|_2^2\right),\\ \Xi^{k+1} &= \Pi_C\left(\Theta^{k+1} + \Upsilon^k\right),\\ \Upsilon^{k+1} &= \Upsilon^k + \Theta^{k+1} - \Xi^{k+1},\end{aligned} \tag{12}$$

where $\Pi_C$ is the projection onto $C$. Hence, $\Pi_C(\Xi)$ is determined by carrying out a singular value decomposition, $\Xi = \Sigma_i\sigma_i u_i v_i^T$, and keeping the top $c$ singular values; that is, $\Pi_c(\Xi) = \sum_{i=1}^{c}\sigma_i u_i v_i^T$.

Here we can initialize $\Theta$ and $b$ as zero w.l.o.g. The primal and the dual residuals at iteration $k+1$ are defined as follows:

$$\begin{aligned}R^{k+1} &= \Theta^{k+1} - \Xi^{k+1},\\ S^{k+1} &= -\rho\left(\Xi^{k+1} - \Xi^k\right).\end{aligned} \tag{13}$$

These residuals converge to zero as ADMM proceeds.

*3.3. Multiple Frequency Bands.* The proposed method can be extended for estimating the spatial filters for multiple frequency bands. Let $X_{b,k} = B_k X$ be the band-pass filtered data by filtering operator $B_k$. The covariance matrix of the signal denoted as $\Sigma_{b,k} = X_{b,k}X_{b,k}^T \in \mathscr{R}^{C\times C}$ is obtained separately for each frequency pass band. Then align them as a large block diagonal matrix (14). To obtain the spatial filters for multiple bands, this block diagonal matrix is substituted for $\Sigma$ in (7).

The solution is expected to effectively select the optimal spatial features from multiple frequency bands:

$$\Sigma = \begin{pmatrix} \Sigma_{b,1} & & & \\ & \Sigma_{b,2} & & \mathbf{0} \\ & & \ddots & \\ \mathbf{0} & & & \Sigma_{b,K} \end{pmatrix}. \quad (14)$$

*3.4. Merits of the Proposed Method.* CSP estimates spatial filters based on a criterion that corresponding components produce minimum variance for one condition and maximum variance for the other and thus increase discriminative ability. However because the spatial filter estimation is decoupled from the inference model, such as logistic regression, optimal filters can only be predicted by using cross-validation of the inference model and select the one which produces the best empirical inference performance.

On the other hand, our proposed model derived from "top-down" approach incorporates spatial filter estimation in the predictive model. Hence by focusing on the prediction performance with suitably chosen regularizer, such as fixed low-rank in our model, it induces sparse decomposition of the signal which corresponds to conventional feature extraction. Hence, it implicitly estimates optimal spatial filters of the best inference model under the assumption.

## 4. Emotion Recognition

To predict the state of emotion experienced by the participants from single EEG segments, a predictive model was employed that estimates from a given short EEG segment (here 5 sec) the probability that the participant experienced positive or negative emotions during that period. For the evaluation, fivefold cross-validation is performed by holding out one-session dataset for the test and the remaining four-session datasets with labels were used to estimate parameters $(\Theta, b)$. For each round, the held-out dataset was used for tests to evaluate the classification error rate. In each round, the classification error rate is computed as the ratio of the number of correctly classified EEG segments divided by the total number of EEG segments in the trial.

*4.1. Data Acquisition.* Twenty-three healthy adult volunteers participated under the informed consent that was approved by the ethical committee of ATR. Among them, ten subjects (males = 3, females = 7, age = 24.5 ± 6.24) were selected for analysis. The EEGs were recorded from 32 gel-based scalp electrodes, as shown in Figure 1, and four EOG placements around the eyes using an eego amplifier (ANT Neuro, Enschede, Netherlands) with 24-bit resolution. The EEGs were sampled at 512 Hz. The protocol of the EEG experiment is described in Figure 2. To elicit emotions, a set of movie clips that were used in Samson et al. [10] was used. The movie clip set includes four classes of different target emotional states: positive, negative, neutral, and mixed. The average length of each clip was about 20 seconds. For each trial, to elicit emotions, four randomly selected movie clips of the same emotional class were played continuously without intervals and followed by self-assessment questions. One session consisted of four trials of four different movie classes. Before each trial, a random color grating pattern was displayed for 90 seconds to wash out the emotional states of the participant. The entire experiment consisted of seven sessions. For the analysis, however, only the first five sessions were used because, during the last two sessions, most participants appeared fatigued or drowsy.

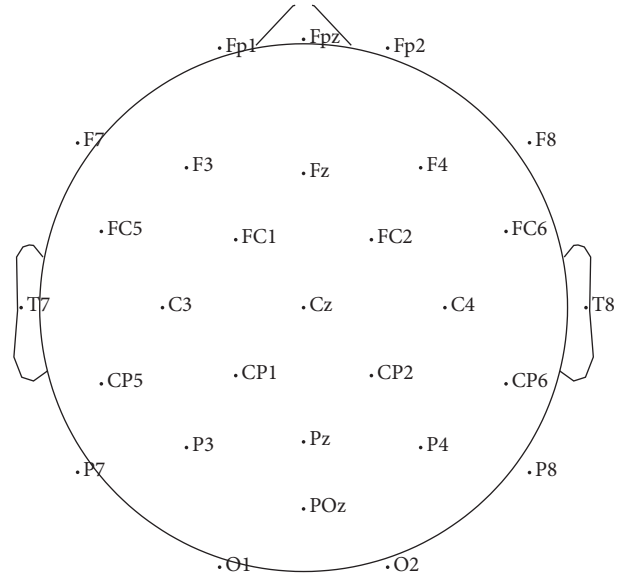


Figure 1: EEG channel locations. For decoding emotions, we use all channels except Fp1, Fpz, and Fp2.

*4.2. Preprocessing.* The EEG signals were downsampled from 512 to 128 Hz and high-pass filtered at 0.5 Hz. The EOG and the muscle artifacts were automatically removed using AAR [11]. Among the 32 channels, only 26 channels were used excluding the reference and prefrontal channels, Fp1, Fpz, and Fp2, which were contaminated severely by the EOG artifacts. The EEG signals were rereferenced by the M1 and M2 means. All the trial data were extracted from the onset of the first movie clip until the offset of the last clip. Then all the trial data were band-pass filtered at 4–47 Hz. Finally, the length of all the trial data was identically set to 80 seconds. Training and testing data were generated by using a sliding window over each bit of trial data. The length of the window was five seconds, and the overlap between windows was two seconds.

## 5. Results

Figure 3 shows the variabilities of the classification error rate for all participants due to the change of the rank constraints. The classification error rate was computed by averaging over folds. It reached plateau after some rank constraints. This figure suggests that an optimal rank constraint exists between 1 and 10 regardless of the participants.

The elapsed time of convergence of the low-rank constrained optimization is shown in Figure 4. The time gradually decreases reciprocally as the rank increases and reaches

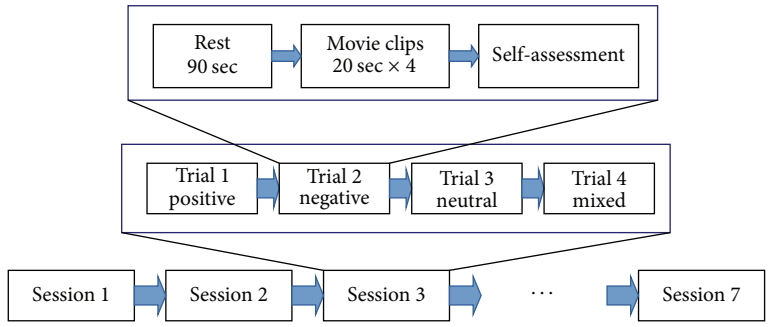


Figure 2: Protocol of the EEG experiment. For each session, we randomly changed the sequence of trials of four movie clip types: positive, negative, neutral, and mixed.

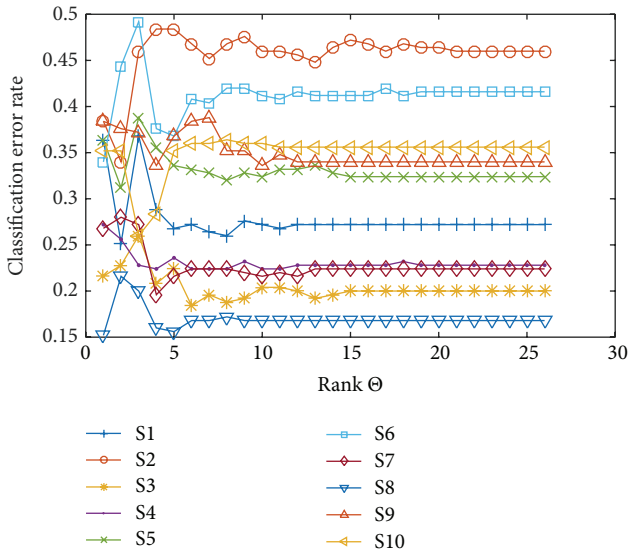


Figure 3: Classification error rate of binary classes (positive or negative) for all subjects. Mean classification error rate changed by increasing low-rank constraint from 1 to 26 (full-rank).

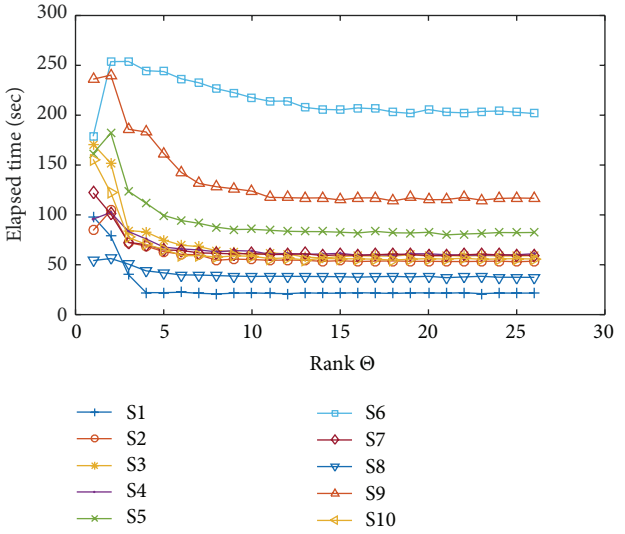


Figure 4: The change of elapsed time of convergence of optimization due to the change of low-rank constraint from 1 to 26 (full-rank) for all subjects.

plateau at some rank constraint. The trend is very similar to that of mean classification error rate in Figure 3. It is also perceived that subject data with higher classification error rates tend to have longer convergence times.

Figure 5 shows the change of mean classification error rate by changing the frequency band of band-pass filter to theta (4–7 Hz), alpha (8–13 Hz), beta (14–29 Hz), gamma (30–47 Hz), and wide band (4–47 Hz) in the preprocessing step. We use rank 6 for all the frequency bands. On average, better performance was obtained for beta and gamma bands compared with lower bands, that is, theta and alpha bands. The best performance was obtained when wide frequency band was used.

For comparative analysis with other methods, the spatial filters were calculated by CSP using identical preprocessed data. Since the proposed method used rank 6 constraint for analysis, six CSP filters were used for the alternative

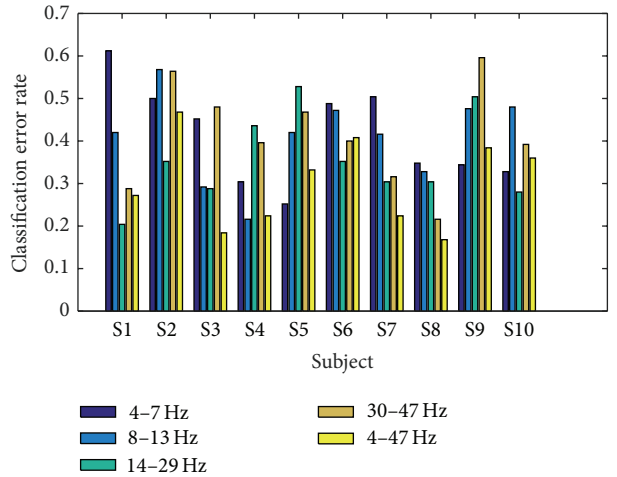


Figure 5: Classification error rate for different frequency bands of band-pass filter.

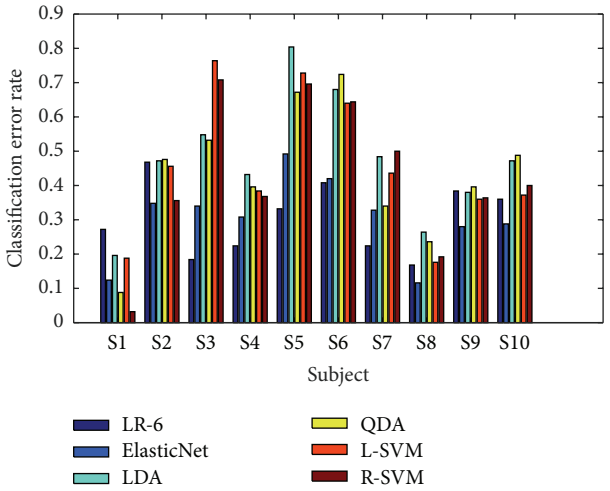


Figure 6: Comparative analysis of classification error rate to fix different methods; the proposed method with low-rank 6 (LR-6), elastic net (ElasticNet), linear discriminant analysis (LDA), quadratic discriminant analysis (QDA), linear SVM (L-SVM), and SVM with RBF kernel (R-SVM).

Table 1: Comparative results of classification error rate. LR-6 specifies the proposed method with rank 6 constraint. In the leftmost column, avg. and std. var. specify mean and standard deviation of classification error rate over folds and subjects.

| | LR-6 | ElasticNet | LDA | QDA | L-SVM | R-SVM |
|---|---|---|---|---|---|---|
| Avg. | 0.302 | 0.304 | 0.473 | 0.435 | 0.450 | 0.426 |
| Std. var. | 0.103 | 0.116 | 0.179 | 0.190 | 0.204 | 0.218 |

methods. CSP filters were selected automatically by three eigenvectors with the highest/lowest eigenvalues. We performed fivefold cross-validation with different classification algorithms, namely, ElasticNet, LDA, QDA, linear SVM (L-SVM), and SVM with RBF kernel (R-SVM). For all methods, we used identical feature vectors by employing selected CSP filters. Note that, for each round, the spatial filters were recalculated using only the training data.

Figure 6 describes subjectwise comparison of the mean classification error rates of the proposed method with rank 6 constraint (LR-6) and the six conventional methods with CSP. Except subject "S1," the proposed method achieved better or comparative results compared with the other methods.

Table 1 describes the comparison results. The classification error rates were obtained by averaging over subjects. The proposed method outperforms CSP-based LDA, QDA, L-SVM, and R-SVM methods and shows comparative performance against ElasticNet, the state-of-the-art method.

*5.1. Discussion.* If all the 23 subjects' data are used for analysis, the mean classification error rate was dropped from 0.302 (±0.103) to 0.412 (±0.131) when using the proposed method (LR-6). This is because the results of excluded subjects show below or just above chance level. The degradation of these results was common irrespective of methods including conventional methods. Therefore, these subjects data were deemed untrustworthy, so we manually select ten subjects for the analysis. The training/test data are non-i.i.d. because of the sliding window approach; that is, there are temporal correlations among neighboring data. But our assumption is that even if i.i.d. assumptions are violated, the proposed method would work well in practice.

The low-rank constrained linear model in (7) can be transformed as follows:

$$f = b + \langle \Theta, \Sigma \rangle \tag{15}$$

$$= b + \sum_{i=1}^{c} \sigma_i \operatorname{Tr}\left(v_i u_i^T X X^T\right) \tag{16}$$

$$= b + \sum_{i=1}^{c} \sigma_i \left(u_i^T X X^T v_i\right). \tag{17}$$

The last equation indicates that the spatial filters, $\{u_i\}_{i=1}^{c}$ and $\{v_i\}_{i=1}^{c}$, are applied to the covariant matrix of $X$ from left and right, and the inner product of the spatially filtered signals is used to form the feature vector. The weighting coefficients of the feature vector correspond to singular values $\{\sigma_i\}_{i=1}^{c}$. Note that spatial filters $u_i$ and $v_i$ are almost identical, possibly with different signs, due to the nature of the original linear model denoted by (7). Hence, it corresponds to computing the power of spatially filtered signals, similarly to CSP-based methods.

The topographies in Figure 7 represent the scalp maps of six representative spatial filters, which are obtained by $k$-mean clustering of estimated spatial filters for all subjects as shown in Figure 12. The spatial filters are defined by the left singular vectors of $\Theta$. The color of topography is mapped from +0.5 (red) to −0.5 (blue).

Figure 8 shows the difference of mean spectral power density (PSD) between positive and negative over all subjects. The mean PSD is calculated by averaging PSDs of all spatially filtered signals by using six spatial filters estimated over all subjects. Hence the mean PSD represents total average PSD of spatially filtered EEG signals. The dotted plots show the deviation from the mean. From this figure, we can observe that positive tends to have larger power than negative especially over beta and gamma frequency bands.

*5.2. Valence versus Neutral.* In order to further examine the differences between positive/negative valence and neutral, two-way binary classifications were conducted for positive versus neutral and negative versus neutral. For the analysis, we employed the proposed method with rank 6 constraint as described above for positive versus negative analysis. The preprocessing is exactly the same as before except for training/test data which is relevant to the target two classes. The data were band-pass filtered at 4–47 Hz.

Figure 9 describes the classification error rates of the two cases: positive versus neutral and negative versus neutral for the same subjects as before. The mean and std. variation of classification errors were as follows: positive versus neutral (0.483 ± 0.131) and negative versus neutral (0.384 ± 0.119).

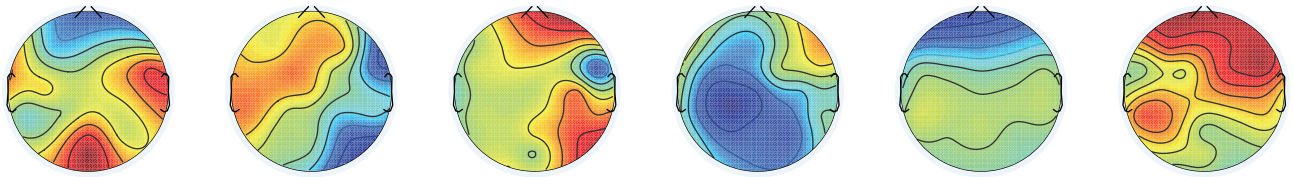

Figure 7: (Positive versus negative) topographies of six significant spatial filters obtained by $k$-mean clustering of all spatial filters estimated for all subjects by using rank 6 constraint. The color is mapped from −0.5 (blue) to +0.5 (red).

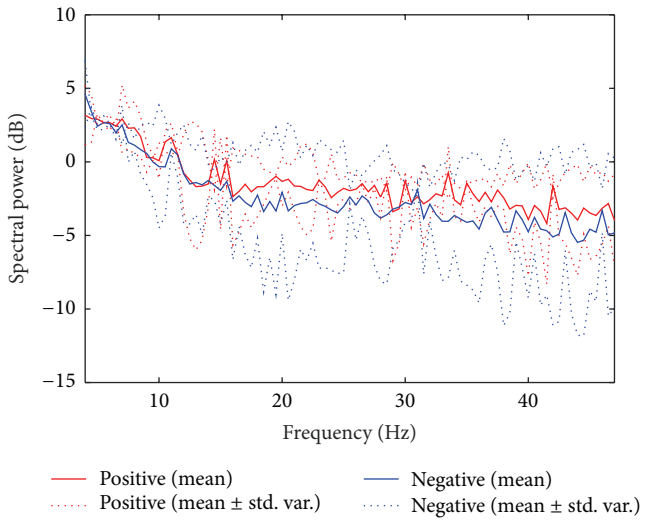


Figure 8: Comparison of mean PSDs between positive and negative. The mean PSD is calculated over all spatially filtered channels and subjects.

From this result, we notice that subjects with high classification performance for positive versus neutral case tend to have low performance for negative versus neutral case.

Figure 10 shows the scalp maps of six representative spatial filters for (a) positive versus neutral and (b) negative versus neutral, which are obtained by $k$-mean clustering of estimated spatial filters as described for Figure 7. Figures 13 and 14 show the estimated spatial filters for all subjects for positive versus neutral and negative versus neutral, respectively.

As we described in Section 2, many researches suggest that hemispherical asymmetry over the frontal cortex is implicated for emotions and motivations. If the assumption is true, our hypothesis is that the scalp maps of estimated spatial filters for valence versus neutral will likely show asymmetrical patterns over the frontal lobe, as such spatial filters should increase inference accuracy.

Among the topographies in Figure 10, about half of them do show asymmetrical patterns over the frontal and left/right temporal lobe area. It is difficult but slightly observable that left or right lateralization corresponds to positive or negative valence as indicated by previous works [6, 7].

Figures 11(a) and 11(b) show the difference of mean PSD between positive/negative and neutral over all spatially filtered channels and subjects. The mean PSD is obtained similarly as positive versus negative case as shown in Figure 8.

From these figures, we can observe that positive has larger power than neutral in beta and gamma bands. On the other hand, negative has similar or slightly lower power than neutral in those bands.

## 6. Conclusion

In this paper, a fixed low-rank spatial filter estimation for BCI systems was proposed with an application of emotion recognition induced by movies. The proposed approach unifies such tasks as feature extraction, feature selection, and classification, which are often independently tackled in a "bottom-up" manner, under a regularized loss minimization problem. We explicitly derived the loss function from the conventional BCI approach and solved its minimization by optimization with a nonconvex fixed low-rank constraint.

The proposed method derived from "top-down" approach incorporates spatial filter estimation in the predictive model. Hence by focusing on the prediction performance with suitably chosen regularizer, such as fixed low-rank in our model, it induces sparse decomposition of the signal which corresponds to conventional feature extraction. Hence, it implicitly estimates optimal spatial filters of the best inference model under the assumption. The result of comparative analysis shows that the proposed method is competitive and has equivalent performance to the best CSP-based alternative.

In the discussion, we show that about half of the significant scalp maps of spatial filters estimated for positive versus negative do show asymmetrical patterns over the frontal and temporal lobe, which agree with the previous research works; that is, asymmetrical patterns over frontal cortex are implicated for emotions and motivations. We also observe that positive state tends to exhibit larger power than negative state over beta and gamma frequency bands. The opposite lateralization of hemispherical activity is weakly admitted for positive and negative cases.

There are some directions for future work and some suggestions for improving performance. First, extending the proposed method to multiclass classification is required to recognize variety of emotional states. Second, source space analysis might be useful to further investigate subcortical activities of emotions. Lastly, obtaining genuine training/test data is of primal importance especially for BCIs depending on interoceptive inputs like thoughts and emotions. One

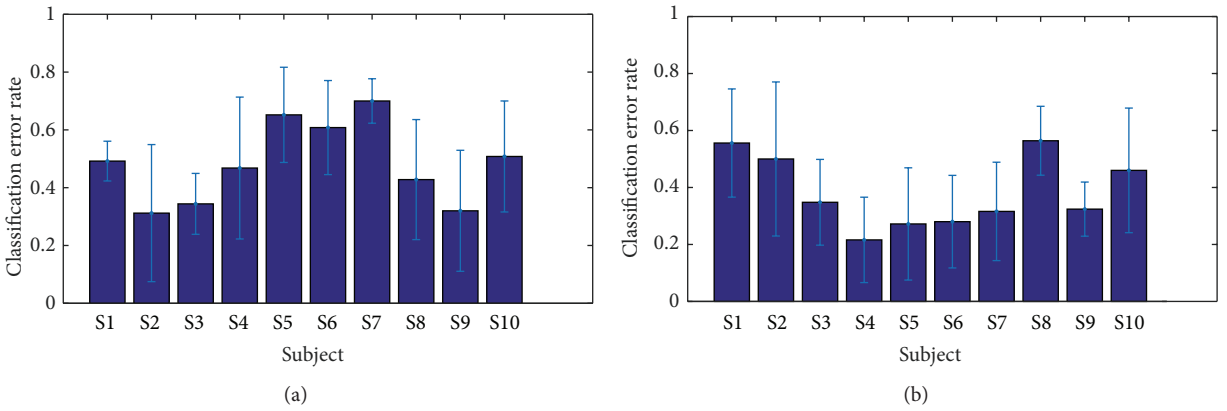


Figure 9: The figures show binary classification error rate of ten subjects in two cases: (a) positive versus neutral and (b) negative versus neutral. Mean classification error rates are (a) 0.483 ± 0.131 and (b) 0.384 ± 0.119.

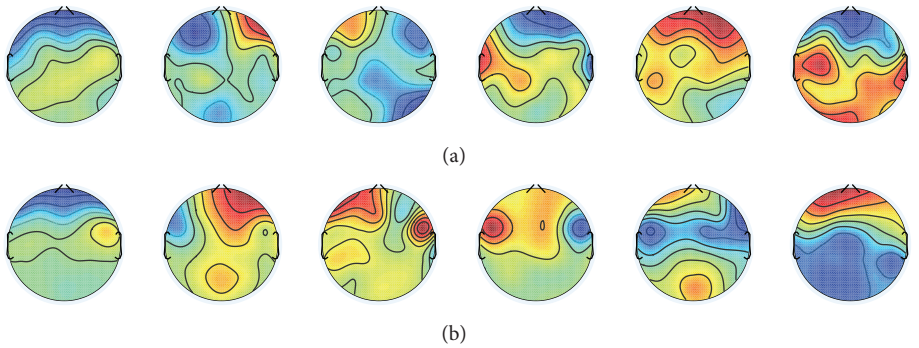


Figure 10: Topographies of six significant spatial filters obtained by $k$-mean clustering of all spatial filters estimated for all subjects by using rank 6 constraint. The color is mapped from −0.5 (blue) to +0.5 (red). (a) Positive versus neutral and (b) negative versus neutral.

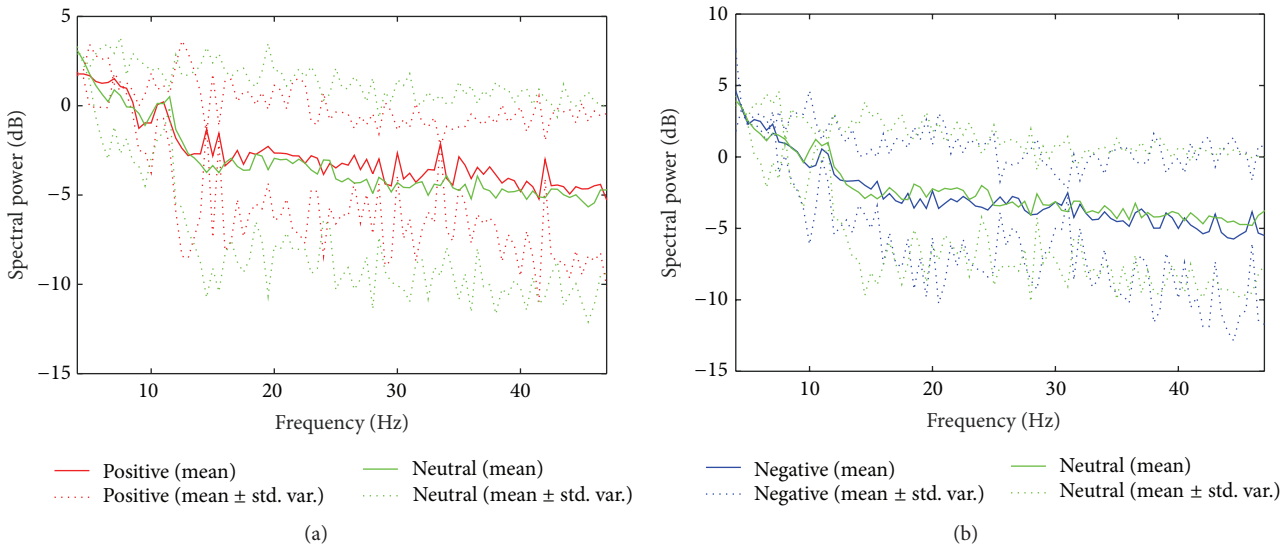


Figure 11: Comparison of mean PSDs between valence and neutral. The mean PSD is calculated over all spatially filtered channels and subjects. (a) Positive versus neutral and (b) negative versus neutral.

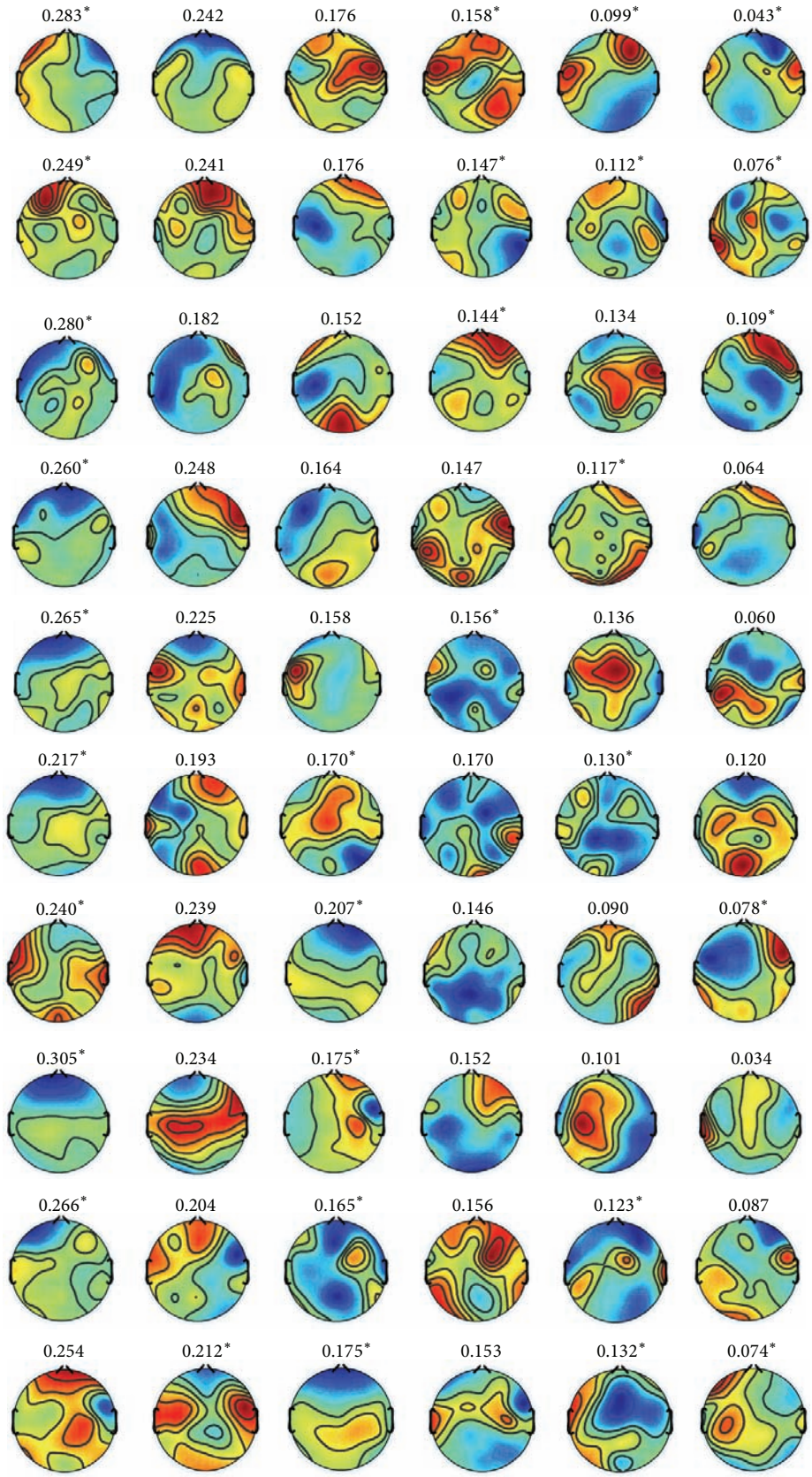


Figure 12: (Positive versus negative) scalp maps of spatial filters obtained by the proposed method with rank 6 constraint for all subjects. The row specifies subjects "S1"–"S10" from top to bottom. The column specifies six spatial filters defined by left singular vectors of $\Theta$ corresponding to the highest six eigenvalues from left to right. The number above each topography is the percentile of corresponding singular value. The superscript $(*)$ indicates that the pair of left and right singular vectors differs in sign.

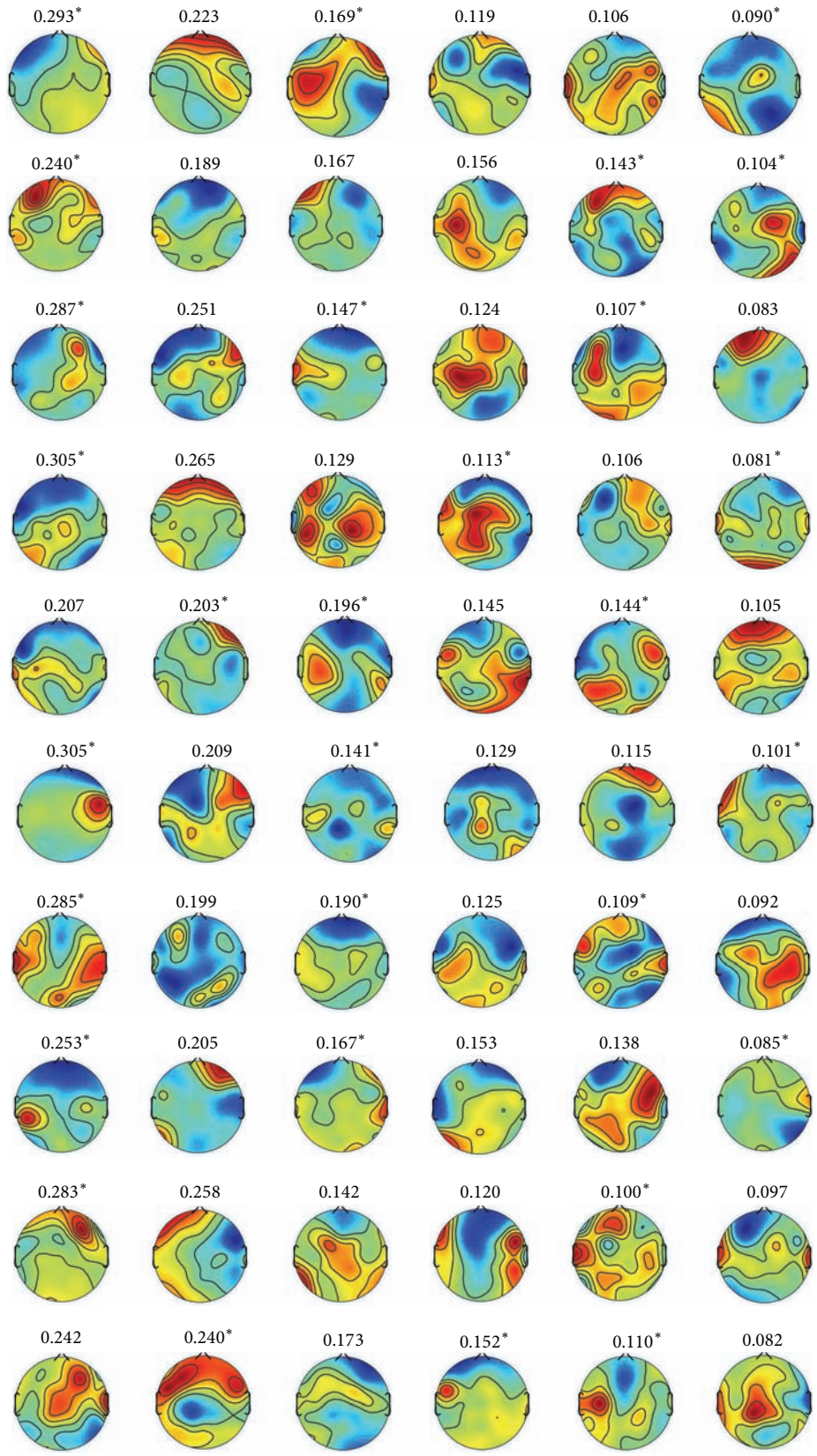


Figure 13: (Positive versus neutral) scalp maps of spatial filters obtained by the proposed method with rank 6 constraint for all subjects. The row specifies subjects "S1"–"S10" from top to bottom. The column specifies six spatial filters defined by left singular vectors of $\Theta$ corresponding to the highest six eigenvalues from left to right. The number above each topography is the percentile of corresponding singular value. The superscript $(*)$ indicates that the pair of left and right singular vectors differs in sign.

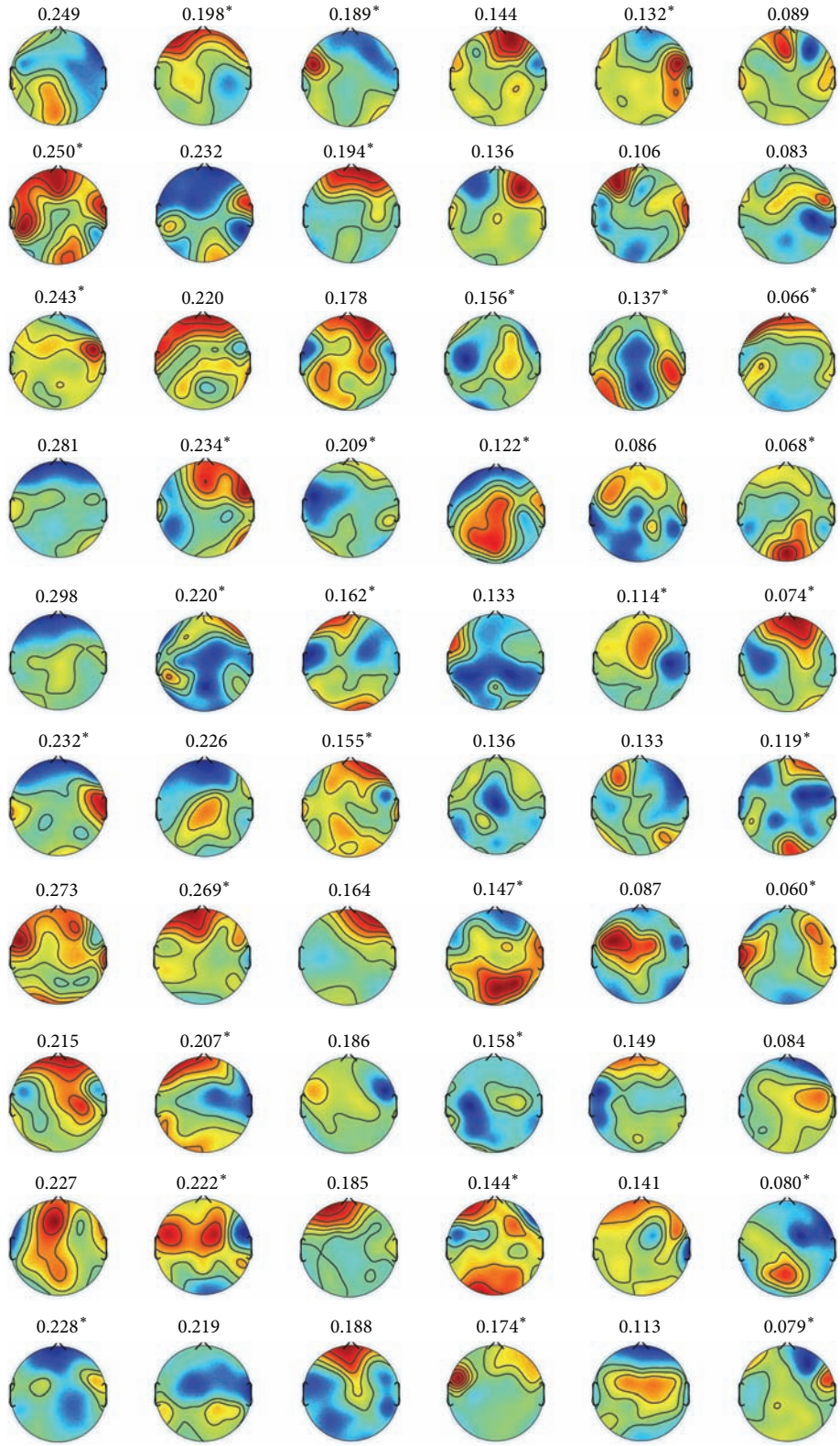


FIGURE 14: (Negative versus neutral) scalp maps of spatial filters obtained by the proposed method with rank 6 constraint for all subjects. The row specifies subjects "S1"–"S10" from top to bottom. The column specifies six spatial filters defined by left singular vectors of $\Theta$ corresponding to the highest six eigenvalues from left to right. The number above each topography is the percentile of corresponding singular value. The superscript $(*)$ indicates that the pair of left and right singular vectors differs in sign.

possible solution is to evaluate labels based on ratings of participants.

## Competing Interests

The authors declare that they have no competing interests.

## Acknowledgments

This research was supported by the ImPACT Program of Council for Science, Technology and Innovation, Japan. The authors wish to thank Dr. Motoaki Kawanabe for the valuable comments and appreciate Dr. Takeshi Ogawa and Dr. Hiroki Moriya for the experimental setup.

## References

[1] B. Blankertz, R. Tomioka, S. Lemm, M. Kawanabe, and K.-R. Müller, "Optimizing spatial filters for robust EEG single-trial analysis," *IEEE Signal Processing Magazine*, vol. 25, no. 1, pp. 41–56, 2008.

[2] R. Tomioka and K.-R. Müller, "A regularized discriminative framework for EEG analysis with application to brain-computer interface," *NeuroImage*, vol. 49, no. 1, pp. 415–432, 2010.

[3] X.-W. Wang, D. Nie, and B.-L. Lu, "Emotional state classification from EEG data using machine learning approach," *Neurocomputing*, vol. 129, pp. 94–106, 2014.

[4] I. Daly, A. Malik, F. Hwang et al., "Neural correlates of emotional responses to music: an EEG study," *Neuroscience Letters*, vol. 573, pp. 52–57, 2014.

[5] E. R. Kandel, J. H. Schwartz, and T. M. Jessell, *Principles of Neural Science*, McGraw-Hill, New York, NY, USA, 2000.

[6] E. Harmon-Jones, "Clarifying the emotive functions of asymmetrical frontal cortical activity," *Psychophysiology*, vol. 40, no. 6, pp. 838–848, 2003.

[7] R. J. Davidson and N. A. Fox, "Asymmetrical brain activity discriminates between positive and negative affective stimuli in human infants," *Science*, vol. 218, no. 4578, pp. 1235–1237, 1982.

[8] F. Lotte and C. Guan, "Regularizing common spatial patterns to improve BCI designs: unified theory and new algorithms," *IEEE Transactions on Biomedical Engineering*, vol. 58, no. 2, pp. 355–362, 2011.

[9] S. Boyd, N. Parikh, E. Chu, B. Peleato, and J. Eckstein, "Distributed optimization and statistical learning via the alternating direction method of multipliers," *Foundations and Trends in Machine Learning*, vol. 3, no. 1, pp. 1–122, 2011.

[10] A. C. Samson, S. D. Kreibig, B. Soderstrom, A. A. Wade, and J. J. Gross, "Eliciting positive, negative and mixed emotional states: a film library for affective scientists," *Cognition and Emotion*, vol. 30, no. 5, 2015.

[11] G. Gómez-Herrero, W. De Clercq, H. Anwar et al., "Automatic removal of ocular artifacts in the EEG without an EOG reference channel," in *Proceedings of the 7th Nordic Signal Processing Symposium (NORSIG '06)*, pp. 130–133, IEEE, Rejkjavik, Iceland, June 2006.

Hindawi Publishing Corporation
Computational Intelligence and Neuroscience
Volume 2016, Article ID 2714052, 8 pages
http://dx.doi.org/10.1155/2016/2714052

*Research Article*

# Macroscopic Neural Oscillation during Skilled Reaching Movements in Humans

**Hong Gi Yeom,[1] June Sic Kim,[2] and Chun Kee Chung[1,2,3]**

[1]*Interdisciplinary Program in Neuroscience, Seoul National University, Seoul 151-742, Republic of Korea*
[2]*Department of Brain and Cognitive Sciences, College of Natural Sciences, Seoul National University, Seoul 151-742, Republic of Korea*
[3]*Department of Neurosurgery, Seoul National University Hospital, Seoul 110-744, Republic of Korea*

Correspondence should be addressed to June Sic Kim; jskim@hbf.re.kr

Received 25 March 2016; Revised 26 May 2016; Accepted 20 June 2016

Academic Editor: Victor H. C. de Albuquerque



The neural mechanism of skilled movements, such as reaching, has been considered to differ from that of rhythmic movement such as locomotion. It is generally thought that skilled movements are consciously controlled by the brain, while rhythmic movements are usually controlled autonomously by the spinal cord and brain stem. However, several studies in recent decades have suggested that neural networks in the spinal cord may also be involved in the generation of skilled movements. Moreover, a recent study revealed that neural activities in the motor cortex exhibit rhythmic oscillations corresponding to movement frequency during reaching movements as rhythmic movements. However, whether the oscillations are generated in the spinal cord or the cortical circuit in the motor cortex causes the oscillations is unclear. If the spinal cord is involved in the skilled movements, then similar rhythmic oscillations with time delays should be found in macroscopic neural activity. We measured whole-brain MEG signals during reaching. The MEG signals were analyzed using a dynamical analysis method. We found that rhythmic oscillations with time delays occur in all subjects during reaching movements. The results suggest that the corticospinal system is involved in the generation and control of the skilled movements as rhythmic movements.

## 1. Introduction

The neural mechanism of skilled movements has been considered to differ from that of rhythmic movement [1]. Skilled movements, such as reaching and grasping, are nonperiodic and are consciously controlled by the brain, while rhythmic movements such as locomotion are repetitive and stereotypical. Although rhythmic movements can be controlled voluntarily, these movements are usually controlled autonomously by the spinal cord and brain stem. A central pattern generator (CPG) in the spinal cord produces periodic oscillatory patterns [1, 2]. The CPG has been considered to be associated with the control of rhythmic movement [3–5].

However, it has been suggested that not only the cortical circuit but also the neural networks in the spinal cord may be involved in skilled movements [6–12]. Moreover, Rokni and Sompolinsky demonstrated that various natural movements can be generated by the linear summation of simple oscillatory components [13]. When considering Fourier theory, it is reasonable to presume that all of the complicated signals can be approximated by the linear summation of sine and cosine signals [14]. The suggestion of generating the various movements from simple components also corresponds to the perspective of dynamic systems, suggesting that most neural activity in the motor cortex will be internal processes that drive desired movements [15]. A recent study reported an important phenomenon. The study, based on neural dynamical analysis, demonstrated that rhythmic oscillations corresponding to the movement frequency also occur during skilled reaching movements [16] as rhythmic movements [16–19]. This implies that diverse skilled movements can be generated via CPG, similar to the neural mechanism of rhythmic movements.

However, in the previous study, a very small motor area in a monkey was measured at a microscopic level. Therefore, whether the rhythmic oscillations are generated in CPG or the cortical circuit in the motor cortex causes the oscillations is unclear. Moreover, the occurrence of the rhythmic

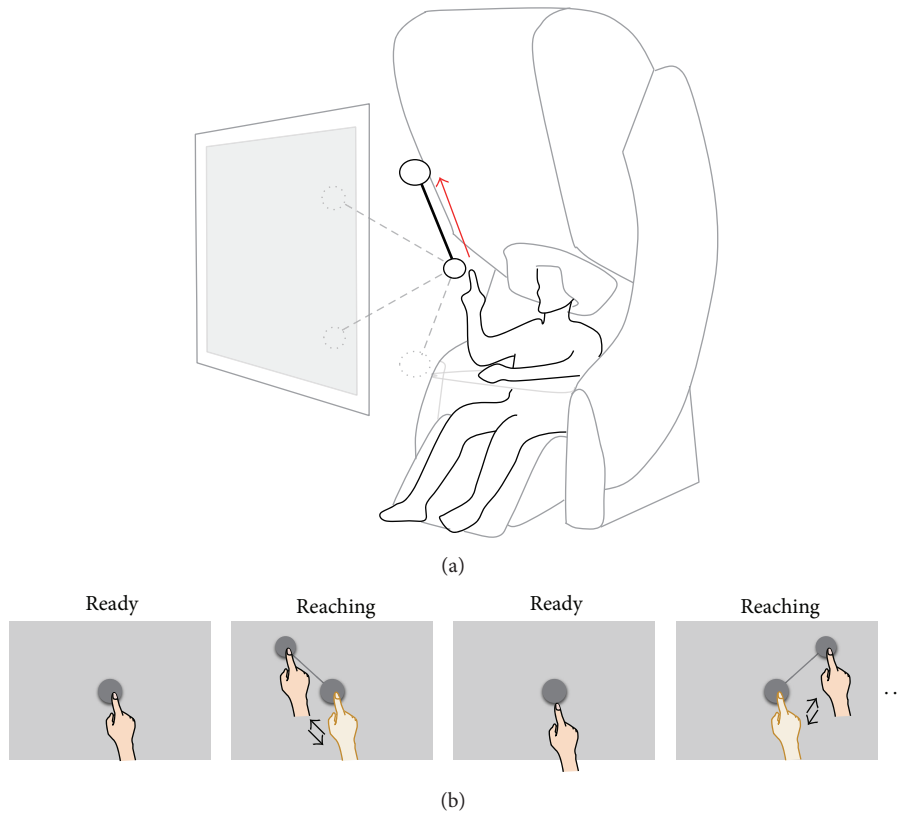


Figure 1: Experiment paradigm. (a) Illustration of the virtual visual stimuli and MEG acquisition system. MEG signals and hand positions were recorded simultaneously during reaching movements. Subjects were instructed to perform a center-out reaching task according to stereographic images on a screen. The target sphere appeared randomly on one of the four corners (upper-left, upper-right, bottom-left, and bottom-right). The red arrow illustrates the example of the reaching movements when the target is shown at the upper-left. (b) Drawings showing the sequence of visual stimuli and instructed behaviors. At the beginning of the experiments, a sphere was shown on the center of the screen. After 4 s, the target was presented for 1 s on one of the four corners. During this time, the subjects were instructed to shift their index finger from the center to the target and return to the center according to the connecting line by moving their right arm as fast as possible. This sequence was repeated during the experiments.

oscillations corresponding to the movement frequency has not been confirmed in humans.

Various pathways connect the cortex and spinal cord. The direct corticomotoneuronal (CM) pathway connects the motor cortex to spinal motoneurons. Indirect pathways might connect other sensorimotor cortices, such as the premotor (PM), supplementary (SMA), cingulate (CMA), and primary somatosensory (S1) areas, to the spinal cord [20]. Therefore, if the rhythmic oscillations occur from the spinal cord and are delivered to the broad motor-related cortex, similar rhythmic oscillations with time delays should be found in macroscopic neural activity (Figures 3(a) and 3(b)). Here, we examine whether similar rhythmic oscillations with time delays are exhibited in macroscopic neural activity during reaching movements in humans. To investigate neural activity, we measured whole-brain MEG signals during reaching movements. We analyze the MEG signals using an analysis method, j principle component analysis (jPCA), where j implies an imaginary part in a complex conjugate. The method reveals the dynamical characteristics of the neural activity [16]. If there are similar oscillatory patterns with time delay, the projections of the oscillations onto the jPC planes will be rotated. Therefore, we can easily investigate whether similar rhythmic oscillations occur or not by examining the projections. Moreover, the results will indicate whether the rhythmic oscillations occur from spinal cords or not.

## 2. Materials and Methods

*2.1. Experiment and Data Acquisition.* Nine healthy subjects (age: 19–37 years; five males and four females) participated in the experiment. All subjects were right-handed (Edinburgh Handedness Inventory scores were above 80). A 306-channel whole-head MEG system (VectorView™, Elekta Neuromag Oy, Helsinki, Finland) was used to measure neural activity during reaching movements (Figure 1(a)). The MEG system has 306 sensors grouped in triplets consisting of 2 planar gradiometers and 1 magnetometer distributed at 102 locations. To record arm position, a three-axis accelerometer (KXM52, Kionix, NY, USA) was attached to the index finger of the right hand using the Velcro band. The accelerometer signals were

recorded simultaneously with the MEG signals. The sampling frequency of the MEG and the accelerometer signals was 600.615 Hz. The experiment was approved by the Institutional Review Board of the Seoul National University Hospital (IRB number 1105-095-363). Subjects were instructed to perform a center-out reaching task according to stereographic images on a screen. To minimize movement artifacts, a cushion was placed under the subject's elbow during the experiment.

At the beginning of the experiments, a sphere was shown on the center of the screen for 4 s and a target sphere with a stick connecting it to the center sphere was presented on one corner for 1 s. The target sphere appeared randomly on one of the four corners (upper-left, upper-right, bottom-left, and bottom-right). During this time, the subjects were instructed to shift their index finger from the center to the target and return to the center according to the connecting line by moving their right arm as fast as possible (Figure 1(b)). This sequence was repeated during the experiments. For each subject, 60 trials were measured for each direction. The distances from the center to the target were ~20 cm. Because we used stereographic images to represent the target, the distance measurement was not accurate. The distances from the center to the target were identical in all subjects. Because the directions of the target were randomly presented, we did not consider the variation of the intertrial interval for habituation effects. Although the reaction times were slightly different (see Section 3), there is no strange trial. Further details are also described elsewhere [21, 22].

*2.2. Signal Preprocessing.* The MEG equipment measures the changes of a magnetic field. Therefore, it is influenced by external signals, such as line noise, and biological artifacts, such as cardiac and muscle activity. To reduce the noise in the MEG signals, the spatiotemporal signal space separation (tSSS) method was applied [23]. The tSSS separates external interference signals of the brain by spatiotemporal methods and eliminates the interference. All data processing was performed using MATLAB 2008b (Mathworks, Natick, MA, USA). We used 204 gradiometer signals among the 306 channels for data analysis because the characteristics of the gradiometer and magnetometer sensors differ and the signal-to-noise ratio (SNR) of the gradiometers is better than that of the magnetometers [24]. The MEG signals were band-pass filtered between 0.5 and 8 Hz. The filtering band was determined by time-frequency analysis based on our previous study [21]. The MEG signals of the frequency band represent the characteristics of reaching movements [21]. To minimize artifacts, independent component analysis (ICA) was applied, which is implemented in EEGLAB [25]. Artifacts such as EOG were removed by eliminating the artifact components. The signals were segmented from −1 to 2 s after the cue onset. After the segmentation, the MEG signals were averaged by trials. The averaged MEG signals were downsampled to 50 Hz. jPCA was applied to the preprocessed signals. The process of the analysis is explained in the next section and in Figure 2.

*2.3. Dynamical Analysis jPCA.* Neural networks in the brain consist of billions of neurons. Although the activities of some neurons in the motor cortex will reflect movement parameters, most neural activities will be an internal process to generate the motor commands [15]. Therefore, the signals are difficult to analyze because the patterns of neural activity are various and complex. To investigate the neural process, a dynamical analysis method, jPCA, was proposed [16]. jPCA describes the dynamical relationship between current and subsequent neural activities on a low-dimensional plane. It represents the dynamic relationship with rotation according to the time flow. If there are consistent phase-differences between neural activities, the projections on the jPC planes will be rotated; however, if there is no consistent change, meaningless small movements will be shown. Moreover, if the sign of the phase-difference changes, the projections will be rotated in the opposite direction. This reveals the change in the dynamic relationship between the current and subsequent neural activities. jPCA is an intuitive method of analyzing the dynamic characteristics of neural activities. jPCA finds informative planes and projects the neural data onto the planes. The projected neural data represents the rotational structure in the data.

The relationship between the current and next neural activities can be expressed as follows:

$$\dot{X} = MX, \tag{1}$$

where $X$ is a matrix of size $n \times ct$ describing the neural activities. The preprocessed MEG signals as described in Section 2.2 were applied to jPCA as $X$. $n$ is the number of MEG channels ($n = 204$). $c$ is the number of conditions ($c = 4$), and $t$ is the number of time points ($t = 151$). $\dot{X}$ is a derivative of $X$ and $M$ represents the relationship between the neural activity and its derivative.

jPCA applies the traditional principal component analysis (PCA) to reduce the dimensionality of $X$ from $n \times ct$ to $k \times ct$ ($k = 6$). The reduced neural activity will be expressed as $X_{\text{red}}$. Equation (1) can be represented as follows:

$$\dot{X}_{\text{red}} = MX_{\text{red}}. \tag{2}$$

$M$ can be calculated by linear regression. $M$ is a combination of symmetric transformation and skew transformation. $M$ can be divided as follows:

$$M = M_{\text{symm}} + M_{\text{skew}}, \tag{3}$$

where $M_{\text{symm}}$ and $M_{\text{skew}}$ are defined as $M_{\text{symm}} = (M + M^T)/2$ and $M_{\text{skew}} = (M - M^T)/2$.

Equation (2) can be expressed as follows:

$$\dot{X}_{\text{red}} = M_{\text{skew}}X_{\text{red}}. \tag{4}$$

Because $M_{\text{skew}}$ has imaginary eigenvalues, it captures the rotational dynamics of neural activity. To express complex eigenvectors $V_1$ and $V_2$ of $M_{\text{skew}}$ on a real plane, the jPC can be defined as $\text{jPC}_1 = V_1 + V_2$ and $\text{jPC}_2 = \text{j}(V_1 - V_2)$.

The projection onto the jPC can be calculated as $X_{\text{jPCA}} = (\text{jPC}_1; \text{jPC}_2) \times X_{\text{red}}$. Further details are provided in [16].

Our results show the projections on one on each jPC (Figure 3(d)) or on the two-dimensional space of $\text{jPC}_1$ and $\text{jPC}_2$ (Figure 4).

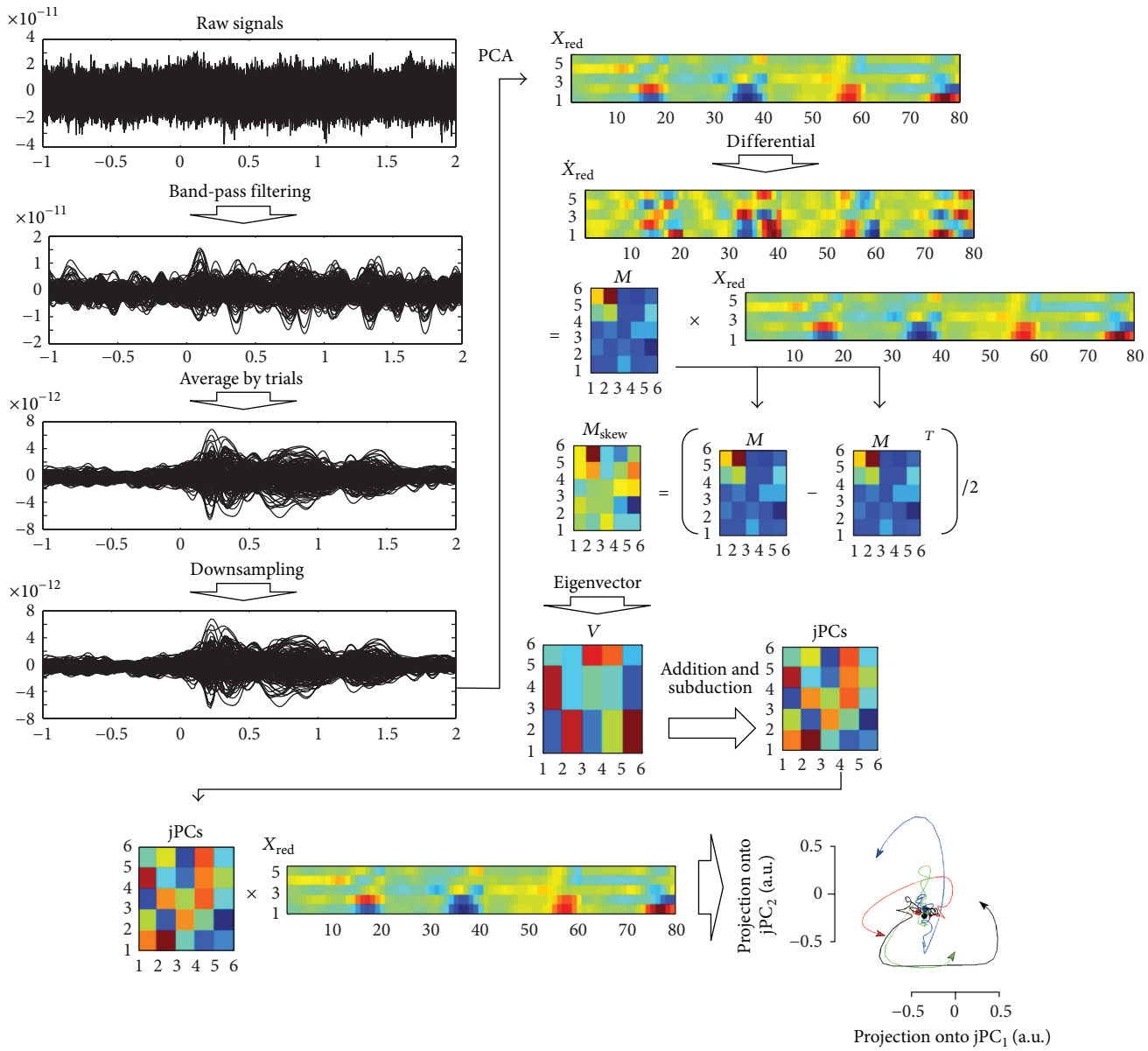


FIGURE 2: Signal process of jPCA analysis. The segmented MEG signals from 1-2 s before the cue onset were band-pass filtered between 0.5 and 8 Hz. After filtering, the MEG signals were averaged by trials. The averaged MEG signals were downsampled at 20 ms. Matrices $M$ and $M_{skew}$ were calculated from downsampled signals. The eigenvectors of $M_{skew}$ produced jPCs. Projections on the jPC plane were illustrated by multiplying jPCs and $X_{red}$.

## 3. Results

Figure 3 shows a simple rhythmic oscillation model that draws a circle on jPC planes and results from jPCA. To draw a circle on jPC planes as in Figure 3(c), the rhythmic oscillations of jPC$_1$ and jPC$_2$ should have a similar pattern. Moreover, the time difference between oscillations should be consistent as in Figure 3(b). Figure 3(d) illustrates jPCs and root-mean square (RMS) of the accelerometer signals over time. Projections on jPC planes are also shown at 0, 100, 200, 300, 400, and 500 ms in Figure 3(e). The different colors of the signals represent the movements of different directions. 0 ms indicates the stimulus onset time. The average movement onset was 316 ± 58 ms (mean ± standard deviation) from stimulus onset. In contrast, the rhythmic oscillations began at 133±69 ms. We compared the onset times between the movements and the rhythmic oscillations using a paired $t$-test. The onsets differed significantly ($p < 0.001$) between the movements and the rhythmic oscillations. After the presentation of visual stimuli, the rhythmic oscillations of jPCs occurred before arm movements, as shown in Figure 3(d). Projections on jPC planes show clearer results. Before movement onset, the projections of the neural oscillations were rotated.

Figure 4 shows the projections on jPC planes for each subject from −100 to 300 ms after presentation of visual stimuli. The duration corresponds to the time taken for

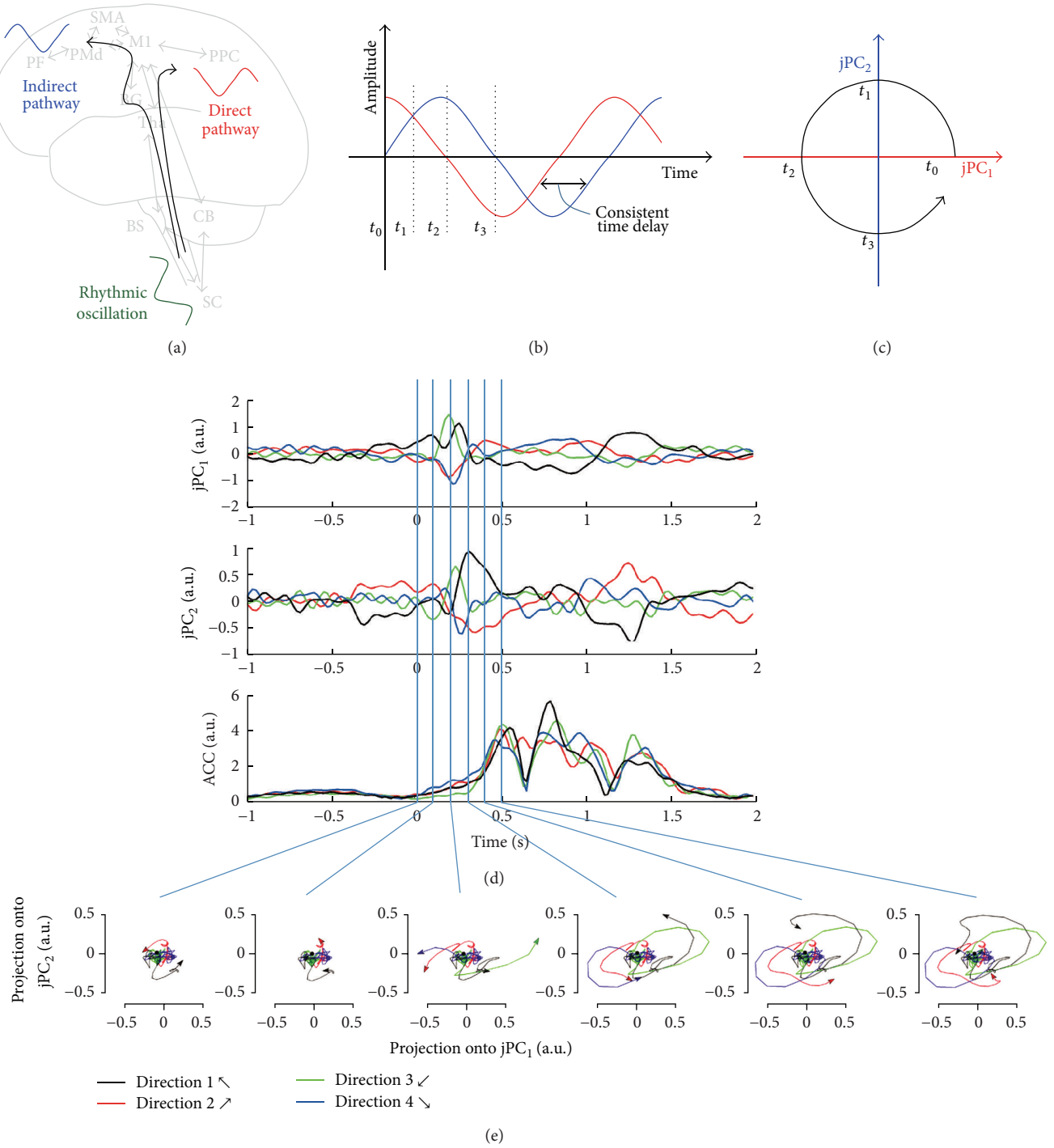


FIGURE 3: Illustration of a simple rhythmic oscillation model to draw a circle on the jPC planes and results of jPCA analysis. (a) Delivery of a rhythmic oscillation to the different area through direct and indirect pathways with different time delays. (b) Oscillations of the different areas with similar patterns and a consistent time delay. (c) Rotation of the oscillations on the jPC planes. (d) jPCs and root-mean squares (RMSs) of accelerometer signals with time. The different-colored signals represent the movements in different directions. 0 ms indicates the stimulus onset time. (e) Projections on the jPC planes are shown at 0, 100, 200, 300, 400, and 500 ms. The projections were rotated prior to movement onset. The results suggest that the oscillations are related not only to movement execution but also to movement preparation.

movement preparation. The projection of the oscillation rotated in the same direction (counterclockwise) for all conditions (reaching different directions) for all subjects. To rotate in the same direction for different conditions, the relation between $jPC_1$ and $jPC_2$ should be invariant irrespective of the movement direction.

Table 1 shows a summary of jPCA. The second row describes the data variance captured by jPC plane. The mean

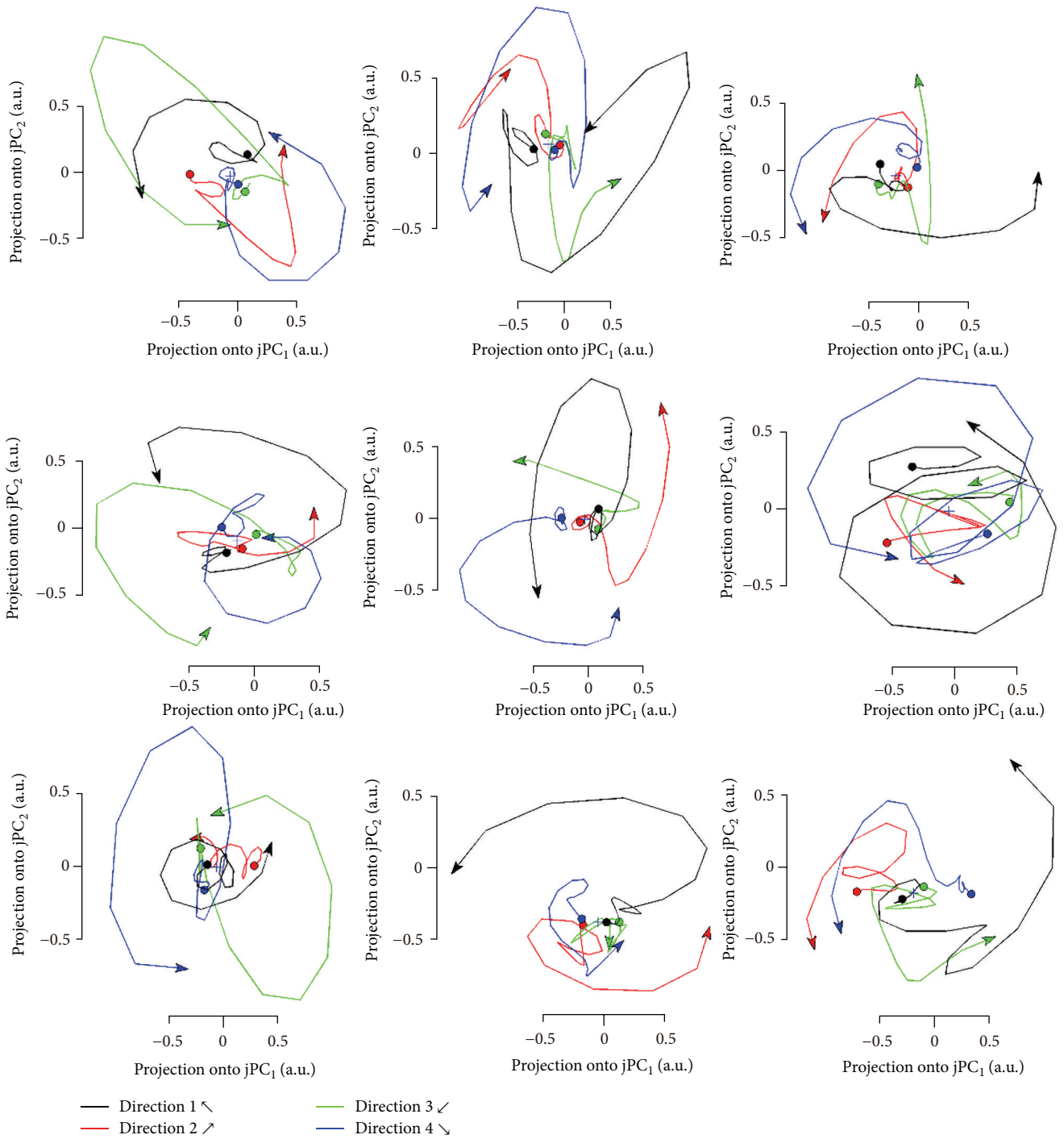


Figure 4: Projections on the jPC planes for all subjects from −100 to 300 ms after presentation of visual stimuli. Each subfigure illustrates the projections from each subject. The different-colored signals represent the movements in different directions. The projection of the oscillation rotated to the same direction (counterclockwise) for all conditions (reaching of different direction) for all subjects. This suggests that the same neural dynamics are involved in reaching movements irrespective of reaching direction.

Table 1: Summary of jPCA. Captured variance, data variance captured by the jPC plane; fit by 2 jPCs, fit quality provided by $M_{skew}$ in the first two jPCs.

| | Sub 1 | Sub 2 | Sub 3 | Sub 4 | Sub 5 | Sub 6 | Sub 7 | Sub 8 | Sub 9 | Mean ± standard deviation |
|---|---|---|---|---|---|---|---|---|---|---|
| Captured variance | 0.226 | 0.382 | 0.180 | 0.212 | 0.190 | 0.231 | 0.242 | 0.243 | 0.212 | 0.235 ± 0.059 |
| Fit by 2 jPCs | 0.164 | 0.226 | 0.157 | 0.168 | 0.245 | 0.250 | 0.237 | 0.401 | 0.271 | 0.235 ± 0.075 |

of the data variance was 0.235 ± 0.059. The third row is fit quality provided by $M_{skew}$, in the first two jPCs. The mean of the fit quality from two jPCs was 0.235 ± 0.075.

## 4. Discussion

In this study, we demonstrated that the neural mechanisms of rhythmic movements and skilled movements are similar. We showed that the corticospinal system is involved in the generation of skilled movements by means of a dynamic analysis of macroscopic neural data. Although our result does not concur with previous knowledge, it supports the suggestion made in recent studies that the spinal cord mediates skilled movements [6–12].

*4.1. Neural Mechanism of Skilled Movements.* It is unclear whether the rhythmic oscillations are generated in the spinal cord or in the motor cortex. We hypothesize that if the rhythmic oscillations are derived by the corticospinal system, oscillations with similar pattern and consistent time delay should be found in macroscopic neural activity (Figures 3(a) and 3(b)). To investigate this hypothesis, we measured and analyzed MEG signals during reaching movements in humans. The results showed that projections on the jPC planes rotated in all subjects (Figure 4). This means that the major components of the neural activity have a similar pattern and consistent time delay. Therefore, it implies the possibility that skilled movements are generated by the corticospinal system. Moreover, the projection of the oscillation rotated in the same direction for all conditions. This suggests that the same neural dynamics are involved in reaching movements, irrespective of reaching direction.

Our perspective corresponds to the suggestion of a common intrinsic structure controlling the reaching movements [16, 26]. When we consider that the cortex also contributes to controlling rhythmic movements [7, 27], the neural mechanisms of rhythmic movements and skilled movements are similar.

Despite numerous studies of a CPG in animals, almost all studies in humans used indirect results [28]. We also did not measure spinal cord activity directly. Therefore, we should be cautious when interpreting the results. Nevertheless, our results provide evidence that the corticospinal system is involved in skilled movement, such as rhythmic movement.

*4.2. Neural Oscillations Involved in Movement Generations.* Iteration of descending motor commands and ascending sensory feedback could be represented by rhythmic patterns. Therefore, the rhythmic oscillations could be considered products generated by sensory feedback, such as kinematic parameter or visual feedback [28–32]. However, our results show that the rhythmic oscillation occurred prior to movement onset (Figures 3(d), 3(e), and 4). Because sensory feedback could not generate the oscillations before the movements, it implies that there is another mechanism of generating the rhythmic oscillations. It has been suggested that neural networks in the spinal cord may also be involved in skilled movements. We hypothesized that if the rhythmic oscillations are made by CPG and delivered to the broad motor-related area through direct and indirect pathways, similar patterns of time delay will be observed at a macroscopic level. We verified our hypothesis using the dynamical analysis method. Therefore, our results suggest that the spinal cord could be involved in the movement generation.

When a subject is aware of a target position in a motor planning task, the reaction time required to reach the target after the go cue was about 240 ms [33]. Because the visual processing requires less than 150 ms [34], and the execution-related time will be about 90 ms. In our experiment, the movement onset time (316 ms) may include the time for visual processing, motor planning, and execution. Therefore, the difference (76 ms) between 316 ms and 240 ms is related to motor planning. Thus, 166 ms (76 + 90 ms) may be required for movement planning and execution. The rhythmic oscillation occurred 183 ms (316 − 133 ms) prior to movement onset, suggesting that the rhythmic oscillations are related to movement generation.

## 5. Conclusions

We showed that neural oscillations occur at a macroscopic level in humans during skilled movements. It seems that a common intrinsic structure generates the oscillations, irrespective of movement direction. The intrinsic structure is involved in not only movement execution but also movement generation. The neural oscillations could be generated in the spinal cord and the oscillations might influence movements by means of corticospinal interaction. This implies that the neural mechanism of skilled movements might be similar to that of rhythmic movements.

## Competing Interests

The authors declare that they have no competing interests.

## Acknowledgments

This study was supported by Grant (NRCTR-EX15002) of the Translational Research Center for Rehabilitation Robots, Korea National Rehabilitation Center, Ministry of Health & Welfare, Korea.

## References

[1] E. R. Kandel, *Principles of Neural Science*, McGraw-Hill, New York, NY, USA, 5th edition, 2013.

[2] K. G. Pearson, "Common principles of motor control in vertebrates and invertebrates," *Annual Review of Neuroscience*, vol. 16, pp. 265–297, 1993.

[3] M. MacKay-Lyons, "Central pattern generation of locomotion: a review of the evidence," *Physical Therapy*, vol. 82, no. 1, pp. 69–83, 2002.

[4] E. Marder and D. Bucher, "Central pattern generators and the control of rhythmic movements," *Current Biology*, vol. 11, no. 23, pp. R986–R996, 2001.

[5] E. Marder and R. L. Calabrese, "Principles of rhythmic motor pattern generation," *Physiological Reviews*, vol. 76, no. 3, pp. 687–717, 1996.

[6] B. Alstermark and T. Isa, "Circuits for skilled reaching and grasping," *Annual Review of Neuroscience*, vol. 35, pp. 559–578, 2012.

[7] T. Drew, S. Prentice, and B. Schepens, "Cortical and brainstem control of locomotion," *Progress in Brain Research*, vol. 143, pp. 251–261, 2004.

[8] A. P. Georgopoulos and S. Grillner, "Visuomotor coordination in reaching and locomotion," *Science*, vol. 245, no. 4923, pp. 1209–1210, 1989.

[9] E. Azim, J. Jiang, B. Alstermark, and T. M. Jessell, "Skilled reaching relies on a V2a propriospinal internal copy circuit," *Nature*, vol. 508, no. 7496, pp. 357–363, 2014.

[10] B. Alstermark, L. G. Pettersson, Y. Nishimura et al., "Motor command for precision grip in the macaque monkey can be mediated by spinal interneurons," *Journal of Neurophysiology*, vol. 106, no. 1, pp. 122–126, 2011.

[11] B. Alstermark, T. Isa, L.-G. Pettersson, and S. Sasaki, "The C3-C4 propriospinal system in the cat and monkey: a spinal pre-motoneuronal centre for voluntary motor control," *Acta Physiologica*, vol. 189, no. 2, pp. 123–140, 2007.

[12] T. Isa, Y. Ohki, B. Alstermark, L.-G. Pettersson, and S. Sasaki, "Direct and indirect cortico-motoneuronal pathways and control of hand/arm movements," *Physiology*, vol. 22, no. 2, pp. 145–153, 2007.

[13] U. Rokni and H. Sompolinsky, "How the brain generates movement," *Neural Computation*, vol. 24, no. 2, pp. 289–331, 2012.

[14] R. N. Bracewell, *The Fourier Transform and Its Applications*, McGraw-Hill, Boston, Mass, USA, 3rd edition, 2000.

[15] K. V. Shenoy, M. Sahani, and M. M. Churchland, "Cortical control of arm movements: a dynamical systems perspective," *Annual Review of Neuroscience*, vol. 36, pp. 337–359, 2013.

[16] M. M. Churchland, J. P. Cunningham, M. T. Kaufman et al., "Neural population dynamics during reaching," *Nature*, vol. 486, no. 7405, pp. 51–56, 2012.

[17] W. B. Kristan Jr. and R. L. Calabrese, "Rhythmic swimming activity in neurones of the isolated nerve cord of the leech," *Journal of Experimental Biology*, vol. 65, no. 3, pp. 643–668, 1976.

[18] K. L. Briggman and W. B. Kristan Jr., "Imaging dedicated and multifunctional neural circuits generating distinct behaviors," *Journal of Neuroscience*, vol. 26, no. 42, pp. 10925–10933, 2006.

[19] K. L. Briggman, H. D. I. Abarbanel, and W. B. Kristan Jr., "Optical imaging of neuronal populations during decision-making," *Science*, vol. 307, no. 5711, pp. 896–901, 2005.

[20] T. Isa, M. Kinoshita, and Y. Nishimura, "Role of direct vs. indirect pathways from the motor cortex to spinal motoneurons in the control of hand dexterity," *Frontiers in Neurology*, vol. 4, article 191, 2013.

[21] H. G. Yeom, J. S. Kim, and C. K. Chung, "Estimation of the velocity and trajectory of three-dimensional reaching movements from non-invasive magnetoencephalography signals," *Journal of Neural Engineering*, vol. 10, no. 2, Article ID 026006, 2013.

[22] H. G. Yeom, J. S. Kim, and C. K. Chung, "Common neural mechanism for reaching movements," in *Proceedings of the 4th International Winter Conference on Brain-Computer Interface (BCI '16)*, pp. 1–3, Gangwon Province, Republic of Korea, Feburary 2016.

[23] S. Taulu and J. Simola, "Spatiotemporal signal space separation method for rejecting nearby interference in MEG measurements," *Physics in Medicine and Biology*, vol. 51, no. 7, pp. 1759–1768, 2006.

[24] M. Hämäläinen, R. Hari, R. J. Ilmoniemi, J. Knuutila, and O. V. Lounasmaa, "Magnetoencephalography—theory, instrumentation, and applications to noninvasive studies of the working human brain," *Reviews of Modern Physics*, vol. 65, no. 2, pp. 413–497, 1993.

[25] A. Delorme and S. Makeig, "EEGLAB: an open source toolbox for analysis of single-trial EEG dynamics including independent component analysis," *Journal of Neuroscience Methods*, vol. 134, no. 1, pp. 9–21, 2004.

[26] T. M. Hall, F. de Carvalho, and A. Jackson, "A common structure underlies low-frequency cortical dynamics in movement, sleep, and sedation," *Neuron*, vol. 83, no. 5, pp. 1185–1199, 2014.

[27] T. Drew, J.-E. Andujar, K. Lajoie, and S. Yakovenko, "Cortical mechanisms involved in visuomotor coordination during precision walking," *Brain Research Reviews*, vol. 57, no. 1, pp. 199–211, 2008.

[28] M. R. Dimitrijevic, Y. Gerasimenko, and M. M. Pinter, "Evidence for a spinal central pattern generator in humans," *Annals of the New York Academy of Sciences*, vol. 860, pp. 360–376, 1998.

[29] K. J. Craik, "Theory of the human operator in control systems; the operator as an engineering system," *The British Journal of Psychology*, vol. 38, no. 2, pp. 56–61, 1947.

[30] R. C. Miall, D. J. Weir, and J. F. Stein, "Manual tracking of visual targets by trained monkeys," *Behavioural Brain Research*, vol. 20, no. 2, pp. 185–201, 1986.

[31] R. C. Miall, D. J. Weir, and J. F. Stein, "Intermittency in human manual tracking tasks," *Journal of Motor Behavior*, vol. 25, no. 1, pp. 53–63, 1993.

[32] R. C. Miall and J. K. Jackson, "Adaptation to visual feedback delays in manual tracking: evidence against the Smith Predictor model of human visually guided action," *Experimental Brain Research*, vol. 172, no. 1, pp. 77–84, 2006.

[33] C. A. Chestek, A. P. Batista, G. Santhanam et al., "Single-neuron stability during repeated reaching in macaque premotor cortex," *The Journal of Neuroscience*, vol. 27, no. 40, pp. 10742–10750, 2007.

[34] S. Thorpe, D. Fize, and C. Marlot, "Speed of processing in the human visual system," *Nature*, vol. 381, no. 6582, pp. 520–522, 1996.

Hindawi Publishing Corporation
Computational Intelligence and Neuroscience
Volume 2016, Article ID 7489108, 10 pages
http://dx.doi.org/10.1155/2016/7489108

*Research Article*

# Comparing the Performance of Popular MEG/EEG Artifact Correction Methods in an Evoked-Response Study

**Niels Trusbak Haumann,[1] Lauri Parkkonen,[2] Marina Kliuchko,[3,4] Peter Vuust,[1] and Elvira Brattico[1]**

[1] *Center for Music in the Brain, Department of Clinical Medicine, Aarhus University and Royal Academy of Music, Aarhus/Aalborg, Nørrebrogade 44, Building 10G, 4th and 5th floor, 8000 Aarhus C, Denmark*
[2] *Department of Neuroscience and Biomedical Engineering, Aalto University School of Science, P.O. Box 12200, 00076 Aalto, Finland*
[3] *Cognitive Brain Research Unit, Institute of Behavioural Sciences, University of Helsinki, P.O. Box 9 (Siltavuorenpenger 1 B), 00014 Helsinki, Finland*
[4] *BioMag Laboratory, HUS Medical Imaging Center, University of Helsinki and Helsinki University Hospital, P.O. Box 340, Hospital District of Helsinki and Uusimaa, 00029 Helsinki, Finland*

Correspondence should be addressed to Niels Trusbak Haumann; niels.haumann@clin.au.dk

Received 29 April 2016; Accepted 23 June 2016

Academic Editor: Victor H. C. de Albuquerque



We here compared results achieved by applying popular methods for reducing artifacts in magnetoencephalography (MEG) and electroencephalography (EEG) recordings of the auditory evoked Mismatch Negativity (MMN) responses in healthy adult subjects. We compared the Signal Space Separation (SSS) and temporal SSS (tSSS) methods for reducing noise from external and nearby sources. Our results showed that tSSS reduces the interference level more reliably than plain SSS, particularly for MEG gradiometers, also for healthy subjects not wearing strongly interfering magnetic material. Therefore, tSSS is recommended over SSS. Furthermore, we found that better artifact correction is achieved by applying Independent Component Analysis (ICA) in comparison to Signal Space Projection (SSP). Although SSP reduces the baseline noise level more than ICA, SSP also significantly reduces the signal—slightly more than it reduces the artifacts interfering with the signal. However, ICA also adds noise, or correction errors, to the waveform when the signal-to-noise ratio (SNR) in the original data is relatively low—in particular to EEG and to MEG magnetometer data. In conclusion, ICA is recommended over SSP, but one should be careful when applying ICA to reduce artifacts on neurophysiological data with relatively low SNR.

## 1. Introduction

Recordings of evoked-responses (also known as event-related potentials, ERPs, or event-related fields, ERFs) with electroencephalography (EEG) or magnetoencephalography (MEG) are widely used methods in cognitive and clinical neuroscience. One of the major challenges in research and clinical applications of evoked-responses is the prevalent strongly interfering electromagnetic signals from external objects and devices in the surrounding MEG or EEG measurement environment as well as nearby mechanical and biological electromagnetic sources originating from the head and other parts of the body of the subject. Since the interfering environmental noise from, for example, laboratory mechanics and electronic devices may be several orders of magnitude stronger than the brain signals of interest (for a review, see, e.g., [1]), it is necessary to remove this noise from the recordings during or after the measurements. Moreover, nonencephalic electromagnetic activity, such as that from the eyes and from the cardiac and facial muscles, is also recorded by EEG or MEG and can be up to a thousand times stronger than the encephalic signal of interest [1]. Since some of these interfering artifactual signals can be synchronous with the brain signal of interest, significant parts of the continuous measurement can be contaminated by artifacts. Hence, to ensure a reliable measurement, it is necessary, in addition to applying an average measure of an evoked-response across

multiple time-locked data segments, also to omit or correct the data contaminated with artifacts.

In the clinical routine, data from patients having a limited control of muscular activity (such as stroke or dementia patients or preterm infants) or with ferromagnetic implants (such as cochlear implantees) typically contain a considerable amount of artifacts. The time constraints of experiments and tests on clinical populations exclude the possibility of a large number of trials that would allow discarding the artefactual ones. A viable alternative to simply rejecting parts of the recorded data is that of correcting the data. Both in clinical patient recordings and in experimental settings with healthy subjects, strong electromagnetic noise from electronic devices, static electricity, and in particular with regard to EEG also the 50/60-Hz power-line noise may interfere significantly with the measurements [2]. When recording EEG in conjunction with transcranial magnetic stimulation (TMS), methods have been developed for reducing the strong TMS artifacts appearing in the recording [3]. In other cases where two neuroimaging modalities are employed simultaneously, special care must also be taken to reduce artifacts originating from the other modality. For recording EEG concurrently with functional magnetic resonance imaging (fMRI), it is necessary to reduce both imaging artifacts caused by the switching gradient fields [4] and ballistocardiogram artifacts caused by the subjects heart beats moving the skin and electrodes in relation to the strong magnetic field within the MRI scanner [5]. Furthermore, in combined EEG/MEG recordings one should be aware that eddy currents in the electrodes induce magnetic fields, which may introduce artifacts in the MEG recordings for signals in higher frequency ranges; however, signals at frequencies below 100 Hz are not critically affected by these types of artifacts [6].

Apart from external artifact sources, it is important to reduce the influence of the internal artifacts originating from the head and the rest of the body of the subject. Typically, MEG and EEG recordings are contaminated by relatively strong artifacts caused by the eyes [2, 7–9]. They can either be eye blinks (picked up mostly by the vertical EOG) contaminating particularly the lower frequencies or be saccades (visible mostly in horizontal EOG) also interfering at higher frequency ranges, where certain saccadic spike artifacts resemble high-frequency muscular artifacts [9]. Another typically interfering internal artifact is due to the electric activity of the cardiac muscle, measured by electrocardiography (ECG or EKG) [2, 10]. Also, noises from different types of muscular activity, seen in electromyographic (EMG) signals, are also a typical issue in MEG and EEG recordings [2, 11]. These muscular artifacts may be caused by mastication (chewing), deglutition (tongue movement), and respiration [2].

Different methods have been developed to reduce the influence of externally and internally originating artifacts. The externally originating interference can be minimized by applying physical shielding techniques in the laboratory [12], by using gradiometer sensors instead of magnetometers, by subtracting measurements of the external noise signals recorded by one or more reference sensors or by applying online or offline spatial filtering methods. MEG systems by Elekta Oy (Helsinki, Finland) comprise both magnetometers and gradiometers and they employ spatial filtering techniques such as Signal Space Projection (SSP) and Signal Space Separation (SSS) and its temporal extension (tSSS) implemented in the Elekta Neuromag® MaxFilter™ software [13]. The SSS method is based on Maxwell equations and the multichannel measurement of the magnetic field distribution; by using a basis comprising spherical harmonic functions, contributions of signal sources within the sensor array (brain signals) can be separated from sources external to the array [13–18]. Since SSS is purely a spatial filter, which only reduces noise originating from the external sources, it retains also those brain signals that oscillate at the same frequency as an external noise source [14]. However, nearby sources of artifacts caused by, for example, movement of magnetic materials, such as dental braces or implants, cannot be sufficiently reduced by applying SSS alone.

The tSSS method is additionally able to filter out interferences from artifactual sources in the space between the brain and the MEG sensor array, by reducing signals in the common subspace through comparisons of the time series in the internal and external spaces. For instance, it has been shown that tSSS makes it possible to locate brain sources on the cortex with beamformer methods in clinical patients, although these patients wore strongly magnetically interfering dental braces; thereby, tSSS seems to allow extending the clinical population compatible with MEG [17].

The internally originating artifacts can be reduced by applying band-pass filtering [19] and component analysis such as Principal Component Analysis (PCA) or Independent Component Analysis (ICA) [20–43] or by recording the artifacts to be removed, identifying their contribution to the data by means of linear regression and subtracting them out [10, 44, 45]. Also, methods for ignoring the artifactual sources have been implemented as part of source analysis algorithms [46, 47]. With regard to the component analysis approaches, PCA is applied to estimate components explaining the highest variance in the data, such as strong artifacts. ICA is able to estimate components that explain variance originating from statistically independent sources, thereby reducing the risk of including signals of interest in the derived artifact components. The ICA algorithms, and, in particular, the infomax version of ICA, have gained popularity as an efficient method for separating the recorded signals into statistically independent components [43]. By inspecting the independent components, only the artifactual components can be rejected to reduce the influence of the artifacts on the data. An alternative method of Signal Space Projection (SSP) has gained some popularity in open source software packages [48, 49]. SSP also decomposes the data into components, often based on a prior PCA; however, in contrast with ICA, these components may not be statistically independent, and therefore there is a risk that artifactual and brain signals of interest may be reduced simultaneously [48].

To investigate the performances and risks of using different popular artifact correction methods, we compared here results achieved by applying SSS, tSSS, ICA, and SSP. We

chose to study the performance of the correction methods on the Mismatch Negativity (MMN) response, which is a well-known evoked-response [50, 51]. In particular, we wanted to investigate (1) whether tSSS improves the data quality in healthy subjects not wearing any magnetically disturbing implants; (2) whether the faster SSS alternative performs as well as the more computationally demanding tSSS; and (3) whether ICA is preferable over SSP (or vice versa) for reduction of typical artifacts in healthy subjects.

## 2. Methods

*2.1. Participants.* A sample of ten volunteers from a larger database named "Tunteet" was chosen (for a description of the experimental protocol, see Kliuchko et al., submitted). The participants were six females and four males. Three participants were nonmusicians, three were amateur musicians, and four were professional musicians. All participants were right-handed, and their average age was 24.8 years (range 18–35 years). Written informed consent was obtained from each participant, and the study was approved by the local ethics committee.

*2.2. Experimental Paradigm.* The participants listened to a melody pattern of 2100 ms, repeated with variations during ~25 minutes. The melody patterns were created from digital piano tones (McGill University Master Samples) and followed the rules of Western tonal music. All melodies started with a triad (300 ms) followed by four single tones (two of 125 ms and two of 300 ms) and an ending tone (575 ms) all separated by 50 ms silent gap. Between all melodies there was a silent gap of 125 ms. Deviations of six types were inserted into the melody patterns to evoke MMN responses to a deviant tone as compared with corresponding unaltered standard. The deviants are explained in Table 1 [52–54].

In total, the tested sample contained 120 brain responses, which comprised the responses to the six standard and six deviant conditions from each of the ten participants.

*2.3. Data Acquisition.* The simultaneous MEG and EEG data were collected at the BioMag Laboratory of the Helsinki University Central Hospital. The measurements were performed in an electrically and magnetically shielded room (ETS-Lindgren Euroshield, Eura, Finland) with Vectorview™ 306-channel MEG system (Elekta Neuromag, Elekta Oy, Helsinki, Finland) equipped with a compatible EEG system. The MEG system had 102 triple-sensor elements, each comprising two orthogonal planar gradiometers and one magnetometer. A 64-channel EEG electrode cap was used. The reference electrode was placed on the nose tip and the ground electrode was on the right cheek. Blinks, as well as vertical and horizontal eye movements, were measured with four electrodes attached above and below the left eye and close to the external eye corners on both sides. Four head position indicator coils were placed on top of the EEG cap. Their positions were determined with respect to the nasion and preauricular points by an Isotrak 3D digitizer (Polhemus, Colchester, VT, USA). MEG and EEG data were recorded with a sample rate of 600 Hz.

During the measurement, subjects were comfortably seated and watched a silenced movie with subtitles. The stimuli were presented with Presentation software (Neurobehavioral Systems, Ltd.). The sound was delivered through a pair of pneumatic headphones at individually adjusted loudness.

*2.4. Artifact Correction.* Elekta Neuromag MaxFilter 2.2 Signal Space Separation (SSS) and temporal Signal Space Separation (tSSS) [13, 16] were applied separately to compare their individual performance. For both SSS and tSSS, we used the default inside expansion order of 8, outside expansion order of 3, automatic optimization of both inside and outside bases, and automatic detection and correction of bad MEG channels. Additionally, for both SSS and tSSS the specific fine calibration and cross talk correction data for the recording site and date were applied. For the tSSS, we used the default subspace correlation limit of 0.980 and raw data buffer length of 10 seconds. The spatially filtered data were saved in 32-bit float format at a sampling rate of 600 Hz.

Correction for internal artifacts with Signal Space Projection (SSP) was performed with the MNE Python version 0.11.0 released with the MNE software version 2.7.4-3485 [55, 56]. We applied the default automatic settings, where two principal components per artifact type are detected for eye artifacts and for cardiac artifacts. Subsequently, the detected ocular and cardiac artifact component projections were removed from the data.

Independent Component Analysis- (ICA-) based correction for internal artifacts was achieved by applying the logistic infomax algorithm implemented in the *runica* function [57] for MATLAB® (MathWorks, Natick, Massachusetts). First, the data were reduced to 64 principal components. The independent components were then estimated for the EEG channels, MEG magnetometers, and MEG planar gradiometers separately. The resulting components were inspected, and one component projection per vertical eye movement, horizontal eye movement, or cardiac artifact type (explaining most variance) was removed from the data, when the artifact component was observed. On average, the total number of observed artifact components per subject was 1.7 (1-2) for the EEG, 1.8 (1–3) for the MEG magnetometers, and 2.0 (1–3) for the MEG gradiometers.

*2.5. Data Analysis.* Event-related EEG and MEG responses were extracted as single-trial epochs with a time window of 0 to 400 ms after the standard or deviant tone onset. The trials were baseline-corrected by applying a baseline of −100 to 0 ms before the tone onset. Since the planar gradiometer sensors measure along two orthogonal directions, the data from each pair of longitudinal and latitudinal sensors were combined by applying the Pythagorean distance formula, as implemented in the FieldTrip toolbox for MATLAB (Donders Institute for Brain, Cognition and Behaviour/Max Planck Institute, Nijmegen, Netherlands) [58]; $d = \sqrt{\text{longitudinal}^2 + \text{latitudinal}^2}$.

Table 1: Deviant tones. *Type of deviant* is the type of change applied to the tone, and *description* explains the change. *Occurrence* describes whether the change is presented in different patterns randomly (single) or is present constantly in each following pattern from the first presentation until the next deviant of the same type occurs (consistent). *Tone number* denotes at which tone of the melody pattern the change may occur. *Melodies with deviants* column shows the percentage of melodies containing the particular type of deviant.

| Type of deviant | Description | Occurrence | Tone number | Melodies with deviants |
|---|---|---|---|---|
| Mistuning | 3% pitch frequency increase | Single | 1st, 2nd, 4th | 14% |
| Timbre | Flute sound | Single | 1st, 3rd, 4th, ending | 8% |
| Timing delay | 100 ms silent gap before the tone | Single | 1st, 2nd, 3rd, ending | 8% |
| Melody modulation | Tone replacement | Consistent | 3rd, 4th | 12% |
| Rhythm modulation | Duration switch between two successive tones | Consistent | 2nd, 3rd | 7% |
| Transposition | Semitone pitch change of a pattern | Consistent | Initial triad | 16% |

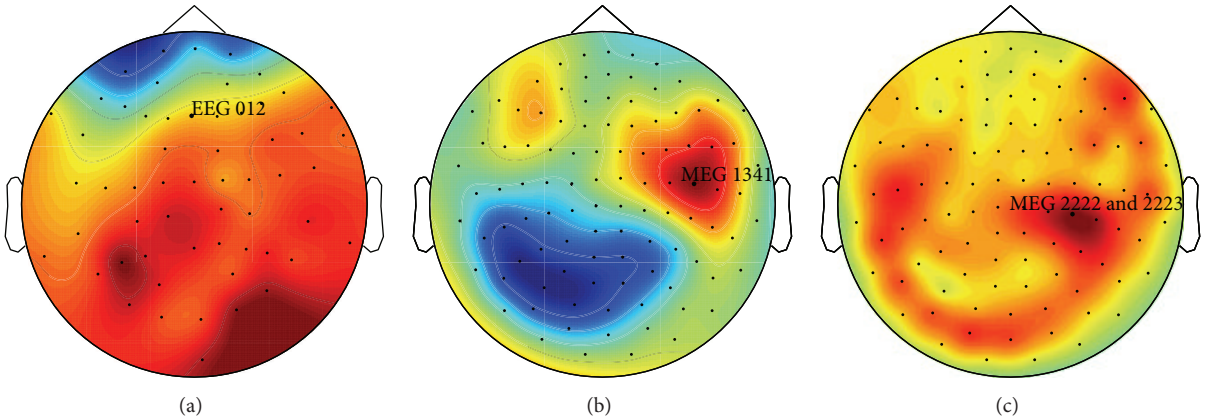


Figure 1: Topographical plots of MMN responses (without correction for internal artifacts). Showing topographical plots of MMN responses to the mistuning deviants, which elicited the strongest and most consistent MMN responses in the tested sample in the EEG (a), MEG magnetometers (b), and MEG gradiometers (c). The plots are based on grand averages from uncorrected data (only preprocessed with tSSS) by applying a time window from 125 to 155 ms after the tone onset.

For the sake of clarity, we performed the subsequent analyses on one channel of each sensor type, those in which the highest MMN amplitude was measured within a typical MMN latency range of 75–200 ms. In this case, we analyzed the event-related waveforms from EEG channel 012 (frontal site), magnetometer channel MEG 1341 (right temporal site), and the combined planar gradiometer channels MEG 2222 and 2223 (right temporal site) (see Figure 1). These analyzed channels behaved reliably and were not detected as bad channels or subjected to any additional correction.

We measured the MMN amplitude in response to each type of deviant tone by taking the average value across the time window from 125 to 155 ms after the tone onset. To compare the noise levels after utilizing each artifact correction method, we first used a baseline standard deviation measure. Since a flat baseline is desirable, we applied a baseline standard deviation (STD) measure to show the flatness of the baseline in a single trial (where lower baseline STD means a more flat baseline) [59]. We calculated the standard deviation across the baseline time points from −100 to 0 ms (in relation to the stimulus onset) in each trial separately and extracted the mean baseline STD across trials. Also, minimal variance in the measured signal across trials is desirable. Therefore, we also calculated the signal STD across trials for each time point in 125 to 155 ms:

$$\sigma_{\overline{x}} = \sqrt{\frac{\sum_{i=1}^{n} (x_i - \overline{x})^2}{N}}, \quad (1)$$

where $x$ is the measured value, $\overline{x}$ is the mean value, $i$ is the trial number, and $N$ is the total number of trials [18] and we averaged these values to obtain the mean signal STD. For additional comparisons, we applied a signal-to-noise ratio measure; SNR = amplitude/$\sigma_{\overline{x}}$ [18].

The Mismatch Negativity (MMN) evoked-response is analyzed by comparing the average response to the deviant stimulus with the average response to the standard stimulus [50, 51]. Also, MMN waveforms are conventionally calculated by subtracting the average response to the standard stimulus from the average response to the deviant stimulus [50, 51]. However, we here analyze the noise levels across multiple single-trial MMN responses, which does not allow us to create difference waveforms by simply subtracting particular

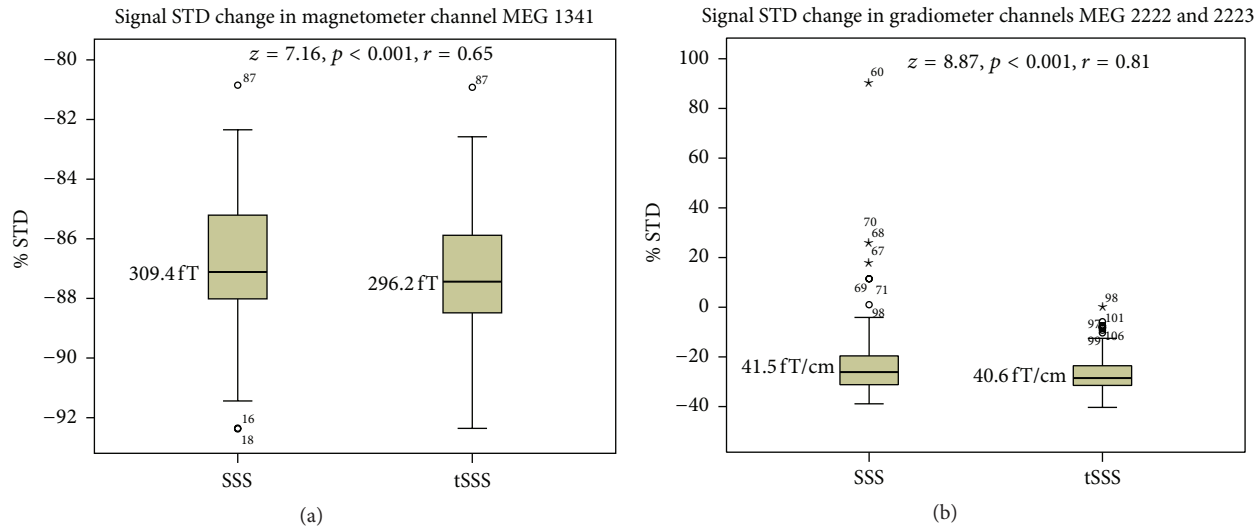


Figure 2: Percentagewise standard deviation (STD) reduction in the signal latency range achieved by applying the SSS or tSSS methods in comparison to the level (at 0% STD) in the raw data recording without spatial filtering. The differences are shown for the amplitude peak channel of the magnetometers (a) and gradiometers (b) in Tukey box plots. Bold horizontal lines indicate medians, brown boxes indicate the first 50 percent of the case range, and vertical lines indicate cases within the 1.5 interquartile range from the edge of the 50% of the cases. Outliers more than 1.5 (circles) or 3.0 (stars) interquartile ranges from the edge of the 50% of the cases are denoted with circles or stars, and case numbers are provided for each outlier. The median values are shown in femtoteslas (fT) and femtoteslas per centimeter (fT/cm). $z$ and $r$ indicate the effect size, and $p$ indicates the level of statistical significance.

pairs of deviant and standard trials among multiple equally possible pairings of trials. The responses to both deviant and standard stimuli are relevant for any subsequent analyses of MMN, and it is therefore important to know the noise levels of responses to both stimuli. Therefore, we here analyzed the noise levels in the responses to both the deviant and standard stimuli.

Statistical comparisons were made with SPSS version 20 (IBM, Armonk, New York, USA). Since the resulting values were not normally distributed, we applied the Wilcoxon signed-rank test to compare the values achieved after utilizing the different artifact correction methods.

## 3. Results

*3.1. SSS and tSSS.* A statistically significant and slightly better reduction of the signal standard deviation (STD) is achieved by applying tSSS in comparison to SSS for for both the MEG magnetometer and gradiometer data (see Figure 2). Importantly, in 6% (7/120) of the tested cases, the signal STD actually increases when applying SSS to the MEG gradiometer data, whereas the signal STD either is retained or decreases when the tSSS method is applied.

*3.2. ICA and SSP.* From grand average waveforms of the event-related responses (across all participants and conditions), it can be seen that the SSP-based artifact correction reduces the signal amplitude, whereas the signal amplitude is similar before and after the artifact correction based on ICA (see Figure 3).

The SSP method results in lower baseline standard deviation (STD) and signal STD in comparison to the ICA method (see Figure 4). The baseline STD even appears to increase when applying the ICA-based artifact correction, in particular with respect to the EEG and magnetometer channels. However, for the gradiometers, ICA yields slightly but statistically significantly better SNR than that achieved by applying the SSP method (see Figure 5).

The SNR achieved by applying the ICA-based artifact correction is similar to that achieved by applying the SSP method with respect to the EEG and magnetometer channels. However, for the gradiometers applying the ICA method results in statistically significantly and slightly better SNR than that achieved by applying the SSP method (see Figure 5).

## 4. Discussion

We compared the noise suppression results achieved with SSS and tSSS on healthy subjects not wearing magnetized material. MaxFilter with tSSS resulted in better suppression of artifacts from external and nearby noise sources in comparison to SSS. In particular, the application of tSSS instead of SSS was important with respect to the MEG gradiometers, since SSS correction in 6% of the cases resulted in an increase of the noise level in the MEG gradiometer data, and thus the reliability of the gradiometer data decreased in comparison to that before SSS. We also compared the performance of ICA and SSP in reducing internal electrophysiological artifacts, originating from eye movements and heart beats of the participants. The ICA-based artifact correction performed better than the SSP method. The SSP method reduced part of the signal of interest along with the artifacts, and the SNR was slightly higher after applying the ICA method than after applying the SSP method. However, after ICA-based artifact

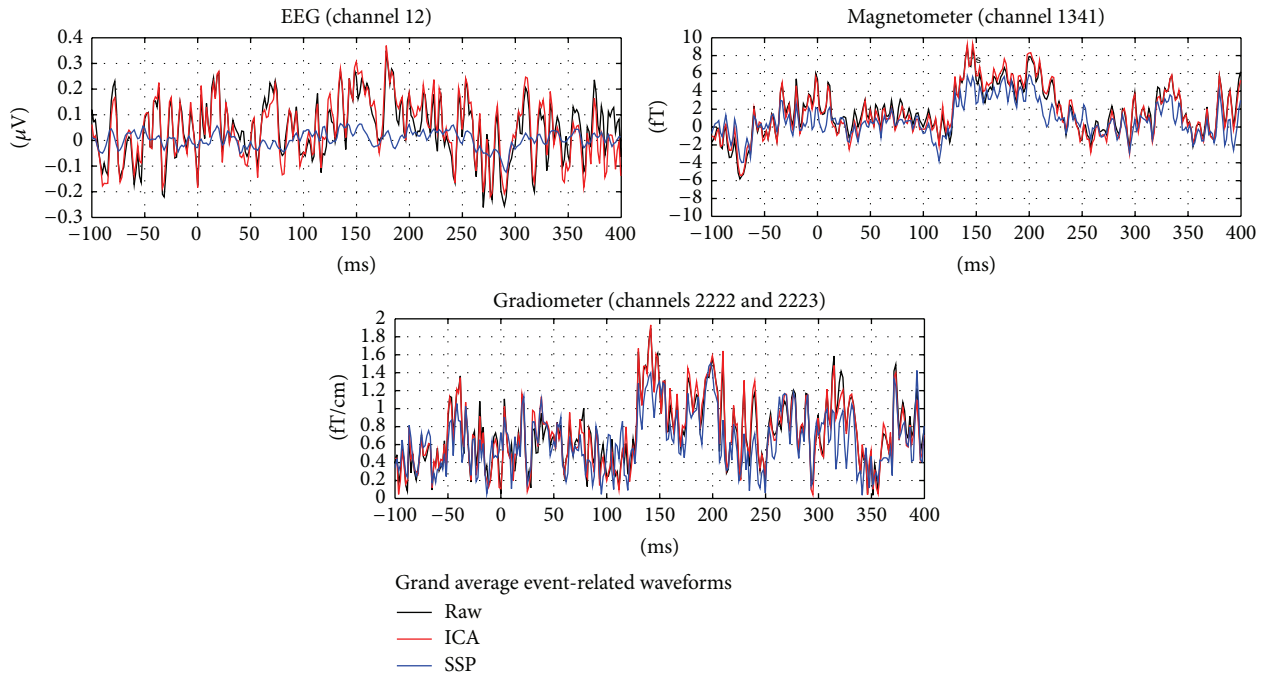


Figure 3: Grand average event-related waveforms. Showing the channels with the signal peak amplitude among the EEG channels, magnetometers, and gradiometers, without any artifact correction (black) and after artifact correction based on Independent Component Analysis (ICA) (red) and Signal Space Projection (SSP) (blue).

correction the baseline noise level increased, in particular in the EEG and magnetometer channels, which have relatively low SNR in the original data. These findings support both the importance of reducing the bias on measures of evoked-responses with EEG and MEG caused by artifacts and the importance of minimizing the bias introduced by errors in artifact correction methods.

With regard to the suppression of external noise, we here observed that the averaged MMN evoked-response in 6% of the cases with the MEG gradiometers even became more unreliable after applying SSS correction than before. Possibly, the influence of nearby artifacts on the evoked-response can become stronger after the external artifacts have been reduced with the SSS. When tSSS is applied the influence of such nearby artifacts on the evoked-responses would be reduced. In general, it seems relevant to further investigate whether correction methods for reducing one type of artifact, such as SSS, in some cases might enhance the influence of other artifacts on the averaged event-related waveform.

The comparisons of the ICA and SSP methods for suppression of internal artifacts revealed particular biases appearing after the corrections. For the SSP method, there is a risk that the artifacts and signals of interest are not described by orthogonal components [48]. We observed this issue after applying the SSP artifact correction method, and we found that part of the signal of interest was reduced along with the influence of the artifacts. For the ICA method, there is another risk that after correction on channels with relatively low SNR is applied—such as correction on EEG channels, magnetometer channels, and channels located distantly from the signal peaks—additional noise is added to these channels. This happens because the errors in estimating the mixing matrix for the ICA will increase when the SNR decreases [60]. Our results emphasized this issue in showing that the baseline noise level increased after applying the ICA-based correction, in particular in the EEG channels and in the MEG magnetometer channels, and also the difference in SNR between applying ICA and SSP was smaller for the EEG channels and MEG magnetometer channels than for the MEG gradiometer channels, suggesting a relatively smaller improvement for the EEG and MEG magnetometer channels after applying the ICA-based artifact correction.

In summary, our test results suggest that tSSS is recommendable for reducing the influence of artifacts originating from external and nearby sources instead of SSS only. We find that the noise level decreases more with tSSS than with SSS in this sample of EEG and MEG data from healthy participants despite the fact that they were not wearing strongly magnetized materials. For the reduction of internal physiological artifacts, we showed that the highest signal-to-noise ratio (SNR) is achieved with ICA-based artifact correction on the tested sample. However, both ICA- and SSP-based artifact corrections are subject to certain limitations. In particular, one must be aware of the risk when processing data with relatively low SNR, such as EEG and MEG magnetometer data, that artifact correction based on ICA may decrease the interference from artifacts while simultaneously increasing the noise level, due to increasing errors in estimating the mixing matrix in the context of data with lower SNR levels.

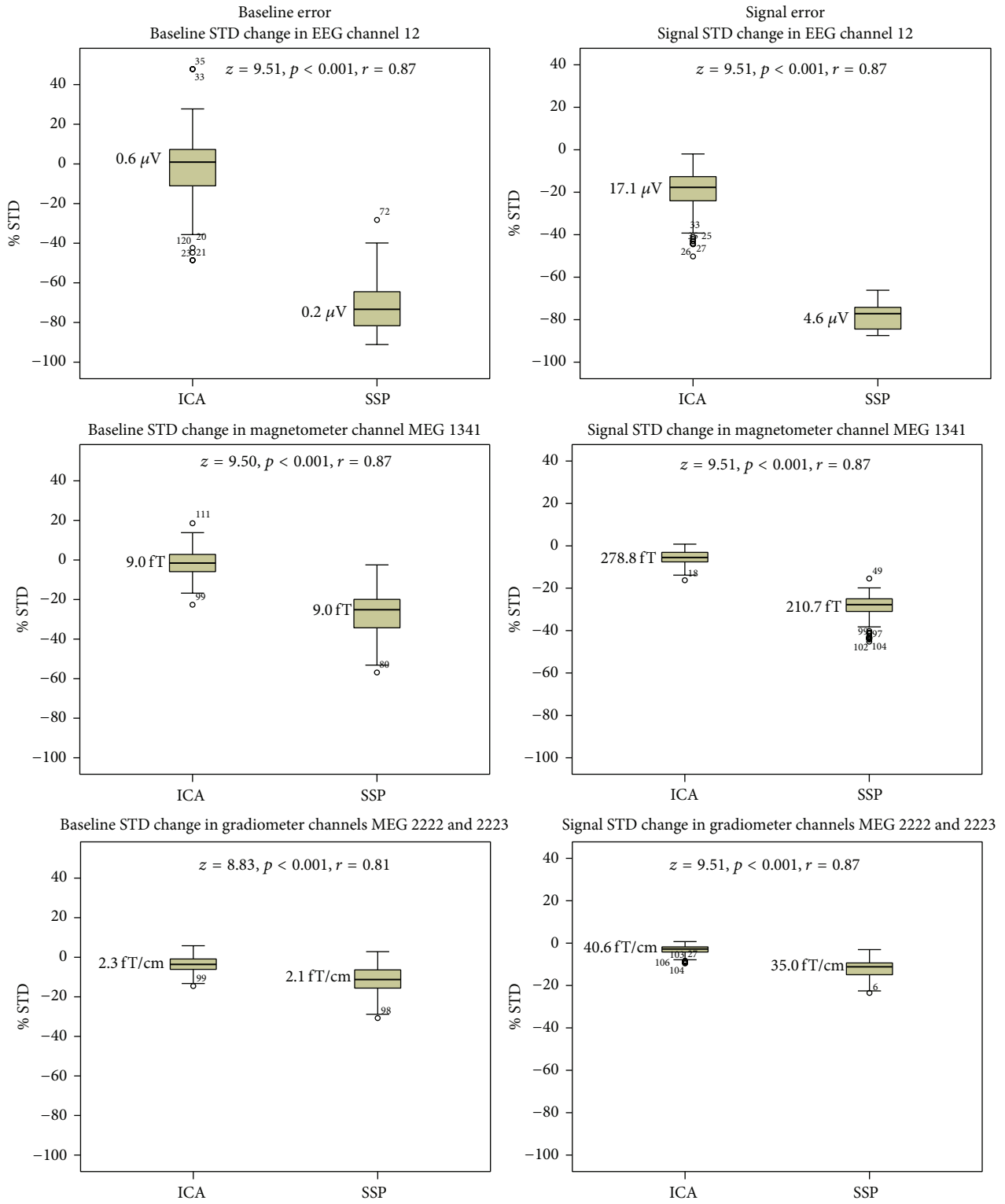


Figure 4: Percentagewise baseline standard deviation (STD) and signal STD reduction achieved by applying ICA or SSP methods in comparison to the level (at 0% STD) in the raw data recording with tSSS only. Median values are shown in microvolts ($\mu$V), femtoteslas (fT), and femtoteslas per centimeter (fT/cm). Outliers more than 1.5 interquartile ranges from the edge of the 50% of the cases are denoted with circles. Case numbers are provided for each outlier.

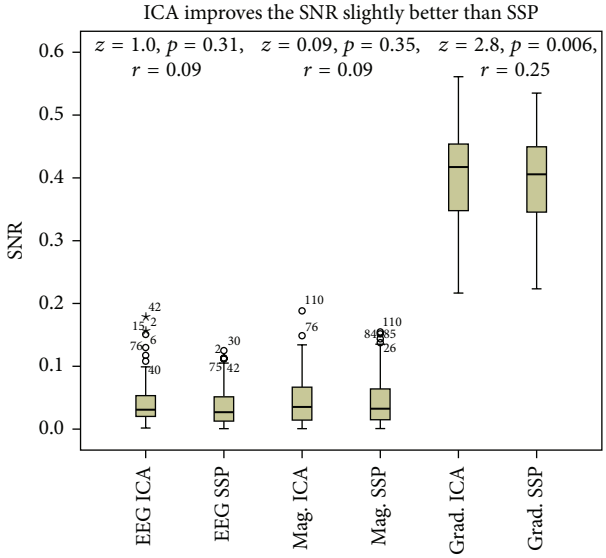


FIGURE 5: Signal-to-noise ratios (SNR) achieved by applying artifact correction based on Independent Component Analysis (ICA) or Signal Space Projection (SSP). Tukey box plot showing the SNR levels achieved by applying the ICA or SSP method in the signal amplitude peak channel of the EEG, magnetometers (Mag.), and gradiometers (Grad.) (the SNR shows the relationship between the signal and noise level in single trials). Outliers more than 1.5 (circles) or 3.0 (stars) interquartile ranges from the edge of the 50% of the cases are denoted with circles or stars, and case numbers are provided for each outlier.

## Competing Interests

The authors declare that they have no competing interests.

## References

[1] M. Hämäläinen, R. Hari, R. J. Ilmoniemi, J. Knuutila, and O. V. Lounasmaa, "Magnetoencephalography—theory, instrumentation, and applications to noninvasive studies of the working human brain," *Reviews of Modern Physics*, vol. 65, no. 2, pp. 413–497, 1993.

[2] W. O. Tatum, B. A. Dworetzky, W. D. Freeman, and D. L. Schomer, "Artifact: recording EEG in special care units," *Journal of Clinical Neurophysiology*, vol. 28, no. 3, pp. 264–277, 2011.

[3] F. Morbidi, A. Garulli, D. Prattichizzo, C. Rizzo, and S. Rossi, "Application of Kalman filter to remove TMS-induced artifacts from EEG recordings," *IEEE Transactions on Control Systems Technology*, vol. 16, no. 6, pp. 1360–1366, 2008.

[4] M. Koskinen and N. Vartiainen, "Removal of imaging artifacts in EEG during simultaneous EEG/fMRI recording: reconstruction of a high-precision artifact template," *NeuroImage*, vol. 46, no. 1, pp. 160–167, 2009.

[5] X. Wan, K. Iwata, J. Riera, T. Ozaki, M. Kitamura, and R. Kawashima, "Artifact reduction for EEG/fMRI recording: nonlinear reduction of ballistocardiogram artifacts," *Clinical Neurophysiology*, vol. 117, no. 3, pp. 668–680, 2006.

[6] R. Murdick and B. J. Roth, "Magneto-encephalogram artifacts caused by electro-encephalogram electrodes," *Medical and Biological Engineering and Computing*, vol. 41, no. 2, pp. 203–205, 2003.

[7] R. J. M. Somsen and B. van Beek, "Ocular artifacts in children's EEG: selection is better than correction," *Biological Psychology*, vol. 48, no. 3, pp. 281–300, 1998.

[8] D. Hagemann and E. Naumann, "The effects of ocular artifacts on (lateralized) broadband power in the EEG," *Clinical Neurophysiology*, vol. 112, no. 2, pp. 215–231, 2001.

[9] C. Carl, A. Açık, P. König, A. K. Engel, and J. F. Hipp, "The saccadic spike artifact in MEG," *NeuroImage*, vol. 59, no. 2, pp. 1657–1667, 2012.

[10] I. Tal and M. Abeles, "Cleaning MEG artifacts using external cues," *Journal of Neuroscience Methods*, vol. 217, no. 1-2, pp. 31–38, 2013.

[11] J. Ma, P. Tao, S. Bayram, and V. Svetnik, "Muscle artifacts in multichannel EEG: characteristics and reduction," *Clinical Neurophysiology*, vol. 123, no. 8, pp. 1676–1686, 2012.

[12] D. Cohen, U. Schläpfer, S. Ahlfors, M. Hämäläinen, and E. Halgren, *New Six-Layer Magnetically-Shielded Room for MEG*, 2002.

[13] S. Taulu and J. Simola, "Spatiotemporal signal space separation method for rejecting nearby interference in MEG measurements," *Physics in Medicine and Biology*, vol. 51, no. 7, pp. 1759–1768, 2006.

[14] T. Song, K. Gaa, L. Cui, L. Feffer, R. R. Lee, and M. Huang, "Evaluation of signal space separation via simulation," *Medical and Biological Engineering and Computing*, vol. 46, no. 9, pp. 923–932, 2008.

[15] T. Song, L. Cui, K. Gaa et al., "Signal space separation algorithm and its application on suppressing artifacts caused by vagus nerve stimulation for magnetoencephalography recordings," *Journal of Clinical Neurophysiology*, vol. 26, no. 6, pp. 392–400, 2009.

[16] S. Taulu and R. Hari, "Removal of magnetoencephalographic artifacts with temporal signal-space separation: demonstration with single-trial auditory-evoked responses," *Human Brain Mapping*, vol. 30, no. 5, pp. 1524–1534, 2009.

[17] A. Hillebrand, P. Fazio, J. C. De Munck, and B. W. Van Dijk, "Feasibility of clinical magnetoencephalography (MEG) functional mapping in the presence of dental artefacts," *Clinical Neurophysiology*, vol. 124, no. 1, pp. 107–113, 2013.

[18] A. Gonzalez-Moreno, S. Aurtenetxe, M.-E. Lopez-Garcia, F. del Pozo, F. Maestu, and A. Nevado, "Signal-to-noise ratio of the MEG signal after preprocessing," *Journal of Neuroscience Methods*, vol. 222, pp. 56–61, 2014.

[19] S. J. Schiff, A. Aldroubi, M. Unser, and S. Sato, "Fast wavelet transformation of EEG," *Electroencephalography and Clinical Neurophysiology*, vol. 91, no. 6, pp. 442–455, 1994.

[20] T.-P. Jung, C. Humphries, T.-W. Lee et al., "Removing electroencephalographic artifacts: comparison between ICA and PCA," in *Proceedings of the IEEE Signal Processing Society Workshop Neural Networks for Signal Processing VIII*, pp. 63–72, Cambridge, UK, August-September 1998.

[21] S. Ikeda and K. Toyama, "Independent component analysis for noisy data—MEG data analysis," *Neural Networks*, vol. 13, no. 10, pp. 1063–1074, 2000.

[22] R. Vigário, J. Särelä, V. Jousmiki, M. Hämäläinen, and E. Oja, "Independent component approach to the analysis of EEG and MEG recordings," *IEEE Transactions on Biomedical Engineering*, vol. 47, no. 5, pp. 589–593, 2000.

[23] J. Iriarte, E. Urrestarazu, M. Valencia et al., "Independent component analysis as a tool to eliminate artifacts in EEG: a quantitative study," *Journal of Clinical Neurophysiology*, vol. 20, no. 4, pp. 249–257, 2003.

[24] C. J. James and O. J. Gibson, "Temporally constrained ICA: an application to artifact rejection in electromagnetic brain signal analysis," *IEEE Transactions on Biomedical Engineering*, vol. 50, no. 9, pp. 1108–1116, 2003.

[25] M. Kawakatsu, "Application of ICA to MEG noise reduction," in *Proceedings of the Independent Component Analysis and Blind Signal Separation (ICA '03)*, pp. 535–541, Nara, Japan, April 2003.

[26] C. A. Joyce, I. F. Gorodnitsky, and M. Kutas, "Automatic removal of eye movement and blink artifacts from EEG data using blind component separation," *Psychophysiology*, vol. 41, no. 2, pp. 313–325, 2004.

[27] Y. Konno, J. Cao, T. Takeda, H. Endo, T. Arai, and M. Tanaka, "Evaluation of brain source separation for MEG data applying JADE, fast-ICA and natural gradient-based algorithm with robust pre-whitening technique," *Journal of Signal Processing*, vol. 8, no. 6, pp. 461–472, 2004.

[28] A. C. Tang, M. T. Sutherland, and C. J. McKinney, "Validation of SOBI components from high-density EEG," *NeuroImage*, vol. 25, no. 2, pp. 539–553, 2005.

[29] W. De Clercq, A. Vergult, B. Vanrumste, W. Van Paesschen, and S. Van Huffel, "Canonical correlation analysis applied to remove muscle artifacts from the electroencephalogram," *IEEE Transactions on Biomedical Engineering*, vol. 53, no. 12, pp. 2583–2587, 2006.

[30] J. Escudero, R. Hornero, D. Abásolo, A. Fernández, and M. López-Coronado, "Artifact removal in magnetoencephalogram background activity with independent component analysis," *IEEE Transactions on Biomedical Engineering*, vol. 54, no. 11, pp. 1965–1973, 2007.

[31] S. P. Fitzgibbon, D. M. W. Powers, K. J. Pope, and C. R. Clark, "Removal of EEG noise and artifact using blind source separation," *Journal of Clinical Neurophysiology*, vol. 24, no. 3, pp. 232–243, 2007.

[32] J. Dammers, M. Schiek, F. Boers et al., "Integration of amplitude and phase statistics for complete artifact removal in independent components of neuromagnetic recordings," *IEEE Transactions on Biomedical Engineering*, vol. 55, no. 10, pp. 2353–2362, 2008.

[33] S. Hoffmann and M. Falkenstein, "The correction of eye blink artefacts in the EEG: a comparison of two prominent methods," *PLoS ONE*, vol. 3, no. 8, Article ID e3004, 2008.

[34] D. Mantini, R. Franciotti, G. L. Romani, and V. Pizzella, "Improving MEG source localizations: an automated method for complete artifact removal based on independent component analysis," *NeuroImage*, vol. 40, no. 1, pp. 160–173, 2008.

[35] J. Escudero, R. Hornero, D. Abásolo, and A. Fernández, "Quantitative evaluation of artifact removal in real magnetoencephalogram signals with blind source separation," *Annals of Biomedical Engineering*, vol. 39, no. 8, pp. 2274–2286, 2011.

[36] A. Hyvärinen, "Testing the ICA mixing matrix based on inter-subject or inter-session consistency," *NeuroImage*, vol. 58, no. 1, pp. 122–136, 2011.

[37] R. J. Korhonen, J. C. Hernandez-Pavon, J. Metsomaa, H. Mäki, R. J. Ilmoniemi, and J. Sarvas, "Removal of large muscle artifacts from transcranial magnetic stimulation-evoked EEG by independent component analysis," *Medical & Biological Engineering & Computing*, vol. 49, no. 4, pp. 397–407, 2011.

[38] B. W. McMenamin, A. J. Shackman, L. L. Greischar, and R. J. Davidson, "Electromyogenic artifacts and electroencephalographic inferences revisited," *NeuroImage*, vol. 54, no. 1, pp. 4–9, 2011.

[39] M. Zima, P. Tichavský, K. Paul, and V. Krajča, "Robust removal of short-duration artifacts in long neonatal EEG recordings using wavelet-enhanced ICA and adaptive combining of tentative reconstructions," *Physiological Measurement*, vol. 33, no. 8, pp. N39–N49, 2012.

[40] G. Lio and P. Boulinguez, "Greater robustness of second order statistics than higher order statistics algorithms to distortions of the mixing matrix in blind source separation of human EEG: implications for single-subject and group analyses," *NeuroImage*, vol. 67, pp. 137–152, 2013.

[41] J. Metsomaa, J. Sarvas, and R. J. Ilmoniemi, "Multi-trial evoked EEG and independent component analysis," *Journal of Neuroscience Methods*, vol. 228, pp. 15–26, 2014.

[42] M. Chaumon, D. V. M. Bishop, and N. A. Busch, "A practical guide to the selection of independent components of the electroencephalogram for artifact correction," *Journal of Neuroscience Methods*, vol. 250, pp. 47–63, 2015.

[43] J. A. Urigüen and B. Garcia-Zapirain, "EEG artifact removal—state-of-the-art and guidelines," *Journal of Neural Engineering*, vol. 12, no. 3, Article ID 031001, 2015.

[44] G. L. Wallstrom, R. E. Kass, A. Miller, J. F. Cohn, and N. A. Fox, "Automatic correction of ocular artifacts in the EEG: a comparison of regression-based and component-based methods," *International Journal of Psychophysiology*, vol. 53, no. 2, pp. 105–119, 2004.

[45] M. Plöchl, J. P. Ossandón, and P. König, "Combining EEG and eye tracking: identification, characterization, and correction of eye movement artifacts in electroencephalographic data," *Frontiers in Human Neuroscience*, vol. 6, article 278, 2012.

[46] J. M. Zumer, H. T. Attias, K. Sekihara, and S. S. Nagarajan, "A probabilistic algorithm integrating source localization and noise suppression for MEG and EEG data," *NeuroImage*, vol. 37, no. 1, pp. 102–115, 2007.

[47] J. M. Zumer, H. T. Attias, K. Sekihara, and S. S. Nagarajan, "Probabilistic algorithms for MEG/EEG source reconstruction using temporal basis functions learned from data," *NeuroImage*, vol. 41, no. 3, pp. 924–940, 2008.

[48] M. A. Uusitalo and R. J. Ilmoniemi, "Signal-space projection method for separating MEG or EEG into components," *Medical and Biological Engineering and Computing*, vol. 35, no. 2, pp. 135–140, 1997.

[49] R. R. Ramírez, B. H. Kopell, C. R. Butson, B. C. Hiner, and S. Baillet, "Spectral signal space projection algorithm for frequency domain MEG and EEG denoising, whitening, and source imaging," *NeuroImage*, vol. 56, no. 1, pp. 78–92, 2011.

[50] R. Näätänen, P. Paavilainen, T. Rinne, and K. Alho, "The mismatch negativity (MMN) in basic research of central auditory processing: a review," *Clinical Neurophysiology*, vol. 118, no. 12, pp. 2544–2590, 2007.

[51] M. I. Garrido, J. M. Kilner, K. E. Stephan, and K. J. Friston, "The mismatch negativity: a review of underlying mechanisms," *Clinical Neurophysiology*, vol. 120, no. 3, pp. 453–463, 2009.

[52] M. Tervaniemi, M. Huotilainen, and E. Brattico, "Melodic multi-feature paradigm reveals auditory profiles in music-sound encoding," *Frontiers in Human Neuroscience*, vol. 8, article 496, 2014.

[53] M. Tervaniemi, L. Janhunen, S. Kruck, V. Putkinen, and M. Huotilainen, "Auditory profiles of classical, jazz, and rock musicians: genre-specific sensitivity to musical sound features," *Frontiers in Psychology*, vol. 6, article 1900, 2016.

[54] V. Putkinen, M. Tervaniemi, K. Saarikivi, N. de Vent, and M. Huotilainen, "Investigating the effects of musical training

on functional brain development with a novel Melodic MMN paradigm," *Neurobiology of Learning and Memory*, vol. 110, pp. 8–15, 2014.

[55] A. Gramfort, M. Luessi, E. Larson et al., "MEG and EEG data analysis with MNE-Python," *Frontiers in Neuroscience*, vol. 7, article 267, 2013.

[56] A. Gramfort, M. Luessi, E. Larson et al., "MNE software for processing MEG and EEG data," *NeuroImage*, vol. 86, pp. 446–460, 2014.

[57] S. Makeig, A. J. Bell, T. Jung, and T. J. Sejnowski, "Independent component analysis of electroencephalographic data," in *Advances in Neural Information Processing Systems*, pp. 145–151, 1996.

[58] R. Oostenveld, P. Fries, E. Maris, and J.-M. Schoffelen, "FieldTrip: open source software for advanced analysis of MEG, EEG, and invasive electrophysiological data," *Computational Intelligence and Neuroscience*, vol. 2011, Article ID 156869, 9 pages, 2011.

[59] H. Nolan, R. Whelan, and R. B. Reilly, "FASTER: fully automated statistical thresholding for EEG artifact rejection," *Journal of Neuroscience Methods*, vol. 192, no. 1, pp. 152–162, 2010.

[60] P. Comon, "Independent component analysis, a new concept?" *Signal Processing*, vol. 36, no. 3, pp. 287–314, 1994.

Hindawi Publishing Corporation
Computational Intelligence and Neuroscience
Volume 2016, Article ID 8984379, 10 pages
http://dx.doi.org/10.1155/2016/8984379

*Research Article*

# Novel Virtual Environment for Alternative Treatment of Children with Cerebral Palsy

**Juliana M. de Oliveira,[1] Rafael Carneiro G. Fernandes,[1] Cristtiano S. Pinto,[1] Plácido R. Pinheiro,[1] Sidarta Ribeiro,[2] and Victor Hugo C. de Albuquerque[1]**

[1]*Programa de Pós-Graduação em Informática Aplicada, Universidade de Fortaleza, Avenida Washington Soares, 1321 Edson Queiroz, 60.811-905 Fortaleza, CE, Brazil*
[2]*Instituto do Cérebro, Universidade Federal do Rio Grande do Norte, Avendia Nascimento de Castro 2155, 59056-450 Natal, RN, Brazil*

Correspondence should be addressed to Victor Hugo C. de Albuquerque; victor.albuquerque@unifor.br

Received 14 January 2016; Revised 27 April 2016; Accepted 23 May 2016

Academic Editor: Stefan Haufe



Cerebral palsy is a severe condition usually caused by decreased brain oxygenation during pregnancy, at birth or soon after birth. Conventional treatments for cerebral palsy are often tiresome and expensive, leading patients to quit treatment. In this paper, we describe a virtual environment for patients to engage in a playful therapeutic game for neuropsychomotor rehabilitation, based on the experience of the occupational therapy program of the Nucleus for Integrated Medical Assistance (NAMI) at the University of Fortaleza, Brazil. Integration between patient and virtual environment occurs through the hand motion sensor "Leap Motion," plus the electroencephalographic sensor "MindWave," responsible for measuring attention levels during task execution. To evaluate the virtual environment, eight clinical experts on cerebral palsy were subjected to a questionnaire regarding the potential of the experimental virtual environment to promote cognitive and motor rehabilitation, as well as the potential of the treatment to enhance risks and/or negatively influence the patient's development. Based on the very positive appraisal of the experts, we propose that the experimental virtual environment is a promising alternative tool for the rehabilitation of children with cerebral palsy.

## 1. Introduction

Virtual environment is a technology able to establish a relationship between the user and the environment created, enabling real-time integration with controlled virtual objects. A virtual environment can be explored through visual and haptic devices, without real restrictions, for example, gravity. The iteration derives from the communication between human actions and the outcome of these actions, processed by the computer generating a response inside the virtual environment. The interaction can be passive, such as watching television, or active, when, for instance, users manipulate their body movements or a particular object inside a virtual scenario [1–3].

Virtual reality is a computational technology that provides artificial sensory feedback, allowing a user to experiment activities and events similar to those that could be found in real life and to develop motor abilities in three-dimensional (3D) virtual environments that resemble the real world [4]. Virtual reality involves three key elements that are required for motor learning: (i) repetitions, because neural plasticity is dependent on repeated stimulation able to produce optimal learning; (ii) sensory feedback, because intense multisensory stimulation is an essential part of rehabilitation for children with cerebral palsy, a systemic disease; and (iii) motivation of the patient [5].

Several studies have been carried out as an alternative tool for rehabilitation of patients with neurologic or genetic syndromes [6–15]. In most cases, the environment was based on games (serious game or exergames) applied to sensorimotor processing. The results are overall very promising, mainly due to the abstraction of traumatic symptoms such as pain and fear, to the escape from the real world, and to the incentive to overcome the challenges posed by virtual environments.

The use of games for clinical rehabilitation has boomed recently because of the availability of low-cost equipment

on the market [16–25]. Another reason for the growing use of this type of treatment is the enhanced attractiveness of interactive environments in addition to the challenges posed by the game in pursuit of conquests/rewards (positive reinforcement) following the conclusion of a specific task. Virtual systems with clinical purposes have an important role in health care: they are easily manipulated by specialists as well as by patients, acting as a motivational source for continued treatment that is less aggressive and tedious than traditional treatments. It is worth emphasizing that the supervision of a clinical expert is extremely necessary for therapeutic success.

Games are incorporated into off-the-shelf commercial entertainment applications or specially developed for clinical purposes. Treatment of cerebral palsy in children is a challenging task for physicians. Lack of motivation and treatment withdrawal due to a delayed perception of patient's progress are two important factors that physicians have to deal with. The use of virtual environments may, thus, be an interesting approach as a complement to conventional treatment for these patients, establishing a new standard in the individual's rehabilitation strategy [6].

It is believed, according to the objectives of traditional treatment, that the rehabilitation process benefits from playful activities because of increased motivation and the reduction of environmental interference that may unfocus the child's attention to other actions which are not therapeutic targets. Given this background, the present work aims to develop a virtual reality game using Unity 3D version 5.2 (characterized as serious game) as an alternative tool of aid to motor and cognitive rehabilitation in children with cerebral palsy. We developed a virtual environment able to interact in real-time with children with cerebral palsy, via motion sensor of the hands and fingers (Leap Motion [26]), with the aim of using play to speed up recovery, by making patients feel more motivated, interested, and confident to carry out motor actions. Importantly, it is possible to perform actions in the virtual environment according to the specific needs of each patient without a direct intervention of specialist. Moreover, the combined recording of the electroencephalogram (EEG) through the device "MindWave" [27, 28] allows the tracking of the patient's clinical evolution in real-time, taking into account variations in the levels of attention and relaxation.

Evaluation of the performance of the proposed system was carried out by eight clinical specialists through a questionnaire that compared several aspects of the novel versus traditional treatments. Beyond this, specialists are submitted to the use of the proposed model, evaluating the potential of the tool, as well as suggesting possible changes or solutions.

A description of the virtual environment and its integration with Leap Motion and MindWave sensors is available at https://github.com/jullianamartins/ProjetoNami.

## 2. Experimental Procedures

Before the implementation of the new virtual environment, several meetings with clinical specialists (occupational therapists, physiotherapists, psychologists, neurologists, and pediatric neurologists) were performed at the Occupational Therapy Center of NAMI (Núcleo de Atenção Médica Integrada: Nucleus for Integrated Medical Attention) of the University of Fortaleza (UNIFOR), Fortaleza, Ceará, Brazil. During these meetings, we defined the age group of the patients from 0 to 8 years old, using as inclusion criterion the presence of major deficits in psychomotor development of the children. The different game phases were set to always increase in difficulty as the patient achieves a goal, that is, goes to the next phase. To model the virtual environment, we used an intuitive, efficient, and effective open source development platform called Unity.

*2.1. Brief Description of Activities.* After selecting the group of patients and during follow-up visits, we selected 6 activities, already present in the conventional treatment, to be modeled and used in the proposed virtual environment. These activities, divided into different levels to encourage the child to always overcome a goal (stimulating cognitive and motor domains), are called "functional play." According to Wallon [29], these can be very simple movements such as flexing arms or legs, shaking fingers, touching objects, balancing the body, or producing sounds.

The purpose of each Phase is as follows:

(1) *Phase 1*. Selecting all objects that contain the same color with the least amount of mistakes and in the shortest time possible. Distinguishing objects with different shapes and colors, developing motor abilities with hands and fingers, and using touch (pointing) through extension and flexing movements of the elbow joints.

(2) *Phase 2*. Selecting all objects that contain the same shape, with minimal errors and in the shortest time possible. Distinguishing objects with different shapes, developing motor abilities through movement using small body muscles, and executing activities that require greater movement detail, such as writing, catching, and manipulating objects with their hands, moving the same joints as in Phase 1.

(3) *Phase 3*. Selecting all objects that contain the same color and taking them to a basket of the same color, with minimal errors and in the shortest time possible. Distinguishing objects with different shapes but the same color, developing skills with hands through the extender and flexor movements of the elbow joint, and distinguishing laterality (right and left).

(4) *Phase 4*. Identifying numbers and letters by dragging them to a basket according to their kind, with minimal errors and in the shortest time possible. Performing associations to distinguish letters and numbers, developing hand motor skills using the flexion and extension movements, and stimulating laterality by distinguishing right and left sides.

(5) *Phase 5*. Selecting all objects that belong to the habitat being presented and taking them to a box. Distinguishing objects belonging to the same habitat according to spatial associations with rural or urban

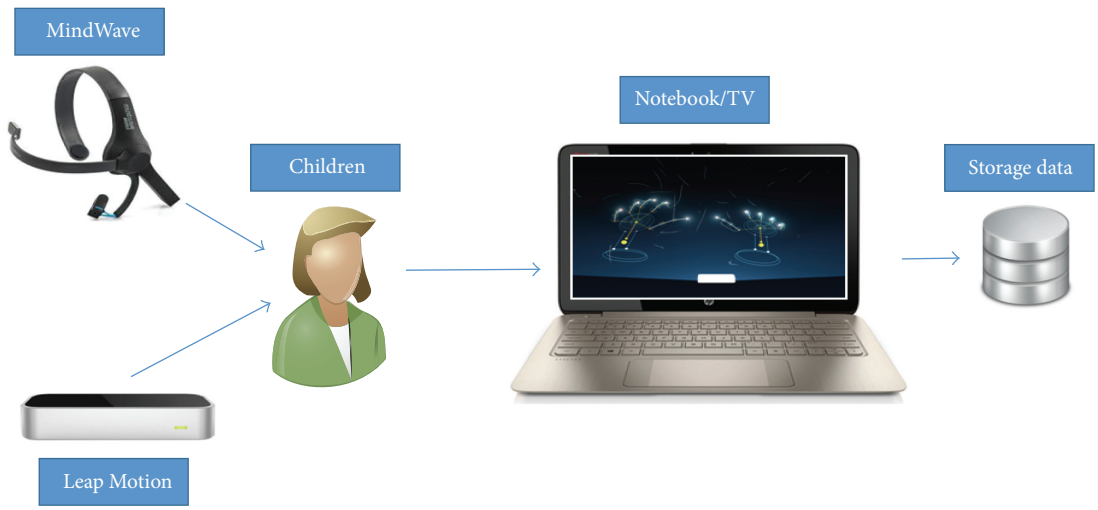


Figure 1: Interaction of patient/children/user with proposed virtual environment.

environments. Developing hand motor skills using the extensor and flexor movements of the elbow joint.

(6) *Phase 6*. Supplementary and without the presence of explicit goals, with the aim of presenting the equipment used to create the virtual environment and of establishing a relationship between motor behavior and the objects in the proposed environment. Stimulating hand movements, through the extension and flexion of the elbow.

Please note that the integration of the child/user with the virtual environment occurs through the motion sensor of the hands and fingers ("Leap Motion"), in which it is possible to select and move objects to reach a specified goal, as explained above. Moreover, during the execution of the activities, the level of attention of the child/user is monitored by the EEG "MindWave" sensor, with the aim of correlating it with the patient's clinical evolution. Attention levels were measured through beta waves in the range of 13 to 30 Hz [30], captured every second during the Phase; when the Phase is completed, the sum of all levels of attention is divided by the execution time of the Phase, and, finally, the average of attention level is measured and stored. In this study, beta frequencies (equivalent to the level of attention [30]) were divided into low beta (13–16.75 Hz) and high beta (18–30 Hz), power was calculated in these bands, and then these values were associated with a range of 0–100 corresponding to different levels of attention of children. Value equal to 0 indicates that the ThinkGear is unable to calculate the level of attention, which can be due to excessive noise. Value between 1 and 20 denotes "strongly reduced" levels of the attention, indicating distraction, agitation, or mental abnormality. A value between 20 and 40 indicates "reduced" levels of the attention. Values from 60 to 80 are considered "slightly elevated" attention. Values from 80 to 100 are considered "elevated," meaning they are strongly indicative of heightened levels of attention. The proposed system is presented in Figure 1.

*2.2. Equipment Integration.* For the development of this virtual environment, we used the framework Unity (5.5.2), in which the user is able to experience immersion in a computer-generated three-dimensional (3D) environment through specialized low-cost equipment.

Unity interacts with the user through the input devices: (i) Leap Motion sensor, in which hand movements are captured with millimeter precision, and (ii) MindWave sensor, which sends attentional feedback to the virtual environment by sending EEG signals in the form of a preprocessed string, so as to supply a range of attentional levels from 0% (no attention) to 100% (maximum attention).

The calculation to measure the level of attention from the EEG signals is based on the analysis of beta waves, as explained below. This information is extracted from a "socket connection" with a port and a standard local address, which allows data to be recorded in JSON format (communication protocol) and sent in real-time to the Unity. The same procedure was applied to the Leap Motion and its Software Development Kit (Leap Manage), which allows reading data in JSON and creating integration for various languages including a script (via plug or SDK) that can be interpreted by Unity. We achieved full integration of the data with the different pieces of equipment, allowing for interactions and enhanced controllability of the system.

*2.2.1. Leap Motion and Unity.* Upload of the Leap Motion library to the Unity is performed through the command "using Leap.Util"; in Unity there is a set of classes aimed at the use of Leap Motion; it is necessary to import the package "*Assets*" with the command "*Unity CoreAsset*," for this project was used at version 2.2.4 [31].

Adding a Controller object to the system, which serves as a connection with the Leap Motion service/daemon, is shown in Box 1.

The library's Leap Motion offers basic gestures, such as the following: (i) circle, which has the action of a finger braiding a circle, (ii) swipe, whose action has a long and

```
class Sample {

   private void verificarPosicao(Frame frame, GameObject objetoParaMovimentar)
   {

      foreach (var h in frame.Hands)
      {
            if (h.IsRight)
            {
                  Leap.Vector position = h.PalmPosition;
                  Vector3 unityPosition = position.ToUnityScaled(false);
                  Vector3 worldPosition = controller.transform.TransformPoint(unityPosition);
                  objetoParaMovimentar.transform.position = new Vector3(worldPosition.x, worldPosition.y, worldPosition.z);
                  Debug.Log("Nome do objeto movim:" + objetoParaMovimentar.name.ToString());

            }
      }

   }
```

Box 1

```
            void Start ()
            {
            handController.GetLeapController ().EnableGesture (Gesture.GestureType.TYPECIRCLE);
            handController.GetLeapController ().EnableGesture (Gesture.GestureType.TYPESWIPE);
            handController.GetLeapController ().EnableGesture (Gesture.GestureType.TYPEKEYTAP);
            handController.GetLeapController ().EnableGesture (Gesture.GestureType.TYPESCREENTAP);
            }
```

Box 2

linear movement of a hand and fingers, (iii) screen tap, which takes action of a move by tapping the finger to simulate touching a monitor vertically, and, finally, (iv) key tap, taking the action of moving by touching a finger, simulating touch of a keyboard key. Box 2 represents the call for habilitation of these movements in the script.

*2.2.2. MindWave and Unity.* The integration of MindWave with Unity is through the ThinkGear Connector (TGC), which uses host settings 127.0.0.1 (localhost), port 13845, and Transmission Control Protocol. Once the *socket* connection is established, the TGC captures the frequency data that the headset sends. When the SWF (Shockwave Flash) files open a socket connection, usually the SWF of this socket automatically prompts one TGC file, called crossdomain.xml, sending the XML in Box 3 to the TGC: "<policy-file-request/>" [32].

In response, the TGC will automatically write the XML in Box 3 for the socket to complete the approval of protocol.

In order for the information established through the protocol to be used by Unity, a new class is created for signal capture. The information captured for use in the application comprises the PoorSignal and Attention functions (see Box 4).

*2.3. Animation.* The first contact of the child/patient/user with the proposed virtual environment is through animation of a book "opening" showing objects and the options to select which Phase the child will play as virtual treatment. The system saves the Phase executed during the last treatment session, as well as the end of each Phase, showing its completion. The animation is accomplished using a set of bones (skeletal representation used to animate objects) on the front of the book and the objects displayed, as shown in Figure 2, in which represent "opening" the book and its rendered image.

After the animation of "closing," corresponding to completion of a given Phase, a bear (Figure 3) with a happy or sad predefined expression is presented as positive or negative reinforcement, respectively, to the child. In order to prevent the child from becoming frustrated and from losing interest in the virtual environment, a specialist can assist them to successfully complete each Phase, increasing the interest for the next Phase.

## 3. Results and Discussions

*Modeling of the Activities.* The six scenarios corresponding to activities that each child will be submitted to, according

```
<?xml version="1.0"?>
<!DOCTYPE cross-domain-policy SYSTEM "http://www.macromedia.com/xml/dtds/cross-domain-policy.dtd">
<cross-domain-policy>
<allow-access-from domain="*" to-ports="*" />
</cross-domain-policy>
```

Box 3

```
void Start()
{
controller = GameObject.Find("ThinkGear").GetComponent<ThinkGearController>();
controller.UpdatePoorSignalEvent += OnUpdatePoorSignal;
controller.UpdateAttentionEvent += OnUpdateAttention;
controller.UpdateDeltaEvent += OnUpdateDelta;
}
```

Box 4

to their clinical evolution or knowledge previously acquired through the conventional treatment, are presented in Figure 4. The goal of each Phase was described in Section 2.1.

Figure 5 shows the use of the alternative treatment tool in a 5-year-old child, considering their behavior during their interaction with the virtual environment through the MindWave and Leap Motion sensors, as well as the usability of the tool for possible adjustments according to the difficulties presented by the child. Initially, we observed that the children tend to face difficulties in task execution, due the proximity of the manipulated object relative to the virtual hand; that is, the virtual hand did not have enough space to move. To solve this problem, the depth scale was adjusted from the virtual environment scenario retreating all scenes in the "$Z$" axis, and, from this adjustment, the virtual hand had more space and could be manipulated to perform the tasks.

*3.1. Validation of the Proposed Virtual Environment.* For validation of the virtual environment, a questionnaire based on the perceptions of specialists at the Occupational Therapy Center of NAMI was considered. According to Pfleeger [33], Wohlin et al. [34], and Wohlin et al. [35], a questionnaire should be used before a technique or tool is submitted to quantitative analysis. The aim of the questionnaire was to assure that important issues related to the study were considered as well as to characterize expectations, perceptions, and opportunities about the real use of the proposed virtual environment as a complementary tool to traditional treatment of children with cerebral palsy.

The questionnaire was carried out after the conclusion of the virtual environment, during an experimental presentation to specialists. The questionnaire was based on activities already undertaken in the conventional treatment, in order to make adjustments and estimate risks. At the end of this process, the system was presented to children.

The questionnaire was composed of 14 questions (11 objective and 3 subjective questions), and was filled out by 8 specialists after exposure to the proposed virtual environment. We found that 87.5% of the specialists considered it highly probable that the proposed virtual environment can assist in the motor rehabilitation of the upper limbs. 50% of experts considered it highly probable that the alternative tool will aid in the cognitive evolution of the patient and enhance the motivation of the patient during the treatment. 37.5% and 62.5% of the experts considered it highly likely and very likely, respectively, that the proposed virtual environment can increase the levels of concentration/attention of children during the treatment, with a positive impact on the evolution of motor and cognitive functions. 12.5%, 25.0%, and 62.5% of the specialists found it extremely likely, very likely, or unlikely, respectively, that the proposed virtual environment can avoid/reduce treatment withdrawal. 37.5% considered it extremely likely, 37.5% considered it very likely, and 25% considered it unlikely that the proposed virtual environment can positively influence the neuroplasticity of children. 87.5% of the experts pointed out that it is very likely and 12.5% pointed out that it is very unlikely that the activities presented in each Phase of the environment/game proposed are aligned with the aims of traditional treatment. When asked whether the virtual environment can jeopardize the motor and cognitive evolution of the children, 12.5% and 87.5% of professionals highlighted that this is very unlikely or not likely, respectively. 25% and 75% of the respondents considered it very likely or unlikely, respectively, that the children may reject using the brainwave sensor. Regarding the possible rejection of using Leap Motion, 12.5% considered it very likely and 87.5% considered it very unlikely to occur.

With regard to the subjective questions, the experts pointed out the following.

*Positive Points*. Positive points are as follows: playful game, with different levels of difficulty, friendly environment, ease of developing new phases with different levels, access to technology, new possibilities of motor and cognitive stimulation, new environment for treatment, motivation, and interest of

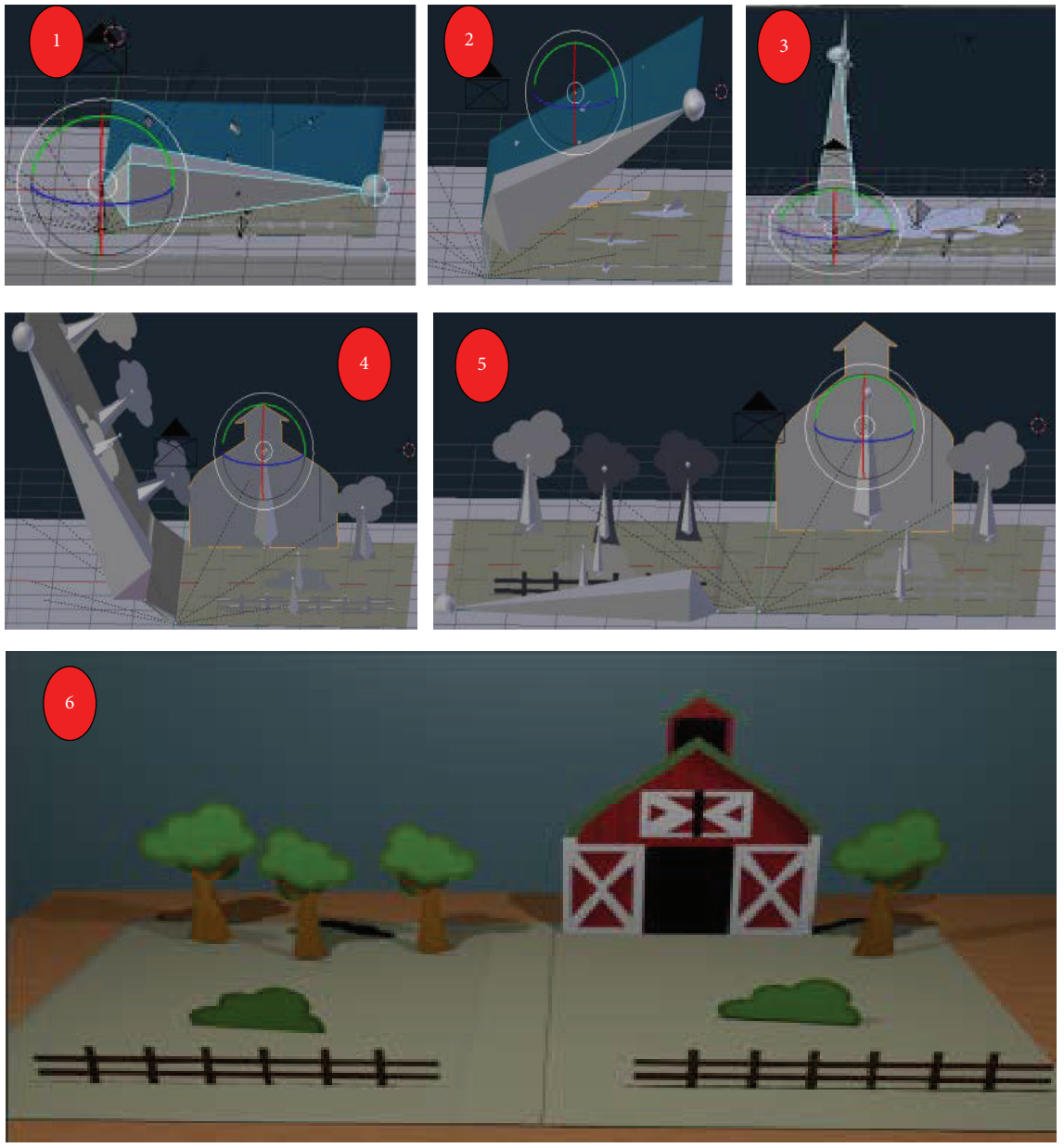


Figure 2: Construction and book opening animation and its rendered image.

the children, enhancement of the attention level, differentiated alternative, and interesting and current tool.

*Negative Points*. Negative points are as follows: concern about overuse, lack of interest in the conventional treatment, possible rejection of the "MindWave" sensor, despite the fact that its use is optional, and difficulty in handling the "Leap Motion" sensor due to the motor restrictions of children, besides other factors.

*Improvements Possibilities*. Improvement possibilities are as follows: adapted chair or another support for children to manipulate the virtual environment using Leap Motion without unnecessary effort, considering the whole body, for example, using sensor Kinect, and updating the environment often to avoid children's disengagement from the task.

The data analysis software ATLAS.ti [36] was used to assess the subjective questionnaire answers by checking how often specific items were listed among the responses. Figure 6 shows the causes that are related to the subjective answers: positive points of the virtual environment, negative points of the virtual environment, and improvement of the virtual environment. It is worth noting the number of times that the positive factor is interconnected with other items, showing great affinity with other answers, differently from negative factors, which have very little connection with the answers.

In consultation with experts in Occupational Therapy and Physical Therapy we established that the group of potential

(a)

(b) (c)

Figure 3: Bear (a) concepts and animation and its (b) sad and (c) happy representation.

users should be selected based on the activities carried out by the expert responsible for monitoring the specific group, who could assess whether the patients could use the proposed virtual environment, given their motor and cognitive levels. The criteria for patients to be included in the study were the following: ataxic, spastic, and dyskinetic cerebral palsy; motor development sufficient for the accomplishment of movements such as walking, running, and jumping; absent or mild spasticity; speed-dependent muscle tone with exacerbation of deep tendon reflexes resulting from hyperexcitability of the stretch reflex; and absence of hypersensitivity to light and attendance to treatment [37].

## 4. Conclusions and Future Perspectives

In this work, we present the development of a new game in virtual reality as an alternative tool to aid the treatment of motor and cognitive impairments in children with cerebral palsy. The integration of the virtual environment with "Leap Motion" was shown to be quite feasible when applied to the rehabilitation of patients with CP, and its integration with MindWave offers a real-time analysis, in which the specialist, to follow the child during the use of this technology, can correlate the level of attention with the evolution of the clinical condition. We found that it was possible to analyze, through testing one child, the possible difficulties and/or facilities of using the proposed method. The application of a questionnaire to specialists allowed assessing the effectiveness and efficiency of the virtual environment, enabling its use in rehabilitation. The specialists were highly optimistic about including the use of the virtual environment in addition to the traditional treatments, as an alternative playful tool for cognitive and motor rehabilitation among children.

As future work, the proposed environment will be included as an auxiliary tool in NAMI, among the complementary activities during the treatment of children with cerebral palsy, analyzing real effectiveness on patient outcomes during a six-month period, periodically assessing the clinical condition of each patient involved.

We intend to analyze the performance of the proposed system for the treatment of other diseases demanding cognitive and motor rehabilitation. If necessary, we will increase

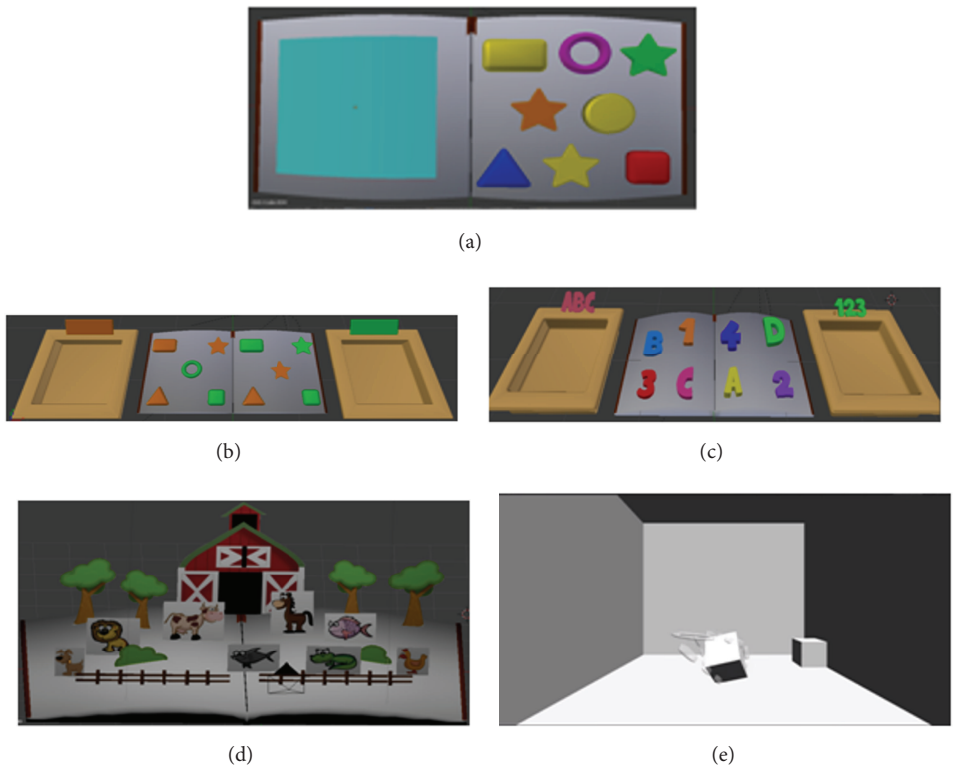


Figure 4: Screenshot of the virtual environment developed used in Phases (a) 1 and 2, (b) 3, (c) 4, (d) 5, and (e) 6.

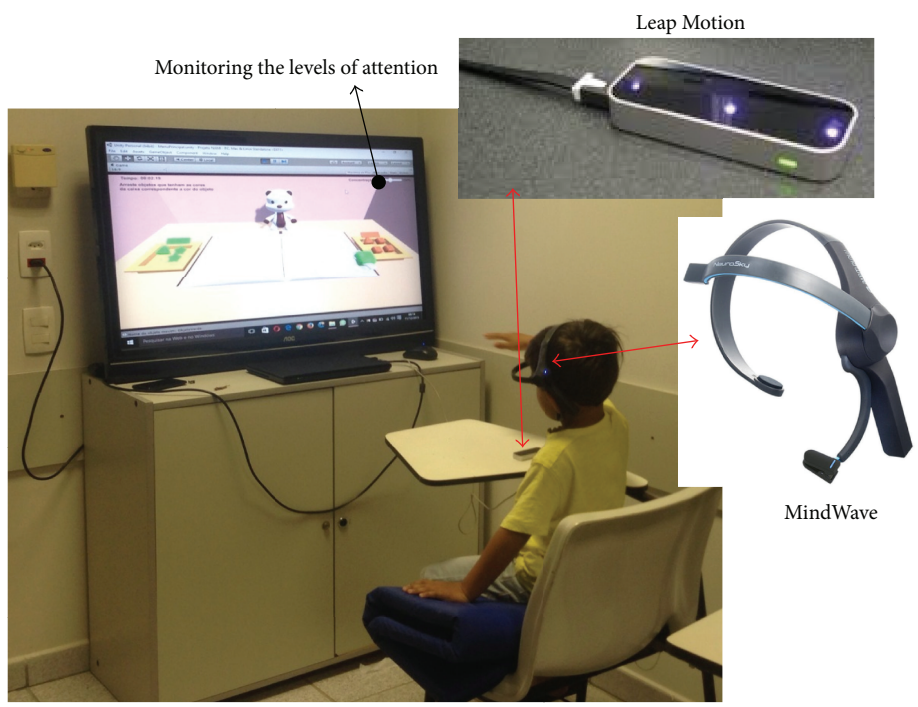


Figure 5: Interaction of the proposed virtual environments with a child.

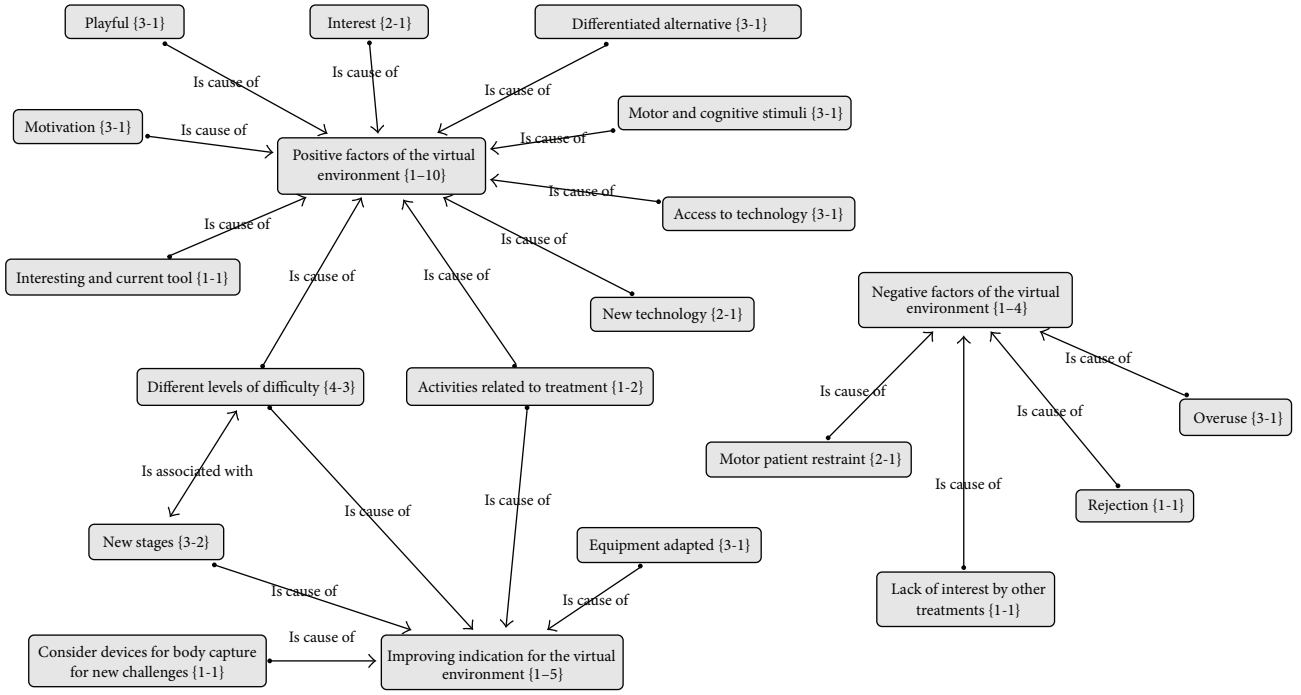


Figure 6: Analysis of the subjective questionnaire answers.

the amount of activities/Phases so as to allow additional levels of difficulty, offering patients new challenges within their limitations. Finally, we plan to assign intelligence to the proposed system, making it able to provide novel changes according to the patient's clinical evolution.

## Competing Interests

The authors declare that they have no competing interests.

## Acknowledgments

The authors thank specialists of the Nucleus for Integrated Medical Assistance (NAMI)/UNIFOR for their support, dedication, and interest in the development and application of the proposed virtual environment. Victor Hugo C. de Albuquerque received support from the Brazilian National Council for Research and Development (CNPq, Grants 470501/2013-8 and 301928/2014-2).

## References

[1] J. N. Latta and D. J. Oberg, "A conceptual virtual reality model," *IEEE Computer Graphics & Applications*, vol. 14, no. 1, pp. 23–29, 1994.

[2] G. Burdea and P. Coiffet, *Virtual Reality Technology*, Wiley-IEEE Press, New York, NY, USA, 2nd edition, 2003.

[3] R. Tori, C. Kirner, and R. Siscoutto, "Fundamentos e tecnologia de realidade virtual e aumentada," in *Proceedings of the 8th Symposium on Virtual Reality*, vol. 2, pp. 2–21, Belém, Brazil, May 2006.

[4] R. C. de la Cuerda, E. Muñoz-Hellín, I. M. Alguacil-Diego, and F. Molina-Rueda, "Telerehabilitation and neurology," *Revista de Neurologia*, vol. 51, no. 1, pp. 49–56, 2010.

[5] E. M. Pereira, F. M. Rueda, I. M. A. Diego, R. C. de la Cuerda, A. D. Mauro, and J. C. M. Page, "Use of virtual reality systems as proprioception method in cerebral palsy: clinical practice guideline," *Neurologia*, vol. 29, no. 9, pp. 550–559, 2014.

[6] B. Bonnechère, B. Jansen, L. Omelina et al., "Can serious games be incorporated with conventional treatment of children with cerebral palsy? A review," *Research in Developmental Disabilities*, vol. 35, no. 8, pp. 1899–1913, 2014.

[7] J. Taylor and K. Curran, "Using leapmotion and gamification to facilitate and encourage rehabilitation for hand injuries: leap motion for rehabilitation," in *Handbook of Research on Holistic Perspectives in Gamification for Clinical Practice*, chapter 9, pp. 183–192, IGI Global, Hershey, Pa, USA, 2015.

[8] M. Khademi, L. Dodakian, H. M. Hondori, C. V. Lopes, A. McKenzie, and S. C. Cramer, "Free-hand interaction with leap motion controller for stroke rehabilitation," in *Proceedings of the 32nd Annual ACM Conference on Human Factors in Computing Systems (CHIEA '14)*, pp. 1663–1668, May 2014.

[9] M. R. Golomb, B. C. McDonald, S. J. Warden et al., "In-home virtual reality videogame telerehabilitation in adolescents with hemiplegic cerebral palsy," *Archives of Physical Medicine and Rehabilitation*, vol. 91, no. 1, pp. 1–8.e1, 2010.

[10] L. Ni, D. Fehlings, and E. Biddiss, "Clinician and child assessment of virtual reality therapy games for motor rehabilitation of cerebral palsy," *Archives of Physical Medicine and Rehabilitation*, vol. 95, no. 10, article e105, 2014.

[11] Y. Salem, S. J. Gropack, D. Coffin, and E. M. Godwin, "Effectiveness of a low-cost virtual reality system for children with developmental delay: a preliminary randomised single-blind controlled trial," *Physiotherapy*, vol. 98, no. 3, pp. 189–195, 2012.

[12] Y.-P. Wuang, C.-S. Chiang, C.-Y. Su, and C.-C. Wang, "Effectiveness of virtual reality using Wii gaming technology in children with Down syndrome," *Research in Developmental Disabilities*, vol. 32, no. 1, pp. 312–321, 2011.

[13] J. Howcroft, S. Klejman, D. Fehlings et al., "Active video game play in children with cerebral palsy: potential for physical activity promotion and rehabilitation therapies," *Archives of Physical Medicine and Rehabilitation*, vol. 93, no. 8, pp. 1448–1456, 2012.

[14] L. Zimmerli, M. Jacky, L. Lünenburger, R. Riener, and M. Bolliger, "Increasing patient engagement during virtual reality-based motor rehabilitation," *Archives of Physical Medicine and Rehabilitation*, vol. 94, no. 9, pp. 1737–1746, 2013.

[15] S.-C. Yeh, M.-C. Huang, P.-C. Wang et al., "Machine learning-based assessment tool for imbalance and vestibular dysfunction with virtual reality rehabilitation system," *Computer Methods and Programs in Biomedicine*, vol. 116, no. 3, pp. 311–318, 2014.

[16] O. Barzilay and A. Wolf, "Adaptive rehabilitation games," *Journal of Electromyography and Kinesiology*, vol. 23, no. 1, pp. 182–189, 2013.

[17] R. Lloréns, C. Colomer-Font, M. Alcañiz, and E. Noé-Sebastián, "BioTrak virtual reality system: effectiveness and satisfaction analysis for balance rehabilitation in patients with brain injury," *Neurologia*, vol. 28, no. 5, pp. 268–275, 2013.

[18] S. Cho, J. Ku, Y. K. Cho et al., "Development of virtual reality proprioceptive rehabilitation system for stroke patients," *Computer Methods and Programs in Biomedicine*, vol. 113, no. 1, pp. 258–265, 2014.

[19] S. J. Lee and M. H. Chun, "Combination transcranial direct current stimulation and virtual reality therapy for upper extremity training in patients with subacute stroke," *Archives of Physical Medicine and Rehabilitation*, vol. 95, no. 3, pp. 431–438, 2014.

[20] A. Mirelman, B. L. Patritti, P. Bonato, and J. E. Deutsch, "Effects of virtual reality training on gait biomechanics of individuals post-stroke," *Gait and Posture*, vol. 31, no. 4, pp. 433–437, 2010.

[21] D. González-Ortega, F. J. Díaz-Pernas, M. Martínez-Zarzuela, and M. Antón-Rodríguez, "A Kinect-based system for cognitive rehabilitation exercises monitoring," *Computer Methods and Programs in Biomedicine*, vol. 113, no. 2, pp. 620–631, 2014.

[22] A. Bufton, A. Campbell, E. Howie, and L. Straker, "A comparison of the upper limb movement kinematics utilized by children playing virtual and real table tennis," *Human Movement Science*, vol. 38, pp. 84–93, 2014.

[23] J. Andrysek, S. Klejman, B. Steinnagel et al., "Preliminary evaluation of a commercially available videogame system as an adjunct therapeutic intervention for improving balance among children and adolescents with lower limb amputations," *Archives of Physical Medicine and Rehabilitation*, vol. 93, no. 2, pp. 358–366, 2012.

[24] G. D. Ferguson, D. Jelsma, J. Jelsma, and B. C. M. Smits-Engelsman, "The efficacy of two task-orientated interventions for children with developmental coordination disorder: neuromotor task training and nintendo Wii fit training," *Research in Developmental Disabilities*, vol. 34, no. 9, pp. 2449–2461, 2013.

[25] L. Fornasari, L. Chittaro, L. Ieronutti et al., "Navigation and exploration of an urban virtual environment by children with autism spectrum disorder compared to children with typical development," *Research in Autism Spectrum Disorders*, vol. 7, no. 8, pp. 956–965, 2013.

[26] Leapmotion. API Overview. Disponible, November, 2015, https://developer.leapmotion.com/documentation/cpp/devguide/Leap_Overview.html?proglang=current.

[27] Neurosky. Brainwave Visualizer. Disponible, November 2015, http://store.neurosky.com/products/brainwave-visualizer.

[28] T. M. Nunes, A. L. V. Coelho, C. A. M. Lima, J. P. Papa, and V. H. C. de Albuquerque, "EEG signal classification for epilepsy diagnosis via optimum path forest—a systematic assessment," *Neurocomputing*, vol. 136, pp. 103–123, 2014.

[29] H. Wallon, *The Psychological Evolution of the Child*, Martins Editora, São Paulo, Brasil, 2010, [Portuguese].

[30] Investigating the NeuroSky MindWave™ EEG Headset, http://www.transportresearchfoundation.co.uk/PDF/PPR726-Investigating-the-NeuroSky-MindWave-EEG-Headset.pdf.

[31] UNITY, "Unity Assets for Leap Motion," https://developer.leapmotion.com/unity#archived.

[32] PROGRAM, Neurosky Develop. Unity, http://developer.neurosky.com/docs/doku.php?id=using_thinkgear_with_unity.

[33] S. L. Pfleeger, "Experimental design and analysis in software engineering," *Annals of Software Engineering*, vol. 1, no. 1, pp. 219–253, 1995.

[34] C. Wohlin, M. Höst, M. C. Ohlsson, B. Regnell, P. Runeson, and A. Wesslén, *Experimentation in Software Engineering: An Introduction*, Kluwer Academic, Norwell, Mass, USA, 2000.

[35] C. Wohlin, M. Höst, and K. Henningsson, "Empirical research methods in software engineering," in *Empirical Methods and Studies in Software Engineering*, vol. 2765 of *Lecture Notes in Computer Science*, pp. 7–23, Springer, Berlin, Germany, 2003.

[36] B. J. Scales, "Qualitative analysis of student assignments: a practical look at ATLAS.ti," *Reference Services Review*, vol. 41, no. 1, pp. 134–147, 2013.

[37] H. A. G. Teive, M. Zonta, and Y. Kumagai, "Treatment of spasticity: an update," *Arquivos de Neuro-Psiquiatria*, vol. 56, no. 4, pp. 852–858, 1998.

Hindawi Publishing Corporation
Computational Intelligence and Neuroscience
Volume 2016, Article ID 5718580, 8 pages
http://dx.doi.org/10.1155/2016/5718580

*Research Article*

# An Analysis of the Effects of Smartphone Push Notifications on Task Performance with regard to Smartphone Overuse Using ERP

**Seul-Kee Kim, So-Yeong Kim, and Hang-Bong Kang**

*Department of Media Engineering, Catholic University of Korea, Bucheon-si, Gyeonggi-do 420-743, Republic of Korea*

Correspondence should be addressed to Hang-Bong Kang; hbkang@catholic.ac.kr

Received 13 January 2016; Revised 28 March 2016; Accepted 5 April 2016

Academic Editor: Victor H. C. de Albuquerque



Smartphones are used ubiquitously worldwide and are essential tools in modern society. However, smartphone overuse is an emerging social issue, and limited studies have objectively assessed this matter. The majority of previous studies have included surveys or behavioral observation studies. Since a previous study demonstrated an association between increased push notifications and smartphone overuse, we investigated the effects of push notifications on task performance. We detected changes in brainwaves generated by smartphone push notifications using the N200 and P300 components of event-related potential (ERP) to investigate both concentration and cognitive ability. ERP assessment indicated that, in both risk and nonrisk groups, the lowest N200 amplitude and the longest latency during task performance were found when push notifications were delivered. Compared to the nonrisk group, the risk group demonstrated lower P300 amplitudes and longer latencies. In addition, the risk group featured a higher rate of error in the Go-Nogo task, due to the negative influence of smartphone push notifications on performance in both risk and nonrisk groups. Furthermore, push notifications affected subsequent performance in the risk group.

## 1. Introduction

Smartphones quickly provide users with various types of information wherever they are, at any time, and enable access to various content via social network services (SNS) and mobile games [1]. In addition, alternative technologies have been installed on smartphones to enable access to content such as GPS, music, and photos, which used to be accessible only through specialized devices like navigation devices, MP3 players, and cameras. Smartphones have become established as tools for day-to-day convenience; however, smartphone addiction has emerged as an increasingly prevalent social issue, which in case of overuse interferes with daily life [2–5].

Smartphone addiction refers to a behavioral disorder in which a person uses content such as SNS, Internet browsing, and mobile games for an excessive amount of time without self-control, such that it interferes with daily life in a manner similar to Internet addiction. Overuse of smartphones negatively affects users, causing psychological conditions such as sleep disorder and attention deficit disorder and physical disabilities such as carpal tunnel syndrome and forward head posture [6–8]. In particular, Kim [9] highlighted push notifications from SNS, multimedia message services (MMS), or applications (apps) as important factor to the excessive use of smartphones. Here, a push notification refers to a frequent alarm that provides users with information regardless of whether they want it or not. This is the opposite concept to pull methods, in which the user directly searches for information. With push notifications, the smartphone providing the information also controls the flow of information. While the advantage of push notifications is that information can be instantly delivered, this information is provided regardless of the users need. Kim [9] reported that the duration and frequency of smartphone usage increased with the number of push notifications, concomitant with an increased risk of developing smartphone addiction.

However, since most studies on smartphone addiction or overuse have included questionnaire-based surveys or behavioral observations [6, 10, 11], these results are based on subjective opinions and might therefore be biased by

individual perception. It was subsequently difficult to investigate changes in behavioral characteristics or cognitive ability caused by smartphone overuse. Therefore, it is necessary to explore them using objective measurements.

In this paper, we analyze brainwaves to detect the effects of smartphone push notifications on task performance with regard to smartphone overuse. Brainwaves refer to the recording of continuous changes in potential between two points on the scalp, which relate to electrical activity in the brain. Brainwave signals vary according to neural activity, the conditions at the time of measurement, and general brain function. We measured event-related potentials (ERPs) in order to study the brainwaves produced in response to a specific stimulus. In many studies, ERP was used to assess both concentration and cognitive ability using repeated tasks, wherein the same stimulus was presented repeatedly, and differences in the averaged potentials induced by the stimulus were analyzed. Specifically, this study investigated the ERP components N200 and P300, which reflect cognitive functions such as attention and concentration [12, 13]. Next, we measured changes in concentration and cognition ability caused by various levels of smartphone overuse.

## 2. Related Works

*2.1. Smartphone Addiction.* Recent studies have addressed the issue of pathological smartphone use. Existing studies on smartphone addiction mostly consist of surveys based on questionnaires and interviews. However, these studies did not reflect continuous evaluation, and doubts have been raised regarding the objectivity of such evaluations. Darcin et al. [14] defined smartphone addiction in college students with regard to social anxiety and loneliness and reported that people who were younger when they first used smartphone-based SNS exhibited a wider range of addictive smartphone habits. In addition, this study found that psychological tendencies, such as loneliness, were strongly linked to excessive smartphone use.

Moreover, Sayrs [15] reported that cognitive states, including stress, productivity, boredom, and loneliness, were related to smartphone use. Lee et al. [1] monitored the usage of GPS apps and other tools in order to objectively measure patterns of pathological smartphone use, performed statistical analysis of the data, and compared the analysis results with Korean smartphone addiction scale (K-SAS) scores. The results identified a strong correlation between K-SAS results and the data obtained by statistical analysis. Based on these findings, Lee et al. [1] proposed a smartphone addiction management system (SAMS). Accordingly, Lin et al. [16] created a mobile app for the identification of smartphone addiction, which indicated that the frequency of smartphone use was strongly linked to smartphone addiction. Park et al. [17] conducted a survey questionnaire consisting of the following items: motivation for social inclusion, motivation for instrumental use, innovativeness, intention to keep using the smartphone, smartphone dependency, and so forth. As a result, they suggested that smartphone dependency was affected by smartphone usage history.

Furthermore, Lee et al. [18] analyzed smartphone usage patterns and habits in a smartphone risk group and a nonrisk group and reported that the duration and frequency of smartphone use correlated with excessive use. Push notifications for incoming messages were strongly linked to smartphone addiction. Despite little difference in the duration of smartphone use between the risk group and the nonrisk group, they identified that previous studies focused on the duration of use as a cause of addiction rather than a characteristic of use. Therefore, they suggested that characteristics of smartphone use other than duration should be investigated. Similarly, Xu et al. [19] argued that despite the introduction of various mobile devices and apps, the understanding of smartphone usage patterns is lacking compared to that of the existing web services. In addition, Xu et al. [19] investigated the usage patterns of apps at a national level and reported various usage patterns according to a smartphone user's pattern of behavior (time, place, object, etc.).

*2.2. Auditory Notification.* Auditory push notifications are a useful tool for notifying users of incoming data and messages. However, push notifications may also cause stress, depending on the user's environment. Previous studies have evaluated the effects of auditory push notifications on behavior but have failed to consider various factors between users, including subjective and environmental differences. To overcome this limitation, performance evaluation methods that can be applied to various environments have been suggested [20]. Yoon and Lee [21] performed a study into the stress levels of users who received push notifications from a smartphone messenger and proposed a design method for push notifications that might reduce stress. Kim [9] investigated the effects of push notifications on the formation of habits for mobile app use and found that increasing the number of push notifications produced a greater frequency of app visits. These results suggest an effect of push notifications on media habit formation.

*2.3. ERP.* ERPs refer to brainwaves that occur in response to a specific stimulus and reflect brain responses associated with sensory, motor, and cognitive events. ERP-based methods of assessment are widely used in behavioral research, since they provide high temporal resolution of neural processes relating to behavior [22]. Most ERP studies focus on stimulus responses relating to sensory and cognitive abilities. Two important components of ERP analysis are P300 and N200. P300 refers to a peak in the positive direction appearing in the interval between 300 and 350 ms after the presentation of auditory stimuli and between 350 and 450 ms after the presentation of visual stimuli. The maximum amplitude appears at parietal electrode sites, and as a component of ERP, it is an important index for the study of information processing in the brain, with particular relevance to cognitive psychology [23, 24].

P300 is divided into P3a and P3b. P3a usually refers to P300 and exhibits maximum amplitude in the frontal and central regions when nontarget stimuli appear amidst repeated target stimuli. P3a relates to attention processing and features a relatively larger amplitude and shorter latency

than P3b. P3b refers to a component that exhibits maximum amplitude in the parietal region in response to target stimuli [25–27]. Since the latency of P300 is typically believed to represent the speed of stimulus classification, a shorter latency reflects superior cognitive ability. The amplitude of P300 reflects stimulus information, wherein a higher level of concentration is accompanied by a larger amplitude. Therefore, a reduction in P300 amplitude is used as an indicator of various psychological symptoms, including alcohol and drug addiction [28].

By contrast, N200 refers to a stimulus-induced negative peak appearing in the interval between 250 and 400 ms (180–325 ms) after stimulus onset. N200 is the greatest in the frontal and central regions and is divided into the following three components: N2a, N2b, and N2c. N2a, also referred to as mismatch negativity (MMN), reflects mismatched responding to a task. MMN is a component induced by an infrequent stimulus that appears amidst a repeated stimulus and is mainly assessed in studies relating to auditory stimuli [13]. Unlike MMN, N2b is not limited to auditory processes but appears in response to both visual and auditory stimuli. N2b is mainly observed using the oddball paradigm and appears in central regions in response to nontarget stimuli. Comparatively, N2c is expressed in posterior regions in response to visual stimuli and in frontal-central regions in response to auditory stimuli. The latency of N2c is an indicator of reaction time in response to the stimulus, and N2c amplitude is larger in response to target stimuli compared to nontarget stimuli. The subcomponents of N200 possess distinct characteristics. N2a does not require concentration on the stimulus and does not appear in conjunction with the P3 component. However, N2b and N2c require concentration on the stimulus and appear together with P3a and P3b, respectively [29].

Cristini et al. [30] used ERPs to assess recurrence risk in patients with alcohol addiction. They reported increased recurrence among patients with alcohol addiction who demonstrated higher P300 amplitudes at the Cz and Pz electrodes. Pandey et al. [31] found that the N200 amplitude of patients with alcohol addiction was not increased between Nogo and Go responses and reported that this was the result of a decline in frontal lobe function. However, no previous study has used ERPs to investigate the differences in response to push notifications with regard to smartphone overuse. Therefore, the aim of this study was to use the Go-Nogo task to study the effects of smartphone push notifications on task performance by analyzing N200 and P300 components [32].

## 3. Research Goals

The aim of this study was to monitor both the amplitude and latency of the ERP components N200 and P300, in order to evaluate the effects of push notifications on task performance, and to identify whether the concentration and cognitive abilities of the smartphone risk group were reduced compared to the nonrisk group. We performed a Go-Nogo task twice, with each round consisting of three sessions. Subjects were given a push notification with a natural intensity during the first session of the first Go-Nogo task. The push notification was also delivered before starting the third session. From this, we investigated the effects of smartphone push notifications before and during the task on subjects' task performance. No push notifications were delivered in the second Go-Nogo task, during which performance was compared depending on the presence or absence of smartphone push notifications.

## 4. Methods

*4.1. Subjects.* Subjects were recruited using an announcement for a study to analyze brainwaves according to the colorfulness of a video, in order to blind them from the nature of the experiment. A presurvey was conducted with questions taken from the smartphone addiction scale (hereafter, S scale) developed by the Korean National Information Society Agency in 2011 [33] and additional questions. Individuals on the boundary between the smartphone risk and nonrisk groups were excluded in order to obtain a distinct difference between the two groups. The experiment took no longer than 2 hours, and subjects were informed about the experiment prior to completion. This excluded the delivery of push notifications but included instructions about filling in a consent form prior to the experiment. Data from 14 subjects was used for analysis, with six in the risk group (3 women and 3 men; mean age, 22 years) and eight in the nonrisk group (5 women and 3 men; mean age, 22.6 years).

*4.2. Go-Nogo Task.* Various figures were presented in the center of a screen with a white background, as shown in Figure 1, and trials were designed so that subjects pressed number 1 when the color of the figure was yellow and pressed nothing when it was green. The length of stimulus presentation was set to 150 ms, and each session was composed of 186 trials, with 148 Go trials and 38 Nogo trials. Subjects were allowed 1 min of practice prior to the main trial, which was composed of three sessions. Each session lasted for approximately 6 min, with 1 min rest between sessions. Therefore, task performance lasted for a total of approximately 18 min.

*4.3. Push Notification.* This experiment used vibration push notifications for all subjects in order to prevent differences in response relating to the smartphone notification sound. Push notifications were delivered twice during the experiment. This is shown in Figure 2. The first push notification (hereafter, P1) was presented during performance of the Go-Nogo task in Session 1, and the second push notification (hereafter, P2) was presented during rest time before starting the Go-Nogo task in Session 3. Push notifications were delivered via a special device, placed behind the subjects so that they were clearly able to recognize the push notification but were not able to check it.

*4.4. EEG (Electroencephalogram) Procedure.* Subjects wore an EEG cap during the experiment to record brainwaves. The experiment was composed of three steps: Task 1 with the push notification, watching a video, and Task 2 without the push notification (hereafter, P3). This is shown in Figure 3. Approximately 18-minute-long Go-Nogo tasks were performed during Tasks 1 and 2. Two push notifications (P1

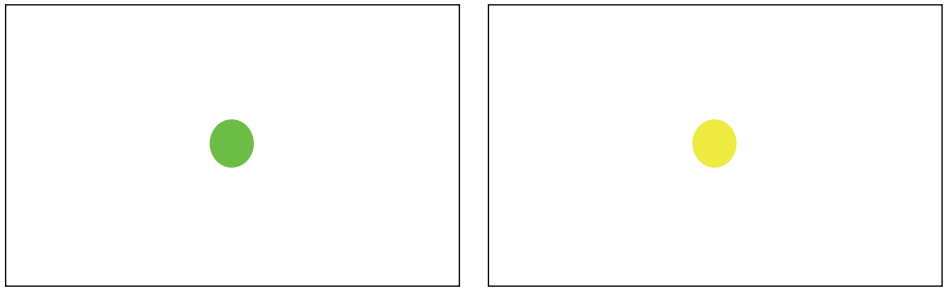


Figure 1: Go-Nogo task: (a) example of Go task and (b) example of Nogo task.

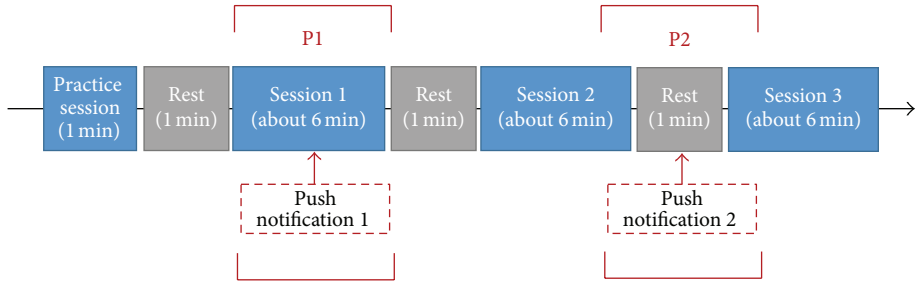


Figure 2: Go-Nogo task procedure.

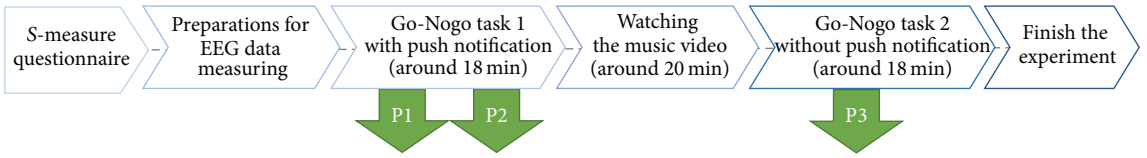


Figure 3: Experimental procedure.

and P2) were delivered when performing Task 1. Subjects watched a video during the rest between the first and the second tasks. A null push notification (P3) was delivered during the second task so that the data could be used as a control. In all experiments, the subjects performed the tasks in a separate space to the tester with illumination intensity of 0, so that they could focus on the task.

## 5. Data Analysis

*5.1. ERP (Event-Related Potential).* For ERP analysis, N200 and P300 were analyzed for Nogo responses in order to examine the differences in task performance between the smartphone risk group and the nonrisk group following the administration of push notifications. A NeuroScan device and the Curry 7 software program were used for the measurement of brainwaves. To minimize noise in the experiment, brainwave data were recorded after impedance was set to 5 or below, while electrodes with an impedance of 10 or over at the end of the experiment were excluded from analysis. Brainwaves were measured based on 10-20 system as shown in Figure 4. Of the 64 channels, FCz in the central frontal region was selected as the representative electrode for ERP

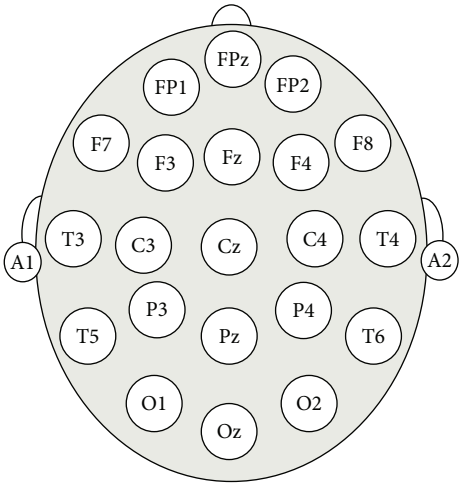


Figure 4: International 10-20 electrode placement system.

measurement, since N200 and P300 could be easily measured and there was less noise in the data. To remove noise from the ERP data, the pre-200 ms and post-800 ms domains in

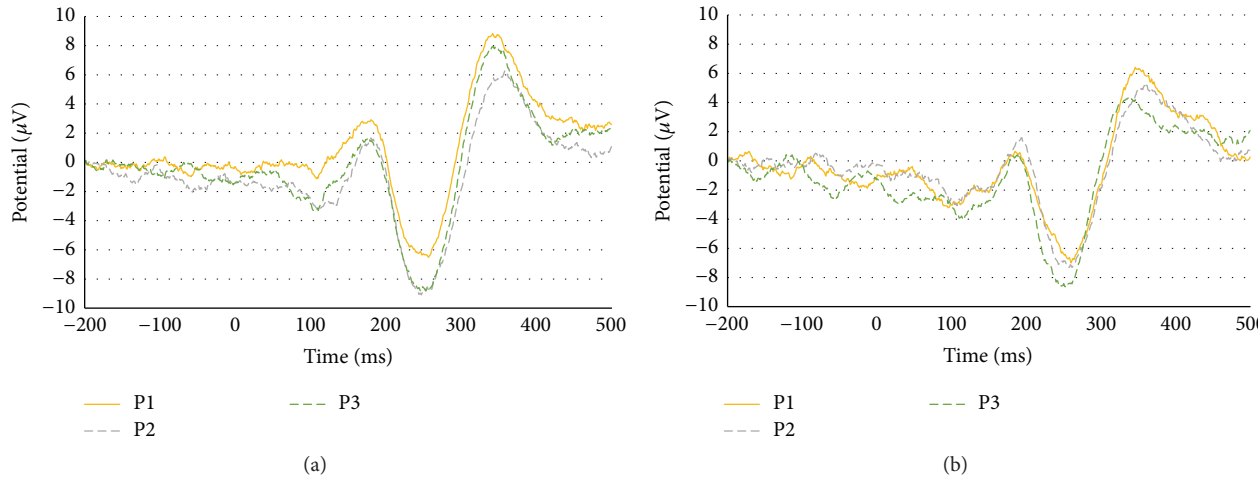


Figure 5: Results of the between-sessions, within-group comparisons: (a) nonrisk group and (b) risk group.

the area outside of the threshold (min 0, max 60) were substituted for the covariance values and the baseline was set to constant. A mean ERP plot of the interval between −200 ms and 500 ms was derived from 38 Nogo trials in each session. Since it was difficult to verify the normal distribution of the amplitude and latency data, we conducted nonparametric statistical testing using the Mann-Whitney $U$ test.

*5.2. Go-Nogo Task.* The two tasks were compared with regard to differences in performance based on smartphone push notifications. First, in order to identify differences according to the timing of push notifications, performance in P1, during which the push notification was delivered during the task, was compared with that of P2, where the push notification was delivered prior to the task. Second, in order to ascertain differences according to the presence or absence of push notifications, P1 performance with push notifications and P3 performance without push notifications were compared. Here, performance referred to error rate and reaction time. The error rate was defined as the rate of Go responses in Nogo trials and the number of Nogo responses within Go trials across all sessions, wherein reaction time referred to the response time in Go trials.

## 6. Results

*6.1. ERP (Event-Related Potential).* ERP data were compared between sessions within each group and between the risk and the nonrisk groups for each session. The results of the between-session, within-group comparisons are presented in Figure 5, where the yellow, gray, and green lines show the ERPs for P1, P2, and P3, respectively. Results for the comparison between the risk and nonrisk groups in each session are presented in Figure 6, where the blue and red lines indicate the nonrisk and the risk group, respectively. The N200 amplitude and latency values are presented in Table 1.

When the amplitudes of the risk group were compared by session, the lowest amplitude (−6.99 $\mu$V) was detected in P1, in which the push notification was presented during the task, and the second lowest amplitude (−7.315 $\mu$V) was detected in P2, in which the push notification was presented before starting the task. P1 (261 ms) and P2 (258 ms) featured similarly long latencies, whereas P3 had a shorter latency (253 ms). These data indicate that P1, in which push notifications were presented during the task, had the greatest impact on concentration and cognitive ability in the risk group.

In the nonrisk group, similar to the risk group, P1 featured the lowest amplitude (−6.503 $\mu$V), whereas the amplitudes of P3 (−8.834 $\mu$V) and P2 (−9.086 $\mu$V) were similar. Latency values were 258 ms for P1, 248 ms for P2, and 247 ms for P3, wherein P1 demonstrated the longest latency, indicating that concentration and cognitive ability declined in the nonrisk group following push notification delivery during the task, whereas notifications before the task had no effect on ability. When the nonrisk group and the risk group were compared in each session, the amplitude of P1 (−6.503 $\mu$V) in the nonrisk group was smaller than that of the risk group (−6.99 $\mu$V). For P2 and P3, by contrast, the amplitudes of the risk group (−7.315 $\mu$V, −8.635 $\mu$V) were lower than those of the nonrisk group (−9.086 $\mu$V, −8.834 $\mu$V). In addition, the risk group demonstrated longer latencies than the nonrisk group in all sessions. This indicates that push notifications delivered during the task affected the nonrisk group; however, subsequent task performance was not affected.

By contrast, the risk group was continuously affected by push notifications delivered during the task, even during subsequent task performance. The amplitude and latency of P300 are presented in Table 2. P300, unlike N200, exhibited no particular trends with regard to amplitude or latency in either session for the risk group or the nonrisk group. When the risk and nonrisk group were compared across sessions, P1, P2, and P3 in the risk group exhibited lower amplitudes than those in the nonrisk group, and P1 and P2 featured longer latencies. These data indicate that the risk group was more affected by push notifications than the nonrisk group.

*6.2. Go-Nogo Task.* Error rate and reaction time for the Go-Nogo task are shown in Figure 7. The risk group featured

Table 1: N200 amplitude and latency.

| | Nonrisk group | | | Risk group | | |
|---|---|---|---|---|---|---|
| Session | P1 | P2 | P3 | P1 | P2 | P3 |
| Amplitude ($\mu$V) | −6.50376 | −9.08664 | −8.83492 | −6.99048 | −7.3151 | −8.63528 |
| Latency | 258 | 248 | 247 | 261 | 258 | 253 |

Table 2: P300 amplitude and latency.

| | Nonrisk group | | | Risk group | | |
|---|---|---|---|---|---|---|
| Session | P1 | P2 | P3 | P1 | P2 | P3 |
| Amplitude ($\mu$V) | 8.83268 | 6.27596 | 7.96026 | 6.410275 | 5.35475 | 4.364368 |
| Latency | 343 | 359 | 347 | 347 | 361 | 338 |

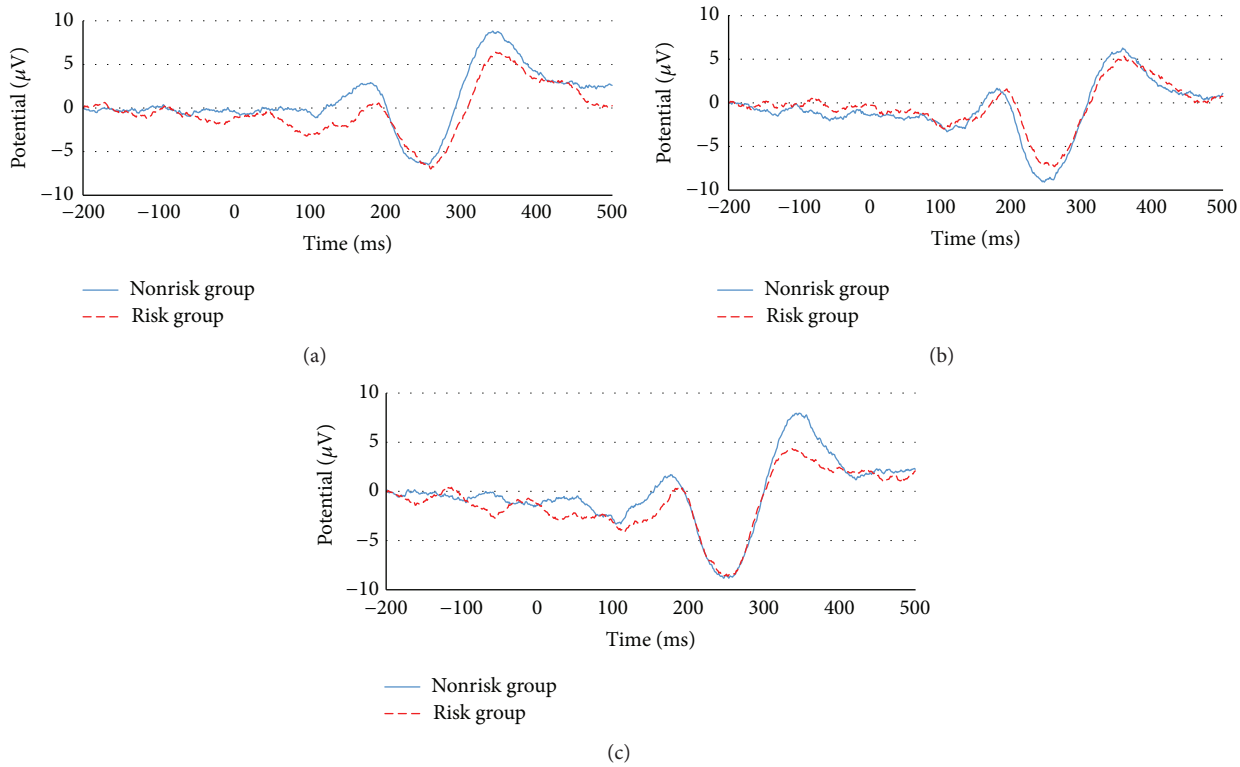


Figure 6: Comparison between the nonrisk group and the risk group in each session: (a) P1 session, (b) P2 sessions, and (c) P3 sessions.

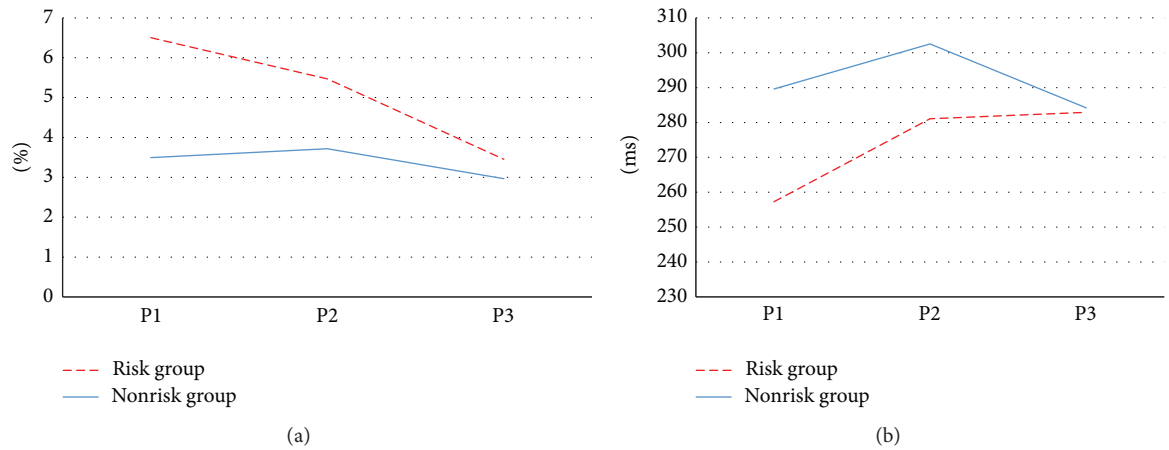


Figure 7: Results of Go-Nogo task: (a) error rate and (b) reaction time.

higher error rate values overall. Performance during P1, when push notifications were delivered during the task, featured the highest error rate. The nonrisk group showed similar error rates for P1, P2, and P3. The risk group exhibited shorter reaction times than the nonrisk group. In addition, no significant differences were identified in reaction time or error rate between P1, P2, and P3 in the nonrisk group, whereas the risk group exhibited shorter reaction times and higher error rates in P1, which then stabilized in P2 and P3. This indicates that the risk group made hastier decisions during P1 than the other sessions, due to the effects of push notification delivery on task performance.

## 7. Discussion

Subjects in the present study performed tasks composed of repeated trials to investigate the effects of push notifications between a smartphone risk group and a nonrisk group. The two tasks were divided into three subsessions (P1, P2, and P3) with varying conditions. Previous studies [3–5] indicated the effects of smartphone addiction using surveys or psychological and behavioral observations. It was possible to determine the effects of smartphone addiction or overuse on physical or psychological health by the users' responses. However, such studies might generate superficial results due to the subjective nature of previous research. Therefore, it is necessary to investigate the physiological effects of smartphone overuse in terms of changes in brainwaves.

To address this problem, we analyzed changes in brainwaves relative to physiological effects or cognitive ability. From the ERP experimental results, we found that differences in concentration and cognition ability correlated with levels of smartphone overuse. Lee et al. [18] found a correlation between smartphone addiction and push notifications. In our study, the smartphone overuse group (the risk group) was more sensitive to push notifications than the nonrisk group. In particular, the risk group demonstrated impaired concentration after hearing the push notification, an observation that was not detected in the nonrisk group.

However, our experiments had several limitations. First, since only FCz electrodes were used in the present study, we were unable to investigate the reaction of parietal or occipital regions. If we compared brainwaves at additional electrode positions, it would be possible to investigate the functional influence of smartphone overuse in various brain regions. In addition, this study utilized the same Go-Nogo task in all sessions to create an experimental environment in which only the push notifications were not controlled.

## 8. Conclusion

In this paper, we explored the effects of smartphone push notification delivery during a task according to the level of smartphone overuse using ERP. From our experimental results, we found that both the smartphone risk group and the nonrisk group demonstrated sensitive reactions to smartphone push notifications during tasks. While the performance of the nonrisk group was unaffected by previously delivered push notifications, the delivery of push notifications affected subsequent task performance in the risk group. In other words, smartphone push notifications produced a decline in task performance in the smartphone risk group, exerting a negative influence on cognitive function and concentration.

ERP was able to measure the negative effects of smartphone overuse in terms of psychological or physical characteristics. Particularly in the risk group, we observed lower N200 amplitude and longer response latency. A higher error rate and longer reaction time were also identified in the risk group during the Go-Nogo task.

In future studies, it might be possible to determine the level of smartphone overuse by measuring responses to push notifications. While this study used a single type of push notification, future studies using various types will be required to investigate sensitivity to different push notifications.

## Competing Interests

The authors declare that they have no competing interests.

## Acknowledgments

This research was supported by Basic Science Research Program through the National Research Foundation of Korea (NRF) funded by the Ministry of Science, ICT and Future Planning (no. 2015R1A2A1A10056304).

## References

[1] H. Lee, H. Ahn, S. Choi, and W. Choi, "The SAMS: smartphone addiction management system and verification," *Journal of Medical Systems*, vol. 38, article 1, pp. 1–10, 2014.

[2] J. Billieux, "Problematic use of the mobile phone: a literature review and a pathways model," *Current Psychiatry Reviews*, vol. 8, no. 4, pp. 299–307, 2012.

[3] M. Samaha and N. S. Hawi, "Relationships among smartphone addiction, stress, academic performance, and satisfaction with life," *Computers in Human Behavior*, vol. 57, pp. 321–325, 2016.

[4] M. Bian and L. Leung, "Linking loneliness, shyness, smartphone addiction symptoms, and patterns of smartphone use to social Capital," *Social Science Computer Review*, vol. 33, no. 1, pp. 61–79, 2015.

[5] S. Kim, J. Kim, and Y. Jee, "Relationship between smartphone addiction and physical activity in Chinese international students in Korea," *Journal of Behavioral Addictions*, vol. 4, no. 3, pp. 200–205, 2015.

[6] K. Hwang, Y. Yoo, and O. Cho, "Smartphone overuse and upper extremity pain, anxiety, depression, and interpersonal relationships among college students," *The Journal of the Korea Contents Association*, vol. 12, no. 10, pp. 365–375, 2012.

[7] C. Jenaro, N. Flores, M. Gómez-Vela, F. González-Gil, and C. Caballo, "Problematic internet and cell-phone use: psychological, behavioral, and health correlates," *Addiction Research & Theory*, vol. 15, no. 3, pp. 309–320, 2007.

[8] Y.-K. Lee, C.-T. Chang, Y. Lin, and Z.-H. Cheng, "The dark side of smartphone usage: psychological traits, compulsive behavior and technostress," *Computers in Human Behavior*, vol. 31, no. 1, pp. 373–383, 2014.

[9] M. Kim, "The effect of push notification alerts on mobile application usage habit," in *Society for Journalism and Communication Studies*, pp. 358–387, 2015.

[10] B. Kim, E. Ko, and H. Choi, "A study on factors affecting smartphone addiction in university students: a focus on differences in classifying risk groups," *Studies on Korean Youth*, vol. 24, no. 3, pp. 67–98, 2013.

[11] W. Lee, "An exploratory study on addictive use of smartphone: developing SAUS (Smartphone Addictive Use Scale)," *Journal of Convergence Information Technology*, vol. 8, no. 12, pp. 403–407, 2013.

[12] J. R. Folstein and C. Van Petten, "Influence of cognitive control and mismatch on the N2 component of the ERP: a review," *Psychophysiology*, vol. 45, no. 1, pp. 152–170, 2008.

[13] U. Roeber, A. Widmann, and E. Schröger, "Auditory distraction by duration and location deviants: a behavioral and event-related potential study," *Cognitive Brain Research*, vol. 17, no. 2, pp. 347–357, 2003.

[14] A. E. Darcin, C. Noyan, S. Nurmedov, O. Yilmaz, and N. Dilbaz, "Smartphone addiction in relation with social anxiety and loneliness among university students in Turkey," *European Psychiatry*, vol. 30, p. 505, 2015.

[15] E. Sayrs, "The effects of smartphone use on cognitive and social functions," TAM Capstone Thesis Paper, 2013.

[16] Y.-H. Lin, Y.-C. Lin, Y.-H. Lee et al., "Time distortion associated with smartphone addiction: identifying smartphone addiction via a mobile application (app)," *Journal of Psychiatric Research*, vol. 65, pp. 139–145, 2015.

[17] N. Park, Y.-C. Kim, H. Y. Shon, and H. Shim, "Factors influencing smartphone use and dependency in South Korea," *Computers in Human Behavior*, vol. 29, no. 4, pp. 1763–1770, 2013.

[18] U. Lee, J. Lee, M. Ko et al., "Hooked on smartphones: an exploratory study on smartphone overuse among college students," in *Proceedings of the 32nd Annual ACM Conference on Human Factors in Computing Systems (CHI '14)*, pp. 2327–2336, Toronto, Canada, May 2014.

[19] Q. Xu, J. Erman, A. Gerber, Z. Mao, J. Pang, and S. Venkataraman, "Identifying diverse usage behaviors of smartphone apps," in *Proceedings of the ACM SIGCOMM Conference on Internet Measurement Conference (IMC '11)*, pp. 329–344, Berlin, Germany, November 2011.

[20] Y. Lee, W. Lin, J. King, L. Ko, Y. Huang, and F. Cherng, "An EEG-based approach for evaluating audio notifications under ambient sounds," in *Proceedings of the SIGCHI Conference on Human Factors in Computing Systems (CHI '14)*, pp. 3817–3826, ACM, Toronto, Canada, 2014.

[21] S. Yoon and K. Lee, "A study on notification system design of smartphone messenger considering the user's stress," *Archives of Design Research*, vol. 28, no. 2, pp. 75–88, 2015.

[22] R. Näätänen, P. Paavilainen, T. Rinne, and K. Alho, "The mismatch negativity (MMN) in basic research of central auditory processing: a review," *Clinical Neurophysiology*, vol. 118, no. 12, pp. 2544–2590, 2007.

[23] J. Polich, "Updating P300: an integrative theory of P3a and P3b," *Clinical Neurophysiology*, vol. 118, no. 10, pp. 2128–2148, 2007.

[24] O. P. Tandon and A. S. Mahajan, "Averaged evoked potentials: event related potentials (ERPs) and their applications," *Indian Journal of Physiology and Pharmacology*, vol. 43, no. 4, pp. 425–434, 1999.

[25] M. D. Comerchero and J. Polich, "P3a and P3b from typical auditory and visual stimuli," *Clinical Neurophysiology*, vol. 110, no. 1, pp. 24–30, 1999.

[26] C. Escera, K. Alho, E. Schröger, and I. Winkler, "Involuntary attention and distractibility as evaluated with event-related brain potentials," *Audiology and Neurotology*, vol. 5, no. 3-4, pp. 151–166, 2000.

[27] J. Polich and J. R. Criado, "Neuropsychology and neuropharmacology of P3a and P3b," *International Journal of Psychophysiology*, vol. 60, no. 2, pp. 172–185, 2006.

[28] S. Sur and V. K. Sinha, "Event-related potential: an overview," *Industrial Psychiatry Journal*, vol. 18, no. 1, pp. 70–73, 2009.

[29] S. H. Patel and P. N. Azzam, "Characterization of N200 and P300: selected studies of the event-related potential," *International Journal of Medical Sciences*, vol. 2, no. 4, pp. 147–154, 2005.

[30] P. Cristini, C. Fournier, M. Timsit-Berthier, M. Bailly, and C. Tijus, "ERPs (N200, P300 and CNV) in alcoholics: relapse risk assessment," *Neurophysiologie Clinique*, vol. 33, no. 3, pp. 103–119, 2003.

[31] A. K. Pandey, C. Kamarajan, Y. Tang et al., "Neurocognitive deficits in male alcoholics: an ERP/sLORETA analysis of the N2 component in an equal probability Go/NoGo task," *Biological Psychology*, vol. 89, no. 1, pp. 170–182, 2012.

[32] M. Falkenstein, J. Hoormann, and J. Hohnsbein, "ERP components in Go/Nogo tasks and their relation to inhibition," *Acta Psychologica*, vol. 101, no. 2-3, pp. 267–291, 1999.

[33] D. Kim, Y. Lee, J. Lee, J. K. Nam, and Y. Chung, "Development of Korean smartphone addiction proneness scale for youth," *PLoS ONE*, vol. 9, no. 5, Article ID e97920, 2014.

Hindawi Publishing Corporation
Computational Intelligence and Neuroscience
Volume 2016, Article ID 3861425, 15 pages
http://dx.doi.org/10.1155/2016/3861425

*Research Article*

# A Prototype SSVEP Based Real Time BCI Gaming System

**Ignas Martišius[1] and Robertas Damaševičius[2]**

[1]*Department of Computer Science, Kaunas University of Technology, Studentu 50-415, LT-51368 Kaunas, Lithuania*
[2]*Department of Software Engineering, Kaunas University of Technology, Studentu 50-415, LT-51368 Kaunas, Lithuania*

Correspondence should be addressed to Robertas Damaševičius; robertas.damasevicius@ktu.lt

Received 15 November 2015; Revised 6 January 2016; Accepted 10 January 2016

Academic Editor: Victor H. C. de Albuquerque



Although brain-computer interface technology is mainly designed with disabled people in mind, it can also be beneficial to healthy subjects, for example, in gaming or virtual reality systems. In this paper we discuss the typical architecture, paradigms, requirements, and limitations of electroencephalogram-based gaming systems. We have developed a prototype three-class brain-computer interface system, based on the steady state visually evoked potentials paradigm and the Emotiv EPOC headset. An online target shooting game, implemented in the OpenViBE environment, has been used for user feedback. The system utilizes wave atom transform for feature extraction, achieving an average accuracy of 78.2% using linear discriminant analysis classifier, 79.3% using support vector machine classifier with a linear kernel, and 80.5% using a support vector machine classifier with a radial basis function kernel.

## 1. Introduction

Since the first experiments of electroencephalography (EEG) on humans in 1929, the EEG of the human brain has been used mainly to evaluate neurological disorders in the clinical environment and to investigate brain functions in the laboratory. An idea that brain activity could be used as a communication channel has gradually emerged. The possibility of recognizing a single message or command considering the complexity, distortion, and variability of brain signals appeared to be extremely remote. Yet EEG demonstrates direct correlations with user intentions, thereby enabling a direct brain-computer interface (BCI) communication channel. BCI requires high computational capacity to analyse brain signals in detail and in real time, and until recently the requisite technology either did not exist or was extremely expensive. The continuing development of computer hardware and software now supports highly sophisticated online analysis of many signal channels at high speed. Also, greatly increased social recognition of the needs and potential contributions of people with severe neuromuscular disorders such as spinal cord injury has generated clinical, scientific, and commercial interest in better communication and control technology. An interdisciplinary field of research has been created to offer direct human-computer interaction via signals, generated by the brain itself.

Brain-computer interface (BCI) technology is a communication channel that enables users to control devices and applications without the direct use of muscles [1]. The development of cognitive neuroscience field has been instigated by recent advances in brain imaging technologies such as electroencephalography, magnetoencephalography, and functional magnetic resonance imaging. The growing field of BCI research is relatively new. The first BCI prototype was created by Dr. Vidal in 1973 [2]. This system was intended to be used as a promising communication channel for persons with severe disabilities, such as paralysis, amyotrophic lateral sclerosis, brain stroke, or cerebral paralysis [3]. Continuation and acceleration of recent progress in BCI research and development have begun to address real world applications spanning activities of daily living, environment control, exercise, locomotion, and verbal communication [4].

The BCI technology, combined with ambient assisted living (AAL) systems, can potentially make the home environment more intelligent and assistive, providing alternative communication means for supporting independent life of elderly people affected by impairments. The quality of life of persons suffering from severe motor disabilities can benefit

from the use of BCI-based assistive technology [5]. Despite recent developments, there are still numerous obstacles to building a usable and effective BCI system. The biggest challenges are related to accuracy, speed, price, and usability. Current BCI systems are inaccurate and have a low information transfer rate. This means that the user needs a long period of time in order to send commands to the device that is being controlled. Another problem is the high cost of EEG equipment, such as an EEG cap and amplifiers [6]. Systems with a high sensor count take a long time to prepare for use and are uncomfortable. Due to these limitations, no BCI system has become commercially successful to this date. Sound knowledge of the data acquisition process, EEG waveform characteristics, signal processing methodologies for feature extraction, and classification is a prerequisite before attempting to design and implement a functional BCI system. These research points have been highlighted by the BCI development community as being both important and necessary, for further BCI development [7–9].

Therefore, BCI technology still has many problems to be solved to transit to feasible assisted living [10] with minimal training effort and support required for independent use at home. One approach is to develop BCI applications based on a user centred design approach to bridge the gap between BCI systems and their end users [11]. Another approach is gamification, that is, the use of elements of a game in a serious nongame context [12]. Redefinition of daily control tasks as enjoyable multimedia applications could define a new level of control possibilities for the disabled but also for healthy users [13].

The goal of this paper is to explore the BCI technology as a gaming controller option, which can require less EEG quality and present low risk interactions. By using low cost devices such as the Emotiv EPOC headset, aimed at consumers rather than scientists and medics, in the system, we sacrifice performance for price and comfort of the system user. Researchers have already applied the Emotiv neuroheadset's technology in a variety of ways: Liu et al. [14] compared the EPOC device to a g.USBamp device in a steady state visually evoked potential (SSVEP) system with good results. It is also used in other paradigms, such as the P300-based system, developed by Duvinage et al. [15]. In this paper we use and compare linear discriminant analysis (LDA) and support vector machine (SVM) classifiers with brainwave data features obtained using wave atom transform (WAT) for the control of a prototype SSVEP based BCI game.

The structure of the remaining parts of the paper is as follows. Section 2 discusses applications of BCI technology. Section 3 describes the typical architecture of BCI systems. Section 4 discusses the more commonly used BCI paradigms. Section 6 describes the materials and methods used. Section 7 presents the experimental results. Finally, Section 8 presents conclusions.

## 2. Applications of BCI Technology

BCI design represents a new frontier in science and technology that requires multidisciplinary skills from fields such as neuroscience, engineering, computer science, psychology, and clinical rehabilitation. BCI research has been successfully used not only for helping the disabled [16], but also as being an additional data input channel for healthy people. It can be exploited as an extra channel in game control [17], augmented reality applications [18], household device control [19], fatigue and stress monitoring [20], and many other applications.

The applications of BCI can be divided into two main categories, medical applications and nonmedical applications, such as multimedia or virtual reality. The first category includes the following:

(i) *Rehabilitation and Prosthetic Device Control*. The BCI technology is used for patients with moderate to severe movement disabilities. Although rehabilitation is impossible in some diseases, such as amyotrophic lateral sclerosis, some of the patients, that is, stroke patients, can sometimes regain some or all lost motor control with effective rehabilitation. Motor imagery (MI) BCI can be used as a means for rehabilitation. In studies [21, 22] among others, patients have tried to grasp objects using BCI controlled robotic prosthetic hands. Robotic arms provided feedback for the patients, aiding their rehabilitation. While rehabilitation results show potential, robotic prosthetic limb control requires a number of control commands, not achievable by BCI systems. The experiments, therefore, are mostly limited to the 1D or 2D movement control.

(ii) *Medical Diagnosis*. BCI technology can be used for developing health monitoring applications that may periodically screen the user for early indicators of neural diseases such as epilepsy [23] and suggest the user to see a doctor for diagnosis.

(iii) *Assistive Mobility*. The most beneficial devices for disabled people are those that let them regain mobility. This is achieved by providing wheelchair control, by means of BCI. BCI-driven spelling devices are used to spell letters or words, allowing for disabled communication. The P300 speller is one of the most famous BCI paradigms [24].

(iv) *BCI Controlled Web and Music Browsers*. Internet access has become the main source of communication on a global scale. The BCI technology enables the development, to make the internet accessible for the disabled. As more aspects of daily life become accessible online (education, retail, personal finance, or business), the potential benefit of connectivity also increases. In a study [25], patients used the P300 paradigm to navigate text, browse forward and backward, use bookmarks, and spell text.

(v) *Mental State Recognition*. Work in this area deals with the recognition of mental states, such as attention levels, to treat attention deficit disorder patients [26], workload, and fatigue [27], useful for an operators cognitive state assessment.

Although the BCI technology is mainly designed with disabled people in mind, it can also be beneficial to healthy

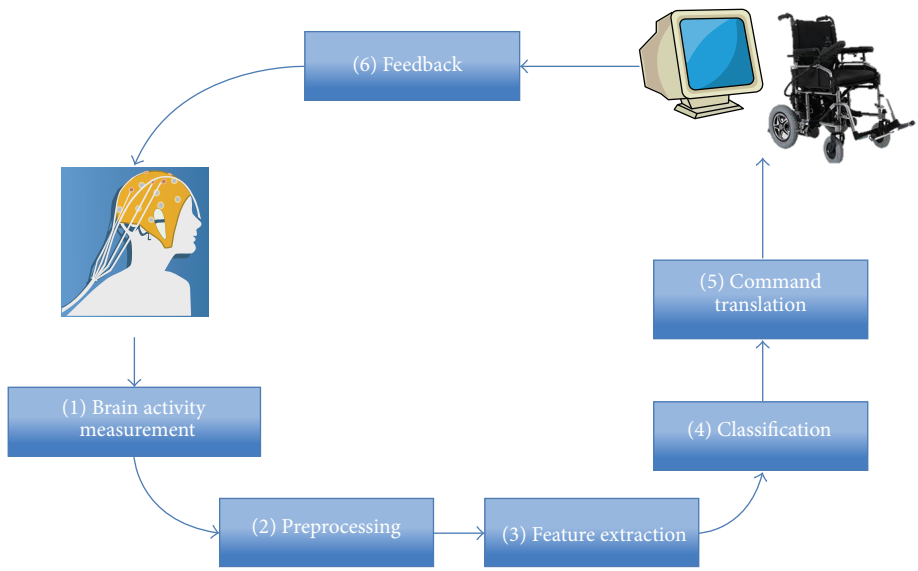


Figure 1: General architecture of an online BCI.

subjects. EEG is particularly suited for this purpose, because it is noninvasive, portable, has a good temporal resolution of a few milliseconds, and is relatively low cost. Therefore the nonmedical applications of BCI include the following:

(i) *Gaming*. All BCI paradigms have been exploited for gaming purposes. BCI is used either as a primary means to control the game or as an extra channel for in game communication, to perform certain user actions, whereas the game is primarily controlled by traditional means. The game examples include a 3-class motor imagery-based asteroid-dodging game, described in [28], and a BCI control interface for a popular game "World of Warcraft" [29]. The SSVEP based games include a 2-class game called Mind-Balance [30], P300-based MindGame [31] as well as Pinball [32], Pacman [33], and Tetris [34].

(ii) *Virtual Reality*. Most existing works focus on either rotating the virtual camera or traveling in the virtual environment. Pineda et al. used a BCI based on the mu rhythm to interact with a "First Person Shooter" video game [35]. A high mu rhythm level triggered left camera rotation, whereas low mu levels triggered right rotations. Other commands in the game were issued by using the keyboard.

## 3. Typical Architecture of BCI Systems

A BCI is an artificial intelligence system that can recognize patterns in brainwaves in these stages: signal acquisition, preprocessing or signal enhancement, feature extraction, classification, and the control interface [36]. Designing a BCI system is a multidisciplinary task, involving knowledge and methods adopted from the areas of computer science, signal processing, neurology, and physiology.

To use a BCI, two stages are required: (1) a training stage, in which (a) the user is trained to willingly control his brain potentials (in the case of operating condition BCI), (b) an offline training stage, which calibrates the training algorithm (in the case of pattern recognition BCI), and (2) the online stage, in which the BCI system is used for control.

In the online mode, the BCI system generally performs a six-step process (see Figure 1): brain activity measurement, preprocessing, feature extraction, classification, command translation, and feedback [37].

(1) Brain activity measurement is the step in which electrodes are used to obtain the user's EEG at specific regions on the scalp, to form input for the BCI system. This step involves determining the number and location of the channels, amplification, analogue filtering, and A/D conversion. Channel locations are selected according to the paradigm used and mental task performed.

(2) The preprocessing step consists of denoising the recorded brain signal in order to enhance the relevant information inside. Denoising can be performed by channel or artefact rejection, DSP signal filtering methods. Preprocessing involves the preparation of the EEG recordings. It is an important stage that decides the filtering, segmentation, and detrending methods used to prepare the EEG data for further stages. Filtering and segmentation (also known as epoching) are used to identify and maximize the information over a certain time or frequency range that is associated with the characteristic brain activity to be elicited. Most cognitive EEG activity is usually in the range of 0.2–40 Hz; thus filtering outside of this range reduces noise. A band-pass filter at the electrical mains frequency is typically performed in addition. After filtering, the segmentation of EEG data is performed. This involves splitting the continuous EEG signal into time-locked windows, which usually overlap or are locked to a stimulus (in case

of synchronous BCIs). Epoching allows for averaging and dramatically simplifies the feature extraction and classification process. Detrending removes any baseline drift associated with the EEG recordings. This is important to ensure the quasi-stationarity of small EEG segments. The sample rate can be converted to represent the data in as few samples as possible to reduce the computational demands of processing a large number of samples. The sampling rate must be chosen to be at least twice that of the maximum frequency contained in the data (Nyquist rate [38]). A sampling rate of 128 Hz can record frequencies up to 64 Hz, thus capturing the entire range of EEG waves.

(3) Feature extraction is a step to describe the signal by a few relevant, command-related values known as "features." This stage often characterizes the BCI design approach. Features that describe the signal in as few components as possible are resilient to noise and artefacts have to be identified and used. Identifying and extracting good features from signals is a crucial step in the design of BCI systems. If the features extracted from EEG are not relevant and do not describe the signal well enough, the classification algorithm which will use these features will have trouble classifying the mental states of the user; the correct recognition rates of mental states will be low, in which case the use of the interface would be impossible or inconvenient. Thus, even if it is sometimes possible to use raw signals as the input of the classification algorithm, it is recommended to select and extract good features in order to maximize the performances of the system by making task of the subsequent classification algorithm easier. Therefore it is often the case that choosing a good preprocessing and feature extraction method has more impact on the final performances than the choice of a good classification algorithm [39].

(4) Classification is a step which assigns a class label to a set of features extracted from the signal. This class label corresponds to the kind of mental state identified. Classification can be performed in various ways ranging from simple thresholding or linear models to complex nonlinear neural network classifiers. The goal of classification is to assign a correct class label to a previously extracted feature vector. This class represents an intention of the BCI user. The key step for identifying neurophysiological signals in a BCI is translating the features into commands [40]. In order to achieve this step, one can use either regression algorithms or classification algorithms, the classification algorithms being by far the most used in the BCI community [41, 42].

(5) Translation into a command is performed by issuing an action, corresponding to the mental state of a user identified, that is, moving the mouse cursor on a computer screen, controlling a speller, or moving a wheelchair.

(6) The feedback step provides the user with information about his/her mental state. This helps the user to consciously control his/her brain activity to increase performance of the executed task.

## 4. Overview of BCI Paradigms

A variety of BCI paradigms have been exploited, such as P300 [43], SSVEP [44], ERD/ERS [45], MI [46], slow cortical potential (SCP) based [47], and hybrid methods [48–50]. We review some of these paradigms in more detail in the following subsections.

*4.1. Spontaneous Potentials.* Spontaneous EEG is measured when there is no stimulus presented to the test subject. In healthy subjects the spontaneous EEG is measured during a prolonged time span in which the brain activity changes constant waves into events with higher or lower frequency. Characteristics of different cognitive processes, mental states, and activation processes can be observed in spontaneous EEG waves. The appearance of certain frequency bands over a specific brain region can be assigned to a certain mental task. The band range limits associated with the brain rhythms, particularly beta and gamma, can be subject to contradiction and are often further subdivided into subbands that can further distinguish brain process activity with a frequency $f$, where $f > 30$ Hz or $f < 0.5$ Hz is often assumed to be of limited clinical utility; although some recent papers have published the existence of cognitive brain process in the beta, gamma, and high gamma bands [51], the literature does not clearly state whether the higher frequency activity (>30 Hz) is of cerebral origin. The EEG rhythms are affected by different actions, thoughts, and mental states. For example, the planning of a movement can block or attenuate the mu rhythm. The fact that mere thoughts affect the rhythmical activity of the brain can be used as the basis for a BCI system.

*4.2. Event Related Potentials (ERP).* The event related brain potentials (ERP) are different from spontaneous brain activity in the way that they appear while the subject is being stimulated and are noted by performing the extensive analysis of the data. The brain generates not only uninterrupted spontaneous activity but also reacts to certain external or internal events with a characteristic potential change. On episodic stimulation, event based activity is registered, which is not displayed, if no stimulation is presented. By presenting the subject with an external stimulus (such as a click sound or a flashing light), a specific reaction and specific EEG components are expected to emerge in the ongoing EEG activity after the stimulus presentation. These ERP are analysed in the time domain using triggers, timestamps of stimulus presentation noted in the EEG. The subject is presented with a stimulus in constant intervals while his/her EEG is being recorded. The data encompassing time after the presentation of the stimulus is then analysed. The arising ERP with amplitude of 1/10 of the spontaneous brain activity is noise-like and is barely noticeable in the EEG data. After computer analysis of time samples following the stimulus and by performing averaging on the signals, the evoked potential becomes clearly visible. As most of the oscillations are not of interest, only

certain frequencies are measured by selecting a time window of about 100 ms to several seconds. The observed potential has amplitude of less than 10 $\mu$V and duration of around 0.5 s. It also has a typical form; after a few milliseconds of stimulus presentation, oscillations with very small amplitude arise. These potential differences are positive or negative changes in brain potential, so one can speak of cortical positivity or cortical negativity [52].

In a typical ERP, first, a small positivity is measured (called P1), followed by a negativity (called N1 or N100, appearing after approximately 100 ms) and again followed by a clear positivity (P3), which is observed after approximately 300 ms after the presentation of the stimulus, reaching its peak at about 400 ms, and known as a P300 wave [53]. The P300 and N100 waves are correlative to the stimulus and therefore observed for medical purposes; that is, in patients with multiple sclerosis, the P300 wave is often longer than in healthy patients. It also serves a purpose for diagnosing other psychological diseases such as schizophrenia, hyperactivity disorders. Apart from the sensory stimulus, ERP are evoked by other event related actions, such as imaginative or physical motorical activity, that is, the movement of arms or legs.

*4.3. Evoked Potentials (EP).* The evoked potentials (EP) are a subset of the ERP that occur in response to or during attention to certain physical stimuli (auditory, visual, somatosensory, etc.). They can be considered to result from a reorganization of the phases of the ongoing EEG signals. The EP can have distinguishable properties related to different stimuli properties, for example, the visual evoked potential (VEP) over the visual cortex varies at the same frequency as the stimulating light [54]. Other EP such as the auditory evoked potential (AEP) are also used [55].

A distinction is made in the literature between a transient EP and a steady state EP (SSEP) based on the stimulation frequency. The former arises when the stimulation frequency is less than 2 Hz. If the stimulus repetition rate is greater than 6 Hz, a periodic response called the SSEP will result. The SSEP are defined by an increase in signal power in the band, equal to the stimulation frequency or integer multiples of that frequency. The amplitude and phase of the SSEP are highly sensitive to stimulus parameters, such as repetition rate, color contrast or sound tone, modulation depth, and spatial frequency. The SSEP was also found to be strongly dependent on spatial attention, being enlarged in the frequency of the target that has the user's attention focused on. The increased SSEP amplitudes reflect an enhancement of neural responses to a stimulus that falls within the range of spatial attention. It is this fundamental idea that justifies the use of the SSEP as a method to identify the attended target among a group of stimuli with sufficiently different stimulation rates.

There are three main modalities of stimulation:

(i) *Auditory One*. Signal tones of a specific frequency or clicks are used as stimuli.

(ii) *Visual One*. Stimulus is presented as a light with a specific blinking frequency.

(iii) *Somatosensory One*. Stimuli are elicited by electrical stimulation of peripheral nerves.

The sequence of stimulation is arranged into paradigms in order to study the responses to certain tasks. The most widely used are as follows:

(i) *No-Task Evoked Potentials*. The subjects are relaxed and instructed to perform no task upon stimulus reception.

(ii) *Oddball Paradigm*. The user is requested to attend to a random sequence composed of two kinds of stimuli with one of these stimuli being less frequent than the other. If the rare stimulus is relevant to the user, its appearance triggers a P300 wave observable in the user's EEG.

*4.4. Steady State Visually Evoked Potentials (SSVEP).* Several studies [56–58] have demonstrated an increase in neural activity excited by a visual stimulus when the test subject directs his attention to the region of visual space containing the stimulus. The results show that attention acts as a "spotlight," enhancing the cortical representation of stimuli presented in attended regions of visual space relative to stimuli presented in the unattended regions of visual space.

Studies show that if two or more stimuli with a varying flicker frequency are presented simultaneously, neural responses are elicited by the flicker, receiving the subjects focus. The response generated by the brain corresponds in frequency to the stimulating frequency and therefore can be detected using the Fourier analysis of the EEG data. In the EEG recordings, these steady state responses are called steady state visually evoked potentials (SSVEP) [59]. If the subject directs his attention to one visual field and ignores the others while performing a target detection task, SSVEP elicited by flicker stimulation in the attended visual field have larger amplitude than SSVEP elicited by the same stimulus in trials where the other field is attended.

The use of frequency tagging to study attention has the obvious advantage of easily separating neural responses into different classes. How attention modulates the SSVEP response may depend on various parameters, such as stimulus frequency [57], stimulus spacing [60], color [61], and shape [62]. It is known that low frequency flickering induces more intensive SSVEP but might cause the users to feel uncomfortable and easily tired.

## 5. Requirements and Limitations of EEG-Based Gaming Systems

Several other factors have to be taken into account when designing a BCI system prototype. To design an end user friendly system, which could be used in everyday activities, that is, wheelchair or mouse cursor control, the system should allow its users to send commands at any time. Such a system must analyse the EEG signals continuously and determine whether the user is intending to issue control commands to the system, that is, in the control state (CS) or if he is in a no control state (NC), indicating that no control commands are issued. If the system detects the user's CS state, it must then decide which control command is being issued. We take this into account, when designing our BCI system.

The biggest problems with most BCIs are low accuracy, reliability, information transfer rate, user acceptability [63], performance variability both within and across subjects [64], and BCI illiteracy of some subjects [65]. Sometimes the output of the system does not match the input. This, of course, can be more or less serious depending on the application. If used for moving the cursor on a computer screen an erroneous output every now and then might be tolerable, but if used for controlling the motion of a physical device, such as a wheelchair, this behaviour becomes unacceptable. Another problem associated with many BCI paradigms is a long input-output delay. Today, the most successful systems work at a transfer rate of less than 30 bits per minute [66]. That might be enough to operate a simple word processor system, but it is too slow to control a wheelchair. Most research today therefore focuses on improving the two factors of speed and accuracy of BCI communication. Even though more and more BCI applications exist, there are still a number of problems BCIs needed to overcome to become interesting for the large public.

The first problem lies with the EEG sensors. Traditional EEG systems like the Biosemi ActiveTwo consist of a cap and up to 256 EEG electrodes. The high sensor count and wires make such a system impossible to use outside the laboratory, because the setup requires one or several assistants and preparation time. Another drawback is the fact that conductive gel needs to be used for leaving residue in the user's hair. The g.SAHARA system produced by g.tec does not require conductive gel, but still needs wires and an electrode cap.

BCI is often the only input modality in applications which have been developed for research projects. This can be problematic: having to control a cursor continually by means of imagined movement results in a high workload. It would probably be better if BCI was one of the multiple modalities used to control an application. Examples of such multimodal applications or hybrid BCIs are the "AlphaWoW" (Alpha-World of Warcraft) [67], where brainwaves in the alpha band are combined with keyboard and mouse inputs, and "Mind the Sheep!" [68], where SSVEP is combined with mouse input. Other examples include a touchless system [69], which combines eye gaze for cursor control with a BCI for making selections, and exergames with Brain Kinect Interface (BKI) for recording and analyzing motion capture signals and EEG signals in order to monitor motor recovery process [70].

The focus of BCI research should shift from reliability to usability and user experience [71]. This is necessary to migrate BCI systems out of the laboratory, into society. Healthy persons can choose from various alternative input modalities. So, for healthy persons to choose a BCI, the user experience and usability must be adequate. Most people have never used a BCI and the novelty of this new technology can be a reason for people to decide to use a BCI instead of alternative input modalities, even if BCI is less reliable and slower. However, if the usability is not good, people will choose a different input modality. Due to the fact that the focus in BCI research has mainly been on the reliability, no standardized methods to assess the user experience for BCI exist, yet. Several researchers (see, e.g., Kübler et al. [11]) use visual analogue scales (VAS) to rate the user satisfaction on a scale from 0 to 10. Such a rating does not provide any in-depth information about the source of satisfaction, but it allows for easy monitoring.

The final limitation to mention here is the amount of data that a BCI can transfer. The EEG measures a mixture of signals originating in neural brain activity. The two lowest functional layers of the brain are mostly locally oriented [72]. By observing brain areas responsible for these signals, it is possible to measure a corresponding signal. The higher sublevels (thoughts, emotions) are assembled on the lower levels and exist only in an abstract way. To measure physical processes on these higher layers would require additional tools to translate the measured low-level signals into the higher-level context. One needs specific "interpreters" for such operations. The problem is the interpretation of this mixture of measured signals. Hence, for the control of highly complex prostheses, EEG signals are not sufficient and can never be in the future. The signals necessary to control the arm, including the consideration of closed loop controls between the brain and the arm, ideally including the fingers and integrated touch sensors, would be too blurred to be the basis for adequate arm movement execution.

## 6. Materials and Methods

*6.1. Hardware.* The EPOC headset, designed by Emotiv Inc., has been selected as the basis for our system. The Emotiv EPOC contains 14 electrodes and 2 reference electrodes, placed in the international 10-10 system [73]; response time is 250–500 ms. The headset is designed as a video game accessory where developers are interested in using the device as a controller. The product chosen for this project was the Research Edition. This provides both the interface for programming with the headset and access to raw EEG data. The headset transmits encrypted data wirelessly. The wireless chip is proprietary and operates in the same frequency range as 802.11 (2.4 GHz). The internal sampling rate of the device is 2048 Hz. The data is then downsampled to 128 Hz before becoming available to the system for capturing the EEG signals. The captured data contains values for each of the 14 electrodes on the EPOC headset.

There are many advantages for using the Emotiv headset over other BCI and EEG devices. Many BCI devices are restrictive due to wiring. The Emotiv headset, however, is wireless and therefore offers free range of motion allowing for easy transport and setup, which is very important in an everyday use setting. Another advantage is that the EPOC does not require conductive gel for electrodes, making it easier to put on and use. Users do not have to wash their hair after using the headset. The main benefit is that it is relatively inexpensive. There are several disadvantages for the EPOC headset as well: it only uses 14 sensors, while many medical grade devices use up to four times that amount. This results in less data coming in from the brain. Additionally, more powerful devices have a sample rate of up to 1000 Hz, as opposed to the 128 Hz that EPOC runs at. Since the EPOC headset is not intended for finer signal detection, the electrodes pick up a lot of noise. Several techniques can be used to increase the Signal-to-Noise Ratio

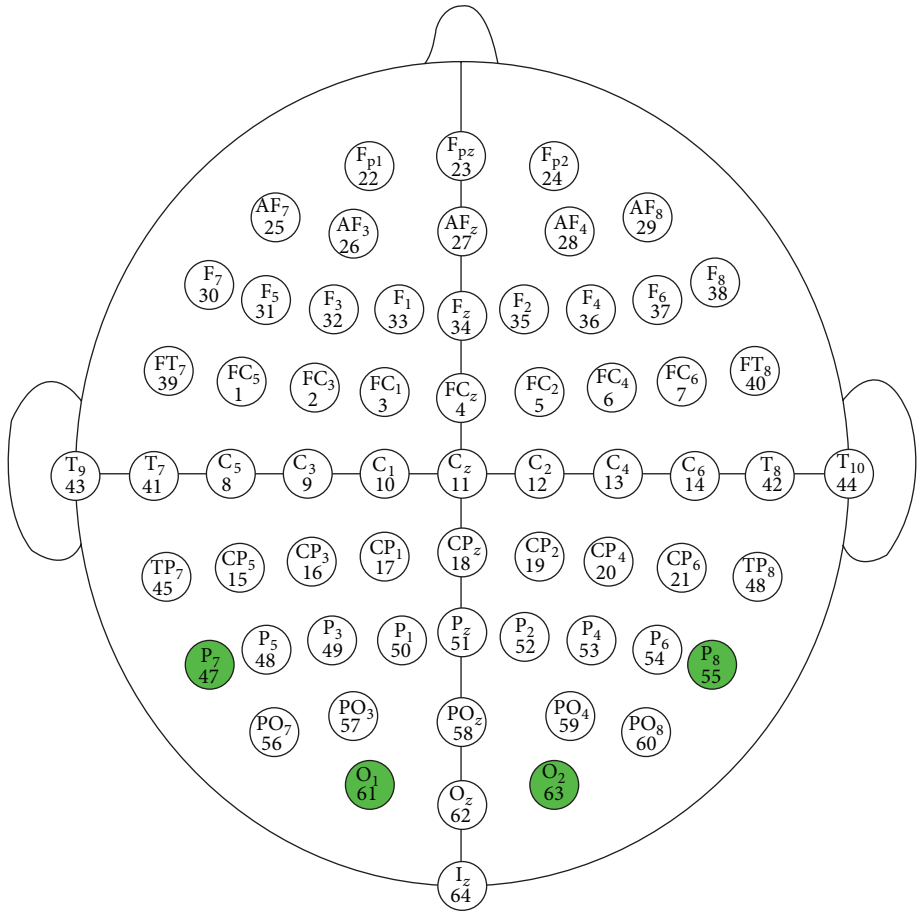


Figure 2: Sensor layout.

(SNR) such as band-pass filtering, averaging or class adaptive denoising [74], DCT compression [75], signal decomposition and thresholding [76], or nonlinear signal operators [77].

*6.2. Software.* The Emotiv Software Development Kit (EDK) was used for interfacing with the EPOC. It is primarily written in C, but the company also provides wrappers for accessing the Application Programming Interface (API) in C++, C#, Java, and MATLAB. MATLAB provides methods for calling functions in C code which allows for straightforward access to the EDK's API.

OpenViBE [78] is an open source graphical programming language used to design BCI applications. The aim of the OpenViBE is to provide open source software for BCI. Key features of this software are its modularity, high performance, real time data acquisition and feedback capabilities, compatibility with various hardware devices, and multiple scripting language support. It can be used to acquire, filter, process, classify, and visualize brain signals in real time.

*6.3. Experimental Setting.* The objective of the experiment was to develop a system that utilizes brain activity to offer control within a real time environment in order to evaluate signal processing algorithms. A 3-class self-paced BCI design with a NC (no control) state was chosen, as this system setup could easily be adapted for wheelchair or mouse cursor control. The system is based on the OpenViBE platform and is comprised of 5 individual scenarios, each performed in sequence. The EEG data is recorded using the Emotiv EPOC headset. Since the headset does not have any sensors over the motor cortex, obtaining even moderate results with the motor imagery (MI) approach is very unlikely. Since the sensors cover the occipital and parietal cortex reasonably, the SSVEP in the multiple visual stimuli selective attention paradigm was chosen for the experiment, due to its well-publicized success and limited subject training requirements.

*6.4. Data Acquisition.* Data acquisition is performed by selecting the channels which will be used for data recording. This allows for individual sensor contact quality evaluation. The signals of interest, in the case of SSVEP, are O1, O2, P7, and P8 (see Figure 2).

The data is acquired in real time by the acquisition client (see Figure 3). The data is processed in the same way as the training data, in order to obtain the same feature vectors that the classifier can then identify. The output of the three classifiers is then input into a SSVEP voter algorithm, which decides on the class label of the current signal. If an NC state is detected, a class label of "0" is assigned to the trial. The control signal can then be used to move the ship and is passed to the

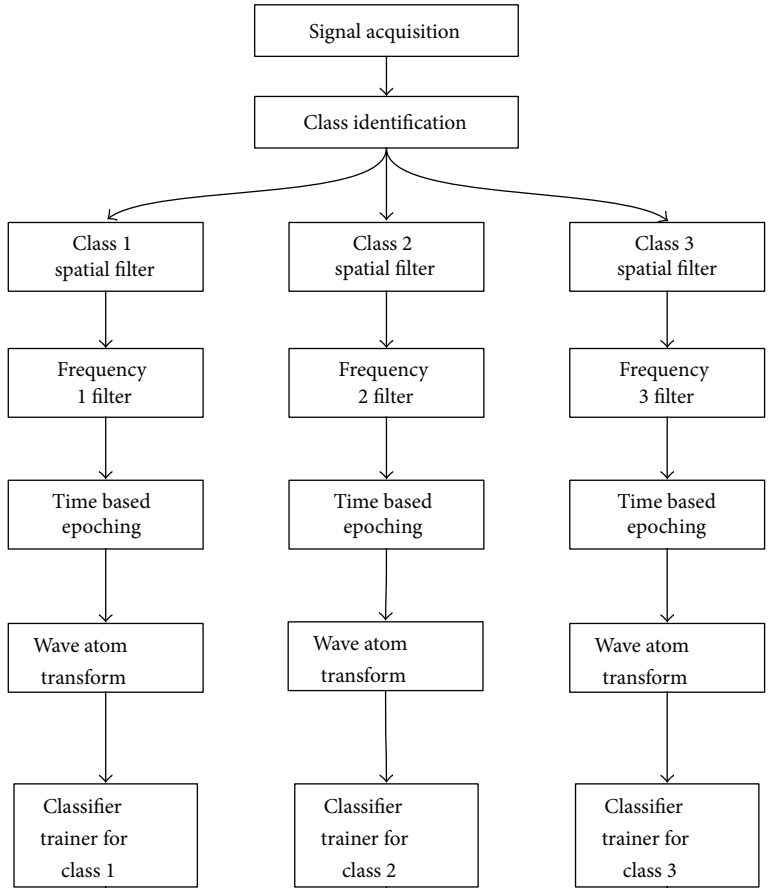


Figure 3: Data flow of prototype BCI shooter game.

ship control application. While in the NC state, no action is performed.

*6.5. Data Preprocessing.* The signals from the sensors are averaged and band-pass filtering of the 6–40 Hz band is performed. The signal is then split into epochs of 2 s, with a 0.5 s interval. An average signal value is obtained by averaging 4 epochs, and an FFT is then performed to visualize the different frequency bands.

Preprocessing steps are then performed in order to denoise the signal and extract relevant information features for the classifier. First, data is split into three groups, according to their corresponding class label, LEFT, RIGHT, and CENTER accordingly. This is done so that a binary classifier could then distinguish whether a trial belongs to a certain class or not, by using the "one versus all" criteria. This allows for the NC class, where output is false for all three classifiers. Next, temporal and spatial filtering is applied to each of the three groups. Specifically, each group of signals is band-pass filtered around the target frequency of interest: for the LEFT class, 29.5–30.5 Hz; CENTER, 19.5–20.5 Hz; RIGHT, 11.5–12.5 Hz. This is done, using a fourth-order Butterworth filter.

*6.6. Feature Extraction.* For feature extraction we use wave atom transform (WAT), a relatively new transform proposed by Demanet and Ying [79]. WAT performs a multiresolution analysis of a signal, that is, decomposing a signal into different frequency subbands. Wave atoms are a variant of wavelets that have sharp frequency localization and offer a sparser expansion for oscillatory functions than wavelets. Wave atoms compose wave fields as a superposition of highly anisotropic, localized, and multiscale waveforms and capture coherence of pattern across and along oscillations. WAT has been previously used mainly in image processing domain for image denoising, image watermarking, image hashing, as well as feature extraction, dimensionality reduction and numerical analysis [80], and analysis of the electrocardiogram (ECG) [81] data.

WAT is a promising approach for EEG processing because of its denoising and feature extraction capabilities and is particularly useful when the signal has discontinuities and sharp spikes as in case of EEG [82]. We expect that WAT coefficients extracted from EEG data samples can retain enough information to permit correct classification, while feature reduction should reduce network training and classification time. Wave atoms are a variant of 2D wavelet packets that retain an isotropic aspect ratio. They are well suited for representing the oscillatory patterns in a signal [80].

To extract features, we first segment the signal, extracting the 5 s long stimulation period from the trial, since only this portion of the signal carries relevant information. Next, each

segment is further divided into epochs of 1 s every 0.2 s, which provides 80% overlap between neighbouring epochs. Then, WAT coefficients are obtained for every epoch, and a feature vector is aggregated. As such, 25 feature vectors are extracted for every trial. They are then used for classifier training.

As a baseline to compare WAT with, we use the band power (BP) feature method. BP performs band-pass filtering a signal in a given frequency band, then in squaring the filtered signal, and finally in averaging the obtained values over a given time window [21]. Band power features are generally computed for several frequency bands previously determined according to the mental states to be recognized. Such features have been notably used with success for MI classification [21] but also for classification of cognitive processing tasks [51]. Features are extracted by training an adaptive common spatial pattern (CSP) filter, then band-pass filtering the signal around the target frequency, as described above, and then performing band power calculation. The BP values are then used as features to train a classifier.

*6.7. Visual User Stimulation.* Visual user stimulation can be performed by using the LED or an LCD computer monitor. However, the LEDs need extra hardware to generate a constant frequency. For the purposes of this experiment, we prefer to use the LCD monitors. The drawback of using a monitor is that a stimulus frequency is limited by the refresh rate. The refresh rate should be multiple times of the stimulus frequencies; that is, for a monitor with 60 Hz refresh rate, 6.67 Hz, 7.5 Hz, 8.57 Hz, 10 Hz, 12 Hz, 15 Hz, and 20 Hz are usually used. When choosing stimulus frequencies it is also important that a frequency is not harmonic of another chosen frequency (e.g., 7.5 Hz and 15 Hz). An SSVEP response can trigger a large amplitude response not only in the main frequency, but also in the harmonic frequency, leading to missclassification. In a 60 Hz refresh rate monitor, for a 10 Hz flicker, it reverses the target colour, usually between some light and dark combination, to produce a flicker, every three frames; for 12 Hz flicker, three frames of dark followed by two frames of light colour are displayed. Therefore, the sequences of certain two frequencies could be combined to get three frequencies with a varying number of frames in each cycle (e.g., 10 Hz and 12 Hz produce 10.5 Hz, 11 Hz, and 11.5 Hz). The EPOC headset has a sampling rate of 128 Hz and therefore has low resolution at higher frequencies. The experiments using SSVEP often include stimulation frequencies of up to 60 Hz, but these should be avoided while using the EPOC. Experiments with different frequencies performed showed that best results for a three- class BCI were obtained by using 30 Hz, 20 Hz, and 12 Hz. Therefore, these frequencies were chosen for the final experimental setup.

*6.8. Training.* The training data acquisition procedure is performed several times, to obtain the training data for each of the three classes. Since the training session is time-bound by the system, it requires a lot of attention and concentration from the user and due to user fatigue has to be limited to a number of trials. In this experimental setup, a number of 20 trials per class were chosen, totalling 60 trials for a single dataset. Classifier training was achieved by gathering 4 EEG

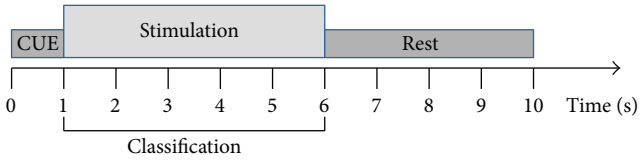


Figure 4: Timing of a single SSVEP trial.

datasets of SSVEP data, acquired from 2 healthy subjects (28 years). Subjects had very few or no previous experience in BCI. During the experiments, they were asked to focus attention on targets, blinking in a defined frequency.

A session was composed of 20 trials of each of the three classes (LEFT, RIGHT, and CENTER), arranged in a random order. The timing of the sessions was organized accordingly: in our protocol, the trial lasted 10 s. First, a yellow arrow is displayed for 1 s, indicating the target, on which the user must focus his attention. From second 1 to second 6, the trial entered stimulation phase. In this phase all three targets start blinking in their corresponding frequencies. The users are specifically ordered not to move the head, relax face muscles, and not to blink during this phase. Stimulation is then followed by a 4 s resting period, at which the user is allowed to rest his gaze, blink, or move the head. The EEG data from this period is not used for classification. This is illustrated in Figure 4.

The recorded EEG data, together with marked events, such as class labels for each trial are saved on the computer. Only relevant channels, in this case, O1, O2, P7, and P8 are used for analysis.

Since both the SVM and LDA are binary classifiers, while dealing with the three-class problem in this case (the user has to select one of the three targets), the classifiers are trained with a one-versus-all paradigm; that is, the first classifier takes features from the first frequency stimulation as the target class and stimulations from the other two frequencies as nontarget. The same is true for the second and third classifier. A voting algorithm is then used to select the class from the three classifier outputs. If all the classifier output a nontarget condition, then the state is said to be NC (no control).

*6.9. Game Interface and Playing.* The colour for the flickering targets was chosen as a combination of white and black. The study [83] analysed how different colours of the targets influence classification quality. For our experiments, the white-black colour combination was chosen, since it gives the highest contrast. The user is presented with an LCD display, containing 3 blinking targets on a black background and a yellow arrow. On cue, the targets start blinking at different frequencies. This is presented in Figure 5(a).

After performing classifier training, subjects are invited to participate in a video-game-like experiment. During this game, the subjects are presented with an interface from Figure 5(b). The "spaceship" comprised two "engines," the two rectangles, and a "cannon," the triangle. The subject is able to rotate the spaceship by focusing his/her attention on one of the rectangular targets.

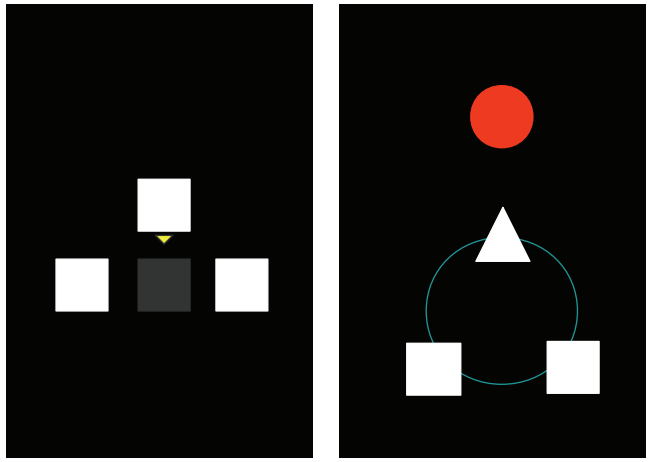

(a) (b)

Figure 5: BCI game interface: training (a) and playing (b).

The ship is turned left or right according to the target in the user's field of attention. By focusing attention on the middle triangle, the user is able to fire the spaceship cannon. A red circular target appears next to the ship at a random location. The aim of the game is to rotate the spaceship and fire its canon to hit the red target. Once the target is hit, it disappears to reappear in another position.

The online game is executed using the OpenViBE scenario shown in Figure 6. The data is acquired in real time by the acquisition client. The data is processed in the same way as the training data, in order to obtain the same feature vectors that the classifier can then identify. The output of the three classifiers is then input into a SSVEP voter algorithm, which decides on the class label of the current signal. The control signal can then be issued to move the ship and is passed to the ship control application. If the NC state is detected, the control signal is not issued and no action is performed.

## 7. Results

To evaluate the system, two datasets have been acquired from two different subjects, marked S1 and S2. Classification has been performed using two feature extraction methods for evaluation, the wave atom transform (WAT) and band power (BP) features (here used as a baseline method to compare against). Two kinds of classifiers have been used, linear discriminant analysis (LDA) [84] and support vector machine (SVM) [85]. The SVM implementation is based on LIBSVM, available at http://www.csie.ntu.edu.tw/~cjlin/libsvm/. For the LDA classifier we used the proprietary implementation of the LDA in the OpenViBE environment. The system was implemented using the OpenViBE environment. All computations were performed on a virtual machine on a PC with Intel Core I5-3570, 3.4 GHz, 4 cores, 3.5 GB RAM.

Since there is a lack of training data, a 10-fold cross-validation is performed and accuracy is measured on the same data used for classifier training. The accuracy metric is chosen for the representation of results, since it is a simple metric that is directly linked to system usability by the user. It likely overestimates the classification result, since the classifier has been trained on the same data. The results most probably indicate higher performances than what the user will actually have during the online classification. We have performed classification using three classification methods and have compared the results.

Table 1: Comparison of classification accuracy.

| Classifier | Features | Accuracy, % | | $F1$ score | |
|---|---|---|---|---|---|
| | | S1 | S2 | S1 | S2 |
| LDA | WAT | 71.5 | 78.2 | 0.64 | 0.67 |
| | BP | 66.2 | 73.2 | 0.56 | 0.62 |
| sLDA | WAT | 70.6 | 77.4 | 0.64 | 0.68 |
| | BP | 68.4 | 73.5 | 0.59 | 0.61 |
| SVM, linear kernel | WAT | 75.5 | 79.3 | 0.64 | 0.68 |
| | BP | 74.3 | 75.1 | 0.64 | 0.66 |
| SVM, RBF kernel | WAT | **78.7** | **82.2** | 0.68 | 0.71 |
| | BP | 74.0 | 77.4 | 0.63 | 0.67 |

S1: subject number 1, S2: subject number 2, LDA: linear discriminant analysis, sLDA: sparse LDA, SVM: support vector machine, RBF: radial basis function, WAT: wave atom transform, and BP: band power.

An evaluation of the system has been conducted using two naïve subjects, named S1 and S2, unfamiliar with the BCI technology. Two feature extraction algorithms have been tested. The first algorithm used wave atom transform (WAT) coefficients. The second algorithm used the band power (BP) in the stimulation frequency band. These features were then used for classifier training. We measured the accuracy and the $F$-measure of each subject, while performing classification with 4 different classifiers (LDA, sparse LDA (sLDA), SVM with linear kernel, and SVM with RBF kernel (with parameter values $C = 1$, gamma = 10)). The results are presented in Table 1.

The results indicate that the WAT-based feature extraction method performed better than BP-based one with all

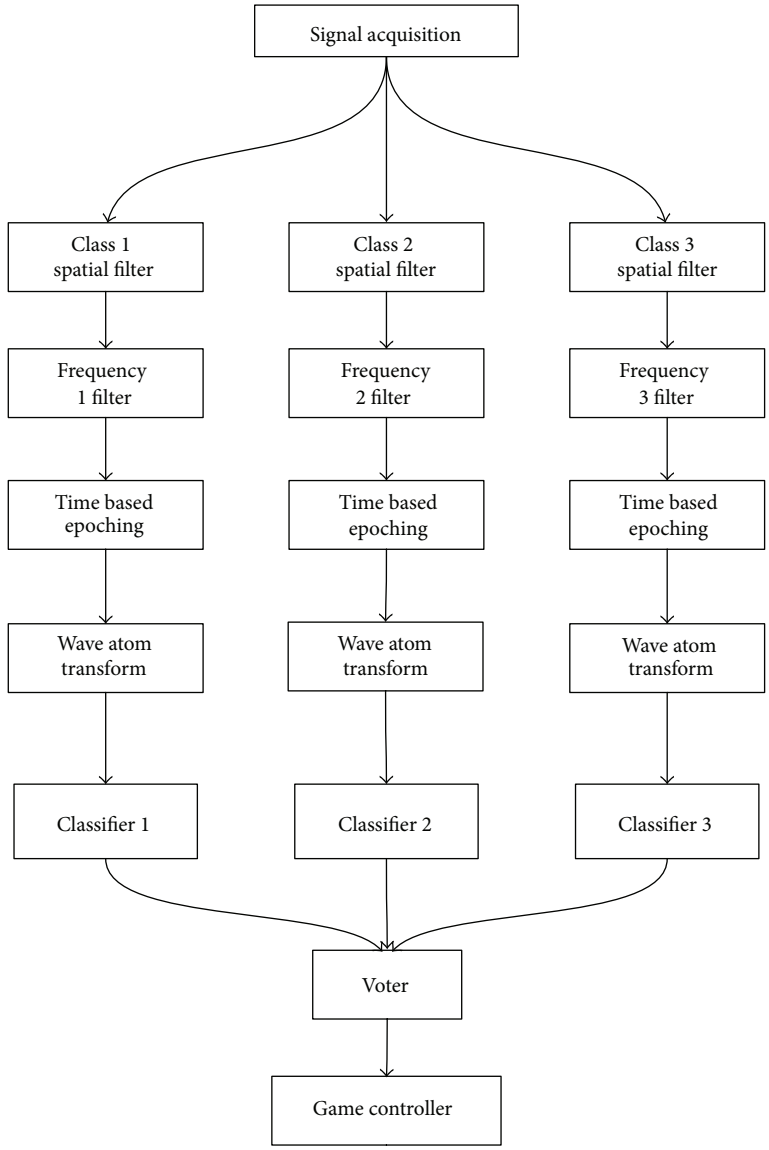


Figure 6: Online test shooter scenario.

four classifiers. This method can also be used in the SSVEP paradigm. Although the best results were achieved by using the SVM classifier with a linear kernel, results obtained with other classifiers are very similar. This shows that the choice of a good feature extraction algorithm is more important in BCI applications. A nonoptimal classifier can produce good results, because most models pick up on good feature data. With good features, one can use a simpler classifier that runs faster. These results also show that it is possible to develop a BCI interface system based on low-cost acquisition devices, such as the Emotiv EPOC, which performs at a reasonable usability level.

Finally, the training times (for training full dataset) for LDA and SVM classifiers are compared in Table 2. In this case, SVM outperforms LDA, too. The processing of 1 s sample of EEG data is performed in 280 ms, which allows the system to perform in real time.

Table 2: Training time of classifiers.

| Classifier | Training time, s |
|---|---|
| LDA | 809 |
| SVM | **618** |

The usability of the developed system was evaluated informally as the number of subjects was too small to perform formal evaluation using, for example, visual analogue scale (VAS). Both subjects complained about discomfort due to the fatigue of eyes after some time of using the system. The fatigue is caused by low frequency flickering of the game interface. The problem could be alleviated by increasing the frequency of flickering; however, it cannot be done due to the characteristics of the EPOC device. The use of a more advanced EEG equipment may solve this problem.

## 8. Conclusion

We have studied the electroencephalogram (EEG) signal processing and classification techniques in order to design brain-computer interface (BCI) systems to be used in the out-of-the-laboratory setting such as AAL environments or smart homes, with these main objectives: (1) improving efficiency in terms of accuracy of the BCI; (2) improving usability and applicability, therefore moving towards the end user; (3) designing a user friendly BCI system based on gamification principles.

We have studied the system performance while using the steady state visually evoked potential (SSVEP) paradigm. We have developed a three-class BCI system, based on SSVEP paradigm and the Emotiv EPOC headset. We have created a scenario, enabling the user to control a virtual spaceship in a game by his/her thoughts. The scenario enables the user to issue 3 control commands and has a no-command (NC) state, allowing for self-paced control. The created scenario includes classifier training, signal preprocessing, and feature extraction.

An online target shooting game, implemented in the OpenViBE environment, has been used for feedback. The wave atom transform (WAT) was chosen for feature extraction. The system achieved an average accuracy of 80.5% for both subjects, while using a support vector machine (SVM) classifier with a radial basis function (RBF) kernel. The use of WAT allowed achieving and improvement in accuracy of 4.8% when compared to the baseline band power (BP) features. These results show that BCI can be used as an interaction technique for complex applications, providing real time operation and feedback. The results also highlight that BCI can be feasible even when using low-resolution low-cost customer-grade EEG acquisition devices. This allows for reduced system cost, mobility, and subject preparation time and, consequently, allows for the subject to be prepared by a nonexpert supervisor. By improving system cost and ergonomics, the BCI technology can be used for the general public who can enjoy entertaining applications, games, and virtual reality.

Concerning the signal processing and classification part of BCI design, we believe that a better approach would be to combine, rather than selecting preprocessing, feature extraction and classification methods. Numerous methods have been proposed and tested in the BCI domain, and while some of them have sometimes been proven to perform better than others, no single method has been identified as being the best. This is partly due to the differences in system users. Therefore, we should focus on combining existing methods together and adapting them to best suit the user. Since different methods exploit different aspects of EEG, these methods could be used together in a complementary way and would probably lead to better results than when using some "single best" method alone.

In future work we plan to develop a real BCI-based game and perform experimentations on a larger number of healthy and motorically impaired subjects as well as performing usability evaluation using visual analogue scale (VAS).

## Conflict of Interests

The authors declare that there is no conflict of interests regarding the publication of this paper.

## Acknowledgment

The authors also would like to acknowledge the contribution of the COST Action IC1303– Architectures, Algorithms and Platforms for Enhanced Living Environments (AAPELE).

## References

[1] J. R. Wolpaw, N. Birbaumer, D. J. McFarland, G. Pfurtscheller, and T. M. Vaughan, "Brain-computer interfaces for communication and control," *Clinical Neurophysiology*, vol. 113, no. 6, pp. 767–791, 2002.

[2] J. J. Vidal, "Toward direct brain-computer communication," *Annual Review of Biophysics and Bioengineering*, vol. 2, no. 1, pp. 157–180, 1973.

[3] A. Kübler, B. Kotchoubey, J. Kaiser, J. R. Wolpaw, and N. Birbaumer, "Brain-computer communication: unlocking the locked in," *Psychological Bulletin*, vol. 127, no. 3, pp. 358–375, 2001.

[4] J. R. Wolpaw, N. Birbaumer, W. J. Heetderks et al., "Brain-computer interface technology: a review of the first international meeting," *IEEE Transactions on Rehabilitation Engineering*, vol. 8, no. 2, pp. 164–173, 2000.

[5] F. Cincotti, D. Mattia, F. Aloise et al., "Non-invasive brain-computer interface system: towards its application as assistive technology," *Brain Research Bulletin*, vol. 75, no. 6, pp. 796–803, 2008.

[6] A. M. Holz, L. Botrel, and A. Kubler, "Bridging gaps: long-term independent BCI home- use by a locked-in end-user," in *Proceedings of the 4th TOBI Workshop*, Sion, Switzerland, January 2013.

[7] R. Kazman, L. Bass, and B. E. John, "Bridging the gaps II: bridging the gaps between software engineering and human-computer interaction," in *Proceedings of the 26th International Conference on Software Engineering (ICSE '04)*, pp. 773–774, May 2004.

[8] A. Kübler, V. K. Mushahwar, L. R. Hochberg, and J. P. Donoghue, "BCI Meeting 2005—Workshop on clinical issues and applications," *IEEE Transactions on Neural Systems and Rehabilitation Engineering*, vol. 14, no. 2, pp. 131–134, 2006.

[9] D. J. Krusienski, M. Grosse-Wentrup, F. Galan et al., "Critical issues in state-of-the-art brain-computer interface signal processing," *Journal of Neural Engineering*, vol. 8, no. 2, Article ID 025002, 2011.

[10] F. Miralles, E. Vargiu, S. Dauwalder et al., "Brain computer interface on track to home," *The Scientific World Journal*, vol. 2015, Article ID 623896, 17 pages, 2015.

[11] A. Kübler, E. M. Holz, A. Riccio et al., "The user-centered design as novel perspective for evaluating the usability of BCI-controlled applications," *PLoS ONE*, vol. 9, no. 12, Article ID e112392, 2014.

[12] S. Deterding, D. Dixon, R. Khaled, and L. Nacke, "From game design elements to gamefulness: defining 'gamification'," in *Proceedings of the 15th International Academic MindTrek Conference: Envisioning Future Media Environments (MindTrek '11)*, pp. 9–15, ACM, Tampere, Finland, September 2011.

[13] R. Krepki, B. Blankertz, G. Curio, and K.-R. Müller, "The Berlin Brain-Computer Interface (BBCI)—towards a new communication channel for online control in gaming applications," *Multimedia Tools and Applications*, vol. 33, no. 1, pp. 73–90, 2007.

[14] Y. Liu, X. Jiang, T. Cao et al., "Implementation of SSVEP based BCI with Emotiv EPOC," in *Proceedings of the 10th IEEE International Conference on Virtual Environments, Human-Computer Interfaces, and Measurement Systems (VECIMS '12)*, pp. 34–37, Tianjin, China, July 2012.

[15] M. Duvinage, T. Castermans, T. Dutoit et al., "A P300-based quantitative comparison between the Emotiv EPOC headset and a medical EEG device," in *Proceedings of the 9th IASTED International Conference on Biomedical Engineering*, vol. 765, Innsbruck, Austria, 2012.

[16] B. Z. Allison, E. W. Wolpaw, and J. R. Wolpaw, "Brain-computer interface systems: progress and prospects," *Expert Review of Medical Devices*, vol. 4, no. 4, pp. 463–474, 2007.

[17] M. Ahn, M. Lee, J. Choi, and S. C. Jun, "A review of brain-computer interface games and an opinion survey from researchers, developers and users," *Sensors*, vol. 14, no. 8, pp. 14601–14633, 2014.

[18] K. Takano, N. Hata, and K. Kansaku, "Towards intelligent environments: an augmented reality-brain-machine interface operated with a see-through head-mount display," *Frontiers in Neuroscience*, vol. 5, article 60, 2011.

[19] E. W. Sellers, T. M. Vaughan, and J. R. Wolpaw, "A brain-computer interface for long-term independent home use," *Amyotrophic Lateral Sclerosis*, vol. 11, no. 5, pp. 449–455, 2010.

[20] I. Käthner, S. C. Wriessnegger, G. R. Müller-Putz, A. Kübler, and S. Halder, "Effects of mental workload and fatigue on the P300, alpha and theta band power during operation of an ERP (P300) brain-computer interface," *Biological Psychology*, vol. 102, no. 1, pp. 118–129, 2014.

[21] G. Pfurtscheller and C. Neuper, "Motor imagery and direct brain-computer communication," *Proceedings of the IEEE*, vol. 89, no. 7, pp. 1123–1134, 2001.

[22] C. Wang, K. S. Phua, K. K. Ang et al., "A feasibility study of non-invasive motor-imagery BCI-based robotic rehabilitation for stroke patients," in *Proceedings of the 4th International IEEE/EMBS Conference on Neural Engineering (NER '09)*, pp. 271–274, IEEE, Antalya, Turkey, April-May 2009.

[23] T. M. Nunes, A. L. V. Coelho, C. A. M. Lima, J. P. Papa, and V. H. C. de Albuquerque, "EEG signal classification for epilepsy diagnosis via optimum path forest—a systematic assessment," *Neurocomputing*, vol. 136, pp. 103–123, 2014.

[24] L. A. Farwell and E. Donchin, "Talking off the top of your head: toward a mental prosthesis utilizing event-related brain potentials," *Electroencephalography and Clinical Neurophysiology*, vol. 70, no. 6, pp. 510–523, 1988.

[25] E. M. Mugler, C. A. Ruf, S. Halder, M. Bensch, and A. Kübler, "Design and implementation of a P300-based brain-computer interface for controlling an internet browser," *IEEE Transactions on Neural Systems and Rehabilitation Engineering*, vol. 18, no. 6, pp. 599–609, 2010.

[26] D. A. Rohani, H. B. Sorensen, and S. Puthusserypady, "Brain-computer interface using P300 and virtual reality: a gaming approach for treating ADHD," in *Proceedings of the 36th Annual International Conference of the IEEE Engineering in Medicine and Biology Society (EMBC '14)*, pp. 3606–3609, IEEE, Chicago, Ill, USA, August 2014.

[27] R. N. Roy, S. Bonnet, S. Charbonnier, and A. Campagne, "Mental fatigue and working memory load estimation: interaction and implications for EEG-based passive BCI," in *Proceedings of the 35th Annual International Conference of the IEEE Engineering in Medicine and Biology Society (EMBC '13)*, pp. 6607–6610, IEEE, Osaka, Japan, July 2013.

[28] D. Coyle, J. Garcia, A. Satti, and T. McGinnity, "EEG-based continuous control of a game using a 3 channel motor imagery BCI: BCI game," in *Proceedings of the IEEE Symposium on Computational Intelligence, Cognitive Algorithms, Mind, and Brain (CCMB '11)*, pp. 1–7, Paris, France, April 2011.

[29] C. Kapeller, C. Hintermüller, and C. Guger, "Augmented control of an avatar using an SSVEP based BCI," in *Proceedings of the ACM 3rd Augmented Human International Conference (AH '12)*, vol. 27, pp. 1–27, 2012.

[30] E. C. Lalor, S. P. Kelly, C. Finucane et al., "Steady-state VEP-based brain-computer interface control in an immersive 3D gaming environment," *EURASIP Journal on Applied Signal Processing*, vol. 2005, pp. 3156–3164, 2005.

[31] A. Finke, A. Lenhardt, and H. Ritter, "The MindGame: a P300-based brain-computer interface game," *Neural Networks*, vol. 22, no. 9, pp. 1329–1333, 2009.

[32] M. Tangermann, M. Krauledat, K. Grzeska et al., "Playing pinball with non-invasive BCI," in *Advances in Neural Information Processing Systems*, vol. 21, pp. 1641–1648, MIT Press, Cambridge, Mass, USA, 2009.

[33] B. Reuderink, A. Nijholt, and M. Poel, "Affective pacman: a frustrating game for brain-computer interface experiments," in *Intelligent Technologies for Interactive Entertainment*, A. Nijholt, D. Reidsma, and H. Hondorp, Eds., vol. 9 of *Lecture Notes of the Institute for Computer Sciences, Social Informatics and Telecommunications Engineering*, pp. 221–227, Springer, Berlin, Germany, 2009.

[34] G. Pires, M. Torres, N. Casaleiro, U. Nunes, and M. Castelo-Branco, "Playing Tetris with non-invasive BCI," in *Proceedings of the IEEE 1st International Conference on Serious Games and Applications for Health (SeGAH '11)*, pp. 1–6, IEEE, Braga, Portugal, November 2011.

[35] J. A. Pineda, D. S. Silverman, A. Vankov, and J. Hestenes, "Learning to control brain rhythms: making a brain-computer interface possible," *IEEE Transactions on Neural Systems and Rehabilitation Engineering*, vol. 11, no. 2, pp. 181–184, 2003.

[36] L. F. Nicolas-Alonso and J. Gomez-Gil, "Brain computer interfaces, a review," *Sensors*, vol. 12, no. 2, pp. 1211–1279, 2012.

[37] S. G. Mason and G. E. Birch, "A general framework for brain-computer interface design," *IEEE Transactions on Neural Systems and Rehabilitation Engineering*, vol. 11, no. 1, pp. 70–85, 2003.

[38] P. Grover, J. Weldon, S. Kelly, P. Venkatesh, and H. Jeong, "An information theoretic technique for harnessing attenuation of high spatial frequencies to design ultra-high-density EEG," in *Proceedings of the 53rd Annual Allerton Conference on Communication, Control, and Computing*, Monticello, Ill, USA, September-October 2015.

[39] G. Pfurtscheller, D. Flotzinger, and J. Kalcher, "Brain-computer interface—a new communication device for handicapped persons," *Journal of Microcomputer Applications*, vol. 16, no. 3, pp. 293–299, 1993.

[40] G. Sun, K. Li, X. Li, B. Zhang, S. Yuan, and G. Wu, "A general framework of brain-computer interface with visualization and virtual reality feedback," in *Proceedings of the 8th IEEE International Symposium on Dependable, Autonomic and Secure Computing (DASC '09)*, pp. 418–423, Chengdu, China, December 2009.

[41] A. Bashashati, M. Fatourechi, R. K. Ward, and G. E. Birch, "A survey of signal processing algorithms in brain-computer interfaces based on electrical brain signals," *Journal of Neural Engineering*, vol. 4, no. 2, pp. R32–R57, 2007.

[42] F. Lotte, M. Congedo, A. Lécuyer, F. Lamarche, and B. Arnaldi, "A review of classification algorithms for EEG-based brain-computer interfaces," *Journal of Neural Engineering*, vol. 4, no. 1, pp. 1–13, 2007.

[43] R. Fazel-Rezai, B. Z. Allison, C. Guger, E. W. Sellers, S. C. Kleih, and A. Kübler, "P300 brain computer interface: current challenges and emerging trends," *Frontiers in Neuroengineering*, vol. 5, article 14, 2012.

[44] Y. Punsawad and Y. Wongsawat, "Hybrid SSVEP-motion visual stimulus based BCI system for intelligent wheelchair," in *Proceedings of the 35th Annual International Conference of the IEEE Engineering in Medicine and Biology Society (EMBC '13)*, pp. 7416–7419, Osaka, Japan, July 2013.

[45] D. Huang, K. Qian, D.-Y. Fei, W. Jia, X. Chen, and O. Bai, "Electroencephalography (EEG)-based brain-computer interface (BCI): a 2-D virtual wheelchair control based on event-related desynchronization/synchronization and state control," *IEEE Transactions on Neural Systems and Rehabilitation Engineering*, vol. 20, no. 3, pp. 379–388, 2012.

[46] G. Reshmi and A. Amal, "Design of a BCI system for piloting a wheelchair using five class MI Based EEG," in *Proceedings of the 3rd International Conference on Advances in Computing and Communications (ICACC '13)*, pp. 25–28, Cochin, India, August 2013.

[47] N. Birbaumer, A. Kübler, N. Ghanayim et al., "The thought translation device (TTD) for completely paralyzed patients," *IEEE Transactions on Rehabilitation Engineering*, vol. 8, no. 2, pp. 190–193, 2000.

[48] Y. Li, J. Pan, F. Wang, and Z. Yu, "A hybrid BCI system combining P300 and SSVEP and its application to wheelchair control," *IEEE Transactions on Biomedical Engineering*, vol. 60, no. 11, pp. 3156–3166, 2013.

[49] M. H. Chang, J. S. Lee, J. Heo, and K. S. Park, "Eliciting dual-frequency SSVEP using a hybrid SSVEP-P300 BCI," *Journal of Neuroscience Methods*, vol. 258, pp. 104–113, 2016.

[50] M. Wang, I. Daly, B. Z. Allison et al., "A new hybrid BCI paradigm based on P300 and SSVEP," *Journal of Neuroscience Methods*, vol. 244, pp. 16–25, 2015.

[51] R. Palaniappan, "Utilizing gamma band to improve mental task based brain-computer interface design," *IEEE Transactions on Neural Systems and Rehabilitation Engineering*, vol. 14, no. 3, pp. 299–303, 2006.

[52] T. Elbert, B. Rockstroh, W. Lutzenberger, and N. Birbaumer, "Biofeedback of slow cortical potentials. I," *Electroencephalography and Clinical Neurophysiology*, vol. 48, no. 3, pp. 293–301, 1980.

[53] H. O. Gulcur, Y. K. Yilmaz, and T. Demiralp, "Classification of P300 component in single trial event related potentials," in *Proceedings of the 2nd International Conference on Biomedical Engineering Days*, pp. 48–50, May 1998.

[54] V. Raudonis, G. Narvydas, and R. Simutis, "A classification of flash evoked potentials based on artificial neural network," *Electronics and Electrical Engineering*, vol. 81, no. 1, pp. 31–36, 2008.

[55] G. Rance, F. W. Rickards, L. T. Cohen, S. De Vidi, and G. M. Clark, "The automated prediction of hearing thresholds in sleeping subjects using auditory steady-state evoked potentials," *Ear and Hearing*, vol. 16, no. 5, pp. 499–507, 1995.

[56] L. Bi, K. Jie, X.-A. Fan, and Y. Li, "A SSVEP brain-computer interface with the hybrid stimuli of SSVEP and P300," in *Proceedings of the 7th International Conference on Complex Medical Engineering (CME '13)*, pp. 211–214, IEEE, Beijing, China, May 2013.

[57] K.-K. Shyu, Y.-J. Chiu, P.-L. Lee, J.-M. Liang, and S.-H. Peng, "Adaptive SSVEP-based BCI system with frequency and pulse duty-cycle stimuli tuning design," *IEEE Transactions on Neural Systems and Rehabilitation Engineering*, vol. 21, no. 5, pp. 697–703, 2013.

[58] P.-L. Lee, C.-L. Yeh, J. Y.-S. Cheng, C.-Y. Yang, and G.-Y. Lan, "An SSVEP-based BCI using high duty-cycle visual flicker," *IEEE Transactions on Biomedical Engineering*, vol. 58, no. 12, pp. 3350–3359, 2011.

[59] D. Regan, "Steady-state evoked potentials," *Journal of the Optical Society of America*, vol. 67, no. 11, pp. 1475–1489, 1977.

[60] S. Resalat, V. Saba, F. Afdideh, and A. Heidarnejad, "High-speed SSVEP-based BCI: study of various frequency pairs and inter-sources distances," in *Proceedings of the IEEE-EMBS International Conference on Biomedical and Health Informatics (BHI '12)*, pp. 220–223, Hong Kong, January 2012.

[61] R. Singla, A. Khosla, and R. Jha, "Influence of stimuli color on steady-state visual evoked potentials based BCI wheelchair control," *Journal of Biomedical Science and Engineering*, vol. 6, no. 11, pp. 1050–1055, 2013.

[62] J. Faller, G. Müller-Putz, D. Schmalstieg, and G. Pfurtscheller, "An application framework for controlling an avatar in a desktop-based virtual environment via a software SSVEP brain-computer interface," *Presence: Teleoperators and Virtual Environments*, vol. 19, no. 1, pp. 25–34, 2010.

[63] S. Amiri, R. Fazel-Rezai, and V. Asadpour, "A review of hybrid brain-computer interface systems," *Advances in Human-Computer Interaction*, vol. 2013, Article ID 187024, 8 pages, 2013.

[64] M. Grosse-Wentrup, "What are the causes of performance variation in brain-computer interfacing?" *International Journal of Bioelectromagnetism*, vol. 13, no. 3, pp. 115–116, 2011.

[65] F. Popescu, B. Blankertz, and K.-R. Müller, "Computational challenges for noninvasive brain computer interfaces," *IEEE Intelligent Systems*, vol. 23, no. 3, pp. 78–79, 2008.

[66] G. Dornhege, *Increasing information transfer rates for brain-computer interfacing [Ph.D. thesis]*, Universitat Potsdam, Potsdam, Germany, 2006.

[67] D. P.-O. Bos, B. Reuderink, B. van de Laar et al., "Human-computer interaction for BCI games: usability and user experience," in *Proceedings of the 10th International Conference on Cyberworlds (CW '10)*, pp. 277–281, Singapore, October 2010.

[68] H. Gürkök, *Mind the sheep! User experience evaluation & brain-computer interface games [Ph.D. thesis]*, University of Twente, Enschede, The Netherlands, 2012.

[69] T. O. Zander, M. Gaertner, C. Kothe, and R. Vilimek, "Combining eye gaze input with a brain-computer interface for touchless human-computer interaction," *International Journal of Human-Computer Interaction*, vol. 27, no. 1, pp. 38–51, 2010.

[70] J. E. Muñoz, R. Chavarriaga, and D. S. Lopez, "Application of hybrid BCI and exergames for balance rehabilitation after stroke," in *Proceedings of the 11th ACM Conference on Advances in Computer Entertainment Technology (ACE '14)*, Funchal, Portugal, November 2014.

[71] G. Kristo, J. Höhne, R. Ortner, B. Reuderink, and N. Ramsey, *BNCI Horizon 2020*, 2015.

[72] M. Solms and O. Turnbull, *The Brain and the Inner World—An Introduction to the Neuroscience of Subjective Experience*, Other Press, New York, NY, USA, 2002.

[73] V. Jurcak, D. Tsuzuki, and I. Dan, "10/20, 10/10, and 10/5 systems revisited: their validity as relative head-surface-based positioning systems," *NeuroImage*, vol. 34, no. 4, pp. 1600–1611, 2007.

[74] I. Martišius and R. Damaševicius, "Class-adaptive denoising for EEG data classification," in *Artificial Intelligence and Soft Computing: 11th International Conference, ICAISC 2012, Zakopane, Poland, April 29-May 3, 2012, Proceedings, Part II*, vol. 7268 of *Lecture Notes in Computer Science*, pp. 302–309, Springer, Berlin, Germany, 2012.

[75] D. Birvinskas, V. Jusas, I. Martisius, and R. Damasevicius, "Fast DCT algorithms for EEG data compression in embedded systems," *Computer Science and Information Systems*, vol. 12, no. 1, pp. 49–62, 2015.

[76] R. Damaševičius, M. Vasiljevas, I. Martisius, V. Jusas, D. Birvinskas, and M. Wozniak, "BoostEMD: an extension of EMD method and its application for denoising of EMG signals," *Electronics and Electrical Engineering*, vol. 21, no. 6, pp. 57–61, 2015.

[77] I. Martisius, R. Damasevicius, V. Jusas, and D. Birvinskas, "Using higher order nonlinear operators for SVM classification of EEG data," *Electronics and Electrical Engineering*, vol. 3, no. 119, pp. 99–102, 2012.

[78] Y. Renard, F. Lotte, G. Gibert et al., "OpenViBE: an open-source software platform to design, test, and use brain-computer interfaces in real and virtual environments," *Presence*, vol. 19, no. 1, pp. 35–53, 2010.

[79] L. Demanet and L. Ying, "Wave atoms and sparsity of oscillatory patterns," *Applied and Computational Harmonic Analysis*, vol. 23, no. 3, pp. 368–387, 2007.

[80] A. A. Mohammed, Q. M. Jonathan Wu, and M. A. Sid-Ahmed, "Application of wave atoms decomposition and extreme learning machine for fingerprint classification," in *Image Analysis and Recognition*, A. Campilho and M. Kamel, Eds., vol. 6112 of *Lecture Notes in Computer Science*, pp. 246–255, Springer, 2010.

[81] H. Xu and G. Zhai, "ECG data compression based on wave atom transform," in *Proceedings of the 3rd IEEE International Workshop on Multimedia Signal Processing (MMSP '11)*, Hangzhou, China, November 2011.

[82] I. Martišius, D. Birvinskas, R. Damaševicius, and V. Jusas, "EEG dataset reduction and classification using wave atom transform," in *Artificial Neural Networks and Machine Learning—ICANN 2013: 23rd International Conference on Artificial Neural Networks Sofia, Bulgaria, September 10–13, 2013. Proceedings*, vol. 8131 of *Lecture Notes in Computer Science*, pp. 208–215, Springer, Berlin, Germany, 2013.

[83] T. Cao, F. Wan, P. U. Mak, P.-I. Mak, M. I. Vai, and Y. Hu, "Flashing color on the performance of SSVEP-based brain-computer interfaces," in *Proceedings of the 34th Annual International Conference of the IEEE Engineering in Medicine and Biology Society (EMBS '12)*, pp. 1819–1822, San Diego, Calif, USA, September 2012.

[84] R. A. Fisher, "The use of multiple measurements in taxonomic problems," *Annals of Eugenics*, vol. 7, no. 2, pp. 179–188, 1936.

[85] V. N. Vapnik, *Statistical Learning Theory*, vol. 2, John Wiley & Sons, New York, NY, USA, 1998.